USAATCOM TR 95-D-8

U.S. ARMY
AVIATION
AND TROOP COMMAND

ADVANCED ROTOR BLADE EROSION PROTECTION SYSTEM

William D. Weigel

KAMAN AEROSPACE CORPORATION
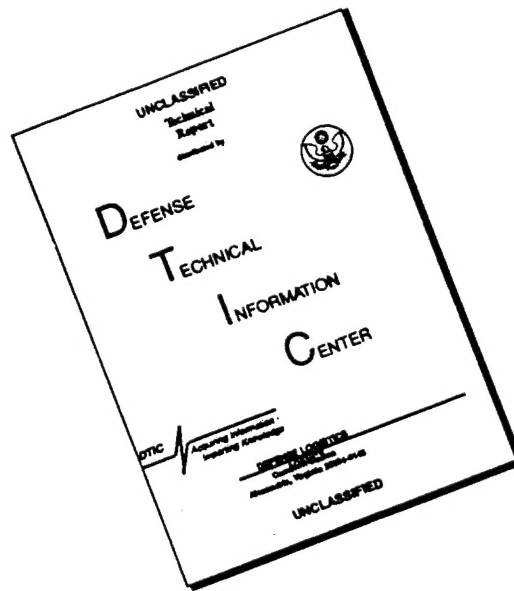BLOOMFIELD, CT O6002-0002

JULY 1996

Final Report

Approved for public release; distribution unlimited.

Prepared for:

AVIATION APPLIED TECHNOLOGY DIRECTORATE
U.S. ARMY AVIATION AND TROOP COMMAND
FORT EUSTIS, VA 23604-5577

19960924 006

DISCLAIMER NOTICE

THIS DOCUMENT IS BEST QUALITY AVAILABLE. THE COPY FURNISHED TO DTIC CONTAINED A SIGNIFICANT NUMBER OF PAGES WHICH DO NOT REPRODUCE LEGIBLY.

AVIATION APPLIED TECHNOLOGY DIRECTORATE
POSITION STATEMENT

This report describes the work accomplished by Kaman Aerospace Corporation (KAC) under U.S. Army Contract DAAJ02-91-C-0045 "Advanced Rotor Blade Erosion Protection System." The primary objective of this program was to develop a superior nonmetallic erosion guard system for rotor blade erosion protection from sand, rain, hydrolysis, and other environmental conditions. An extensive industry survey was conducted to identify suitable materials. This was a very comprehensive effort and included foreign materials. After screening tests, two materials were chosen --- 3M NPE 2916 and Miles Inc. 535330A. NPE 2916 exhibits more than four times the rain resistance and twice the sand resistance of the current PO655 material. Miles 535330A exhibits equivalent rain resistance and six times the sand resistance of PO655. Both of these materials were found to be free of the hydrolysis problems encountered with the current PO655 material.

The AH-1 Cobra K747 blade was chosen by the contractor as a testbed for the new materials. This blade uses a full length molded leading edge erosion guard. Therefore, a molded form of erosion guard was required. Three erosion guards of each material were designed and successfully fabricated with the manufacturing processes documented. Four of these guards were installed on rotor blades and are being evaluated at Ft. Rucker.

A dynamic finite element model for water drop impact was developed under this program. It is a significant improvement over previously available analyses. Further work with this model would be useful in expanding knowledge of water drop interaction with polymers.

The draft Design Criteria Document referenced in this report has been updated to reflect lessons learned during this development effort. It should be published and used as a guide by designers for rotor blade erosion guard development.

Mr. Donald N. Arents of the Air Vehicle Structures Division, served as project engineer for this effort.

REPORT DOCUMENTATION PAGE

Public reporting burden for this collection of information is estimated to average 1 hour per response, including the time for reviewing instructions, searching existing data sources, gathering and maintaining the data needed, and completing and reviewing the collection of information. Send comments regarding this burden estimate or any other aspect of this collection of information, including suggestions for reducing this burden. to Washington Headquarters Services, Directorate for Information Operations and Reports, 1215 Jefferson Davis Highway, Suite 1204, Arlington, VA 22202-4302, and to the Office of Management and Budget, Paperwork Reduction Project (0704-0188), Washington, DC 20503.

1. AGENCY USE ONLY (Leave blank)	2. REPORT DATE July 1996	3. REPORT TYPE AND DATES COVERED FINAL FROM AUG 91 TO SEP 94

4. TITLE AND SUBTITLE	5. FUNDING NUMBERS
ADVANCED ROTOR BLADE EROSION PROTECTION SYSTEM	
6. AUTHOR(S) WEIGEL, WILLIAM D.	DAAJ02-91-C-0045

7. PERFORMING ORGANIZATION NAME(S) AND ADDRESS(ES)	8. PERFORMING ORGANIZATION REPORT NUMBER
KAMAN AEROSPACE CORPORATION BLOOMFIELD, CT 06002-0002	R-2034

9. SPONSORING/MONITORING AGENCY NAME(S) AND ADDRESS(ES)	10. SPONSORING/MONITORING AGENCY REPORT NUMBER
AVIATION APPLIED TECHNOLOGY DIRECTORATE U.S. ARMY AVIATION AND TROOP COMMAND FORT EUSTIS, VA 23604-5577	USAATCOM TR 95-D-8

11. SUPPLEMENTARY NOTES

12a. DISTRIBUTION/AVAILABILITY STATEMENT	12b. DISTRIBUTION CODE
APPROVED FOR PUBLIC RELEASE; DISTRIBUTION UNLIMITED.	

13. ABSTRACT (Maximum 200 words)

Two new hydrolysis-free elastomeric materials have been identified, tested and fabricated into full-length leading edge erosion guards. The were applied to K747 composite main rotor blades for operational flight evaluation on the AH-1 Cobra helicopter. One exhibits more than four times the rain resistance and twice the sand resistance as the current material. The other has six times the sand resistance and equivalent rain resistance.

A worldwide survey was conducted to identify potentially suitable materials. Moldable and castable materials, films and tapes, sprayable coatings and two-component, room temperature curing systems were subjected to hydrolysis testing and whirling arm rain erosion testing. A selected group was then subjected to whirling arm sand erosion and impact testing in a Kaman-funded test facility constructed for this program. Solar radiation, fungus, salt fog, low temperature, temperature shock and decontamination testing completed the environmental tests. Army design criteria and qualification test procedures were updated. A three-dimensional, dynamic, finite element stress wave analytical model of a raindrop impacting elastomeric material was developed. A unique test procedure was devised for measuring large strain, high strain rate, dynamic material properties required for input into the analytical model.

14. SUBJECT TERMS			15. NUMBER OF PAGES
Rotor Blade Erosion, Sand Erosion, Rain Erosion, Impact, Hydrolysis, Stress Wave Analysis, Strain Rate, Viscoelasticity			288
			16. PRICE CODE

17. SECURITY CLASSIFICATION OF REPORT	18. SECURITY CLASSIFICATION OF THIS PAGE	19. SECURITY CLASSIFICATION OF ABSTRACT	20. LIMITATION OF ABSTRACT
UNCLASSIFIED	UNCLASSIFIED	UNCLASSIFIED	UNLIMITED

NSN 7540-01-280-5500

Standard Form 298 (Rev. 2-89)
Prescribed by ANSI Std. Z39-18
298-102

PREFACE AND ACKNOWLEDGEMENTS

CONTENTS

FIGURES

TABLES

INTRODUCTION

The performance of helicopter rotor blade erosion protection systems has become exceedingly important. Recent operational experiences have forced Army helicopters to function in extremely hostile environmental conditions and emphasized the need for improved materials and designs of rotor blade erosion protection systems.

Although many types of equipment must contend with either solid or liquid particle impact, helicopter rotor blades are unique in having to withstand severe exposure to both. Neither Kaman nor any other manufacturer has evolved a totally satisfactory protective system for both sand and rain erosion. Since most manufacturers have to deal with either solid or liquid particle erosion, each problem has generally been attacked individually. State-of-the-art, optimized material systems have been developed for each environment, but these do not perform as well as desired in the other environment.

It has been demonstrated in earlier research[1] that most suitably chosen elastomeric systems perform outstandingly well in solid particle erosion service, at least an order of magnitude better than the best known metals. See Figure 1. In contrast, elastomer life under nearly normal impingement angles in rain is lower than that of metals. However, it is significant to note that components such as radomes and antenna housings, requiring nonmetallic dielectric coatings for protection against rain erosion, generally employ elastomeric materials. As a class, elastomers exhibit much better sand erosion protection than metals and are second only to metals in rain erosion resistance. In comparison to the metal leading edge erosion guards in general use, an elastomeric guard reduces the radar cross section of the blade, is inherently less costly to fabricate, easier to install, more amenable to field repair and replacement, and provides a better balance of rain and sand erosion life in the Army helicopter operating environment.

Army data shows that the metal erosion guards employed on the B-540 metal main rotor blades for the AH-1 Cobra helicopter exhibited low flight time between replacement as a result of sand erosion[2]. The elastomeric erosion guard originally developed for the K747 composite main rotor blade for the same helicopter performed to the Army's specified sand and rain erosion resistance requirements[3]. It was fabricated from Estane 82-083-1828, a thermoplastic polyurethane material supplied by B.F. Goodrich. Although satisfactory from the standpoint of sand and rain erosion performance, it proved to be undesirably vulnerable to foreign object impact damage during in-ground-effect (IGE) and operational nap-of-the-earth (NOE) maneuvers. As a result of this experience, an erosion guard with improved resistance to impact was developed[4]. It was fabricated from P0655, a thermosetting polyurethane material supplied by Custom Urethane Elastomers, Inc. (CUE Inc.) formerly Fluorocarbon Inc.

Configurations

No. 1	Base Line .025 Stainless Steel
No. 2	.032 Stainless Steel
No. 3	.031 Stellite 6B
No. 4	.032 Titanium 6Al-4V
No. 5	.016 Electroformed Nickel
No. 6	.032 Electroformed Nickel
No. 8	.030 Polyurethane PO 655
No. 9	.030 Polyurethane Estane - Tapered
No. 10	.060 Polyurethane PO 655
No. 11	.060 Polyurethane Estane - Tapered

Test Conditions

Olin Whirl Rig
Velocity - 530 mph (777 fps)
Sand Rate - 144 gm/min

Figure 1. Sand Erosion Wear Rate, Comparative Summary. (From Ref. 1)

2

The P0655 polyurethane erosion guard performed well in rain, sand and impact conditions but began to exhibit hydrolytic degradation in hot-moist service environments. This led to a gradual softening of the elastomer and required erosion guard replacement after 3-4 years in hot-moist climates such as Southeastern U.S., Hawaii, Korea and Pakistan. Hydrolytic degradation did not occur at a high rate in cooler climates such as Germany where considerably longer operating life has been experienced.

Despite the impact damage susceptibility of the Estane erosion guard and the hydrolytic instability of the P0655 material, a recent Army-funded study ranked the combined performance of these erosion protection systems as the most cost-effective on Army helicopters[2]. Of all the rotor blades employed during Operation Desert Storm in the Mideast, the K747 main rotor blade required the least amount of maintenance.

In the same study, a stress wave analysis was performed to examine the effect of raindrop impingement on erosion guard materials. The analysis was one dimensional and did not include failure criteria in the model. It provided the magnitude of uniaxial stress and strain levels but it was left to the user to decide whether or not the calculated results would lead to failure. Material properties were measured on a split-Hopkinson pressure bar which is normally used to obtain properties of metals. There have been some concerns regarding the validity of properties of polymeric materials obtained in this manner.

In summary, there has been a hydrolytic degradation problem associated with elastomeric leading edge erosion guards which otherwise exhibit a good balance of rain, sand and impact resistance. This program begins with a worldwide survey for potentially suitable materials and, using a down-select elimination process, proceeds through a series of environmental and mechanical tests, culminating with a choice of two new hydrolysis-free materials. These were fabricated into full-length erosion guards and applied to helicopter rotor blades for operational flight evaluation by the Army.

Additionally, it has been desirable to expand analytical and test methodology to improve understanding of rain erosion mechanisms. General Research Corporation (GRC) was contracted by Kaman to perform the analytical requirements and large strain, high strain rate material testing for this program. A 50 mm powder gun and a unique specimen loading system was used to measure dynamic material properties required for input into the GRC-developed, three-dimensional, dynamic finite element stress wave computational model of a raindrop impacting an elastomeric material.

TECHNICAL APPROACH

The first task of the Advanced Rotor Blade Erosion Protection System (ARBEPS) program was a materials identification, evaluation and selection function. It began with a survey of material suppliers and aircraft manufacturers for potential candidate materials. Determining which materials to evaluate was considered a key element for the successful performance of the entire program. Knowledge of the relationship of polymer molecular structure to material properties was important to assure that the most likely to succeed candidate materials were introduced.

The material survey and identification process was followed by an extensive screening program consisting of a battery of environmental, erosion and impact tests. All the materials were first subjected to a hydrolysis test to reveal any possible degradation which could occur in a hot-wet environment. Many of these were then subjected to a rain erosion test. As described earlier, most elastomeric urethanes perform quite well in sand erosion; however, the degree to which different elastomers perform in rain erosion varies dramatically. Therefore hydrolysis and rain erosion testing were used as the primary down-selection process which greatly reduced the number of materials required for subsequent testing.

Following the hydrolysis and rain erosion testing, a selected group of materials were subjected to a whirling arm sand erosion test in the Kaman-funded test facility built especially for this program. A whirling arm sand erosion test was considered representative of the type of particle erosion experienced by rotor blades in an operational world sand environment.

Whirling arm impact testing was conducted in the same test facility by injecting hardwood dowels of progressively increasing diameters into the path of the test coupon and assessing the damage to the erosion protection material. This test simulates tree branch strikes which Army helicopters experience during the course of certain operations.

The hydrolysis, rain erosion, sand erosion and impact tests were considered to be the most significant of all the material testing performed. A series of other tests were performed to insure against unexpected environmental degradation which could occur. Those tests included solar radiation, fungus, salt fog, low temperature, temperature shock and decontamination.

A radar cross section assessment was performed to determine what changes might occur if a different urethane elastomer was used in place of the current P0655.

In parallel with the materials evaluation tasks, a stress wave/parametric analysis effort was begun by General Research Corporation (GRC) under a contract from Kaman. This was undertaken to expand the analysis methodology discussed earlier. A three-dimensional, dynamic finite element stress wave computational model of rain drop impacts at normal and oblique impact angles was developed at GRC.

In order to realistically evaluate the transient response of the erosion protection system for raindrop impacts, dynamic material properties at 10^4 to 10^5 s^{-1} strain rates and large strain levels representative of raindrop collisions were required for input into the computational

4

model. Since material properties were not generally available at these strain rates, GRC's effort was expanded to determine these properties on selected candidate materials using a GRC ballistic range. A novel and ingenious test procedure, incorporating a 50 mm powder gun and a unique specimen loading system, generated the required dynamic material properties, including ultimate tensile stress and strain to failure, at the high strain rates experienced by rotor blade erosion protection materials impacted by rain drops. Using as input the newly acquired material properties obtained at the relevant strain rates, the computational model was exercised to perform parametric analyses for examining the influence of dynamic material properties, thickness of material, angle of attack and raindrop size on the ability of the material to function effectively as a rain erosion protection system.

After all the testing was performed and the results studied and discussed, several of the overall best materials were proposed for the design task of the program. The materials selected and the analytical methodology developed in this program have generic applicability to all Army helicopters. Because Kaman designed and produced over 4000 K747 composite main rotor blades for the Army AH-1 Cobra helicopter, the K747 was chosen as the demonstration blade for evaluating materials and designs developed within this program. Figure 2 shows the K747 composite main rotor blade configuration, details and primary materials.
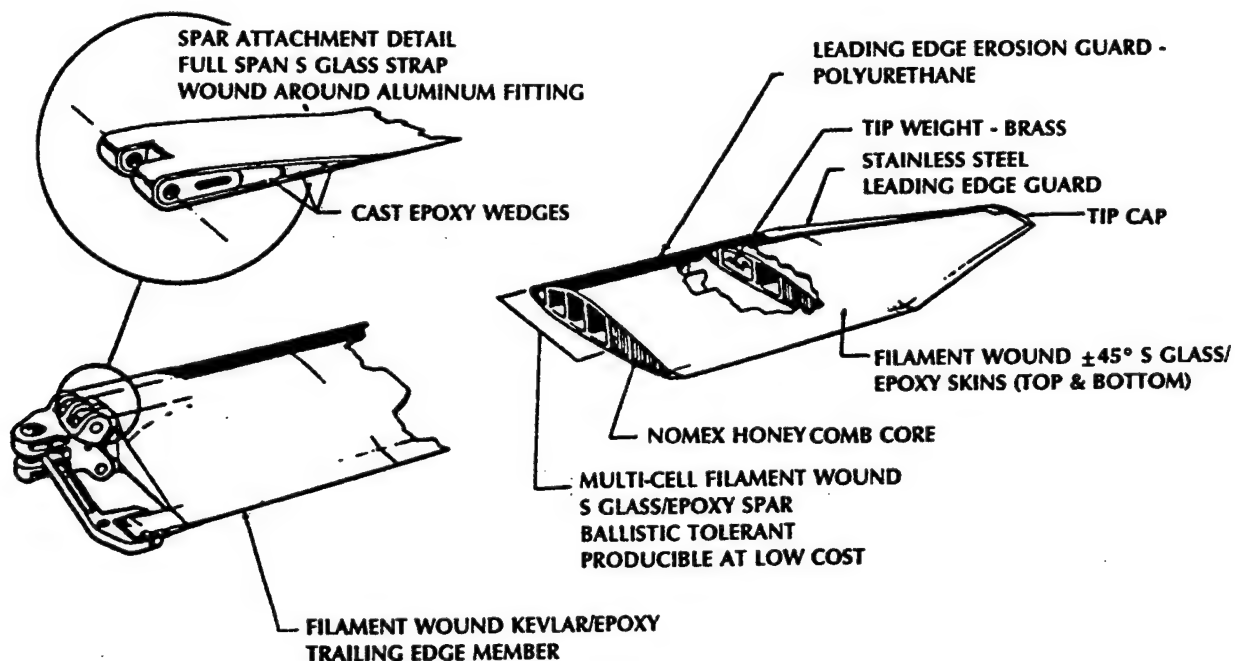
Figure 2. K747 Blade Configuration.

5

Two materials were recommended by Kaman for further evaluation as leading edge erosion guards. Both had excellent hydrolysis resistance. One, NPE 2916, exhibited outstanding rain erosion resistance and better sand erosion resistance than the current P0655 erosion guard material. The other, 535330A, possessed superior sand erosion resistance and equivalent rain erosion resistance compared to P0655. It was determined that both materials should be submitted for operational evaluation as full-length erosion guards.

The next program task was a detail design and manufacturing process development for fabricating full-length erosion guards from both materials. NPE 2916 material was supplied as thermoplastic sheet stock and a process was developed for heat forming erosion guards at Kaman. The 535330A material was a two-part casting compound. A process was developed for fabricating erosion guards in the same matched metal mold used to fabricate the standard P0655 production erosion guards at CUE, Inc.

After the detail designs were approved by the Army, three full-length leading edge erosion guards were fabricated from each material. Two of each were bonded to Government furnished K747 main rotor blades and the blades were prepared for flight. The short outboard stainless steel leading edge guard shown in Figure 2 was not installed over the new elastomeric erosion guards in order to achieve accelerated wear data from flight testing in harsh environments.

Following a Flight Safety Review, the four blades with the new erosion guards installed were delivered to Ft. Rucker for operational evaluation. The two spare erosion guards were delivered to AATD, Ft. Eustis, VA.

MATERIALS EVALUATION

MATERIALS SURVEY AND IDENTIFICATION

The materials survey was conducted using form letters and telephone contacts to organizations primarily within but not limited to the U.S. Form letters varied slightly depending on the business of the addressee, whether an aircraft manufacturer or materials supplier, and the particular type of material supplied by the vendor, such as coatings, tapes and molded materials. Telephone calls were made directly to product development chemists and engineers who were already known by Kaman personnel or who were introduced through vendor technical representatives.

Considerable care and effort was given to the discussion of the blade operational requirements so the material suppliers could better recommend potential candidate materials for the program. Hydrolysis resistance was stressed as extremely important and, based on previous rain erosion testing of molded materials, a Shore A hardness range of approximately 60 to 70 was suggested.

Commercially available polyurethane elastomers are primarily based on two different precursor or prepolymer types, those which contain ester links and those which contain ether links in the molecular chain or backbone. The ester or polyester types are known for their excellent mechanical properties, such as tensile strength and tear resistance, and the ether or polyether types are known for their resistance to hydrolysis. Hydrolysis in this case is a mechanism whereby an ester group in the primary backbone chain can be split into its two original organic acid and alcohol reactant groups. The result is a broken bond in the molecular backbone, similar to a broken or missing link in a chain. When this occurs in an elastomeric polymer, the usual effect is a gradual change from a tough, resilient material to a soft, pliable one with reduced mechanical and environmental properties. In some cases where the molecules formed are small enough to be leached out with moisture, the material which remains becomes brittle and eventually cracks or tears. Both types of failures were observed in this study.

Table 1 describes a total of 62 potential candidate materials which were identified for initial evaluation. Some materials were chosen because they are currently in use on Army helicopter rotor blades, or because they are part of erosion guard repair kits and/or erosion protection enhancement kits. Some were known to be polyester type urethanes, but if they could provide outstanding protection and be easily replaceable, they were considered. Most helpful were those material suppliers who were willing to describe in general terms the formulation of their products. Knowing the general molecular structure of the materials leads to a much greater understanding of the role of certain chemical groups on various aspects of erosion protection systems. That information has been included in the sample description.

TABLE 1. CANDIDATE MATERIALS

Sample No.	Chemical Type	Company Name	Sample Name	Hydrolysis Pass/Fail	Description
		MOLDED MATERIALS			
1	Rubber/Nylon	CUE Inc.	Nyrim 2300	P	Rubber/Nylon Block Copolymer. 98A/75D.
2	Urethane	CUE Inc.	CE868	P	Polyether/MDI. 60A
3	Urethane	CUE Inc.	CE870	P	Polyether/MDI. 75A.
4	Urethane	CUE Inc.	PO655	F	Polyester/MDI/Polyol. 60A. (Current K747 Erosion Guard Material).
5	Urethane	Goodrich, B. F.	74-451-170	F	Lightly Crosslinked Polyester Urethane. 73A. Has UV Stabilizer.
6	Urethane	Novex Inc.	Z.48.1	P	PTMEG/PPDI/Polyol. 90A.
7	Urethane	Polyurethane Specialties	PCA 6-3 65A	P	PTMEG/MDI/Glycol-Polyol Blend. 65A
8	Urethane	Polyurethane Specialties	PCA 6-3 80A	P	PTMEG/MDI/Glycol. 80A.
9	Urethane	Polyurethane Specialties	PCA 708S 60A	F	Polycaprolactone/MDI/Glycol-Polyol Blend. 60A. Hydrolysis stabilized.
10	Urethane	Polyurethane Specialties	PCA 708S 75A	P	Polycaprolactone/MDI/Glycol. 75A. Hydrolysis stabilized.
11	Urethane	Task Research Inc.	TSK L101	P	Polyether Urethane. 96A/54D. (Current UH-1 CMRB Erosion Guard Material).
12	Urethane	Uniroyal Chemical	PP150-50A	F	PTMEG/PPDI/Polyol. 50A.
13	Urethane	Uniroyal Chemical	PP150-60A	F	PTMEG/PPDI/Polyol. 60A.
14	Urethane	Uniroyal Chemical	Vibrathane 6060	F	Polycaprolactone/TDI/MOCA. 58A.
15	Urethane	Uniroyal Chemical	Vibrathane B 836	F	PTMEG/MDI/Polyol. 55A.
17	Urethane-Urea	Miles Inc.	535330A	P	PTMEG/rMDI Urethane-Urea. 85A.
19	Urethane	Miles Inc.	535330C	P	PTMEG/t,t-rMDI/Glycol. 83A.
20	Urethane	CONAP	DPTU-19140	P	CHDI Polyether Urethane. 92A.
21	Neoprene	Fairprene Industrial Prods.	NS-6572	F	Neoprene Deicing/Erosion Boot Material. 71A. Used on Propellers.
22	Urethane	Uniroyal Chemical	JC-010992	P	PTMEG/CHDI/Polyol. 69A.
23	Urethane	Miles Inc.	535336A	P	PTMEG Blend/rMDI/Curative Blend. 51A. Low Rebound. 8% Resilience.
24	PVC	E.A.R Div.,Cabot Corp.	C-1002	P	Thermoplastic PVC. Low Rebound. Damping Elastomer. 56A.
25	Urethane	E.A.R Div.,Cabot Corp.	HDS-06	P	Polyether Urethane. Low Rebound. Damping Elastomer. 58A.
26	Urethane	IAI Mata Helicopters	MTA-2151664	F	Polyester Urethane. 69A. (Israeli LE Material. 6 Years In Service).

8

TABLE 1. CANDIDATE MATERIALS

Sample No.	Chemical Type	Company Name	Sample Name	Hydrolysis Pass/Fail	Description
27	Urethane	Miles Inc.	535330B	P	PTMEG/MDI/Glycol. 69A.
28	Urethane	IAI Mata Helicopters	PU-V-18	F	Identified as Polyether Urethane. 85A. Israeli Candidate LE Material.
29	Urethane-Urea	Miles Inc.	535382A	P	PTMEG/rMDI Urethane-Urea. 96A/40D. 48% Resilience.
30	Urethane-Urea	Miles Inc.	535382B	P	PTMEG/rMDI Urethane-Urea. 94A. 44% Resilience.
31	Urethane-Urea	Miles Inc.	535382C	P	PTMEG/rMDI Urethane-Urea. 81A. 41% Resilience.
32	Urethane-Urea	Miles Inc.	535382D	P	PTMEG/rMDI Urethane-Urea. 70A. 55% Resilience.
33	Urethane	Miles Inc.	535383A	P	PTMEG/rMDI/Curative Blend. 82A. Energy Absorbing. 15% Resilience.
34	Urethane	Miles Inc.	535383B	P	PTMEG/rMDI/Curative Blend. 71A. Energy Absorbing. 12% Resilience.
35	Urethane	Miles Inc.	535383C	P	PTMEG Blend/rMDI/Curative Blend. Energy Absorbing. 59A. 8% Resilience.
36	Urethane	Uniroyal Chemical	6982A	F	Polycaprolactone/MDI/Curative Blend. 60A.
37	Urethane	Uniroyal Chemical	6982B	F	Polycaprolactone/MDI/Curative Blend. 80A.
38	Urethane	Uniroyal Chemical	6982C	F	Polycaprolactone/MDI/Glycol. 93A.
39	Urethane-Urea	Miles Inc.	535385A	P	PTMEG/t,t-rMDI Urethane-Urea. 73A. 57% Resilience.
40	Urethane-Urea	Miles Inc.	535385B	P	PTMEG/t,t-rMDI Urethane-Urea. 90A. 55% Resilience.
41	Urethane	Miles Inc.	535387A	P	PTMEG/t,t-rMDI/Curative Blend. 95A. 48% Resilience.
42	Urethane	Miles Inc.	535387D	P	PTMEG/t,t-rMDI/Curative Blend. 90A. 50% Resilience.
43	Urethane	Miles Inc.	535387E	P	PTMEG/t,t-rMDI/Curative Blend. 86A. 49% Resilience.
44	Urethane	Uniroyal Chemical	6978	P	PTMEG/PPDI/CHDM & PTMEG. 66A.
45	Urethane	3M Co.	NPE 2916	P	.060" Aliphatic Polyether TP Urethane. 80A. Has UV/Antioxidation Inhibitors.

TAPES

T1	Urethane	3M Co.	8663	F	.016" Aliphatic Polyester TP Urethane/.002" PS Adhesive (Desert Storm Mtl).
T2	Urethane	3M Co.	NPB 2803	F	.012" Aliphatic Polyester TP Urethane/.002" High Shear PS Adhesive.
T3	Urethane	3M Co.	NPE 2846	P	.012" Aliphatic Polyether TP Urethane/.002" High Shear PS Adhesive.
T4	Urethane	Fasson UK Ltd.	Stoneguard 2000	F	.0075" Polyester Urethane/.0014 Acrylic PS Adhesive.(Used on UK Helicopters).

9

TABLE 1. CANDIDATE MATERIALS

Sample No.	Chemical Type	Company Name	Sample Name	Hydrolysis Pass/Fail	Description
T5	Urethane	Flormel Adhesive Products	281	F	.0055" Polyester Urethane/Acrylic PS Adhesive.
T6	Neoprene	Safeway Products	Neoprene Stock	F	.020" Neoprene Deicer Boot Material. Used on Propellers.
COATINGS					
C1	Urethane	Lord Chemical Products	M331/M201	P	Black.
C2	Urethane	Lord Chemical Products	M112/M201	P	Clear version of 331 Black.
C3	Urethane	Lord Chemical Products	M1433/M201	P	Gray. VOC Compliant.
C4	Silicone	Martin Marietta	MI-15 TopCoat	P	Fiber-filled Topcoat for thermal protection coating.
C5	Silicone	Martin Marietta	R-2550	P	MI-15 Clear Topcoat. No Fiber.
C6	Urethane	AGC Inc.	AGCoat 1R/3R	P	Polyether Urethane.
C7	Urethane	Tnemec Co. Inc.	Tnemec 143	P	Polyether Urethane.
C8	Urethane	CAAP Co.	Caapcoat AS-P108/B-274	F	AS-P108 Antistatic Topcoat/B-274 Erosion Coating
C9	Urethane-Urea	United Coatings	Elastuff 504	P	Polyether Urethane-Urea.
C10	Epoxy-Urethane	Dexter Crown-Metro	8B6	F	Epoxy Crosslinked With Urethane.
2-PART SYSTEMS					
B1	Urethane	Task Research Inc.	TSK L100	P	Polyether 2-Part Urethane. (Used for erosion guard field repair).
B2	Urethane	United Coatings	Elastuff 120 Mastic	P	Polyether 2-Part Urethane.
B3	Urethane-Urea	Cal Polymers	NF 1500 Special	F	2-Part Urethane-Urea.

10

In general, the material suppliers were very helpful, supplying product information, recom-mendations and samples. 3M, Miles and Uniroyal were especially cooperative, formulating a variety of candidate materials to specifically meet the blade operational criteria set forth by Kaman early in the program.

The materials consist of molded specimens, tapes, coatings and two-part systems (100% solids/no solvents). The molded specimens represent the form of material expected to be used for main rotor blade leading edge erosion guards. Materials described as molded include those which are also cast, calendered or extruded. Coatings and tapes represent the forms of materials which could possibly be considered for tail rotor erosion protection. The two-part systems are expected to be used for field repairs of either main or tail rotor protection systems.

Almost all the materials are urethanes and urethane derivatives. The remainder include a small number of silicone, neoprene, PVC and rubber/nylon copolymer types.

HYDROLYSIS

All 62 materials were tested for possible degradation in a hot-wet environment. The temperature/humidity levels of the MIL-STD-810E humidity test were increased to a constant 82°C (180°F)/95-100% relative humidity to identify materials which may eventually degrade by the molecular chain scission mechanism of hydrolysis. Due to the large number of samples tested, four separate groups were run. Figure 3 shows the apparatus used for this test. About an inch of distilled water was placed in the bottom of a large plastic container. Samples were placed in small aluminum dishes and stacked on racks. The container was then covered and sealed except for a small opening to relieve pressure. The semi-sealed container was placed in an air circulating oven which was maintained at 82°C (180°F). Materials were visually inspected and tested for durometer hardness prior to exposure and periodically throughout the exposure cycle. The failure mode of most of the materials was a fairly rapid drop in the hardness value within the first several hundred hours of exposure followed by an eventual melting of the material. Several of the materials became brittle and developed cracks. The neoprene samples, 21 and T6, did not melt or crack but swelled irreversibly, especially the thin sample T6. Even after being removed from the test environment and allowed to dry, the samples remained swollen to such a degree that they were considered undesirable. The results of the hydrolysis tests are summarized in Table 1 and described in greater detail in Table 2.

All of the four groups of tests were run to a minimum duration of approximately 1200 hours. Whether the samples passed or failed was determined at that limit. Four of the samples passed at 1200 hours but failed at longer exposure times. Others may have exhibited similar charac-teristics had they been exposed longer. Note that the current K747 erosion guard material, sample 4, failed after 300 hours. This same material in service begins to show signs of hydrolysis after approximately 3 years of operation in severely hot and humid climates, thus 100 hydrolysis test hours relates to approximately 1 year of service exposure in this case. If that relationship is linear then 1200 hours of test exposure would relate to a minimum of 12 years of service in severe hot and humid climates. Many of the samples passed after nearly 4000 hours of exposure.
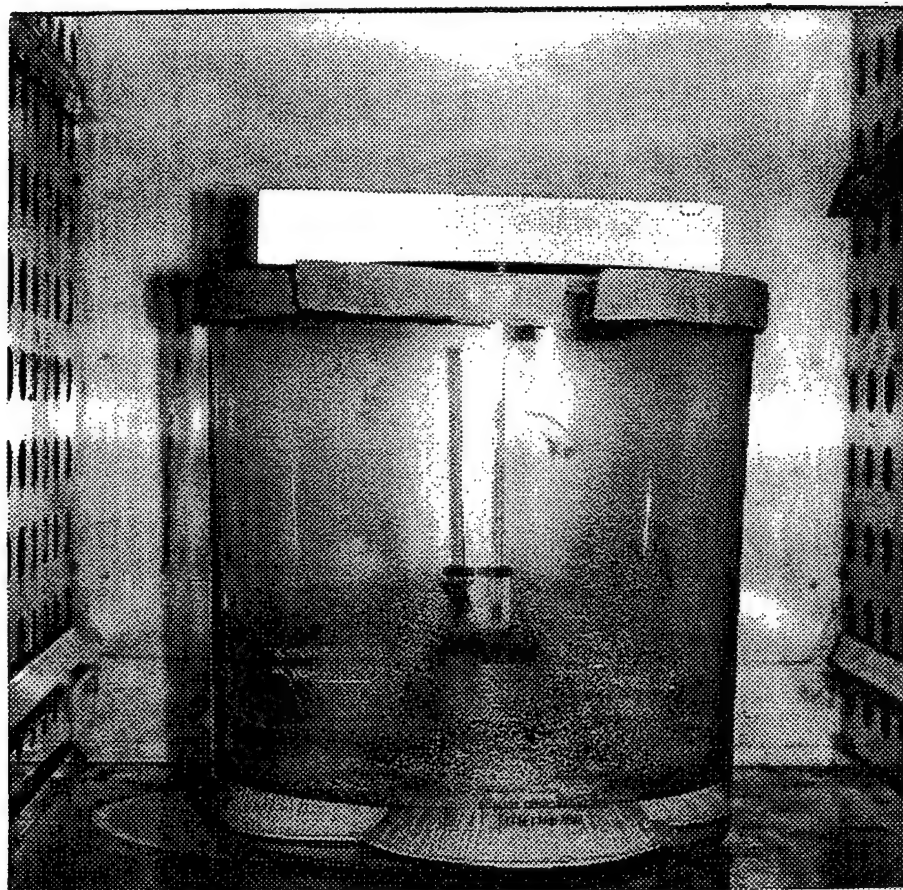
Figure 3. Apparatus Used for Hydrolysis Testing.

TABLE 2. HYDROLYSIS SUMMARY

Sample No.	Sample Name	1200 Hour Hydrolysis Pass/Fail	Observations
	MOLDED MATERIALS		
1	Nyrim 2300	P	Passed 1157 hrs.
2	CE868	P	Passed 1157 hrs.
3	CE870	P	Passed 1157 hrs.
4	PO655	F	Failed 305 hrs. Melted.
5	74-451-170	F	Failed 800 hrs.
6	Z.48.1	P	Passed 1157 hrs.
7	PCA 6-3 65A	P	Passed 1157 hrs.
8	PCA 6-3 80A	P	Passed 1157 hrs.
9	PCA 708S 60A	F	Failed 1157 hrs. Melted.
10	PCA 708S 75A	P	Passed 1157 hrs.
11	TSK L101	P	Passed 1157 hrs.
12	PP150-50A	F	Failed 305 hrs. Melted.
13	PP150-60A	F	Failed 1157 hrs. Sticky.
14	Vibrathane 6060	F	Failed 305 hrs. Melted.
15	Vibrathane B 836	F	Failed 1157 Hrs. Sticky.
17	535330A	P	Passed 1225 hrs.
19	535330C	P	Passed 1225 hrs.
20	DPTU-19140	P	Passed 1225 hrs.
21	NS-6572	F	Failed 1225 hrs. Swelling.
22	JC-010992	P	Passed 1225 hrs.
23	535336A	P	Passed 1225 hrs.
24	C-1002	P	Passed 1225 hrs.
25	HDS-06	P	Passed 1225 hrs.
26	MTA-2151664	F	Failed 253 hrs. Soft. Melted at 800 hrs.
27	535330B	P	Passed 1225 hrs.
28	PU-V-18	F	Failed 566 hrs. Melted. Cracked.
29	535382A	P	Passed 3960 hrs.
30	535382B	P	Passed 3960 hrs.
31	535382C	P	Passed 3960 hrs.
32	535382D	P	Passed 3960 hrs.
33	535383A	P	Passed 3960 hrs.
34	535383B	P	Passed 3960 hrs.
35	535383C	P	Failed 3241 hrs. Melted. Stuck to Pan.
36	6982A	F	Failed 566 hrs. Soft. Stuck to pan.
37	6982B	F	Failed 801 hrs. Breaking up. Weak.
38	6982C	F	Failed 1229 hrs. Breaking up. Tacky.
39	535385A	P	Passed 3862 hrs.
40	535385B	P	Passed 3862 hrs.
41	535387A	P	Passed 3862 hrs.
42	535387D	P	Failed 3145 hrs. Melted.
43	535387E	P	Failed 3145 hrs. Melted.
44	6978	P	Passed 3862 hrs.
45	NPE 2916	P	Passed 3862 hrs.

13

TABLE 2. HYDROLYSIS SUMMARY

| Sample No.	Sample Name	1200 Hour Hydrolysis Pass/Fail	Observations
	TAPES		
T1	8663	F	Failed 566 hrs. Tacky. Cracked at 800 hrs.
T2	NPE 2803	F	Failed 566 hrs. Tacky. Cracked at 800 hrs.
T3	NPE 2846	P	Passed 1225 hrs.
T4	Stoneguard 2000	F	Failed 566 hrs. Cracked.
T5	281	F	Failed 566 hrs. Cracked.
T6	Neoprene Stock	F	Failed 566 hrs. Excessive Swelling.
	COATINGS		
C1	M331/M201	P	Passed 1225 hrs.
C2	M112/M201	P	Passed 1225 hrs.
C3	M1433/M201	P	Passed 1225 hrs.
C4	MI-15 TopCoat	P	Passed 1225 hrs.
C5	R-2550	P	Passed 1225 hrs.
C6	AGCoat 1R/3R	P	Passed 3960 hrs.
C7	Tnemec 143	P	Failed 3241 hrs. Blistered.
C8	Caapcoat B-274/AS-P108	F	Failed 566 hrs. Soft.
C9	Elastuff 504	P	Passed 3960 hrs.
C10	8B6	F	Failed 1229 hrs. Cracks easily.
	2-PART SYSTEMS		
B1	TSK L100	P	Passed 3960 hrs.
B2	Elastuff 120 Mastic	P	Passed 3960 hrs.
B3	NF 1500 Special	F	Failed 400 hrs. Tacky.

14

RAIN EROSION

Seventy-four materials or material configurations were tested for rain erosion resistance using the University of Dayton Research Institute (UDRI) whirling arm rain erosion test facility at Wright Patterson Air Force Base, Ohio[5]. The materials were applied to leading edge airfoil substrates made of fiberglass/epoxy or aluminum. Dimensions of each are shown in Figure 4. Molded materials were bonded to fiberglass substrates. Coatings, tapes and two-part systems were applied primarily to aluminum substrates. Figure 5 shows a test specimen attached to the outboard leading edge of a test blade of the UDRI rain erosion rig. The tangential midspan velocity of the specimens was 733 fps (500 mph). Rain drop size was 2 mm and a rainfall rate of 1 inch per hour was used. Failure was determined as the time when the erosion protection system wore through to the substrate. Rain erosion test results are shown in Table 3 and are ranked according to rain erosion resistance in Table 4. Some of the molded samples, Nos. 6, 19 and 20, developed a bondline failure prior to eroding to the substrate and are identified by an appropriate note. Although the erosion time has been listed for those materials, they are not considered usable for erosion systems due to the potential dangers involved when material becomes unbonded from a rotor blade.

All the molded specimens were bonded with a thin fiberglass fabric in the bondline except for samples 5A, 6A, 20A, 22A and 23A. Style 120 glass fabric, used in the bondline of the K747 erosion guard, greatly enhances the erosion guard removal operation. The presence of fabric delayed the onset of immediate bondline failure of material No. 6 in rain testing; however, it did not improve the immediate bondline failures of material No. 20. The reasons for the difference are unknown.

Sample 45, NPE 2916, exhibited by far the best rain erosion resistance of all samples tested. The test was halted due to a premature failure on one end of one of the two specimens. The failure was attributed to excessive pressure caused by the clamp which holds the specimen to the test rotor. The same type of premature failure was beginning to occur on the other specimen. The remaining surface of test material between the clamps was almost as unblemished as when the test was started. There were no pits, gouges or torn material to indicate the early stages of erosion failure.

The tape sample NPE 2846 of sample T7, bonded to a glass-epoxy airfoil substrate, revealed substrate damage starting 21 minutes into the test. For this reason, it was deemed not suitable for protection of composite substrates despite the fact that the material survived 240 minutes without failing. The same material on an aluminum substrate, sample T3, failed after 50 minutes. 3M Co. improved the material by adding UV and antioxidation stabilizers to the formulation. This sample, T3U on an aluminum substrate, survived 240 minutes without failure. The cause for the difference in rain erosion resistance could not be determined with certainty. The most reasonable explanation presented by the material supplier was that later samples containing the UV/antioxidant additives exhibited better caliper (consistency of thickness) than the earlier samples due to an improved fabrication process. Thickness variations may have contributed to localized weak areas within the earlier tape samples.
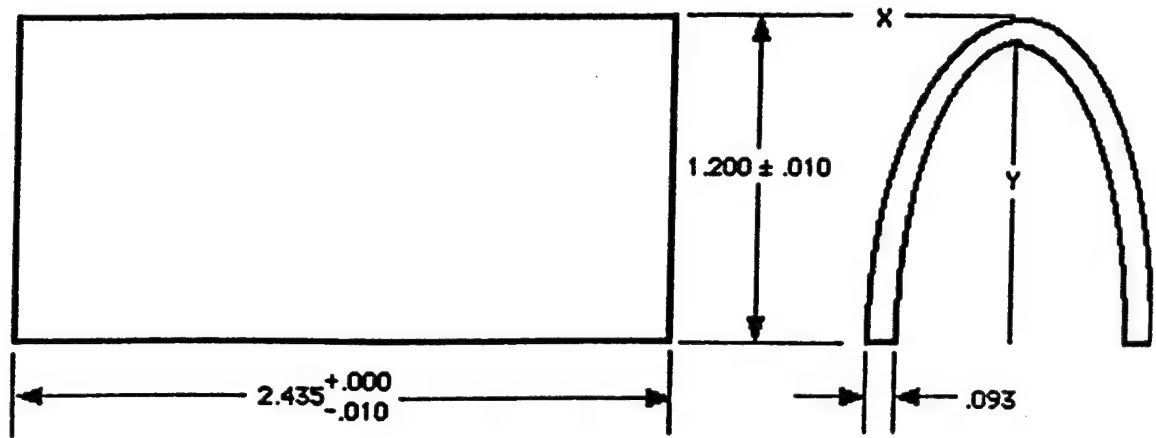
a. Glass-Epoxy
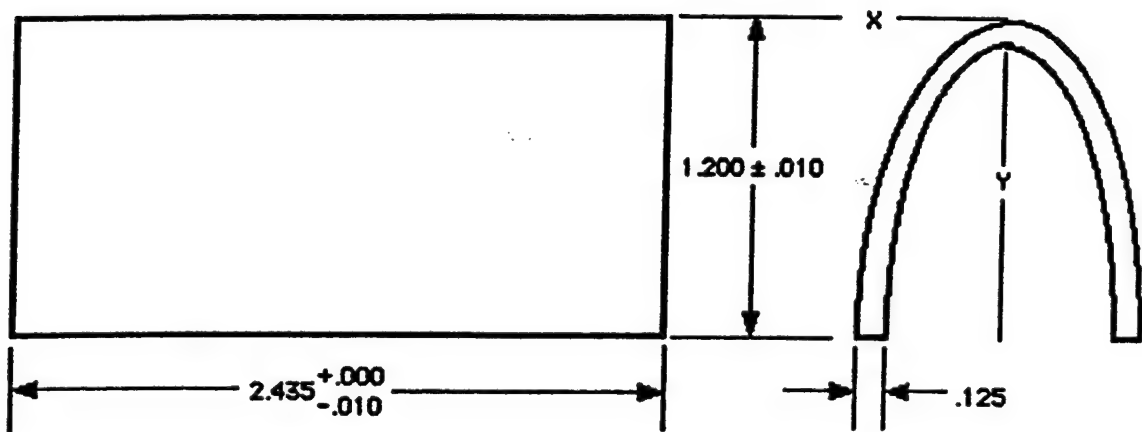
b. Aluminum
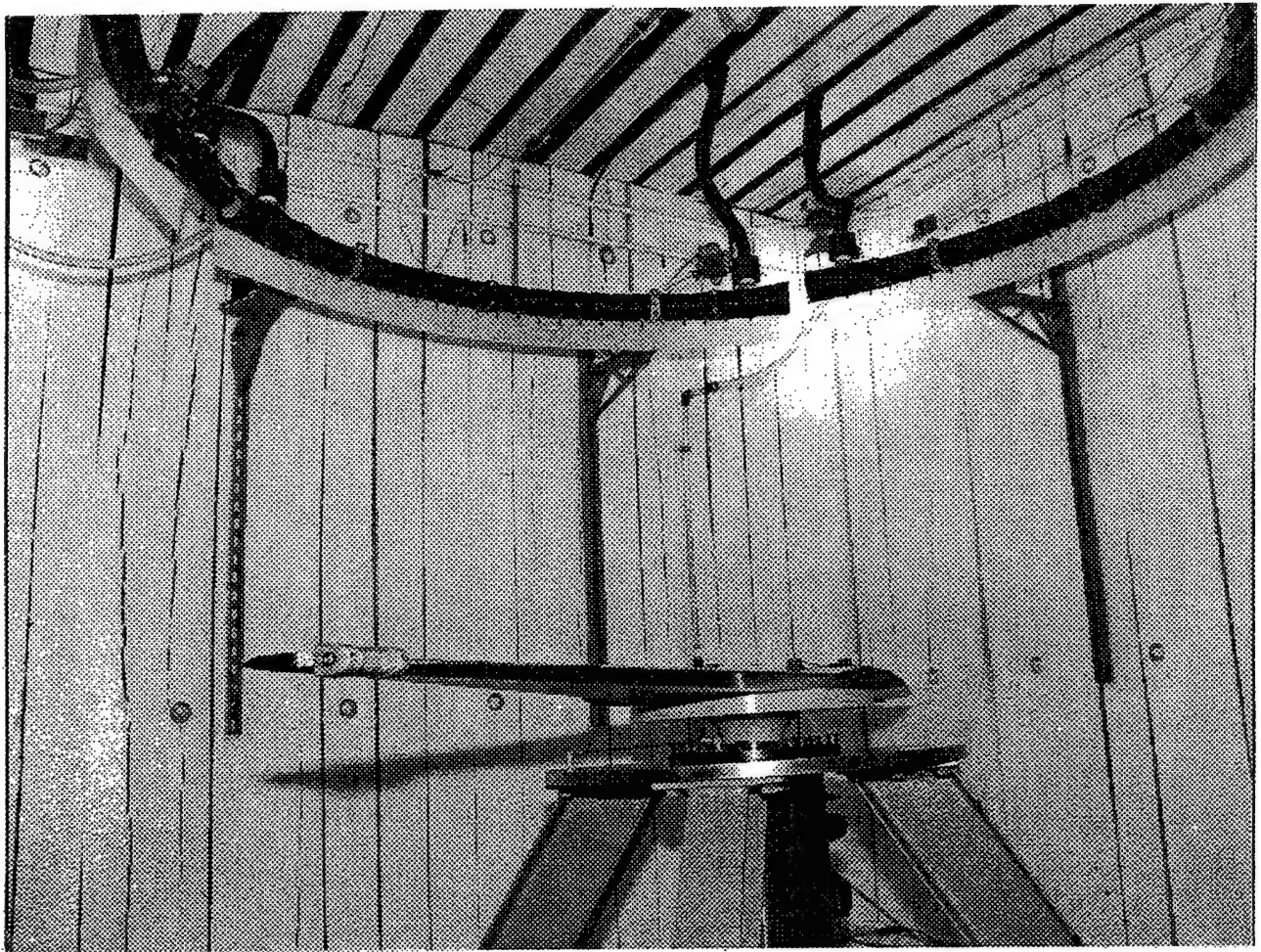
Figure 4. Leading Edge Airfoil Substrates.

16

Figure 5. Specimen Attached to Rotor Blade of UDRI Rain Erosion Test Rig.

17

TABLE 3. RAIN EROSION TEST RESULTS

Sample No.	Sample Name	Thickness (Inch)	Adhesive Notes	Substrate Notes	Time (Min)	General Notes
	MOLDED MATERIALS					
1	Nyrim 2300	0.071	1	1	80	
2	CE868	0.076	1	1	81	
3	CE870	0.070	1	1	85	
4	PO655	0.076	1	1	240	
5	74-451-170 (5 layers)	0.071	1	1	105	1,2
5R	74-451-170 (Monolayer)	0.077	1	1	117	
6	Z.48.1	0.082	1	1	150	3
7	PCA 6-3 65A	0.071	1	1	97	
8	PCA 6-3 80A	0.073	1	1	90	
9	PCA 708S 60A	0.072	1	1	97	
10	PCA 708S 75A	0.078	1	1	70	
11	TSK L101	0.071	1	1	35	
12	PP150-50A	0.070	1	1		See T10
13	PP150-60A	0.070	1	1	123	
14	Vibrathane 6060	0.072	1	1		See T8
15	Vibrathane B 836	0.069	1	1	106	
17	535330A	0.077	1	1	220	
19	535330C	0.074	1	1	90	3
20	DPTU-19140	0.075	1	1	240	3
20A	DPTU-19140	0.076	1	1	5	1,3
21	NS-6572	0.080	2	1	218	
22A	JC-010992	0.077	1	1	70	
23A	535336A	0.063	1	1	130	
24	C-1002	0.077	2	1	42	
25	HDS-06	0.059	2	1	21	
29	535382A	0.068	1	1	58	
30	535382B	0.067	1	1	73	
31	535382C	0.066	1	1	220	
32	535382D	0.067	1	1	40	
33	535383A	0.071	1	1	62	
34	535383B	0.060	1	1	68	
35	535383C	0.065	1	1	110	
36	6982A	0.072	1	1	100	1
37	6982B	0.073	1	1	60	1
39	535385A	0.078	1	1	155	
40	535385B	0.068	1	1	90	
41	535387A	0.075	1	1	80	
42	535387D	0.062	1	1	117	
43	535387E	0.062	1	1	60	
44	6978	0.063	1	1	280	
45	NPE 2916	0.060	9	1	1060	1

Note: For Moldings, Suffix "A" = No Glass Fabric In Bondline.
Suffix "R" = Repeat Using Monolayer Sample.

TABLE 3. RAIN EROSION TEST RESULTS

Sample No.	Sample Name	Thickness (Inch)	Adhesive Notes	Substrate Notes	Time (Min)	General Notes
	TAPES					
T1	8663	0.016	10	2	122	
T3	NPE 2846	0.012	7	2	50	
T3U	NPE 2846U	0.012	7	2	240	1
T4	Stoneguard 2000	0.0075	10	2	16	
T5	281	0.0055	10	2	29	
T6	Neoprene Stock	0.020	8	2	32	
T7	NPE 2846	0.012	7	1	240	1,3
T8	NPE 2846 Over Sample #14	.012/.072	7/1	1	90	4
T9	NPE 2873 (Thinner NPE 2846)	0.006	7/3	2	40	
T10	NPE 2873 Over Sample #12	.006/.070	7/1	1	31	5
T11	NPE 2846 (2 Layers)	0.024	7	1	77	6
T12	NPE 2846 (3 Layers)	0.036	7	1	7	6
	COATINGS					
C1	M331/M201	0.012	3	2	19	
C2	M112/M201	0.012	3	2	26	
C3	M1433/M201	0.012	3	2	20	
C4	MI-15 TopCoat	0.012	4	2	0.5	
C5	R-2550	0.012	4	2	0.5	
C6	AGCoat 1R3R	0.012	5	2	85	
C6A	AGCoat 1R3R	0.012	11	2	7	7,8
C6A+	AS-P108/AGCoat 1R3R	.002/.012	11	2	54	7
C7	Tnemec 143-5001/143-5002	.014/.014	6	2	24	9
C7A	Tnemec 143-5002	0.010	6/11	2	46	9
C8	AS-P108/Caapcoat B-274	.002/.014	3	2	29	
C8A	AS-P108/Caapcoat B-274	.002/.014	11	2	75	
C9	Elastuff 504	0.022	3	2	34	9
C9A	Elastuff 504	0.022	11	2	102	
C9A+	AS-P108/Elastuff 504	.002/.022	11	2	185	
C10	8B6	0.012	3	2	26	
C10A	8B6	0.012	11	2	27	

Note: For Coatings, Suffix "A" = Mil-P-23377 TyII Epoxy Primer
Suffix "+" = AS-P108 Over Non-Caapcoat Coating

Sample No.	Sample Name	Thickness (Inch)	Adhesive Notes	Substrate Notes	Time (Min)	General Notes
	2-PART SYSTEMS					
B1	TSK L100	0.023	3	2	16	9
B2	Elastuff 120 Mastic	0.017	3	2	7	9
	OTHER					
FG	Unprotected Glass-Epoxy	0.093	-	1	29	

TABLE 3. RAIN EROSION TEST RESULTS

Page 3 of 3

Adhesive Notes
1. Kaman KPS 146 Epoxy Adhesive
2. Bostik 7132 Urethane (22:1) Adh.
3. Lord 9924V Wash Primer
4. Dow Corning 1200 Silicone Primer
5. AGC AGCoat 7A/B Primer
6. Tnemec 66-1211 Epoxy Primer
7. 3M High Strength PS Acrylic/Promoter 86
8. 3M Scotch-Grip 1300-L Rubber Adhesive
9. 3M EC-2216 Clear Epoxy Adhesive
10. Standard Strength PS Acrylic/Promoter 86
11. Mil-P-23377 TyII Epoxy Primer/Alodine

Substrate Notes
1. 0.093 Glass-Epoxy Airfoil
2. 0.125 Aluminum Airfoil

General Notes
1. Test halted. Premature failure at clamp location.
2. Material was calendered from 5 different layers. Upper 3/5 peeled off in large pieces. Unsafe for rotor blade use. See sample 5R for test of monolayer of same material.
3. Bondline or substrate failure occurred prior to erosion failure.
4. Both tape and molded urethane split at same location.
5. Premature failure. Specimen too thick. Damage probably caused during mounting of specimen to test rig.
6. Tape adhesion failure, 1st layer to substrate. No damage to glass-epoxy substrate.
7. Premature failure. Distinctive intercoat adhesion failure of erosion coating to primer. Cause traced to excessive use of tack rag during sample coating operation.
8. Premature failure. Cause traced to cotton fibers imbedded in surface from contact with cloth before full cure of AGCoat 1R3R.
9. Porosity in erosion coating.

TABLE 4. RAIN EROSION TEST RESULTS (RANKED)

Sample No.	Sample Name	Thickness (Inch)	Adhesive Notes	Substrate Notes	Time (Min)	General Notes
	MOLDED MATERIALS					
45	NPE 2916	0.060	9	1	1060	1
44	6978	0.063	1	1	280	
4	PO655	0.076	1	1	240	
20	DPTU-19140	0.075	1	1	240	3
17	535330A	0.077	1	1	220	
31	535382C	0.066	1	1	220	
21	NS-6572	0.080	2	1	218	
39	535385A	0.078	1	1	155	
6	Z.48.1	0.082	1	1	150	3
23A	535336A	0.063	1	1	130	
13	PP150-60A	0.070	1	1	123	
5R	74-451-170 (Monolayer)	0.077	1	1	117	
42	535387D	0.062	1	1	117	
35	535383C	0.065	1	1	110	
15	Vibrathane B 836	0.069	1	1	106	
5	74-451-170 (5 layers)	0.071	1	1	105	1,2
36	6982A	0.072	1	1	100	1
7	PCA 6-3 65A	0.071	1	1	97	
9	PCA 708S 60A	0.072	1	1	97	
8	PCA 6-3 80A	0.073	1	1	90	
19	535330C	0.074	1	1	90	3
40	535385B	0.068	1	1	90	
3	CE870	0.070	1	1	85	
2	CE868	0.076	1	1	81	
1	Nyrim 2300	0.071	1	1	80	
41	535387A	0.075	1	1	80	
30	535382B	0.067	1	1	73	
10	PCA 708S 75A	0.078	1	1	70	
22A	JC-010992	0.077	1	1	70	
34	535383B	0.060	1	1	68	
33	535383A	0.071	1	1	62	
37	6982B	0.073	1	1	60	1
43	535387E	0.062	1	1	60	
29	535382A	0.068	1	1	58	
24	C-1002	0.077	2	1	42	
32	535382D	0.067	1	1	40	
11	TSK L101	0.071	1	1	35	
25	HDS-06	0.059	2	1	21	
20A	DPTU-19140	0.076	1	1	5	1,3
12	PP150-50A	0.070	1	1	See T10	
14	Vibrathane 6060	0.072	1	1	See T8	

Note: For Moldings, Suffix "A" = No Glass Fabric In Bondline.
Suffix "R" = Repeat Using Monolayer Sample.

TABLE 4. RAIN EROSION TEST RESULTS (RANKED)

Sample No.	Sample Name	Thickness (Inch)	Adhesive Notes	Substrate Notes	Time (Min)	General Notes
	TAPES					
T3U	NPE 2846U	0.012	7	2	240	1
T7	NPE 2846	0.012	10	1	240	1,3
T1	8663	0.016	7	2	122	
T8	NPE 2846 Over Sample #14	.012/.072	7/1	1	90	4
T11	NPE 2846 (2 Layers)	0.024	7	1	77	6
T3	NPE 2846	0.012	7	2	50	
T9	NPE 2873 (Thinner NPE 2846)	0.006	7/3	2	40	
T6	Neoprene Stock	0.020	8	2	32	
T10	NPE 2873 Over Sample #12	.006/.070	7/1	1	31	5
T5	281	0.0055	10	2	29	
T4	Stoneguard 2000	0.0075	10	2	16	
T12	NPE 2846 (3 Layers)	0.036	7	1	7	6
	COATINGS					
C9A+	AS-P108/Elastuff 504	.002/.022	11	2	185	
C9A	Elastuff 504	0.022	11	2	102	
C6	AGCoat 1R3R	0.012	5	2	85	
C8A	AS-P108/Caapcoat B-274	.002/.014	11	2	75	
C6A+	AS-P108/AGCoat 1R3R	.002/.012	11	2	54	7
C7A	Tnemec 143-5002	0.010	6/11	2	46	9
C9	Elastuff 504	0.022	3	2	34	9
C8	AS-P108/Caapcoat B-274	.002/.014	3	2	29	
C10A	8B6	0.012	11	2	27	
C10	8B6	0.012	3	2	26	
C2	M112/M201	0.012	3	2	26	
C7	Tnemec 143-5001/143-5002	.014/.014	6	2	24	9
C3	M1433/M201	0.012	3	2	20	
C1	M331/M201	0.012	3	2	19	
C6A	AGCoat 1R3R	0.012	11	2	7	7,8
C4	MI-15 TopCoat	0.012	4	2	0.5	
C5	R-2550	0.012	4	2	0.5	

Note: For Coatings, Suffix "A" = Mil-P-23377 TyII Epoxy Primer
                     Suffix "+" = AS-P104 Over Non-Caapcoat Coating

Sample No.	Sample Name	Thickness (Inch)	Adhesive Notes	Substrate Notes	Time (Min)	General Notes
	2-PART SYSTEMS					
B1	TSK L100	0.023	3	2	16	9
B2	Elastuff 120 Mastic	0.017	3	2	7	9
	OTHER					
FG	Unprotected Glass-Epoxy	0.093	-	1	29	

TABLE 4. RAIN EROSION TEST RESULTS (RANKED)

Page 3 of 3

Adhesive Notes
1. Kaman KPS 146 Epoxy Adhesive
2. Bostik 7132 Urethane (22:1) Adh.
3. Lord 9924V Wash Primer
4. Dow Corning 1200 Silicone Primer
5. AGC AGCoat 7A/B Primer
6. Tnemec 66-1211 Epoxy Primer
7. 3M High Strength PS Acrylic/Promoter 86
8. 3M Scotch-Grip 1300-L Rubber Adhesive
9. 3M EC-2216 Clear Epoxy Adhesive
10. Standard Strength PS Acrylic/Promoter 86
11. Mil-P-23377 TyII Epoxy Primer/Alodine

Substrate Notes
1. 0.093 Glass-Epoxy Airfoil
2. 0.125 Aluminum Airfoil

General Notes
1. Test halted. Premature failure at clamp location.
2. Material was calendered from 5 different layers. Upper 3/5
   peeled off in large pieces. Unsafe for rotor blade use.
   See sample 5R for test of monolayer of same material.
3. Bondline or substrate failure occurred prior to erosion failure.
4. Both tape and molded urethane split at same location.
5. Premature failure. Specimen too thick. Damage probably caused
   during mounting of specimen to test rig.
6. Tape adhesion failure, 1st layer to substrate. No damage to
   glass-epoxy substrate.
7. Premature failure. Distinctive intercoat adhesion failure of
   erosion coating to primer. Cause traced to excessive use of
   tack rag during sample coating operation.
8. Premature failure. Cause traced to cotton fibers imbedded in
   surface from contact with cloth before full cure of AGCoat 1R3R.
9. Porosity in erosion coating.

An attempt to protect the glass-epoxy substrate from damage by using multilayers of the NP 2846 tape are shown in samples T11 and T12. The substrates were protected but the tapes failed at 77 and 7 minutes, respectively, due to failure of the high strength, pressure sensitive acrylic adhesive at the interface between the first layer of tape and the substrate. Apparently the shear forces caused by the additional mass of extra layers of tape were sufficient to overcome the shear strength of the adhesive in this high centrifugal force (CF) field. These results preclude use of multilayers of tape with pressure sensitive adhesive on outboard locations of tail rotor blades where the CF loading is extreme.

SAND EROSION

Whirling arm sand erosion testing was based on the requirements of the Design Criteria Document (DCD) and the Qualification Test Procedures (QTP) previously developed by Haynie[2]. Testing was performed in the Kaman-funded Whirling Arm Sand Erosion and Impact Test Facility built especially for this program. As a result of earlier hydrolysis and rain erosion testing, the number of samples were reduced considerably and only 18 materials were subjected to sand erosion testing. Samples 4, 11, T1 and B1, although undesirable from the hydrolysis or rain erosion test results, are included in subsequent testing as controls because they are currently used on Army rotor blades.

The 8.04 foot diameter test rotor is housed in a circular enclosure, 21 feet in diameter and 15 feet high. See Figure 6. This conforms to the rotor-to-enclosure size ratio recommended in the QTP. The facility employs a 200 hp, 1800 rpm motor which is connected to a hydraulic speed reducer. The output is fed into two intermediate gearboxes, through appropriate shafting and into a tail rotor gearbox to satisfy the required maximum output shaft speed of up to 1900 rpm. Although the test coupon speed of 733 fps requires only 1750 rpm, the as-designed capability provides for sufficient margin to ensure meeting the rpm requirements independent of power requirements. The center of the test enclosure contains a vertical steel mast and pedestal with a horizontally mounted rotor assembly. The rotor gearbox contains a pitch change mechanism to allow presetting and/or varying of the specimen angle of attack during the dynamic phases of testing. A semi-torus shaped floor was installed to encourage circulation of sand particles during testing.

Figure 7 is a schematic of the test coupon showing the candidate material, substrate and overall dimensions. The substrates are the same as those used for the UDRI rain erosion testing. Figures 8 and 9 (top) show the arrangement of the test specimen on the test blade for sand erosion testing. The sand injection device for introducing sand into the chamber is primarily a funnel into which the sand is poured (Figure 10). An air injector insures that the sand enters the chamber. This method, when used with the rotor operating at predetermined test conditions, causes the sand to become immediately airborne and disperse itself throughout the chamber.

Table 5 lists the test conditions used during sand erosion testing. All material samples were tested at these conditions. Rig vibration prevented rotation at sample centerline speeds of 733 fps, and sample speeds were adjusted to 711 fps (485 mph). Blade tip pitch angle, specimen angle of attack and downward velocity, V_V, at the specimen were determined during rig calibration testing.
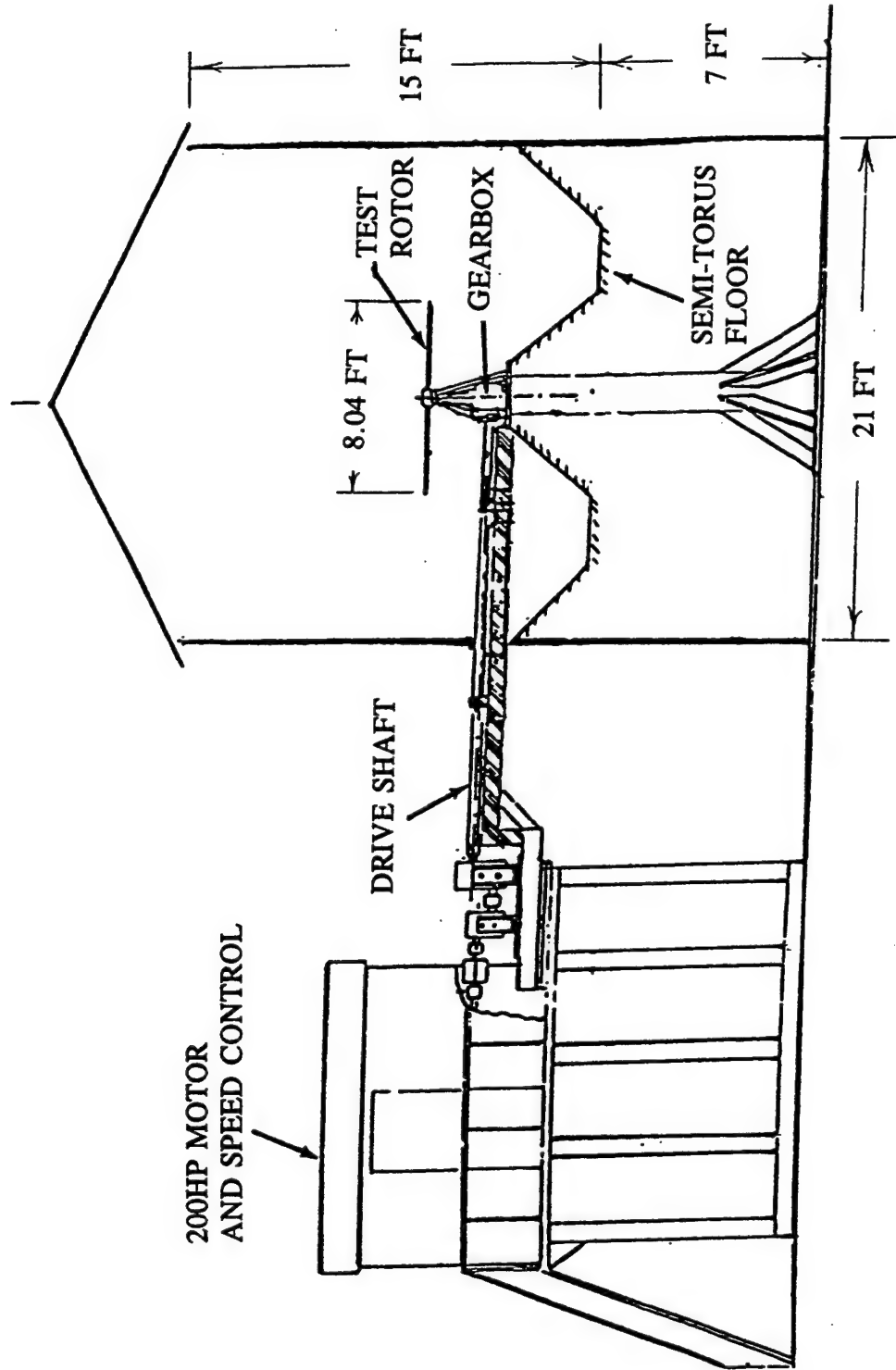
24

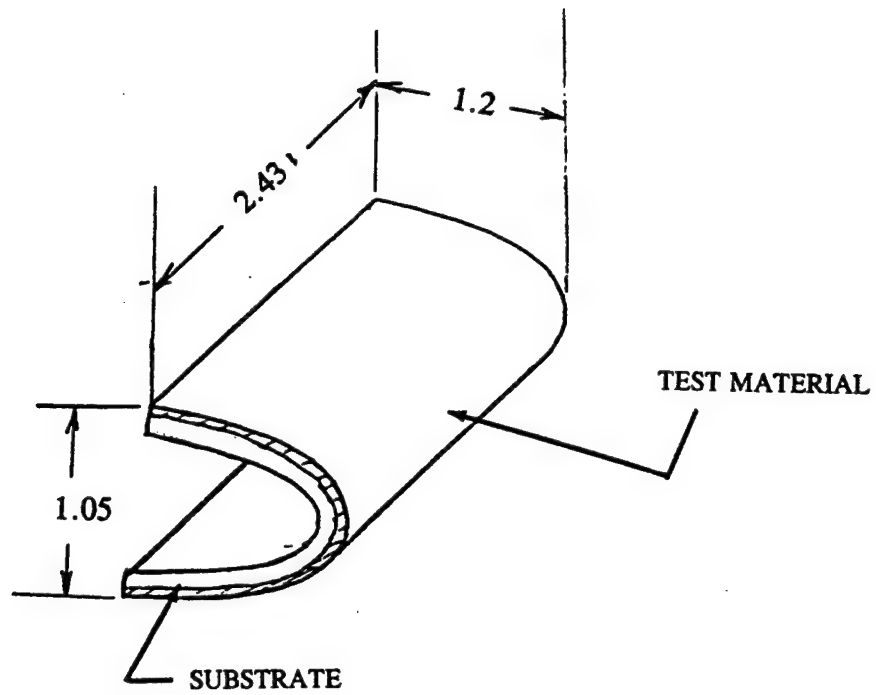**Figure 6. Kaman Whirling Arm Sand Erosion and Impact Test Facility.**

25

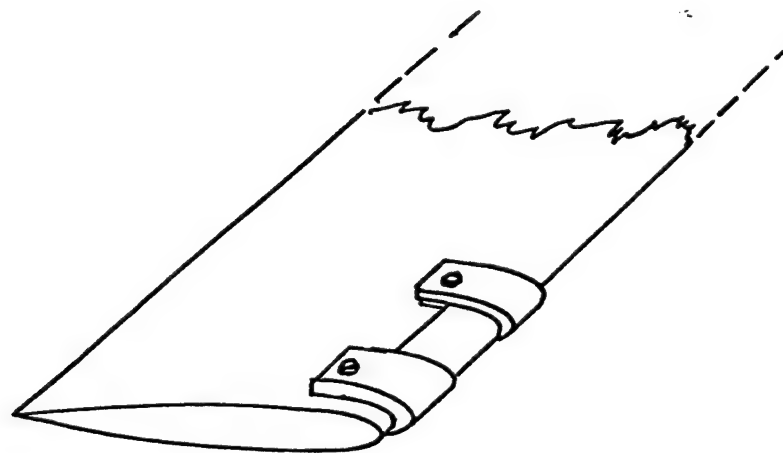**Figure 7. Sand Erosion and Impact Test Specimen.**

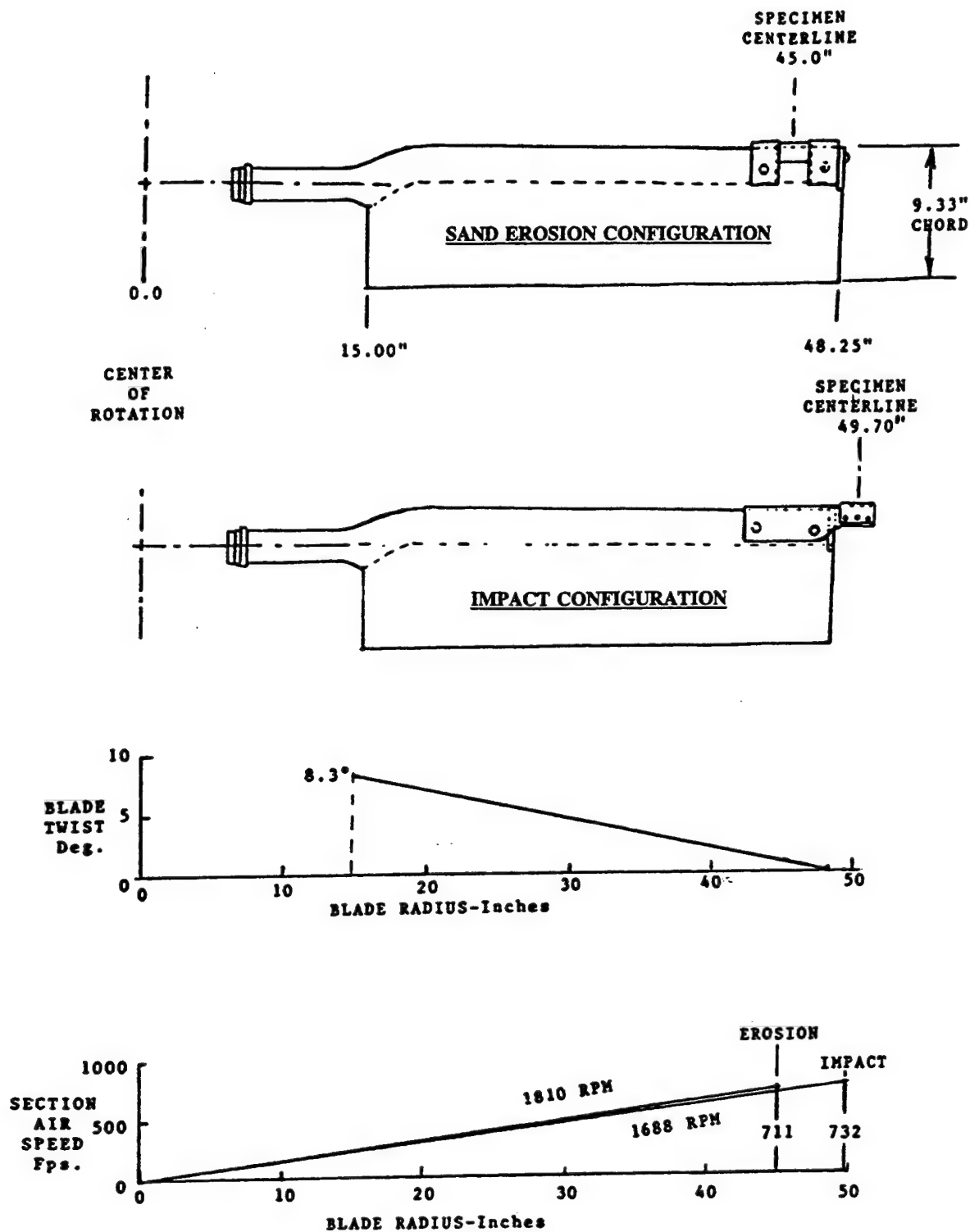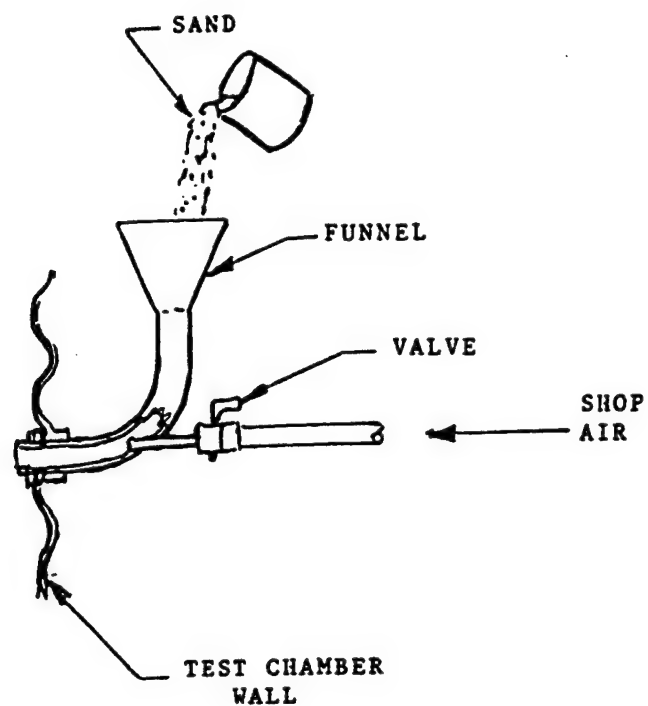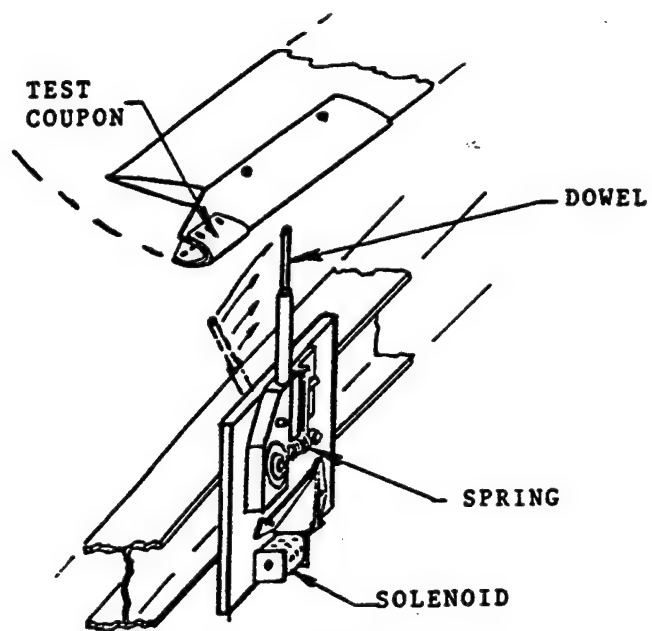**Figure 8. Attachment Arrangement for Sand Erosion Tests.**

Figure 9. Erosion and Impact Blade Configurations.

27

a. SAND INJECTION DEVICE

b. DOWEL INJECTION DEVICE

Figure 10. Sand and Dowel Insertion.

28

TABLE 5. TEST CONDITIONS FOR SAND EROSION TESTS

Test Rotor Rotational Speed	1810 rpm
Drive Shaft Rotational Speed	3300 rpm
Blade Tip Speed	762 fps
Specimen Centerline Tangential Velocity	711 fps
Blade Tip Pitch Angle	7.5 deg
Specimen Angle of Attack (Relative to Air)	1.4 deg
Downwash Velocity, V_V, Under Specimen	85.62 fps

Sand to air density was determined through the use of a sand collector device shown in Figure 11. This device was placed under the rotor at the specimen centerline radius. The entrance at the top of the collector was placed 5½ inches below the rotor plane where some of the air coming through the annulus traversed by the test specimen is captured by the collector. The air flows down the vertical pipe into a settling chamber with a screen to prevent the sand from escaping. The ratio of sand to air was then determined by dividing the weight of sand collected over the test period by the calculated volume of airflow entering the sand collector.

From preliminary testing it was determined that ¾ lb of sand inserted at the beginning of erosion tests of 10-minute duration was sufficient to determine measurable quantities of wear on the specimens and give reasonable results. Technical information for the sand used is described on the product data sheet in Appendix A.

Table 6 shows the results of the sand erosion tests. Sample weight loss and the weight of sand collected over the 10-minute test period were determined. Sample No. 4 was run several times to insure consistency during the testing. The sand to air density was calculated as described above and was found to be reasonably consistent. There is, however, some variation and this was taken into account when making comparisons. A normalized weight loss column is included where the weight loss was divided by the sand to air density. To further simplify the results, the samples were compared using the material currently in use on the K747 blade as the baseline material. Therefore, the normalized weight loss for Samples No. 4A and 4B was divided by the normalized weight loss obtained for each material. Using that basis, the larger the number, the better the material can resist sand erosion. Table 7 lists the materials ranked in order of their comparison ratio number.
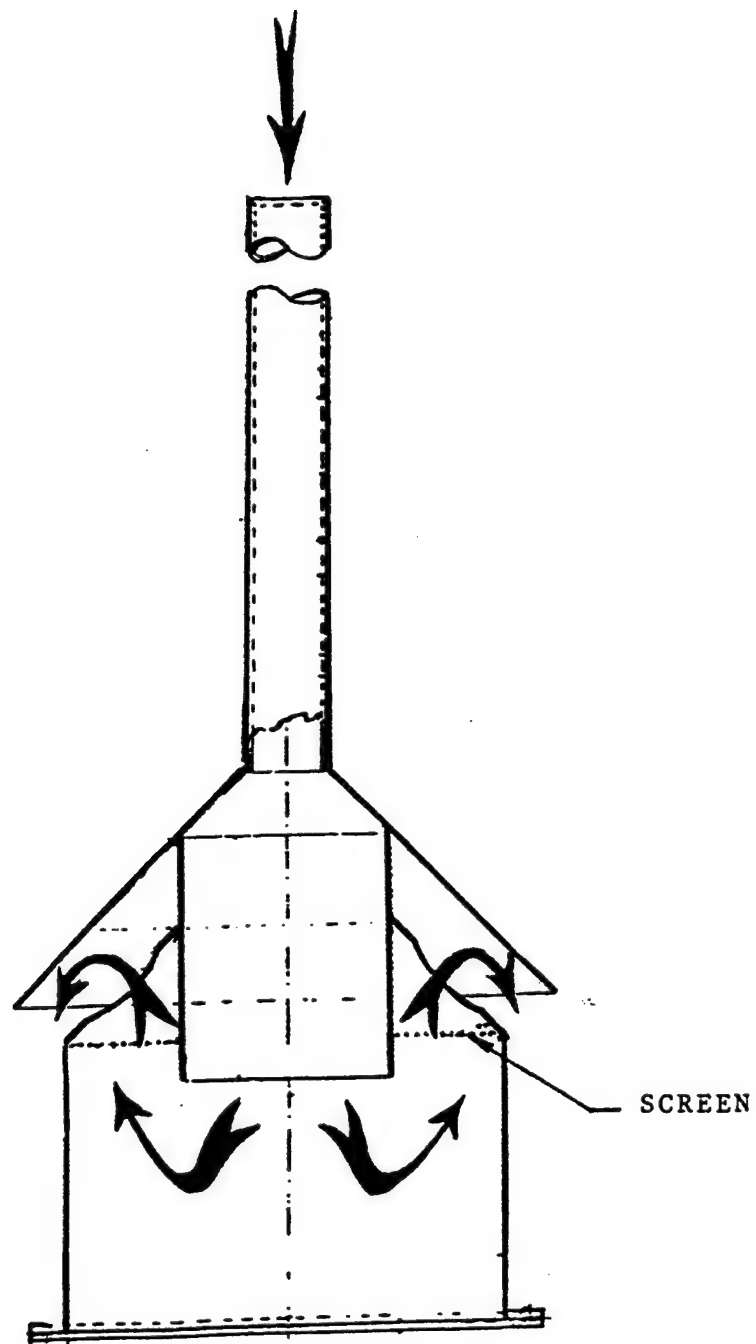
Figure 11. Sand Collector.

SCREEN

TABLE 6. SAND EROSION TEST RESULTS

Sample No.	Sample Name	Thickness (Inch)	Adhesive Notes	Substrate Notes	Collector Sand (gm)	Sand/Air Density (gm/cu ft)	Test Blade	Sample Wt Loss (gm)	Normalized Wt Loss (gm)	Comparison Ratio
	MOLDED MATERIALS									
4	PO655	0.076	1	1	2.918	0.01800	A	0.025	1.39	1.0
							B	0.024	1.33	
4R	PO655 (Repeat)	0.076	1	1	2.878	0.01776	A	0.026	1.46	1.0
							B	0.025	1.41	
11	TSK L101	0.071	1	1	2.759	0.01702	A	0.049	2.88	0.5
							B	0.046	2.70	
17	535330A	0.077	1	1	3.201	0.01975	A	0.006	0.30	6.1
							B	0.003	0.15	
21	NS-6572	0.080	1	1	2.665	0.01644	A	0.021	1.28	1.1
							B	0.020	1.22	
23	535336A	0.063	1	1	2.571	0.01586	A	0.020	1.26	1.1
							B	0.020	1.26	
31	535382C	0.066	1	1	2.645	0.01632	A	0.015	0.92	2.0
							B	0.008	0.49	
39	535385A	0.078	1	1	2.679	0.01653	A	0.042	2.54	0.6
							B	0.040	2.42	
42	535387D	0.062	1	1	2.702	0.01667	A	0.018	1.08	1.3
							B	0.017	1.02	
44	6978	0.063	1	1	2.801	0.01728	A	0.073	4.22	0.3
							B	0.066	3.82	
45	NPE 2916	0.060	2	1	2.700	0.01666	A	0.009	0.54	2.1
							B	0.013	0.78	
	TAPES									
T1	8663	0.016	3	2	2.696	0.01663	A	0.002	0.12	7.8
							B	0.004	0.24	
T3	NPE 2846	0.012	3	2	2.775	0.01712	A	0.009	0.53	2.7
							B	*	*	

31

TABLE 6. SAND EROSION TEST RESULTS

Sample No.	Sample Name	Thickness (Inch)	Adhesive Notes	Substrate Notes	Collector Sand (gm)	Sand/Air Density (gm/cu ft)	Test Blade	Sample Wt Loss (gm)	Normalized Wt Loss	Comparison Ratio
T3U	NPE 2846U	0.012	3	2	2.707	0.01670	A	0.001	0.06	5.8
							B	0.007	0.42	
	COATINGS									
C6+	AS-P108/AGCoat 1R3R	0.012	4	2	2.969	0.01832	A	0.025	1.36	1.0
							B	0.024	1.31	
C8A	AS-P108/Caapcoat B-274	.002/.014	5	2	2.808	0.01732	A	0.037	2.14	0.7
							B	0.036	2.08	
C9A	Elastuff 504	0.022	5	2	2.836	0.01750	A	0.009	0.51	1.7
							B	0.019	1.09	
C9A+	AS-P108/Elastuff 504	.002/.022	5	2	3.052	0.01883	A	0.025	1.33	0.9
							B	0.033	1.75	
	2-PART SYSTEMS									
B1	TSK L100	0.023	6	2	2.669	0.01647	A	0.055	3.34	0.4
							B	0.058	3.52	

* Data Recording Error

Adhesive Notes

1. Kaman KPS 146 Epoxy Adhesive
2. 3M EC-2216 Clear Epoxy Adhesive
3. 3M High Strength PS Acrylic/Promoter 86
4. AGC AGCoat 7A/B Primer
5. Mil-P-23377 TyII Epoxy Primer/Alodine
6. Lord 9924V Wash Primer

Substrate Notes

1. 0.093 Glass-Epoxy Airfoil
2. 0.125 Aluminum Airfoil

32

TABLE 7. SAND EROSION TEST RESULTS (RANKED)

Sample No.	Sample Name	Thickness (Inch)	Adhesive Notes	Substrate Notes	Collector Sand (gm)	Sand/Air Density (gm/cu ft)	Test Blade	Sample Wt Loss (gm)	Normalized Wt Loss (gm)	Comparison Ratio
MOLDED MATERIALS										
17	535330A	0.077	1	1	3.201	0.01975	A	0.006	0.30	6.1
							B	0.003	0.15	
45	NPE 2916	0.060	2	1	2.700	0.01666	A	0.009	0.54	2.1
							B	0.013	0.78	
31	535382C	0.066	1	1	2.645	0.01632	A	0.015	0.92	2.0
							B	0.008	0.49	
42	535387D	0.062	1	1	2.702	0.01667	A	0.018	1.08	1.3
							B	0.017	1.02	
21	NS-6572	0.080	1	1	2.665	0.01644	A	0.021	1.28	1.1
							B	0.020	1.22	
23	535336A	0.063	1	1	2.571	0.01586	A	0.020	1.26	1.1
							B	0.020	1.26	
4	PO655	0.076	1	1	2.918	0.01800	A	0.025	1.39	1.0
							B	0.024	1.33	
4R	PO655 (Repeat)	0.076	1	1	2.878	0.01776	A	0.026	1.46	1.0
							B	0.025	1.41	
39	535385A	0.078	1	1	2.679	0.01653	A	0.042	2.54	0.6
							B	0.040	2.42	
11	TSK L101	0.071	1	1	2.759	0.01702	A	0.049	2.88	0.5
							B	0.046	2.70	
44	6978	0.063	1	1	2.801	0.01728	A	0.073	4.22	0.3
							B	0.066	3.82	
TAPES										
T1	8663	0.016	3	2	2.696	0.01663	A	0.002	0.12	7.8
							B	0.004	0.24	
T3U	NPE 2846U	0.012	3	2	2.707	0.01670	A	0.001	0.06	5.8
							B	0.007	0.42	

33

TABLE 7. SAND EROSION TEST RESULTS (RANKED)

Sample No.	Sample Name	Thickness (Inch)	Adhesive Notes	Substrate Notes	Collector Sand (gm)	Sand/Air Density (gm/cu ft)	Test Blade	Sample Wt Loss (gm)	Normalized Wt Loss	Comparison Ratio
T3	NPE 2846	0.012	3	2	2.775	0.01712	A	0.009	0.53	2.7
							B	*	*	
	COATINGS									
C9A	Elastuff 504	0.022	5	2	2.836	0.01750	A	0.009	0.51	1.7
							B	0.019	1.09	
C6+	AS-P108/AGCoat 1R3R	0.012	4	2	2.969	0.01832	A	0.025	1.36	1.0
							B	0.024	1.31	
C9A+	AS-P108/Elastuff 504	.002/.022	5	2	3.052	0.01883	A	0.025	1.33	0.9
							B	0.033	1.75	
C8A	AS-P108/Caapcoat B-274	.002/.014	5	2	2.808	0.01732	A	0.037	2.14	0.7
							B	0.036	2.08	
	2-PART SYSTEMS									
B1	TSK L100	0.023	6	2	2.669	0.01647	A	0.055	3.34	0.4
							B	0.058	3.52	

* Data Recording Error

Adhesive Notes

1. Kaman KPS 146 Epoxy Adhesive
2. 3M EC-2216 Clear Epoxy Adhesive
3. 3M High Strength PS Acrylic/Promoter 86
4. AGC AGCoat 7A/B Primer
5. Mil-P-23377 TyII Epoxy Primer/Alodine
6. Lord 9924V Wash Primer

Substrate Notes

1. 0.093 Glass-Epoxy Airfoil
2. 0.125 Aluminum Airfoil

34

IMPACT

The impact tests were conducted in the same whirling arm test facility described above for sand erosion testing. The clamps which hold the sand erosion specimens were removed from one of the blades and replaced with attachment hardware that extends beyond the tip end of the blade. The impact specimen was secured to the outboard end of this hardware. This configuration is shown in Figures 9 and 12.

Impact testing was conducted by injecting hardwood dowels of progressively increasing diameters of ½ in., ¾ in., and ⅞ in. into the path of the whirling test coupon. The Design Criteria Document would require a dowel of 1⅛ in. diameter to equal 12% of the blade's thrust-weighted chord length which was thought at the time to be too destructive to the test rotor. During sand erosion rig calibration, the blade structure was weakened when approximately 1/16 in. of the aluminum leading edge blade spar had been eroded away while the blades were run unprotected for a short time in a sand cloud.

The spring-loaded dowel injection device is shown in Figure 10. The dowel holder is cocked and held in place by a latching mechanism. When an electrical solenoid is activated from within the control room, the latching mechanism releases the cocked dowel holder and the dowel is pulled forward into the path of the test specimen.

The airfoil shaped leading edge substrates which hold the candidate materials are the same as those described above for the UDRI rain erosion tests and the Kaman sand erosion tests. Conditions for the impact tests are listed in Table 8. The specimen centerline tangential velocity was 733 fps (500 mph). A grease pencil was used to coat the leading edge surface of the material to aid in determining the exact location of the dowel strike. After each impact an assessment of the damage was determined before the next greater diameter dowel was used.

Impact damage was difficult to measure quantitatively. When damage occurs, quantities of material become unbonded from the substrate and are removed. Prior to that time some compression can be noted in the material for some of the specimens. Table 9 is a qualitative assessment of the damage done by the dowel after each impact. The type or location of the impact and a damage assessment are described. The Pass Test column is an indication of whether or not the material provides protection for the blade after impact. Table 10 is a summary of the damage and categorization of the data. Table 11 ranks the materials in the order of impact damage.

35
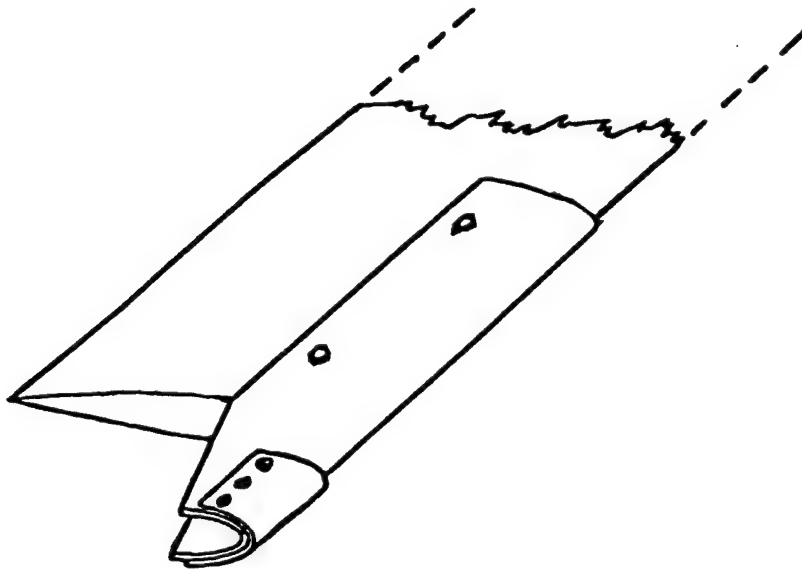
Figure 12. Attachment Arrangement for Impact Tests.

TABLE 8. TEST CONDITIONS FOR THE IMPACT TESTS

Test Rotor Rotational Speed	1688 rpm
Drive Shaft Rotational Speed	3079 rpm
Blade Tip Speed	711 fps
Specimen Centerline Tangential Velocity	733 fps
Specimen Impact Angle	0 deg

TABLE 9. IMPACT DAMAGE ASSESSMENT

Spec No.	Dowel Dia (in.)	Type or Location of Impact	Width of Pattern (in.)	Damage Assessment	Pass Test	Permanent Deformation (in.)
4A	1/2	Close to IB edge	5/16	Vertical splitting close to specimen edge, good resistance in pattern center and OB. Bad underside scuffing due to dowel stump. No scuffing.	Yes	1/64
	3/4	Close to tip	7/16	Edge fragmentation. Good resistance in pattern center. No scuffing.	Yes	1/64
	7/8	Inboard of Center	1/2	Square pattern 1/2 in. wide. Substantial scuffing in square with material loss.	Yes	1/64
4B	1/2	1/2 in. from tip	3/8	No significant damage. Light scuffing.	Yes	1/64
	3/4	1-5/16 in. from IB	1/4	No significant damage. Light scuffing.	Yes	1/64
	7/8	3/4 in. from tip	3/4	No significant damage. Scuffing.	Yes	1/64
11	1/2	1/4 in. from tip	1/2	Slight scuffing. Good resistance.	Yes	1/64
	3/4	7/16 in. from tip	3/4	Slight scuffing. Good resistance.	Yes	1/64
	7/8	At tip	3/8	Material removed from underside. Slight unbonding near specimen edge at stagnation point. Good resistance on IB portion of pattern. Slight Scuffing.	Yes	1/64
17	1/2	1/2 in. IB of center	3/8	Little scuffing. Vertical pattern.	Yes	0
	3/4	Center strike	3/4	Slight scuffing.	Yes	1/64
	7/8	Premature dowel break diagonal strike across IB edge	5/8	Substantial material loss and peeling, initial split in direction of diagonal, probably occurred initially 1/4 in. from IB edge of specimen.	No[1]	---

37

TABLE 9. IMPACT DAMAGE ASSESSMENT

Spec No.	Dowel Dia (in.)	Type or Location of Impact	Width of Pattern (in.)	Damage Assessment	Pass Test	Permanent Deformation (in.)
21	1/2	1/2 in. IB of center	3/8	Little scuffing. Vertical pattern.	Yes	0
	3/4	3/8 in. from tip	5/8	Slight scuffing. Good resistance.	Yes	1/64
	7/8	9/16 in. from IB	5/8	Circle of distressed material of 5/16 in. dia & 5/8 in. dia.	Yes	1/64
23	1/2	3/8 in. from tip	1/2	Very light scuffing.	Yes	0
	3/4	1/4 in. from tip	1/2	Some edge break-up due to OB location. Slight scuffing.	Yes	0
	7/8	OB of center	3/4	Good bond. Slight scuffing. Good resistance.	Yes	0
31	1/2	3/4 in. from tip	3/8	Light scuffing. No visible damage.	Yes	0
	3/4	1st strike at IB edge	3/8	Some unbonding at edge due to edge strike.	--	--
		2nd strike 5/16 in. from IB	5/8	No damage. Light scuffing.	Yes	0
	7/8	5/16 in. IB of center	3/4	Substantial unbonding. Square 1/2 in. pattern. Splitting & peeling at nose.	No	1/64
39	1/2	OB of center	7/16	Slight scuffing. Little damage.	Yes	1/64
	3/4	IB of center. Secondary strike near IB edge	3/4	Slight scuffing. Little damage.	Yes	1/64
	7/8	Impact 3/8 in. from tip	3/4	Substantial unbonding & material removal.	No	--

38

TABLE 9. IMPACT DAMAGE ASSESSMENT

Spec No.	Dowel Dia (in.)	Type or Location of Impact	Width of Pattern (in.)	Damage Assessment	Pass Test	Permanent Deformation (in.)
42	1/2	5/8 in. from tip	7/16	Square pattern. No visible scuffing. Good resistance.	Yes	0
	3/4	1st strike, 3/8 in. from tip	1/2	No visible scuffing. Good resistance.	Yes	0
		2nd strike, 3/4 in. from tip	1/2	No visible scuffing. Good resistance.	Yes	0
	7/8	1 in. from tip	5/8	Substantial unbonding, cracking and loss of material.	No	--
44	1/2	1st strike, at tip	1/8	Material break-up OB edge.	--	--
	1/2	2nd strike, 7/16 in. from tip	1/2	Slight scuffing. Good resistance.	Yes	0
	3/4	Just OB of center	5/8	Square pattern, slight scuffing. Good resistance.	Yes	0
	7/8	1/2 in. from tip	1	Substantial unbonding & material loss.	No	--
45	1/2	3/8 in. from tip	1/2	No damage. Very slight scuffing.	Yes	1/64
	3/4	Center impact	3/4	No damage. Very slight scuffing.	Yes	1/64
	7/8	1/2 in. from IB edge	3/4	Slight scuffing. Good bond & resistance.	Yes	1/64
T1	1/2	13/16 in. from tip	5/8	Slight scuffing. No visible damage.	Yes	1/64
	3/4	1st strike, 1/16 in. IB of spec.	1/4	Slight scuffing. Some edge fraying.	Yes	1/64
		2nd strike, 3/16 in. from tip	3/4	Slight scuffing. No visible damage.	Yes	1/64
	7/8	5/8 in. from tip	3/4	Splitting, unbonding & peeling	No	1/32

TABLE 9. IMPACT DAMAGE ASSESSMENT

Spec No.	Dowel Dia (in.)	Type or Location of Impact	Width of Pattern (in.)	Damage Assessment	Pass Test	Permanent Deformation (in.)
T3	1/2	At tip	1/4	No visible damage.	Yes	1/64
	3/4	1/4 in. from tip	1/2	Substantial unbonding, ripping and tearing.	No	--
	7/8	5/8 in. from tip	1	Substantial loss of material, extruding, unbonding, ripping & tearing.	No	--
T3U	1/2	Center strike	1/2	Light scuffing except compression.	Yes	1/64
	3/4	11/16 in. from tip	7/8	Rectangular pattern. Some movement of material.	Yes	1/64
	7/8	7/8 in. from tip	1	Severe damage. Material pushed back, peeling, etc.	No	--
C6+	1/2	5/16 in. from tip	5/8	No discernible damage.	Yes	1/64
	3/4	3/8 in. from tip	3/4	No discernible damage.	Yes	1/32
	7/8	1/2 in. from tip	1	Slight scuffing.	Yes	3/64
C8A	1/2	3/8 in. from tip	1/2	No damage. Slight scuffing.	Yes	1/64
	3/4	5/16 in. from tip	5/8	No damage. Slight scuffing.	Yes	1/32
	7/8	7/8 in. from tip	1	Rectangular pattern, Light scuffing.	Yes	3/64
C9A	1/2	1st strike, 1/4 in. from tip	3/8	No visible damage.	Yes	1/64
	1/2	2nd strike, 3/4 in. from tip	1/4	No visible damage.	Yes	1/64
	3/4	5/8 in. from IB	5/8	No visible damage.	Yes	1/64
	7/8	7/8 in. from tip	1	No visible damage except compression	Yes	3/64

40

TABLE 9. IMPACT DAMAGE ASSESSMENT

Spec No.	Dowel Dia (in.)	Type or Location of Impact	Width of Pattern (in.)	Damage Assessment	Pass Test	Permanent Deformation (in.)
C9A+	1/2	1/4 in. from tip	1/2	No visible damage except compression	Yes	1/32
	3/4	3/4 in. from tip	9/16	No visible damage except compression	Yes	3/64
	7/8	1/2 in. from tip	5/8	No visible damage except compression	Yes	1/16
B1	1/2	3/8 in. from tip	1/2	No damage. No scuffing.	Yes	1/64
	3/4	5/8 in. from tip	3/4	No damage. No scuffing.	Yes	1/32
	7/8	3/8 in. from tip	3/4	No damage. No scuffing.	Yes	3/64

NOTE: (1) May be invalid. Strike occurred at or very close to edge.

TABLE 10. IMPACT DAMAGE SUMMARY

Sample No.	Sample Name	Thickness (Inch)	Adhesive Notes	Substrate Notes	1/2" Dowel	3/4" Dowel	7/8" Dowel
	MOLDED MATERIALS						
4	PO655	0.076	1	1	1	1	1
11	TSK L101	0.071	1	1	1	1	2
17	535330A	0.077	1	1	1	1	4,5
21	NS-6572	0.080	1	1	1	1	1
23	535336A	0.063	1	1	1	1	1
31	535382C	0.066	1	1	1	2	4
39	535385A	0.078	1	1	1	1	4
42	535387D	0.062	1	1	1	1	4
44	6978	0.063	1	1	1	1	4,6
45	NPE 2916	0.060	2	1	1	1	1
	TAPES						
T1	8663	0.016	3	2	1	2	4
T3	NPE 2846	0.012	3	2	1	3	4
T3U	NPE 2846U	0.012	3	2	1	2	4
	COATINGS						
C6+	AS-P108/AGCoat 1R3R	0.012	4	2	1	1	1
C8A	AS-P108/Caapcoat B-274	.002/.014	5	2	1	1	1
C9A	Elastuff 504	0.022	5	2	1	1	1
C9A+	AS-P108/Elastuff 504	.002/.022	5	2	1	1	1
	2-PART SYSTEMS						
B1	TSK L100	0.023	6	2	1	1	1

Adhesive Notes

1. Kaman KPS 146 Epoxy Adhesive
2. 3M EC-2216 Clear Epoxy Adhesive
3. 3M High Strength PS Acrylic/Promoter 86
4. AGC AGCoat 7A/B Primer
5. Mil-P-23377 TyII Epoxy Primer/Alodine
6. Lord 9924V Wash Primer

Substrate Notes

1. 0.093 Glass-Epoxy Airfoil
2. 0.125 Aluminum Airfoil

Impact Code

1. No Damage
2. Moderate Damage. Will Still Protect Blade.
3. Moderate Damage. Will Not Protect Blade.
4. Severe Damage. Blade Protection Gone.
5. May be Invalid. Strike Occurred at or very near Edge.
6. May be Invalid Due to Prejudicial Previous Strike Edge Damage.

TABLE 11. IMPACT DAMAGE SUMMARY (RANKED)

Sample No.	Sample Name	Thickness (Inch)	Adhesive Notes	Substrate Notes	1/2" Dowel	3/4" Dowel	7/8" Dowel
	MOLDED MATERIALS						
4	PO655	0.076	1	1	1	1	1
21	NS-6572	0.080	1	1	1	1	1
23	535336A	0.063	1	1	1	1	1
45	NPE 2916	0.060	2	1	1	1	1
11	TSK L101	0.071	1	1	1	1	2
17	535330A	0.077	1	1	1	1	4,5
39	535385A	0.078	1	1	1	1	4
42	535387D	0.062	1	1	1	1	4
44	6978	0.063	1	1	1	1	4,6
31	535382C	0.066	1	1	1	2	4
	TAPES						
T1	8663	0.016	3	2	1	2	4
T3U	NPE 2846U	0.012	3	2	1	2	4
T3	NPE 2846	0.012	3	2	1	3	4
	COATINGS						
C6+	AS-P108/AGCoat 1R3R	0.012	4	2	1	1	1
C8A	AS-P108/Caapcoat B-274	.002/.014	5	2	1	1	1
C9A+	AS-P108/Elastuff 504	.002/.022	5	2	1	1	1
C9A	Elastuff 504	0.022	5	2	1	1	1
	2-PART SYSTEMS						
B1	TSK L100	0.023	6	2	1	1	1

Adhesive Notes
1. Kaman KPS 146 Epoxy Adhesive
2. 3M EC-2216 Clear Epoxy Adhesive
3. 3M High Strength PS Acrylic/Promoter 86
4. AGC AGCoat 7A/B Primer
5. Mil-P-23377 TyII Epoxy Primer/Alodine
6. Lord 9924V Wash Primer

Substrate Notes
1. 0.093 Glass-Epoxy Airfoil
2. 0.125 Aluminum Airfoil

Impact Code
1. No Damage
2. Moderate Damage. Will Still Protect Blade.
3. Moderate Damage. Will Not Protect Blade.
4. Severe Damage. Blade Protection Gone.
5. May be Invalid. Strike Occurred at or very near Edge.
6. May be Invalid Due to Prejudicial Previous Strike Edge Damage.

43

SOLAR RADIATION

Solar radiation testing was performed by the Q-Panel Company of Cleveland, OH, using the guidelines of MIL-STD-810E, Method 505.3, Procedure II. Each 24 hour cycle consisted of 20 hours of ultraviolet (UV) exposure at 70°C (158°F) and 4 hours of no-light condensation at 50°C (122°F), following the operating procedures of ASTM G 53, Standard Recommended Practice for Operating Light and Water Exposure Apparatus (Fluorescent UV-Condensation Type) for Exposure of Nonmetallic Materials. The type of lamp used was UVB-313 and the specimens were rotated daily to assure a similar exposure for all specimens. The UVB-313 is more aggressive than UVA-340, which simulates the UV spectrum of sunlight very closely, but the UVB-313 was chosen so results could be obtained within the initial task time frame of this program. Also major materials suppliers such as 3M Co. and DuPont use the UVB-313 lamps for preliminary testing of their materials. The samples were cycled for a maximum of 2016 hours (84 days), less if they failed before that time. Several of the original materials were reformulated with UV and/or antioxidation inhibiting chemicals. Although some improvement is evident from the increased number of hours to failure in Miles samples 39, 42 and 44, the additives do not perform as well as those in 3M Co. samples 45, T1 and T3U. Test results are shown in Table 12 and the materials are ranked according to their UV resistance in Table 13.

The failures of these materials must be kept in perspective. The UVB-313 lamps emit radiation of shorter and more destructive wave length than that found in natural sunlight or UVA-340 lamps. It is possible that phenomena which developed in this test may not occur at all or may occur only after long periods of time in the presence of natural sunlight or UVA-340 lamps. Most of the materials tested were unpigmented and in their natural color. It is known that the presence of carbon black pigment adds some measure of UV protection and had it been present in the natural color materials, the results may have been different. Finally, some of the materials were affected in a purely textbook fashion, characteristic of urethane elastomers. The surface appears to get harder and shrink while the deeper material appears unaffected. Upon shrinking, fine shallow surface cracks develop and expand, exposing fresh underlying unaffected material. Under magnification, these cracks do not appear as true cracks but rather as shallow rounded depressions or rills. To be consistent, this condition was reported as a failure; however, the effect of this condition on the overall effectiveness of the erosion protection system was considered on an individual basis.

FUNGUS

Fungus testing was performed by East-West Technology Corp of West Babylon, NY, in accordance with MIL-STD-810E, Method 508.4, Procedure I. The material specimens were exposed to the five fungus spores listed in the test. Incubation conditions consisted of daily cycles of 20 hours at 30 ± 1°C (86 ± 2°F) and 95 ± 5% relative humidity, followed by a 4-hour period in which at least 2 hours consisted of 25 ± 1°C (77 ± 2°F) and 95-100% relative humidity. The remaining 2 hours were transitions during which the conditions were maintained at 24-31°C (75-88°F) and 90-100% relative humidity. After the 28-day incubation period, there was no visible evidence of fungal growth. Table 14 lists the materials tested.

TABLE 12. SOLAR RADIATION TEST RESULTS

Sample No.	Sample Name	Color	Pass/ Fail	Time To Pass/Fail (Hours)	Description
	MOLDED MATERIALS				
4	PO655	Black	F(4)	336	Surface Wrinkling.
11	TSK L101	Black	P	2016	Sl Chalky, Oily, Minor Orange Peel.
17	535330A	Natural	F(3)	1008	Many Fine Surface Cracks.
17U	535330A (1)	Natural	F(3)	1008	Many Fine Surface Cracks.
21	NS-6572	Black	P	2016	Surface Spotted & Chalky.
23	535336A	Natural	F	123	Melted.
23U	535336A (1)	Natural	F	336	Tacky.
39	535385A	Natural	F	123	Many Surface Cracks. Weak.
39U	535385A (1)	Natural	F	336	Cracked. Weak.
42	535387D	Natural	F	267	Swelled. Many Severe Cracks. Weak.
42U	535387D (1)	Natural	F	1344	Brittle. Cracked Apart.
44	6978	Natural	F	336	Cracked Apart. Weak.
44UA	6978 (2)	Natural	F	1008	Cracked Apart. Weak.
44UB	6978 (1)	Natural	F	1344	Surface Cracks. Weak.
45	NPE 2916	Natural	P	2016	Sl Chalky Surface & V Sl Yellowing.
	TAPES				
T1	8663	Natural	P	2016	Some Yellowing.
T3	NPE 2846	Natural	F	123	Many Cracks To Substrate.
T3U	NPE 2846U (1)	Natural	P	2016	V Sl Yellowing.
	COATINGS				
C6	AGCoat 1R3R	Black	P	2016	Chalky.
C8	AS-P108/Caapcoat B-274	Black	P	2016	Chalky.
C9	Elastuff 504	Blue	P	2016	Chalky. Blue Color Disappeared.
	2-PART SYSTEMS				
B1	TSK L100	Sl Black	F(3)	1344	Many Fine Surface Cracks.

Notes
1. Same As Original Sample But With UV/Antioxidant Stabilizers.
2. Same As Original Sample But With UV Stabilizer Only.
3. Characteristic UV Surface Phenomenom. Underlying Material Not As Weak As Others Which Failed. Miles Now Uses Improved UV/Antioxidation Stabilizers. See Page 52.
4. Surface Wrinkles. Not The Characteristic UV Surface Phenomenom Discussed In Text Of Report.

TABLE 13. SOLAR RADIATION TEST RESULTS (RANKED)

Sample No.	Sample Name	Color	Pass/ Fail	Time To Pass/Fail (Hours)	Description
	MOLDED MATERIALS				
11	TSK L101	Black	P	2016	Sl Chalky, Oily, Minor Orange Peel.
21	NS-6572	Black	P	2016	Surface Spotted & Chalky.
45	NPE 2916	Natural	P	2016	Sl Chalky Surface & V Sl Yellowing.
42U	535387D (1)	Natural	F	1344	Brittle. Cracked Apart.
44UB	6978 (1)	Natural	F	1344	Surface Cracks. Weak.
17	535330A	Natural	F(3)	1008	Many Fine Surface Cracks.
17U	535330A (1)	Natural	F(3)	1008	Many Fine Surface Cracks.
44UA	6978 (2)	Natural	F	1008	Cracked Apart. Weak.
4	PO655	Black	F(4)	336	Surface Wrinkling.
23U	535336A (1)	Natural	F	336	Tacky.
39U	535385A (1)	Natural	F	336	Cracked. Weak.
44	6978	Natural	F	336	Cracked Apart. Weak.
42	535387D	Natural	F	267	Swelled. Many Severe Cracks. Weak.
23	535336A	Natural	F	123	Melted.
39	535385A	Natural	F	123	Many Surface Cracks. Weak.
	TAPES				
T1	8663	Natural	P	2016	Some Yellowing.
T3U	NPE 2846U (1)	Natural	P	2016	V Sl Yellowing.
T3	NPE 2846	Natural	F	123	Many Cracks To Substrate.
	COATINGS				
C6	AGCoat 1R3R	Black	P	2016	Chalky.
C8	AS-P108/Caapcoat B-274	Black	P	2016	Chalky.
C9	Elastuff 504	Blue	P	2016	Chalky. Blue Color Disappeared.
	2-PART SYSTEMS				
B1	TSK L100	Sl Black	F(3)	1344	Many Fine Surface Cracks.

Notes

1. Same As Original Sample But With UV/Antioxidant Stabilizers.
2. Same As Original Sample But With UV Stabilizer Only.
3. Characteristic UV Surface Phenomenom. Underlying Material Not As Weak As Others Which Failed. Miles Now Uses Improved UV/Antioxidation Stabilizers. See Page 52.
4. Surface Wrinkles. Not The Characteristic UV Surface Phenomenom Discussed In Text Of Report.

TABLE 14. FUNGUS, SALT FOG AND TEMPERATURE TEST RESULTS

Sample No.	Sample Name	Fungus Pass/ Fail	Salt Fog Pass/ Fail	Low Temp Pass/ Fail	Temp Shock Pass/ Fail
	MOLDED MATERIALS				
4	PO655	P	P	P	P
11	TSK L101	P	P	P	P
17	535330A	P	P	P	P
21	NS-6572	P	P	P	P
23	535336A	P	P	P	P
39	535385A	P	P	P	P
42	535387D	P	P	P	P
44	6978	P	P	P	P
45	NPE 2916	P	P	P	P
	TAPES				
T1	8663	P	P	P	P
T3	NPE 2846	P	P	P	P
T3U	NPE 2846U	(1)	P	P	P
	COATINGS				
C6	AGCoat 1R3R	P	P	P	P
C8	AS-P108/Caapcoat B-274	P	P	P	P
C9	Elastuff 504	P	P	P	P
	2-PART SYSTEMS				
B1	TSK L100	P	P	P	P

Notes

1. Not tested as T3U. T3U is same urethane as sample 45
   and therefore will pass. T3U is same as T3 but with
   UV & antioxidant stabilizers.

47

T3U was not tested, but samples 45 and T3 were. T3U is T3 with UV and antioxidation inhibitors added. Sample 45 is T3U at 0.060 inch thick and without the high strength pressure sensitive adhesive. Therefore, T3U will also pass the Fungus Test.

SALT FOG

Salt fog testing was performed in accordance with MIL-STD-810E, Method 509.3, Procedure I using a 5% salt solution, 35°C (95°F) and a fall-out rate of 0.5-3 ml/80 cm²/hr. After 14 days of continuous salt spray, the materials exhibited no signs of degradation. Table 14 lists the materials tested.

LOW TEMPERATURE

Low temperature testing was performed in accordance with MIL-STD-810E, Method 502.3, Procedure I. The specimens were visually examined before the test, after 4 hours at -54°C (-65°F) and after stabilizing at room temperature. No cracking or degradation of any kind was observed. Additionally, the materials were then stabilized at -54°C (-65°F) again and removed from the cold chamber one at a time and flexed immediately. No cracking or degradation was observed on any of the 16 samples. Table 14 lists the materials tested.

TEMPERATURE SHOCK

Temperature shock testing was performed in accordance with MIL-STD-810E, Method 503.3. The 16 materials were visually examined before and after three complete temperature cycles. After placing the specimens in the high temperature chamber, the temperature was adjusted to 104°C (220°F). After 1 hour at 104°C (220°F), the specimens were transferred between the chamber 104°C (220°F) and the -54°C (-65°F) chamber for three complete cycles. Transfer time between chambers was less than 1 minute. Specimens were allowed to stabilize at the test temperatures prior to each transfer. There were no visible changes in any of the specimens. Table 14 lists the materials tested.

DECONTAMINATION

Decontamination testing was performed in accordance with the guidelines of ASTM D 543 and ASTM D 1308 using distilled water and decontamination fluid DS2. The molded materials were used as is and the coatings and tapes were applied to 0.025 inch thick aluminum strips. The material specimens for the distilled water tests were visually examined, weighed, measured for thickness and immersed in distilled water. They were visually inspected after 1 hour, 8 hours and after 1, 3, 7 and 14 days. They were weighed and measured for thickness after 14 days. Results are listed in Table 15. There were no significant changes except that the swelling which occurred with sample 21 in the hydrolysis test is confirmed by the large weight gain of this 14-day soak in distilled water. The fact that water intruded under the

TABLE 15. DISTILLED WATER DECONTAMINATION TEST RESULTS

Sample No.	Day 0	Weight Day 14	Diff.	Day 0	Thickness Day 14	Diff.	Visual Appearance Day 14
		MOLDED MATERIALS					
4	5.4514	5.5169	0.0655	0.068	0.070	0.002	No Change
11	4.2538	4.2995	0.0457	0.055	0.056	0.001	No Change
17	5.4837	5.5090	0.0253	0.080	0.081	0.001	No Change
21	7.1807	7.4221	0.2414	0.078	0.080	0.002	No Change
23	4.5726	4.6221	0.0495	0.063	0.064	0.001	No Change
39	4.8108	4.8302	0.0194	0.071	0.072	0.001	No Change
42	4.4816	4.5034	0.0218	0.063	0.064	0.001	No Change
44	5.1153	5.1594	0.0441	0.074	0.075	0.001	No Change
45	4.0141	4.0355	0.0214	0.059	0.060	0.001	No Change
		TAPES					
T1	4.8215	4.8299	0.0084	0.037	0.038	0.001	No Change
T3	4.4637	4.4661	0.0024	0.035	0.036	0.001	No Change
T3U	4.4862	4.4905	0.0043	0.034	0.034	0.000	No Change
		COATINGS					
C6	8.0439	8.0487	0.0048	0.055	0.055	0.000	No Change
C8	8.0079	8.0127	0.0048	0.056	0.056	0.000	No Change
C9	7.9071	7.9136	0.0065	0.056	0.057	0.001	No Change *
		2-PART SYSTEMS					
B1	8.8585	8.8758	0.0173	0.068	0.069	0.001	No Change *

* Water under coating edges on Day 7.

49

edges of samples C9 and B1 after 7 days has no negative implications because the aluminum strips were not etched and primed for optimum adhesion and corrosion protection.

The samples for the DS2 decontamination tests were visually examined and weighed prior to immersing in DS2 decontamination agent. Visual changes were noted after 1, 2 and 2½ hours. The normal Army procedure for decontaminating equipment with DS2 is to rinse the decontaminating agent away within 30 minutes. In unusual cases it may remain on the equipment for 1 hour. Test results are shown in Table 16. Note that all the materials survived a 1-hour soak in acceptable condition except sample 4, P0655, which began leaching black material into the fluid. Of the 3M Co. materials, samples 45, T1 and T3U turned amber, probably because each contains the same UV and antioxidation inhibitors. T3 does not have them and did not turn amber. T3 is T3U without inhibitors.

RADAR CROSS SECTION ASSESSMENT

The radar cross section (RCS) assessment was conducted for Kaman by AT Team, an electromagnetic physics and low observables consultant firm from Mesa, Arizona. Based on knowledge of the geometry and materials of the K747 blade, it was concluded that no significant RCS variation is anticipated and that the radar detectability of the helicopter with modified K747 blades will remain unchanged. The RCS assessment is provided in Appendix B.

50

TABLE 16. DS2 DECONTAMINATION TEST RESULTS

| Sample | Weight | | | Visual Appearance | | |
No.	Hr 0	Hr 2.5	Diff.	Hr 1.0	Hr 2.0	Hr 2.5
MOLDED MATERIALS						
4	5.2537	4.0578	-1.1959	Leaching Black.	Leaching Black. Stuck To Bottom.	Leaching Black.
11	4.5362	5.0430	0.5068	Good	Good	Good
17	4.7814	4.8235	0.0421	Good	Good	Good
21	7.1184	7.2182	0.0998	Good	Good	Good
23	4.7348	5.2592	0.5244	Good	Good	Good
39	4.8362	4.8548	0.0186	Good	Good	Good
42	4.4410	4.5516	0.1106	Good	Good	Good
44	4.9101	5.2949	0.3848	Good	Stuck To Bottom.	Stuck To Bottom.
45	4.7410	4.9466	0.2056	Turned Amber.	Turned Amber.	Turned Amber. Sl Soft But OK.
TAPES						
T1	4.5966	3.9883	-0.6083	Turned Amber.	Completely Disintegrated.	Completely Disintegrated.
T3	3.7909	3.9673	0.1764	Good	Good	Sl Soft but OK.
T3U	3.9900	4.2468	0.2568	Turned Amber.	Turned Amber.	Film Shriveled. DS2 In Bondline.
COATINGS						
C6	4.7287	7.9914	3.2627	Good	Starting To Leach.	Leaching Material.
C8	7.9459	7.4764	-0.4695	Good	Deteriorating Rapidly.	Disintegrating
C9	7.9038	8.0091	0.1053	Good	Good	Sl Soft but OK.
2-PART SYSTEMS						
B1	8.4333	8.4902	0.0569	Good	Good	Good

DISCUSSION OF MATERIALS EVALUATION

The material properties judged to be most important for erosion protection are hydrolysis, rain erosion, sand erosion, impact resistance and solar radiation. The candidate materials selected to undergo the complete series of tests are shown in the summary table (Table 17). All of these materials passed the other testing, specifically, fungus, salt fog, low temperature, temperature shock and decontamination testing, except for sample 4 which leached out black material after 1 hour in DS2 fluid.

The materials on Table 17 were ranked first by hydrolysis, then by rain erosion, sand erosion and impact. All materials which possess a suffix "U" have had UV and antioxidation inhibitors added to the original sample except 44UA which has only the UV stabilizer. They were received later in the program, and it was not possible to subject them to the entire test series. Tape sample T3U completed the tests shown but the molded material "U" samples were tested for solar radiation only.

MOLDED MATERIALS

The results show that sample 45 is the best candidate material for rain erosion. It is the identical aliphatic polyether urethane formulation as that of tape sample T3U discussed below. Rain erosion results of 1060+ minutes are outstanding, and the sand erosion resistance is more than twice that of sample 4, the current K747 blade erosion guard material. Figure 13 shows sample 45 after rain and sand erosion testing. It survived the 7/8 in. dowel impact testing with only slight scuffing and would continue to protect the blade.

Sample 44, although second best on rain erosion, performed poorly in sand erosion. It also failed the 7/8 in. dowel impact and solar radiation tests. The improvements to solar radiation by UV and antioxidation additives are evident from the increased number of hours to failure, but the improved samples still failed.

Sample 17 is the best candidate material for sand erosion. It performed about as well as sample 4 in rain erosion but was six times better in sand erosion. Impact resistance was good through the 3/4 in. dowel. Although the results indicate an impact failure with the 7/8 in. dowel, it may have been invalid because an unusual diagonal strike occurred very close to the inboard end of the specimen. Had it not occurred, sample 17 may have survived the 7/8 in. dowel impact. This was one of the materials which must have its solar radiation result considered on an individual basis. The surface was characteristically affected by the UV radiation but the underlying material appeared stronger than most of the other samples which failed. Subsequent to this evaluation, Miles tested an improved UV and antioxidation additive package in 535330A. After 1000 hours of UV testing, the sample surface was unaffected. Because of the excellent condition of the sample with no surface cracking present, it is reasonable to expect that the material will pass 2000 hours of UV testing. Miles now uses this improved additive package in 535330A to replace the one tested in sample 17U.

TABLE 17. SUMMARY TABLE

Sample No.	Sample Name	1200 Hr Hydrolysis Pass/Fail	Rain Erosion (Minutes)	Sand Erosion (Ratio)	Impact Resistance 7/8" Dowel	Solar Radiation Pass/Fail	Solar Radiation Pass/Fail (Hours)
	MOLDED MATERIALS						
45	NPE 2916	P	1060 +	2.1	1 **	P	2016
44	6978	P	280	0.3	4	F	336
44UA	6978 (2) *	-	-	-	-	F	1008
44UB	6978 (1)	-	-	-	-	F	1344
17	535330A	P	220	6.1	4	F(4)	1008
17U	535330A (1)	-	-	-	-	F(4)	1008
39	535385A	P	155	0.6	4	F	123
39U	535385A (1)	-	-	-	-	F	336
23	535336A	P	130	1.1	1	F	123
23U	535336A (1)	-	-	-	-	F	336
42	535387D	P	117	1.3	4	F	267
42U	535387D (1)	-	-	-	-	F	1344
11	TSK L101	P	35	0.5	2	P	2016
4	PO655	F	240	1.0	1	F(5)	336
21	NS-6572	F	218	1.1	1	P	2016
	TAPES						
T3U	NPE 2846U on Aluminum	P	240 +	5.8	4	P	2016
T7	NPE 2846 on Glass-Epoxy	P	240 + (3)	-	-	F	123
T3	NPE 2846 on Aluminum	P	50	2.7	4	F	123
T1	8663 on Aluminum	F	122	7.8	4	P	2016
	COATINGS						
C9A+	AS-P108/Elastuff 504	-	185	0.9	1	-	-
C9A	Elastuff 504	P	102	1.7	1	P	2016
C6	AGCoat 1R3R	P	85	-	-	P	2016
C6+	AS-P108/AGCoat 1R3R	-	-	1.0	1	-	-
C8A	AS-P108/Caapcoat B-274	F	75	0.7	1	P	2016
	2-PART SYSTEMS						
B1	TSK L100	P	16	0.4	1	F(4)	1344

* General Notes

1. Same as original sample number but with UV/Antioxidant stabilizers.
2. Same as original sample number but with UV stabilizers only.
3. NPE 2846 tape looks good after 240 minutes but damage to the glass-epoxy substrates occurred at 21 and 75 minutes into test.
4. Characteristic UV surface phenomenon. Underlying material not as weak as others which failed. Miles now uses improved UV/antioxidation stabilizers. See page 52.
5. Surface wrinkles. Not the characteristic UV surface phenomenon discussed in text of reprt. Underlying material not as weak as others which failed.

** Impact Code

1. No damage.
2. Moderate damage. Will still protect blade.
3. Moderate damage. Will not protect blade.
4. Severe damage. Blade protection gone.

53
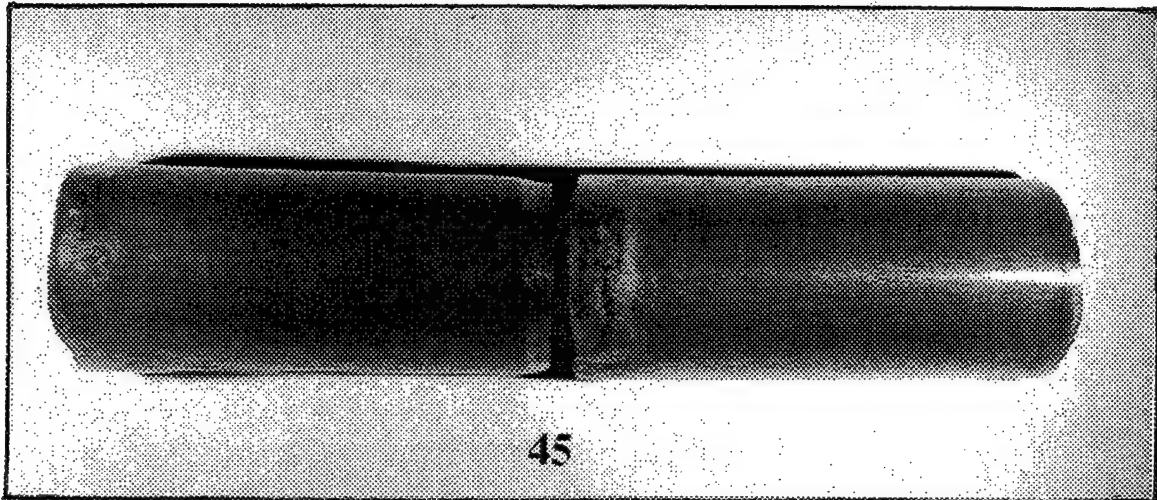
a. Rain erosion specimens after 1060 minutes.
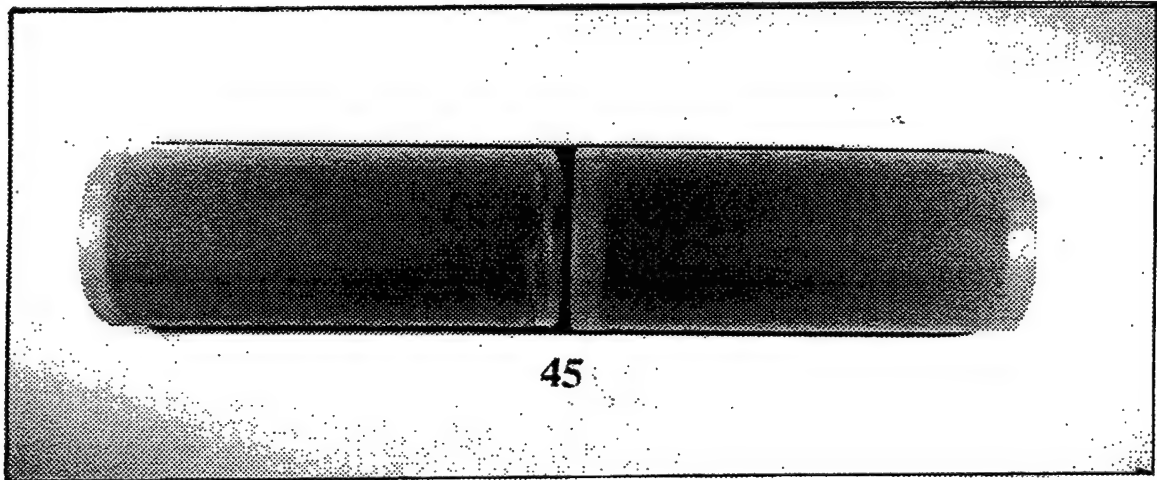
b. Sand erosion specimens.

Figure 13. Sample 45 Rain and Sand Erosion Specimens

Samples 39, 23 and 42 definitely failed the solar radiation tests, developing severe cracking and even melting. The rain erosion results were not as good as most of the other materials. Sand erosion was relatively unimpressive and only sample 23 passed the impact test.

The rain erosion performance of sample 11, the current erosion guard material on the UH-1 composite main rotor blade (CMRB), was not very good, surviving only 35 minutes, and sand erosion was only half that of sample 4. It passed hydrolysis, solar radiation, and the ⅞ in. dowel impact.

Sample 4, the current K747 AH-1 blade erosion guard material, survived rain erosion testing for 240 minutes, was the baseline material for sand erosion and showed little impact damage from the ⅞ in. dowel. Figure 14 shows sample 4 after rain and sand erosion testing. The effect of solar radiation was different than that of the other materials. Surface wrinkling occurred and the fine, shallow surface cracks or rills characteristic of UV damaged urethane elastomers were not evident. Whatever this may indicate is of little consequence because the poor hydrolysis resistance makes the material undesirable for long-term use in hot humid climates.

The neoprene material, sample 21, performed quite well except for the hydrolysis test in which an unusual degree of swelling was observed. On the molecular level, this material probably doesn't exhibit the polymer chain scission which is generally associated with the ester type of urethane elastomers. The most reasonable explanation for the swelling is that the material is highly loaded with a hygroscopic filler which absorbed the moisture and caused excessive swelling of the sample. Thus, while the material has been used as a deicing/erosion guard for propellers, it would be undesirable for long-term use on helicopter rotor blades in hot humid climates.

TAPES

Of the tape materials evaluated, only those of the aliphatic polyether type of urethane survived the hydrolysis test. Sample T1 is an aliphatic polyester type of urethane which failed the hydrolysis test but was fully evaluated because it is currently part of erosion protection enhancement kits for Army helicopter rotor blades. It exhibited the best sand erosion resistance of all the materials tested, but rain erosion of 122 minutes was only half that of sample T3U.

Sample T3U, which is the identical urethane formulation of molded sample 45, also exhibited excellent rain erosion results. After 240 minutes, the specimens were unblemished and would likely survive much longer. Solar radiation resistance was excellent as described above. Sand erosion, although almost six times better than sample 4 in erosion wear rate, was found to be unacceptable. After only 10 minutes of testing, small splits had developed and one had opened down to the substrate. Subsequently it filled with sand and began to lift from the
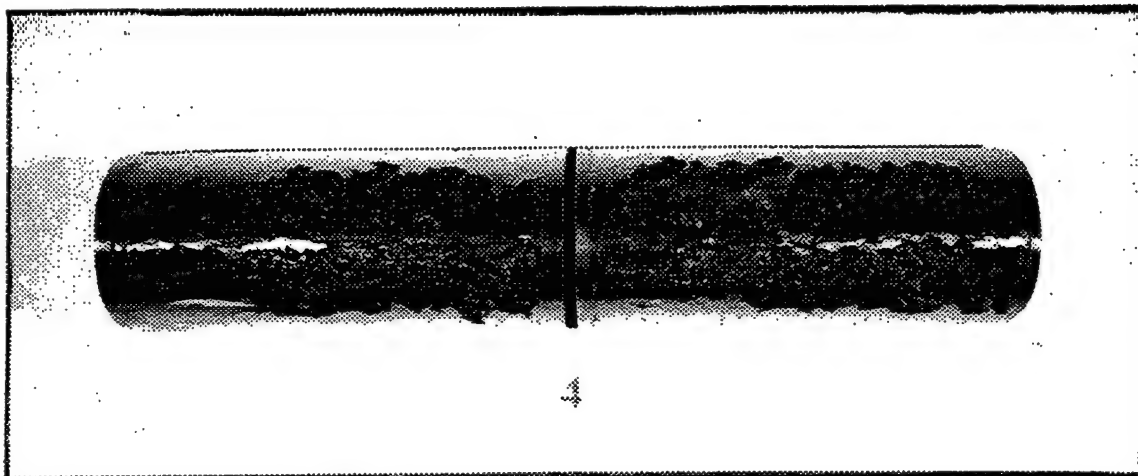
a. Rain erosion specimens. Failed after 240 minutes.
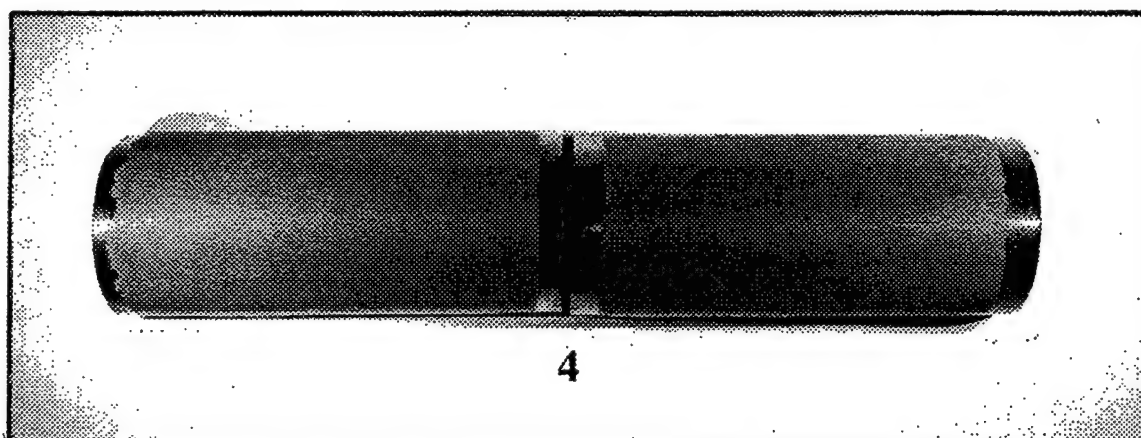
b. Sand erosion specimens.

Figure 14. Sample 4 Rain and Sand Erosion Specimens.

surface. Figure 15 shows T3U after rain and sand erosion testing, and Figure 16 shows the split along the leading edge with sand particles under the tape. T3U survived the ¾ in. dowel impact although some movement or sliding of the material was observed. Failure occurred at the ⅞ in. dowel impact as did all the tape samples tested. This is believed to be a function of thickness and/or the type of adhesive (pressure sensitive) used, as the 0.060 inch thick molded sample 45, bonded with a thermosetting epoxy adhesive, passed with only slight scuffing. Figure 17 shows samples T3U and 45 after impact testing with the ⅞ in. dowel.

Sample T3 survived only 50 minutes of rain erosion, but this is believed due to the inconsistency of thickness described earlier in the Rain Erosion section. Sand erosion was also not as good as T3U. This was apparently enhanced by the improved fabrication process of sample T3U. T3 did not contain UV or antioxidant stabilizers and failed early in the solar radiation testing. The later samples of the same material contained the additives and survived solar radiation testing in excellent condition.

The rain erosion of sample T7, on fiberglass-epoxy airfoil substrates, was as good as sample T3U on aluminum, except that damage to the fiberglass-epoxy substrates became apparent after 21 minutes on one sample and 75 minutes on the other. For this reason, these thin, pressure-sensitive adhesive backed tapes will not be considered for rain erosion protection of composite substrates.

COATINGS

Of the coatings selected to undergo the entire series of tests, sample C9A, Elastuff 504, has exhibited the best overall performance as an erosion protection material. When topped with AS-P108 antistatic topcoat, the rain erosion time increases substantially from 102 to 185 minutes. However, the sand erosion resistance is reduced by about 50%. This is due to the reduced sand erosion characteristic of the topcoat and not to the Elastuff 504. Without the topcoat, Elastuff 504 has approximately twice the sand erosion resistance of P0655.

Elastuff 504 was evaluated as either clear or blue in color. The blue version contains a very small amount of a user added blue dye as a visual aid to help the painter determine the amount of coating build while painting. The blue eventually fades out from the UV radiation in sunlight. It has no known detrimental effect on the coating.

Sample C6, AGCoat 1R3R, has slightly less rain erosion at 85 minutes than sample C9A. As a result of obtaining 83 extra minutes of rain erosion by the addition of the AS-P108 topcoat to Elastuff 504, it was decided to also evaluate the AGCoat 1R3R for sand erosion and impact with the AS-P108 in place as sample C6+. To the extent that the sand erosion tests were run, the sand erosion results of C6+ are mostly due to the topcoat and not a true reflection of the underlying coating. Since sample C9A has better rain and sand erosion, sample C6 was not recommended for further evaluation.

57
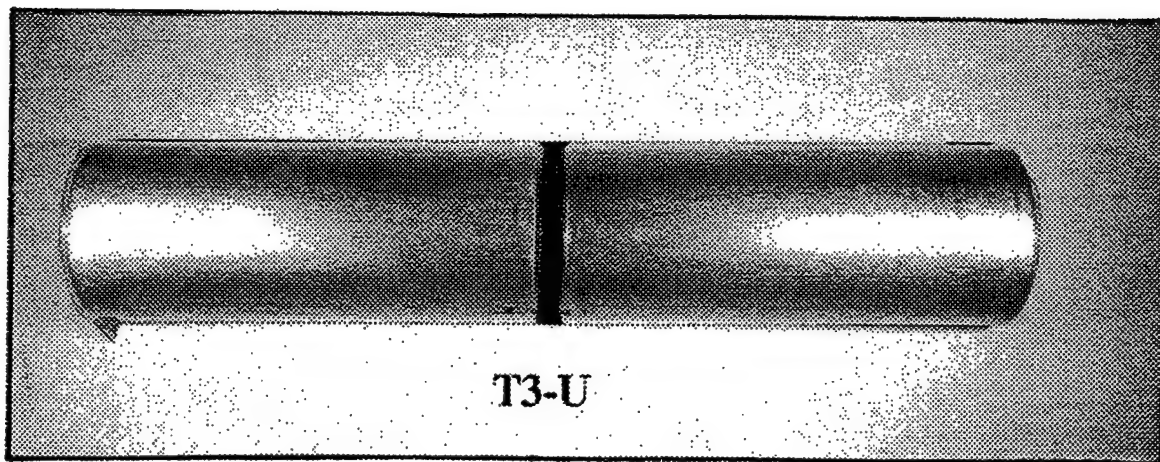
a. Rain erosion specimens. No failure after 240 minutes.
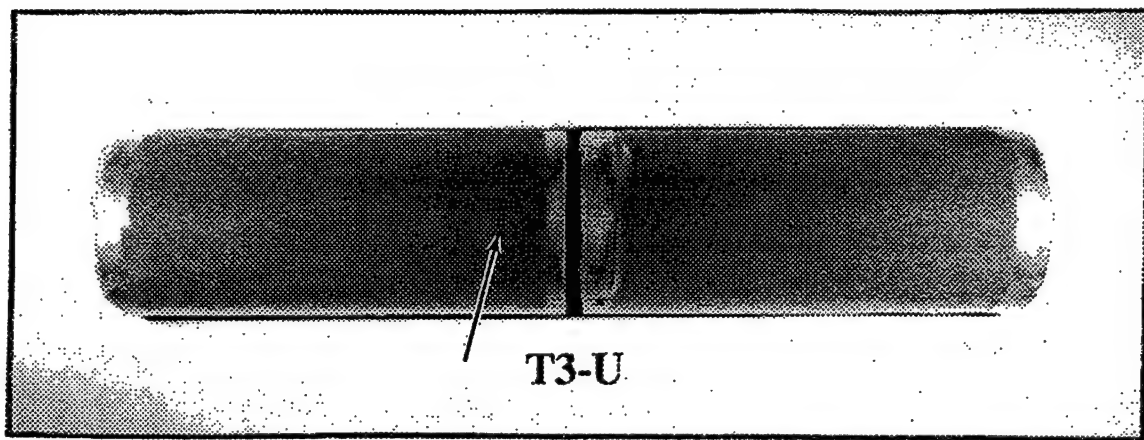
b. Sand erosion specimens. Arrow indicates split in tape.

Figure 15. Sample T3U Rain and Sand Erosion Specimens.
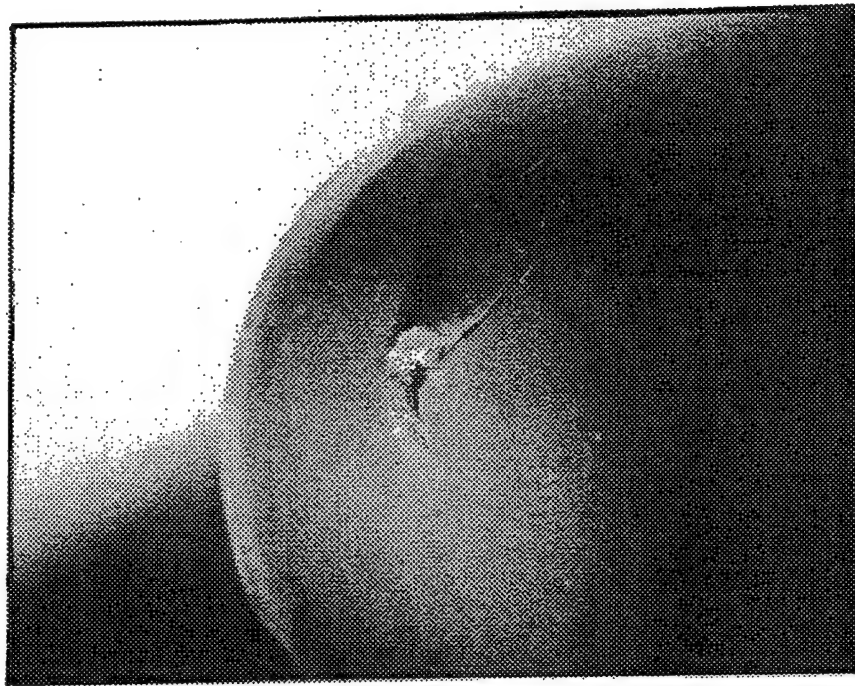
Figure 16. T3U Sand Erosion Specimen. Leading Edge Split with Sand Particles Under the Tape. Mag. 8X.
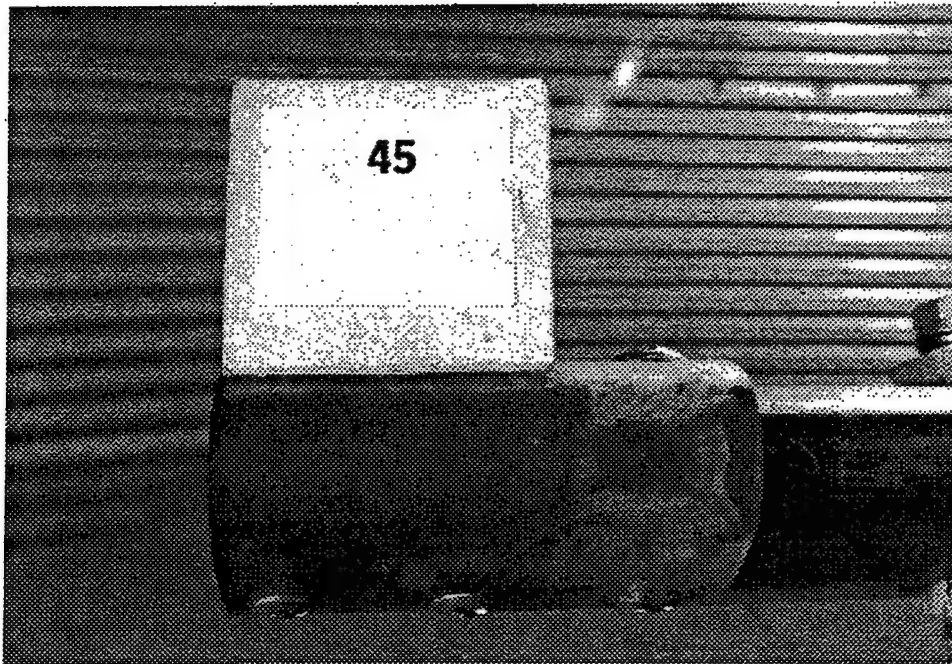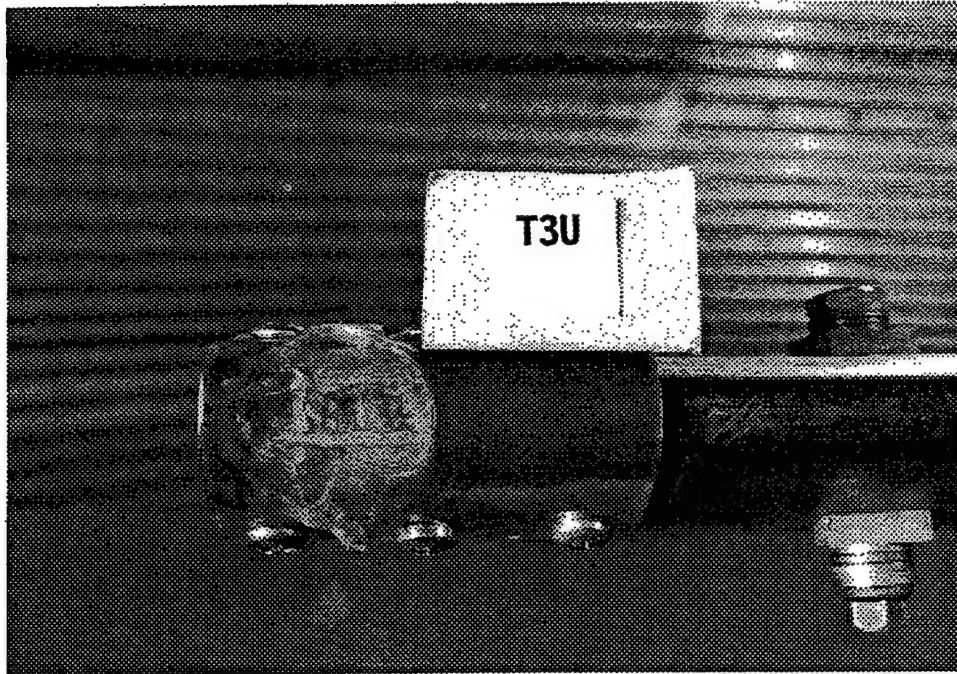
Figure 17. Samples T3U and 45 After ⅞ In. Dowel Impact.

Sample C8A is qualified as a rain-resistant coating system per MIL-C-83281A and was expected to run for 150 minutes minimum in the rain test. The reason for lasting only 75 minutes is unknown. Sand erosion is slightly less than sample 4 and similar to C9A+ and C6+. As discussed above, sand erosion results are primarily those of the AS-P108 topcoat. AS-P108 was not tested for hydrolysis by itself. It was tested with its recommended basecoat of Caapcoat B-274 as C8A, and together they failed hydrolysis. C8A was not recommended for further evaluation on helicopter rotor blades.

TWO-PART SYSTEMS

The only two-part system selected for the complete series of tests was sample B1, TSK L100, because it was part of an erosion guard repair kit for Army helicopter rotor blades. Rain erosion was poor at only 16 minutes, and sand erosion is less than half that of sample 4. Sample B2 lasted only 7 minutes in rain erosion testing and sample B3 failed hydrolysis.

MATERIAL EVALUATION AND THE DESIGN CRITERIA DOCUMENT

The Design Criteria Document (DCD) is from an earlier Army-funded study[2]. Its intention was to establish minimum requirements for the design and wear life of erosion protection systems. Compliance was to be demonstrated by testing in accordance with the Qualification Test Procedures (QTP). These documents were used as guidelines during the materials evaluation effort. The following discusses the testing as it relates to them.

The requirements of the QTP were carefully considered in the design of the Kaman-funded Whirling Arm Sand Erosion and Impact Test Facility. The test rotor at 8.04 feet in diameter is 18.3% of the full-scale K747 blade and therefore meets the 15% minimum QTP require-ment. Additionally, the rotor gearbox contains a pitch change mechanism to allow presetting and/or varying of the specimen angle of attack during the dynamic phases of testing. A semi-torus shaped floor was installed to encourage circulation of sand particles during testing. The minimum cross section of the enclosure at 21 feet is more than the required minimum of five times the radius of the rotating arm. Rain erosion testing by UDRI is performed with an enclosure-to-blade ratio much smaller than this and there appears to be no reason for requiring a larger one for rain erosion.

The airfoil geometry of the K747 blade was not used in testing. As a matter of convenience, the same airfoil shaped leading edge substrates used for rain erosion testing were chosen for the sand erosion and impact testing. This was judged adequate when a comparison of materials for a leading edge guard is being sought. For qualification of a specific leading edge erosion guard, the QTP implies that the test airfoil should be of the same geometry as that of the erosion guard being qualified.

The average sand cloud density at 0.0172 gms/cu ft was 23% greater than the 0.0140 gms/ cu ft requirement based on disk loading for the AH-1S helicopter and Figure A-2 of the DCD. It was required to be within 50% of that value. White quartz sand was used which had the required MOH hardness of 7 and was of similar particle size distribution with a slightly tighter

61

range. It was a little sharper, based on its Krumbein number of 0.1 versus 0.2 of the QTP. The sand product data sheet is attached as Appendix A.

During the sand tests, the tangential centerline velocity of the test coupon was 711 fps (485 mph) instead of 746 fps (509 mph), the tip speed of the K747 blade in hover. The intention was to run at 733 fps (500 mph), the same velocity as the rain erosion tests, but resonance was encountered at that velocity. Also a slight but variable imbalance in the blades occurred daily due to the need to brush coat the blades with an erosion protective coating after each day of testing. The sand erosion testing was therefore run at 95.3% of the QTP required velocity.

The DCD requires that the erosion protection system (EPS) be capable of operation in a sand cloud for a minimum of 10 percent of the blade design life. Blades with an unlimited life shall have a repairable EPS. The K747 blade has a 10,000 hour blade design life and the EPS is repairable. For a repairable EPS, the EPS Design Life (EPSDL) shall be capable of 12 hours of flight for each equivalent man-hour required for repair according to the following:

$$\text{EPSDL} = 12 \left[\text{Repair man-hours} + \frac{\text{Material Costs}}{(1.5)(\text{SIC labor rates})} \right]$$

To calculate the EPSDL requirement for the K747 erosion guard, the following information applies:

1. Repair man-hours will be the same as for the full length P0655 EPS, listed as 21 hours in Reference 2.

2. The latest SIC labor code 372 hourly wage is $17.16 for December 1992.

3. The total material cost to the Army is the current $1121 for 1993.

The minimum EPSDL for the K747 erosion guard becomes

$$\text{EPSDL} = 12 \left[21 \text{ hrs} + \frac{\$1121}{(1.5)(\$17.16)} \right] = 775 \text{ hrs}$$

From Reference 2, the mean flight-hours of the K747 erosion guard in 1985 was reported as equal to or greater than 300 hours. The population of K747 blades at that time included many with erosion guards of the old Estane material which, in a Kaman hydrolysis study using identical conditions as those herein, failed by melting in less than 90 hours. From recent data, the average flight-hours on 17 P0655 erosion guards replaced by US Army Aviation Units in Korea was 962 hours. Therefore, even with its inherently poor hydrolytic stability, the actual flight-hours per each man-hour of repair of the current P0655 erosion guard is 14.9, exceeding the DCD minimum of 12 flight-hours by 24%.

According to Kaman's K747 blade service representative, the primary causes for erosion guard replacement are material softening (hydrolysis) and foreign object impact damage from stones, gravel, tree branches, etc. These impact-damaged erosion guard failures are prejudiced by the degradation of the P0655 impact resistance properties caused by hydrolysis. There have been no known cases of erosion guards replaced strictly for sand erosion, and only one shipset was reported as removed due to rain damage. In that case, it was believed that the helicopter encountered hail which is a severe form of impact rather than rain erosion.

Using the relationship discussed in the Hydrolysis section of this report which states that 100 hydrolysis test hours relates to approximately 1 year of service exposure in hot and humid climates, the Miles 535330A material will survive hydrolysis-free for at least 12 years and the 3M Co. NPE 2916 material will survive hydrolysis-free for at least 38 years. This is a time-temperature-humidity function and is not related to flight hours.

Based on the EPSDL for P0655, a leading edge erosion guard fabricated from Miles 535330A will not fail due to hydrolysis for at least four times longer than the current P0655, which would indicate a hydrolysis-free EPSDL of 3860 flight-hours (962 x 1225 ÷ 305). Using the same relationship, a guard fabricated from 3M Co. NPE 2916 would indicate a hydrolysis-free EPSDL of 12,180 flight-hours (926 x 3862 ÷ 305), 20% greater than the 10,000 flight-hour K747 blade design life. The only reason for indicating less time and fewer flight hours for the Miles material is because its hydrolysis test was stopped at 1225 hours whereas the 3M Co. material hydrolysis test was allowed to accumulate 3862 hours. It is possible that the Miles material would also survive hydrolysis-free for as long as the 3M Co. material.

To estimate how long the K747 erosion guard will survive in sand is presented as follows. The QTP requires that sand erosion test be run at the tip velocity of the K747 blade in hover which is 746 fps. For the reasons discussed above, Kaman's sand erosion tests were performed at 711 fps or 95.3% of the QTP requirement. Since the sand was somewhat sharper than required, assume that the velocity and sand differences offset each other.

The average sample weight loss for P0655 was 0.025 gm and its measured density was 1.25 gm/cc. Average sand density for the P0655 tests was 0.01788 gm/cu ft and the visible effective eroded area of the specimens was 4.2 sq in. (2.1 in. spanwise and 1 in. each chord-wise on top and bottom).

Thus the average depth of material removed in 1 hour is:

$$\frac{\dfrac{.025 \text{ gm}}{1.25 \text{ gm/cm}^3} \times \dfrac{1 \text{ in.}^3}{16.39 \text{ cm}^3} \times \dfrac{60 \text{ min/hr}}{10 \text{ min}} \times \dfrac{.014 \text{ gm/ft}^3}{.01788 \text{ gm/ft}^3}}{4.2 \text{ in.}^2} = 0.0014 \text{ in/hr}$$

The maintenance manual for the K747 blade permits modifying the blade by removing the outboard stainless steel leading edge guard. The blade can then be flown with just the P0655 erosion guard. The outboard 36 inches of the P0655 erosion guard gradually increases in

63

thickness from 0.10 to 0.25 inch at the leading edge. Using the wear rate measured for P0655, the erosion guard would last for 179 flight-hours [0.25 in. ÷ 0.0014 in/hr] in sand erosion of the intensity described by the DCD. This is 23% of EPSDL, more than twice that required by the DCD. Using the same reasoning, the values for erosion guards of 535330A and NPE 2916 are compared to P0655 in Table 18.

TABLE 18. COMPARISON OF SAND EROSION RATES

	P0655	535330A	NPE 2916
Sample Wt Loss (gm)	0.025	0.0045	0.011
Density (gm/cc)	1.25	1.03	1.07
Sand Density (gm/cu ft)	0.01788	0.01975	0.01666
Wear Rate (in/hr)	0.0014	0.00027	0.00075
Sand Flight Hours	179	926	333
% of EPSDL	23	119	43

By the above calculations, the Miles 535330A erosion guard would last twelve times longer than required to meet the DCD for sand erosion and it would almost qualify as a lifetime erosion guard for the K747 in regard to sand erosion.

These calculations are based on extrapolated wear rates only and not on actual times to failure. All the materials except Elastuff 504 exhibited microscopic surface splits after the test. This is probably an indication that the materials will fail earlier by some fatigue mechanism rather than the time predicted by their erosion rates. Running the samples to failure would determine whether the 10% of EPSDL requirement is reasonable for the sand erosion test parameters of the DCD.

For rain erosion, the DCD requires that a repairable EPS be capable of flying in rain for 1.5% of the EPSDL in a 0.5 in/hr rainfall and for 0.5% of the EPSDL in 1 in/hr rainfall during forward flight at 85% of the maximum normal cruise speed in level flight (V_H). Reference 2 assumes that as long as the material has time to unload between impacts and the particle size distribution of a 1 in/hr rainfall is used, then results are directly proportional to intensity. This assumption has been incorporated into the QTP. Thus, by combining the two intensities, the EPS shall be capable of flying in rain for 1.25% of the EPSDL in a 1 in/hr rainfall. In the K747 case, the EPS is therefore required to survive for 9.7 hours in a 1 in/hr rainfall.

At 85% V_H, the test speed described in the DCD, the relative tip velocity of the AH-1S helicopter main rotor blade is 939 ft/sec. The QTP varies from the DCD by stating that higher test specimen velocities "may" be used other than the tip velocity of the rotating wing in hover, which is 746 ft/sec. The rain erosion tests herein were conducted at 733 ft/sec

64

which is a common specification requirement and the same velocity as tests previously conducted by Kaman.

Only one of the materials recommended for the detail design task, 3M Co. NPE 2916, has the potential for meeting the current DCD rain erosion requirement. Samples of 0.060 inch thickness were tested for 1060 minutes (17.7 hours) at 733 ft/sec and the surface of each remains unblemished except for a premature failure caused by the end clamps of the test rotor. If the rain erosion rate is considered linear with respect to velocity, then at 85% V_H, 939 ft/sec, the NPE 2916 rain erosion results would decrease to 13.8 hours which is 42.3% greater than the DCD requirement. It is believed, however, that rain erosion rate increases exponentially with increasing velocity. The degree to which this would reduce the 733 ft/sec test results is unknown. However, since the material had not failed and the surface was still in good condition after 17.7 hours, there is reason to believe that it will meet the DCD requirement of 9.7 hours. Using the same analogy, the 535330A and P0655 materials would both fail after approximately 3 hours, 31% of the same requirement.

The impact tests using ½ in., ¾ in., and ⅞ in. hardwood dowels relate to 5.33%, 8.00% and 9.33% respectively of the thrust-weighted chord length. The DCD requires that strikes of hardwood branches with a diameter of 6% of the blades thrust-weighted chord length shall not require unscheduled maintenance other than minor painting, and that strikes of 12% shall not cause an aborted mission. The 535330A passed at 5.33% and may have passed at 9.33% as explained earlier. NPE 2916 passed at 9.33%. It is therefore possible that both materials will pass at 12% without causing an aborted mission requirement.

These discussions show that significant improvements in erosion protection systems have been attained as a result of the materials evaluation effort.

PROCESS DEVELOPMENT

NPE 2916

The initial plan for fabricating a full-length NPE 2916 erosion guard was to form it in the production mold at CUE Inc., the company that produces the current erosion guard from PO655 for the K747 blade. NPE 2916 is a thermoplastic material and can be heat-formed using heat and pressure. The production tool is normally heated to 230°F during the curing of PO655. The upper male plug is machined aluminum and the lower female mold is nickel-plated epoxy. Because alignment of the tool is critical, it was decided that the mold should be maintained at the same temperature to prevent possible damage to the tool or alignment.

Preliminary molding trials at Kaman were begun using a small laboratory press to determine molding parameters. A cylindrical steel plug was machined to act as an insert around which attempts would be made to flow the NPE 2916 without development of porosity or other unforeseen problems. Five molding trials were run which showed that the material would mold successfully at 500 psi and 230°F for 5 minutes.

Molding trials were begun at CUE Inc. using 0.020 in. thick material samples in a small laboratory airfoil-shaped mold at 220-230°F. Initial moldings using four layers were porous. Subsequent trials using tapered layers continued to result in porous parts. Single layer samples of 0.250 in. thick material succeeded in reducing porosity; however, the material tore upon removal from the mold. Finally, 0.120 in. thick, single-layer material was tried in the production tool for the 46.5 in. long outboard replacement erosion guard, commonly called the short boot, for the K747 blade. Even at temperatures up to 250°F, the tool was unable to develop enough pressure to fill the cavity. Due to these tooling limitations, further efforts to form NPE 2916 in this manner were abandoned.

Emphasis was then focused on the contingent plan, a staggered-width, multilayered approach using heat, vacuum and pressure to form the erosion guards at Kaman. This process was similar to that used for the original Estane erosion guards for the K747 blade. Multiple layers with staggered widths were used to develop the tapered top and bottom aft edges of erosion guard. On the top surface of the blade, the erosion guard tapers down in thickness in the aft 1 inch of blade width; on the bottom surface the taper occurs in the aft 2 inches.

Seven laboratory trials were required to determine the important parameters for forming void-free laminates with minimum outflow of material at the laminate edges. It was determined that autoclave pressures were not required. A void-free part could be fabricated using a vacuum bag/oven technique only. Six plies of 0.020 in. thick NPE 2916 provided the best acceptable taper. The first two plies were identical in size. Each of the remaining four plies was staggered back ¼ in. from the edge of the one underneath it. This stackup was vacuum-bagged and fused at 275°F for 30 minutes while gradually increasing vacuum to 28-29 inches Hg. Figure 18 shows a typical vacuum bag assembly from a laboratory trial.

66
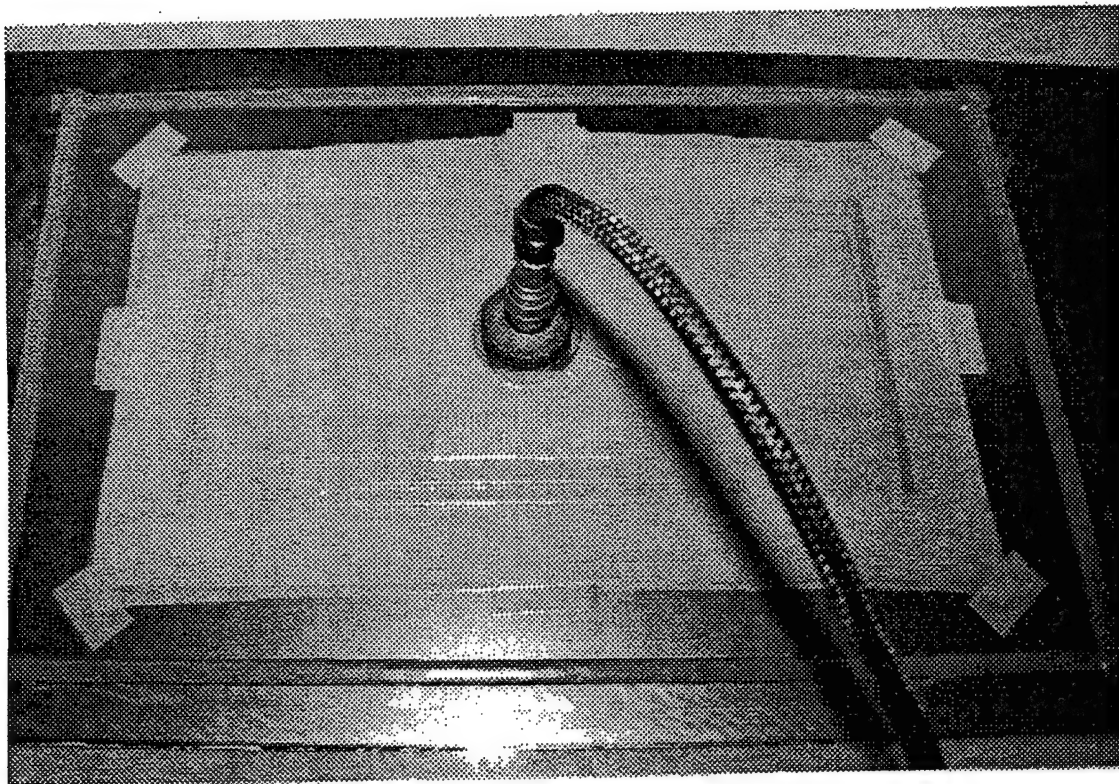
Figure 18. Laboratory Vacuum Molding Trial of NPE 2916.

After establishing the above processing parameters, the ply patterns for the full-length erosion guards were developed. The plies would be fused or melted together on a flat plate using vacuum bag pressure and an oven. This would yield a flat erosion guard similar to those of the original Estane erosion guards of the early K747 blades. Since the outboard 40 inches of the K747 leading edge is swept back from the straight inboard leading edge, ply pattern development required consideration of the sweep angle and the chordwise arc lengths at various spanwise stations. Arc lengths were determined from CAD drawings and the ply patterns were developed. Coordinates from the pattern of each ply were used to program a computer-controlled, automated ply cutting machine used for cutting fiberglass and graphite fabrics, film adhesives and prepreg materials.

535330A

The 535330A material is a two-part castable urethane system similar in processing characteristics to the current K747 erosion guard PO655 material. In addition to the prepolymer (Part A) and the curative (Part B), it is common practice to incorporate a third component, a color concentrate, to impart the desired color to the finished item. PO655 derives its black color from a color concentrate containing carbon black pigment in a urethane-compatible resin. During the course of this study, it was learned from conversations with government and industry scientists that the type of pigment can influence rain erosion resistance of elastomeric

erosion guards and erosion-resistant paints. Specifically, carbon black pigment was identified as having a detrimental effect while certain dyes and inorganic pigments did not degrade rain erosion resistance to any significant degree. This prompted a search for a suitable black coloring agent for 535330A.

Potential use of dyes was discussed with technical representatives and dye chemists from Ciba-Geigy's Dyestuff division. After explaining the harsh UV and weathering environment that a leading edge erosion guard is expected to endure for many years, the use of dyes was rejected for further consideration. Based on carbon arc, lightfastness data, it was concluded that all of the dyes being considered could be expected to sublime and change color or to fade after long exposure to UV radiation. Carbon blacks and inorganic pigments were recommended for long-term color stability.

Concern about the type of pigment in NPE 2916 was discussed with 3M Co. It was confirmed that it contained a Ni/Cr/Mn black inorganic pigment, but the source was proprietary. Ten U.S. pigment suppliers were contacted, namely Plasticolors, Inc., Harshaw Chemical Corp., Du Pont, Ciba-Geigy Pigment Div., Cerdec Corp., Cookson Pigments, Toyo, Inc., Shepard Color Co., Englehard Corp. and Ferro Color Div. None had a Ni/Cr/Mn black inorganic pigment that did not contain Fe. Cerdec had a Ni/Cr/Mn/Fe pigment, 10333 Black, which had an average particle size of 2.9 microns. To minimize the potential for polymer crack initiation from the fatiguing impact of raindrops, it was considered desirable to obtain the smallest particle size possible. Cerdec was willing to produce a fine particle version of 10333 Black and supplied samples of a 0.45 micron size pigment identified as 154-9-A.

A color concentrate was produced using 154-9-A, the 535330A curative (Part B) and a small amount of a dispersant, Anti-Terra-U100, which greatly enhances pigment wet-out. The color concentrate was sent to CUE Inc. for evaluation in laboratory batches of 535330A. They found that the pigment produced a deep brownish color rather than the desired black. Discussions with Cerdec confirmed that in a tinting comparison, 154-9-A is reddish and that grinding it to a very small particle size enhances the redness. Another pigment, Black 2980, was suggested. It is a Co/Cr/Fe pigment and available off the shelf at 0.9 micron. One of its common uses is the tinting of automobile windshields. A color concentrate was formulated with this pigment and it produced an acceptable black color in 535330A.

After reviewing the processing parameters and the health and safety aspects of 535330A, process engineers at CUE decided that a trial run was necessary to test the ability of the equipment to safely pump, meter, mix and degas the new material. The viscosity of the 535330A prepolymer is about four to five times more viscous than the materials normally processed. It also is more sensitizing from a health and safety point of view. The trial run, using a more conventional prepolymer with a viscosity similar to that of 535330A, was successfully completed. This showed that 535330A could be processed normally in the standard production equipment.

DETAIL DESIGN

Two detail design drawings were developed. Drawing XK747-216, Appendix C, describes the geometry, materials, processes and quality requirements for two leading edge erosion guards, one made from NPE 2916 and one made from 535330A. It also describes the materials, process and quality requirements for the 535330A color concentrate. Drawing XK747-215, Appendix D, describes the configuration, materials, processes, blade balance and quality requirements of test blades with the experimental erosion guards. The detail design drawings were accepted by AATD and approval was granted for fabrication and installation of the full-length erosion guards.

A detail design review was held at Kaman. Items discussed were the detail design drawings, specifications associated with the drawings, process development of 535330A at CUE, process development of NPE 2916 and flight test plans for the new erosion guards. Laboratory samples, vacuum bag tooling and laboratory equipment used in the process development efforts of NPE 2916 were observed.

Flight test options for the modified blades were discussed. It was decided that the most program value would be gained if three helicopters were used. One would be equipped with a 535330A protected blade and an NPE 2916 protected blade. Another would use a 535330A protected blade and standard PO655 protected blade. A third would be equipped with an NPE 2916 protected blade and a standard PO655 protected blade. The standard PO655 protected blades, used as controls, would be flown without their stainless steel erosion guards. They would match the configuration of the experimental blades, yield a direct comparison of erosion data and allow more rapid accumulation of data. Of less value to the program would be to equip two helicopters each with one 535330A protected blade and one NPE 2916 protected blade. Of least value would be to equip one helicopter with both blades having 535330A erosion guards and one with both blades having NPE 2916 guards.

FABRICATION OF FULL-LENGTH EROSION GUARDS

NPE 2916

For the first full-length erosion guard fabricated with NPE 2916, six staggered-width plies of 0.020 in. sheet stock were cut on Kaman's computer-controlled, automated ply cutting machine. They were stacked, vacuum-bagged and fused together using a final vacuum of 28+ in. Hg for 30 minutes at 275°F. Figure 19 shows the layup of plies before vacuum-bagging. The quality of this erosion guard was excellent. A shiny external surface had been achieved by forming it against a 0.0005 in. thick fluoropolymer film that had been stretched tight and taped to an aluminum base plate.

A dry-fit bonding trial was performed using this first NPE 2916 erosion guard. An unacceptable wrinkle developed on the upper surface at station 224.4, the spanwise location on the blade where the leading edge sweeps back from the inboard straight line of the blade leading edge. Because the NPE 2916 guards are formed flat and have to be wrapped around the blade leading edge, a buckle or wrinkle was expected at the aft edges of the erosion guard on the top or bottom surfaces at this station. The extent to which the elastomeric material could accommodate it was unknown. Under vacuum, the material was forgiving enough to absorb the lower surface wrinkle during the resin squeegeeing operation. However, the change in geometry of the upper surface is greater and the wrinkle could not be squeegeed smooth.

For the second erosion guard, the ply cutter computer program was modified to cause a small wedge-shaped thickness reduction in the upper surface trailing edge at station 224.4. Attempts to tape the 0.0005 in. fluoropolymer film to the base plate without wrinkling were unsuccessful. A 0.002 in. fluoroplastic film, Airtech 4600 White, claimed by its manufacturer to be good to 400°F, was substituted to produce a glossy external surface. However, the film appeared to shrink and cause wrinkles when subjected to the 275°F forming temperature. This in turn caused a regularly spaced series of chordwise wrinkles in the external surface of the guard.

The third NPE 2916 erosion guard was also fabricated with the same wedge-shaped thickness reduction at station 224.4, upper surface. It was formed against the release paper supplied with the material sheet stock to provide a matte finish to the guard outer surface. Although the formed guard did not release as well from the paper as it did from the fluoroplastic film, it did release with care and provided a uniformly, wrinkle-free matte finish.

No wedge-shaped reduction of thickness at station 224.4 was incorporated into the fourth and final NPE 2916 erosion guard. Since the original dry-fit bonding trial of the first NPE 2916 guard, observations were made of the bonding of production erosion guards to production blades. It was learned that the wrinkling observed during the dry-fit bonding operation was due to the placement of a vacuum hose at station 224 and not to the inability of the material to conform to the blade at that location. The vacuum bag wrinkles because it is gathered in that area to rise over the vacuum hose. Those wrinkles in the vacuum bag pull wrinkles into the erosion guard itself. Placement of a vacuum hose at this location during bonding of the production guards does not present the same problem because the PO655 guard is molded into
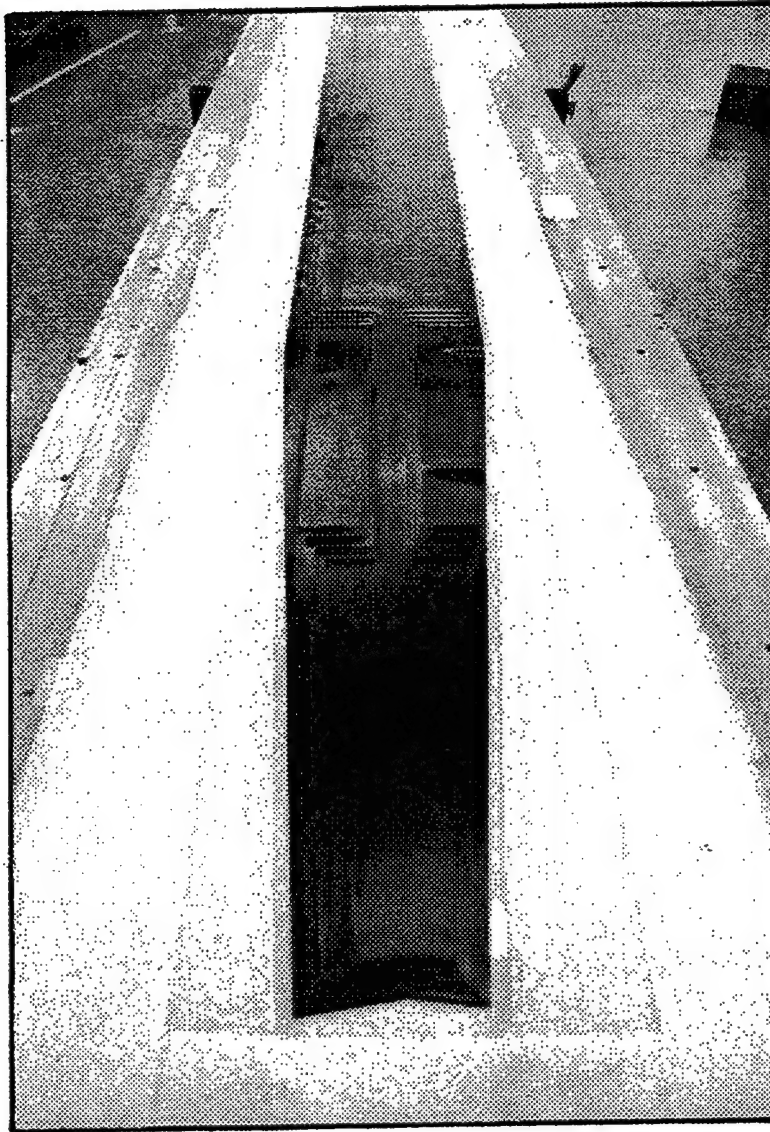
Figure 19. Layup of Plies for NPE 2916 Erosion Guard Before Vacuum-bagging.

a C-shaped cross section with the swept-back configuration molded into it. This is in contrast to the NPE 2916 guards that are molded flat. The fourth erosion guard was formed against the same type of release paper used for the third guard and it looked equally good. Both the third and fourth guards with their matte finish were selected for bondment to blades for operational evaluation.

<u>535330A</u>

The first attempt to fabricate full-length erosion guards at CUE from 535330A was performed by Miles and CUE personnel using a Miles recommended cure of 230°F for 45 minutes. All of the guards developed holes and rips upon removal from the tool.

A second attempt was made by the author and CUE personnel. A standard production PO655 erosion guard had been allowed to stay overnight in the heated and closed mold. Upon its removal from the mold, a hole at station 246 lower surface and rips at stations 176 lower surface and 142 upper surface were observed. These were above the trim line and presented no problems. CUE personnel said that, based on their previous trials, if the guard had been fabricated from 535330A instead of PO655, the rips would have progressed past the trim line, making it unacceptable. Thickness measurements of the guard upper and lower surfaces at those stations suggested that the male plug apparently shifts upon tool closure toward the sides of the female tool where the hole and rips occur. To offset this tool shifting, three 0.010 in. thick brass shim strips ending 2 inches above the trim line were positioned on the lower female tool at the stations described above. Figure 20 shows the shim at station 246 lower surface.
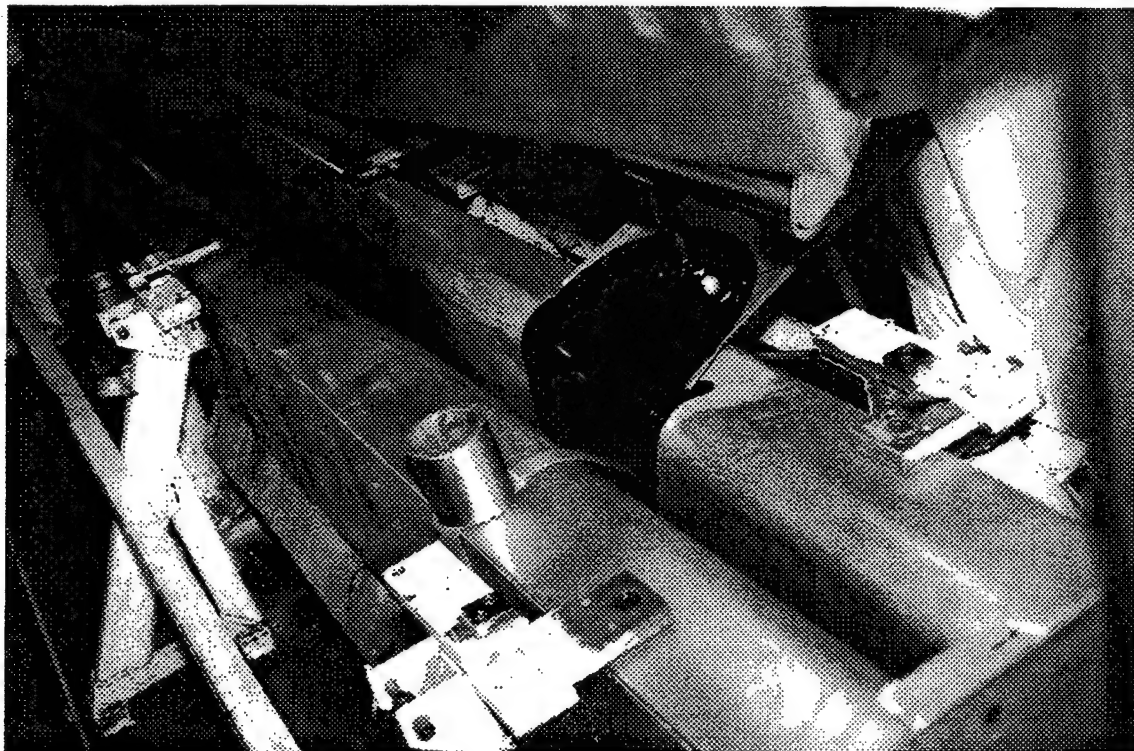
Figure 20.   Casting 535330A into Tip End of Mold Cavity. Note Brass Shim at Station 246 Lower Surface.

72

The first experimental unit was poured using automatically metered and mixed 535330A. As with the PO655 material, 24 lb of the mixture were poured into the outboard end of the female mold and 6 lb were poured into the inboard end. A mechanical problem was encountered which caused a delay when attempting to close the mold. After a 45 minute cure, the part was carefully demolded. The material did not fill the outboard end completely. This was probably a result of the delayed mold closure which allowed material to flow away from the slanted outboard end. Some minor rips developed during demolding but all were above the trim line. Had the outboard end filled properly, this would have been an acceptable erosion guard.

A second experimental unit was repeated identical to the first but this time the mold closed properly. There was just enough material to fill the outboard end. Again some minor rips were present but the material had developed enough strength such that the rips all terminated above the trim line. The part was acceptable.

The third unit was a repeat of the second except that the pour ratio was 27 lb outboard and 3 lb inboard, as was the case for all successive units. There was better material fill at the outboard end and the part was also acceptable.

Units four and five were identical repeats of unit three; however, unit four had two rips and unit five had three rips below the trim line. This made them unacceptable for use. One rip on unit five was at a new location, station 77 lower surface. As a result, a fourth brass shim strip was positioned at that station for successive units.

Since the parts were apparently getting weaker as evidenced by an increasing number of damaging rips, mold surface temperatures were measured with a surface pyrometer. The upper male plug surface was only 170°F and the lower female surface was 200-210°F. The reason for the difference is that only the lower female half of the tool has heating elements. The upper male plug obtains its heat by heat transfer from the lower female half when the tool is closed. Before these experimental trials were started, the tool had been closed and heated overnight with a PO655 guard in place. This allowed both mold halves to attain equilibrium temperatures before the production guard was removed. The PO655 guard is normally demolded after a 2-hour in-the-mold cure and then oven postcured for 18 hours at 230°F. During these experimental trials, the mold had been opened more frequently and for longer times than usual, thus causing the mold to run cooler than expected.

Unit six was run similar to four and five except that the cure time was increased to 1¼ hour. Due to excess porosity, the part was not acceptable. The prepolymer line was checked for porosity and it also contained many gas bubbles. The pump was then run until the porosity disappeared from the line. A reason for gas bubbles in the line was never determined.

Units seven and eight were fabricated similarly to six and both were acceptable. All units except discarded unit six were postcured for 18 hours at 230°F. Units two and three were selected for bondment to blades for operational evaluation.

INSTALLATION OF THE ARBEPS EROSION GUARDS

Four K747-003-403 composite main rotor blades suitable for modification with the full-length experimental erosion guards were located at Ft Drum, NY. Upon their arrival at Kaman, they were subjected to an incoming visual and sonic inspection to determine their as-received condition. The inboard hardware, outboard stainless steel erosion guards and the elastomeric PO655 erosion guards were removed from all the blades. They were then prepared for bonding to accept the full-length experimental erosion guards fabricated above.

Full-length 535330A erosion guards were bonded to two of the prepared blades following standard procedures employed for the current PO655 erosion guards. The internal guard surfaces were prepared for bonding by solvent wiping with MEK and by scuffing aggressively with 60 grit disc sanders as shown in Figure 21. This procedure removes final traces of silicone mold release agent that inevitably transfers to the part during the casting operation at CUE. The guards were bonded with KPS 146 (Kaman Process Specification No. 146) adhesive. This is a room temperature curing epoxy mixture containing 100 pbw (parts by weight) Epon 826 epoxy resin, 10 pbw Versamid 125 polyamide curing agent and 6 pbw diethylenetriamine curing agent. One ply of 120 style glass fabric was used in the bondline to insure a minimum bondline thickness and to aid in subsequent removal of the erosion guard. Figure 22 shows excess adhesive being squeegeed from the bondline during vacuum bag bonding operation. A 1-in. x 6-in. strip of erosion guard material is also bonded to the blade at the same time using the same process and adhesive mixed batch. It is a 180-degree peel test sample and a standard process control procedure whenever an erosion guard is bonded to a blade. The guard and sample are vacuum-bagged and held in place under vacuum overnight to allow the adhesive to set. After a minimum cure time of 24-hours, the process control peel test is performed. Both blades passed the required minimum of 10 lb per inch of width.

No silicone release agent was used during the fabrication of NPE 2916 guards. To determine the value of scuffing the internal bonding surface of the NPE 2916 guards, a cursory bonding experiment was performed. Two 1-in. x 6-in. peel test sample strips each of 535330A and NPE 2916 material were solvent wiped and scuffed. Another peel test sample strip of NPE 2916 was solvent wiped but not scuffed. These were bonded to a K747 blade spar according to the same procedure used for bonding erosion guards to production blades. After a three-day cure at room temperature, a 180-degree peel test was performed. Test results are shown in Table 19. Although the unscuffed NPE 2916 sample surpassed the minimum 10 lb per inch of width requirement, it was decided that to obtain maximum strength, scuffing would be performed on the NPE 2916 guards.

Two of the NPE 2916 full-length erosion guards were bonded to the other K747 blades by methods similar to those of the original flat Estane erosion guards. When these were solvent wiped, it was observed that the surface texture was permanently affected by MEK, 1,1,1-trichloroethylene or isopropyl alcohol. Aliphatic naphtha proved to be satisfactory and was the only solvent used thereafter.

74

Figure 21. Scuffing Internal Surface of 535330A Erosion Guard in Preparation for Bonding.
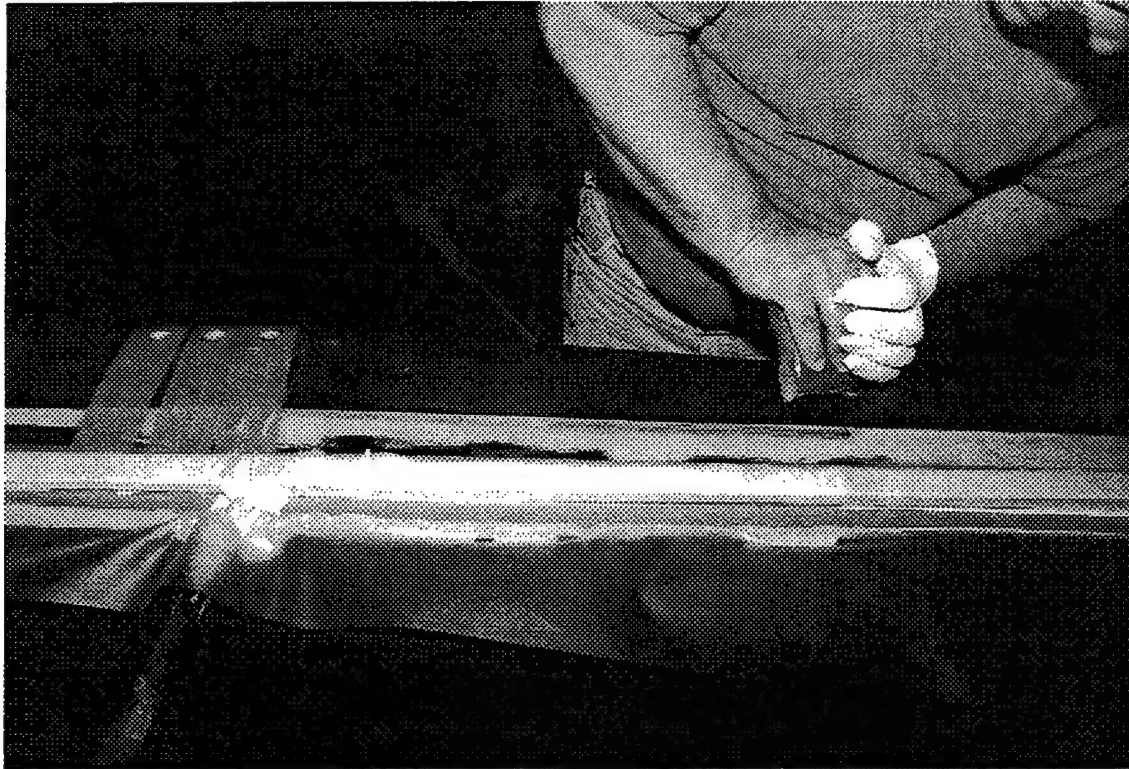
Figure 22.   Squeegeeing Excess Adhesive from Bondline during Vacuum Bag Bond Operation.

TABLE 19. PEEL TEST SAMPLES

Material	Condition	lb/in.
535330A	Scuffed	28 >30
NPE 2916	Scuffed	28 >30
NPE 2916	Unscuffed	16

On the last K747 blade with the NPE 2916 erosion guard, the process control peel test sample failed at 6-8 lb per inch of width. The last inch of the specimen was left bonded to the blade for later testing. After 5 more days at room temperature it was retested and again only developed 6 lb per inch peel strength. When the process control test fails, it is standard procedure to test the actual erosion guard. Therefore, a 1-inch-wide test cut was made on the inboard bottom surface of the erosion guard. It developed a satisfactory 16-lb-per-inch peel strength. The test area was repaired following established repair procedures.

When the above process control peel test specimen was bonded to the blade spar, it was inadvertently placed upside down with the smooth top surface against the wet adhesive bond line. It was removed, turned around and replaced properly with the abraded side toward the bond line. This may have contributed to low peel strength. During fabrication of the panel from which the 1-inch-wide peel test specimen was taken, a sheet of silicone rubber was directly against the panel top surface and probably contaminated it with trace amounts of silicone oil. When the specimen was placed against the epoxy adhesive, it may have contaminated it and caused the low strength. Even small amounts of silicone oils are notorious for contaminating bonding surfaces, adhesives and coatings. Solvent cleaning followed by surface grinding are required to remove it from elastomeric bonding surfaces.

The current K747 blade configuration has a 43.5-inch-long, stainless steel, leading edge guard covering the outboard end of the PO655 guard as shown in Figure 2. Its purpose is to enhance rain and impact resistance. Conversely, its resistance to sand erosion is much worse as evidenced by the sand erosion wear rates shown in Figure 1 for stainless steel versus poly-urethane. During extensive desert operations, the blades can be modified in the field and flown without the stainless steel guards. After the guard is removed, six stainless steel shields are installed with new self-locking screws as shown in Figure 23. These shields are elongated countersunk washers that cover attachment cutouts in the PO655 guard. The cutouts are through holes which allow the shields to seat directly against the attachment posts bonded in the blade. A process was developed whereby most of the attachment holes were cut in the experimental erosion guards using a ⅞-inch OD hole saw during prebond dry-fit operations. K747 blades that have the stainless steel erosion guard so removed are called field-modified. This configuration was chosen for the test blades so erosion effects would appear sooner. They were 3-scale balanced to match field-modified production blades.
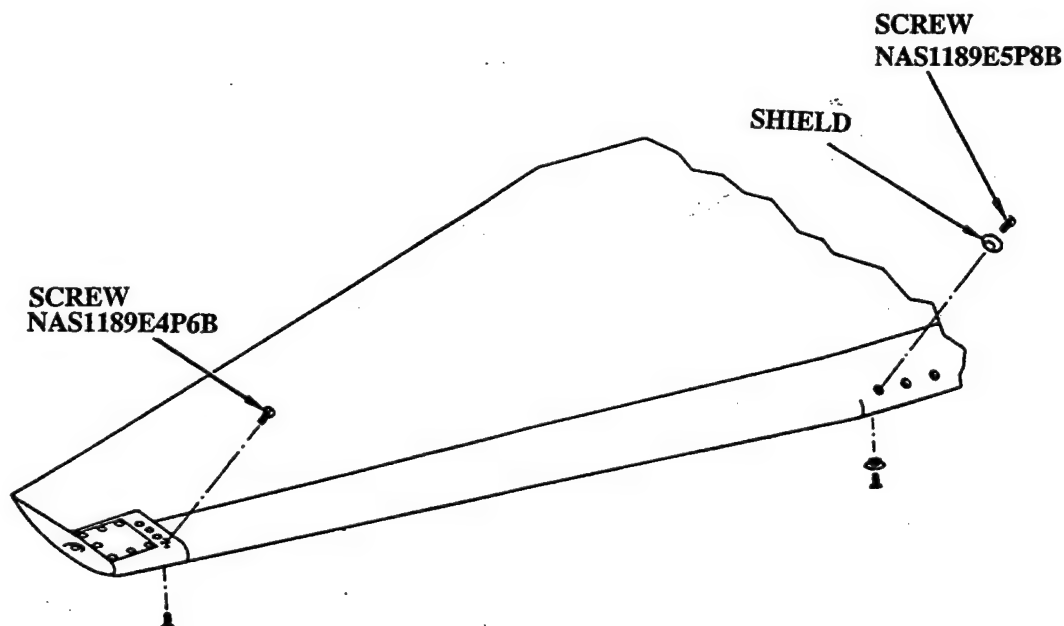
Figure 23. Installation of the Shields.

77

SAFETY-OF-FLIGHT REVIEW

A safety-of-flight review was held at Kaman to determine the airworthiness of the blades with the new materials. It was attended by representatives from ATCOM, St. Louis; AATD, Ft. Eustis; and Kaman.

A background of leading edge erosion guard performance and the reasons for initiating the ARBEPS program were presented. The ARBEBS program was reviewed, including the materials survey/selection process and the testing which resulted in two materials chosen for full-scale operational evaluation. Drawings for the erosion guards and blade modification (Appendices C and D) were examined and the different methods of fabrication for each material were discussed. Examples of full-length erosion guards fabricated from each material were presented and blades in various stages of boot bondment were shown. Incoming inspection records of the test blades, bonding process instructions and process control peel test results were reviewed.

An Airworthiness Substantiation Document, previously prepared by Kaman and approved by AATD, was examined and discussed. It is a comprehensive System Safety Hazard Analysis of the safety risks assumed for the ARBEPS prior to full-scale flight testing. Those risks were identified and treated as follows:

> Hazards associated with loss or partial loss of the erosion guard in flight are controlled to the same level and in the same manner as on the basic K747 blade. The blade and method of attaching (bonding) the guard to the blade remain unchanged. Materials and processes used in attaching the erosion guard also remain unchanged. Verification of the bonding process and the adequacy of the bond attained is achieved through the use of peel test samples. Criteria for the peel test samples are identical to those required for the K747 blade.

> Hazards associated with voids and discontinuities between the erosion guard and blade during manufacture and repair are controlled to the same level and in the same manner as on the basic K747 blade. Total weight, chordwise center of gravity, and span moment are controlled to the same level and in the same manner as on the existing blade.

> Flight with the outboard stainless steel leading edge removed from the blade is an accepted practice and authorized by training manual TM-55-1520-236-23-1.

It was concluded that the new designs introduce no additional hazards beyond those of the production K747 blades and that the existing methods of hazard control are not degraded by the new designs.

ARBEPS FLIGHT TESTING

Upon completion of the safety-of-flight review, all four blades were made ready-for-issue. The root end hardware was attached and the blades were marked by white stenciled characters on the inboard lower surfaces for easy identification from the ground. All four blades were delivered to the Aviation Center at Fort Rucker, AL, and two spare erosion guards, one each of 535330A and NPE 2916, were delivered to AATD at Ft Eustis, VA. Correlation of erosion guard materials to blade serial numbers are shown in Table 20.

TABLE 20. CORRELATION OF EROSION GUARD MATERIALS TO BLADE SERIAL NUMBERS

Blade S/N	Blade P/N	Erosion Guard P/N	Erosion Guard Material
A3653	XK747-215-001	XK747-216-011	535330A (Miles)
A4777	XK747-215-001	XK747-216-011	535330A (Miles)
A5270	XK747-215-003	XK747-216-013	NPE 2916 (3M)
A5699	XK747-215-003	XK747-216-013	NPE 2916 (3M)

The Army decided to use two helicopters for flight testing. Each of the two-bladed helicopters was equipped with one blade having a 535330A erosion guard and the other having one of NPE 2916.

STRESS WAVE/PARAMETRIC ANALYSIS

In parallel with the materials survey, identification and evaluation tasks, Kaman contracted General Research Corporation (GRC) to: (1) develop a stress wave computational model of a raindrop impact with an elastomeric erosion guard material, and (2) use the model to examine the influence of various parameters on the erosion protection material.

To realistically evaluate the transient response of the erosion protection system for raindrop impacts, dynamic material properties at 10^4 to 10^5 s^{-1} strain rates and large strain levels were required for input into the computational model. A literature survey was performed and suppliers of property measurement equipment were contacted by GRC. A few techniques were able to approach 10 percent strain levels; however, greater than 50 percent was required. GRC proposed a novel and ingenious test procedure incorporating a 50 mm powder gun and a unique specimen loading system. The required dynamic material properties were generated by that technique, including ultimate tensile stress and strain to failure. Surprisingly, the poly-urethanes tested under large strain conditions do not exhibit the anticipated tendency toward more brittle behavior at the 10^4 to 10^5 s^{-1} strain rates associated with water-drop impacts. Instead, they display surprisingly low moduli during large strain extensions.

Using as input the newly acquired material properties at the relevant strain rates, the computational model was exercised to determine the influence of parameters, such as dynamic material properties, material thickness, angle of attack, and raindrop size on the ability of the material to function as a rain erosion protection system.

The analytical and testing contributions by GRC are described in their entirety in Appendix E.

CONCLUSIONS

As a result of this program, two new hydrolysis-free materials have been identified, tested, fabricated into full-length leading edge erosion guards and applied to government-furnished helicopter rotor blades for operational flight evaluation at Ft. Rucker, AL. One material, NPE 2916 from 3M Company, exhibits more than four times the rain resistance and twice the sand resistance as P0655, the current erosion guard material on the K747 blades. The other material, 535330A from Miles, Inc., has six times the sand resistance of P0655 and equivalent rain resistance.

The same 3M material as above, when produced in a 0.012-inch-thick tape with a new high shear pressure sensitive adhesive, also delivers outstanding rain erosion resistance. Although the sand erosion testing indicates a slow wear rate, the development of surface splits progressed to the bondline and allowed sand intrusion after only 10 minutes of testing. These results confirmed Army reports of similar occurrences on erosion protection tape used in operation Desert Storm. Pinholes would develop in the tape. These would fill with sand and grow until large sections of tape would tear loose. Impact resistance of all tapes tested was poor. They would split upon impact and slide outboard as a result of the centrifugal force effect of the whirling blades.

A sprayable, hydrolysis-free erosion protection coating, Elastuff 504 by United Coatings, exhibited good rain and sand erosion resistance. Elastuff 504 was the only material which did not develop small surface splits from the sand erosion test. Potential locations for use are leading edges for tail rotor blades and highly erosion susceptible afterbody areas on main and tail rotor blades.

Of the small number of two-part systems tested, TSK L100 performed adequately as a repair material. Rain erosion, sand erosion and solar radiation properties are not as good as those of the above materials; however, as a repair material it can be reapplied as often as necessary. Because it cures relatively quickly, the helicopter can be returned to operational status in a reasonably short period of time.

In addition to identifying new leading edge guard materials, this program provided the opportunity for a direct comparison of erosion protection materials currently in use or in the Army inventory. These are P0655, TSK L101, TSK L100 and 8663.

Based on the results of the materials evaluation task, the Design Criteria Document (DCD) and the Qualification Test Procedures (QTP) have been modified to include the hydrolysis requirement. Sand particle size distribution and Krumbein number have also been updated to reflect those used in this program. Upgraded DCD and QTP are presented in Appendixes F and G.

The dynamic three-dimensional finite element analysis developed for this program provides a significant advance over previously available analyses. The duration and general features of a waterdrop impacting a highly deformable polymeric layer can now be quantified with respect to the material properties of the layer.

Another significant advancement was development of a powder gun flyer plate test procedure for obtaining fundamental material properties including strain-to-failure measurements of elastomeric polymers at large strains and high strain rates. Surprisingly, the polyurethanes tested under large strain conditions do not exhibit the anticipated tendency toward more brittle behavior at 10^4 to 10^5 s^{-1} strain rates. Instead, they display low modulii during large strain extensions. The strain-to-failure measurements did not display a large variation from material to material. All of the polymeric materials remained rubbery with minimal strains-to-failure of around 300 percent.

Insertion of the measured material properties into the finite element model, the first time a realistic simulation of the waterdrop impact has been achieved, shows that the maximum calculated tensile strains for waterdrop impacts were around 80%. On the basis of these results, a single waterdrop impact would not be capable of initiating erosion failure for the materials evaluated. Although ultimate strain and modulus are significant, additional factors may need to be considered to develop a means for ranking erosion resistance. It has been hypothesized that high strain fatigue may be a potential contributor to erosion damage.

In summary, the technology of erosion protection has been advanced as a result of this program. New commercially available erosion protection materials have been proven effective by extensive testing. Full-length leading edge erosion guards have been fabricated in production facilities. Demonstration blades using the new materials are being flight evaluated. Design criteria and qualification test procedures have been modified to update erosion-resistant material requirements. A three-dimensional finite element analysis program which models a raindrop impacting an elastomeric material has been developed, as was a new and unique test method for determining material properties not previously measurable. Improved procedures for evaluating erosion protection systems and the analytical tools for increasing the understanding of erosion protection have been established.

REFERENCES

(1) Falcone, A.S., Clark, F., and Maloney, P., "**Elastic Pitch Beam Tail Rotor Operational Suitability Investigation**," USAAMRDL-TR-74-60, Contract DAAJ02-71-C-0063, U.S. Army Air Mobility Research and Development Laboratory, Fort Eustis, Virginia, July 1974.

(2) Haynie, D.A., "**Rotor Blade Erosion Protection System**," USAAVSCOM TR-88-D-24, Contract DAAK51-84-C-0033, Aviation Applied Technology Directorate, US Army Aviation Research and Technology Activity (AVSCOM), Fort Eustis, VA, February 1989.

(3) Hintermister, R., "**Test Report for Demonstrations of the AH-1 Improved Main Rotor Blade Erosion Protection System**," Kaman Aerospace Corporation Report T-668-1, Contract DAAJ01-75-C-0806, U.S. Army Aviation Systems Command (AVSCOM), St Louis, MO, February 1977.

(4) White, M.L., "**Development and Qualification of an Improved Leading Edge Guard for the K747 Main Rotor Blade**," Kaman Aerospace Corporation Report T-778, Contract DAAK50-80-G-0003, U.S. Army Aviation Systems Command (AVSCOM), St Louis, MO, 22 September 1982.

(5) Hurley, Charles, J., Schmidt, George F. Jr., "**Development and Calibration of a Mach 1.2 Rain Erosion Test Apparatus**," U of Dayton Res. Inst., AFML-TR-70-240, October 1970.

NEW ENGLAND SILICA, INC.

PRODUCT DATA
MYSTIC WHITE® QUARTZ NO. 90 SILICA SAND

TYPICAL SIZE ANALYSIS:
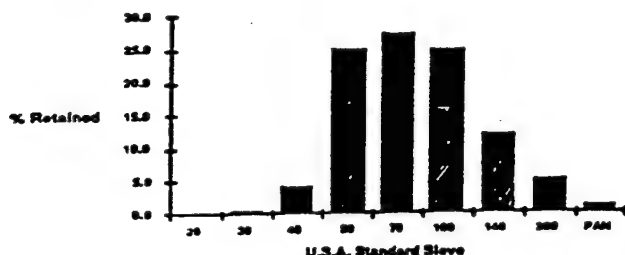
Plant: Ledyard, Connecticut
Form Number: 52032
Date: November, 1990

ORDER PLACEMENT INFORMATION:

Telephone: (203)289-7778
Truck Shipping Point: Plant Site Ledyard, CT
Rail Shipping Point: South Windsor, CT
Available in Bulk & 100-lb. Bags

U.S.A. Std. Sieve	Millimeter Designation	% Retained On Sieve		% Retained Cumulative	% Passing
		Mean	Range	Mean	Mean
20	.850	0.0	0-T	0.0	100.0
30	.600	0.3	0-1	0.3	99.7
40	.425	4.0	0-8	4.3	95.7
50	.300	25.0	15-35	29.3	70.7
70	.212	27.5	18-35	56.8	43.2
100	.150	25.0	15-35	81.8	18.2
140	.106	12.0	7-20	93.8	6.2
200	.075	5.0	0.5-8	98.8	1.2
PAN	-	1.2	0-3	100.0	-

TYPICAL PHYSICAL PROPERTIES:

Mineral	Quartz
Color	White
Grain Shape	Angular
Sphericity (Krumbein)	0.1
Roundness (Krumbein)	0.1
Hardness (Moh)	7.0
Specific Gravity	2.57
Melting Point	3100°F
Moisture Content Dry (Max. %)	0.5
Fineness Modulus	0.82
pH	Neutral

Bulk Density -
Compacted (lbs/ft³)	90
Uncompacted (lbs./ft³)	87
Theoretical Surface Area (cm²/gm)	154.9
Actual Surface Area (cm²/gm)	238.5
Coefficient of Area	1.54
Base Permeability	50
Acid Demand (pH - 4)	2.0
AFS Grain Fineness	64.0
Crushing Strength (psi)	24,500

TYPICAL CHEMICAL ANALYSIS: (Percent Reported as Oxide)

SiO2 (Silicon Dioxide)	97.46
Fe2O3 (Iron Oxide)	0.07*
Al2O3 (Aluminum Oxide)	1.50
Na2O (Sodium Oxide)	0.03
TiO2 (Titanium Dioxide)	0.04
CaO (Calcium Oxide)	0.08
MgO (Magnesium Oxide)	0.06
K2O (Potassium Oxide)	0.51
LOI (Loss-on-Ignition)	0.25

* Includes Fe

APPENDIX B
RADAR CROSS SECTION ASSESSMENT

Without measured radar cross section (RCS) data on the current production K747 blade and the K747 blade with a new candidate erosion protection coating, a definitive evaluation is not possible. No measured values are available for the permittivity (dielectric constant) of the current erosion protection system (EPS) or of a new EPS. Hence the RCS assessment is based on the following technical judgment.

Most modern search radars are two delay line canceler moving target indicator (MTI) radars. As such, with modern clutter rejection techniques, these radars perceive very slow moving objects as clutter and apply electronic canceling to them as if they were clutter. As the outboard section of a rotor blade is moving almost mach 1, it is always well above the velocity of clutter rejection and hence represents the most detectable component of the rotor system. This program does not change the blade's radar scattering for blade components beyond Station 217.5 as a Stainless Steel Leading Edge Erosion Guard covers the blade from Station 217.5 to Station 261 on the current production blade. The program results only in the potential modification of the electromagnetic scattering from the inner portion (within Station 217.5) of the rotor blade. Most, if not all, threat search radars will partially reject the radar return from the inner portion of the blade.

The K747 blade has numerous potential sources of electromagnetic scattering for any given threat radar. Figure B-1 defines the various scattering centers (i.e. edges) of the K747 blade and Figure B-2 depicts the angles at which the peak of the reflections would be found. The scattering pattern of each edge will vary due to its physical dimensions and component material electromagnetic properties. The primary scattering sources are the primary leading edge inboard of Station 224.4, the tapered leading edge section from Station 224.4 outboard (7 degrees off the primary leading edge), the tip cap (Station 264), the primary trailing edge inboard of Station 224.4, and the trailing edge from Station 224.4 outboard (21 degrees off the primary trailing edge). Associated with each edge is the "traveling wave" return from the "trailing edge", if any, of that scattering center. These are referred to on Figure B-2 as secondary scattering centers. Secondary scattering returns are significantly lower than primary scattering returns. As only the primary leading and trailing edges line up, the K747 has five (5) primary and two (2) secondary scattering sources as indicated in Figure B-2.

Note that in Figure B-2 the blade root is located at - 180 degrees, the trailing edges of the blade between - 180 and 0 degrees, the tip cap at 0 degrees, and the leading edges between 0 and + 180 degrees.

The current production as well as the potential candidate EPS materials are elastomeric polyurethanes. Elastomeric polyurethanes range in permittivity (dielectric constant) from 2.1 on the low side to 2.6 on the high side. As the erosion boot is bonded to a much thicker
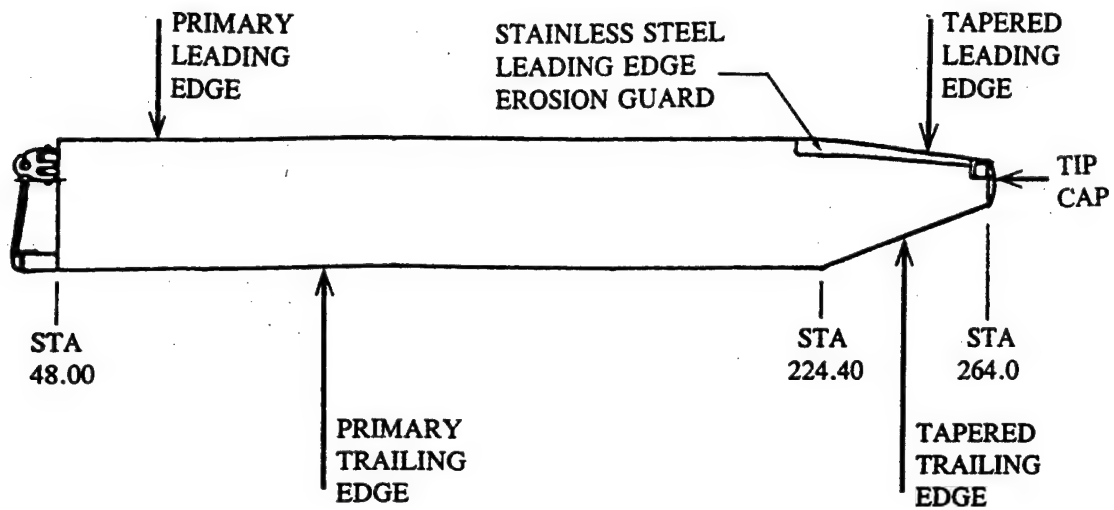
Figure B-1. K747 Blade, Various Scattering Centers.

PRIMARY SCATTERING CENTERS ──────────
SECONDARY SCATTERING CENTERS ── ── ── ── ── ──
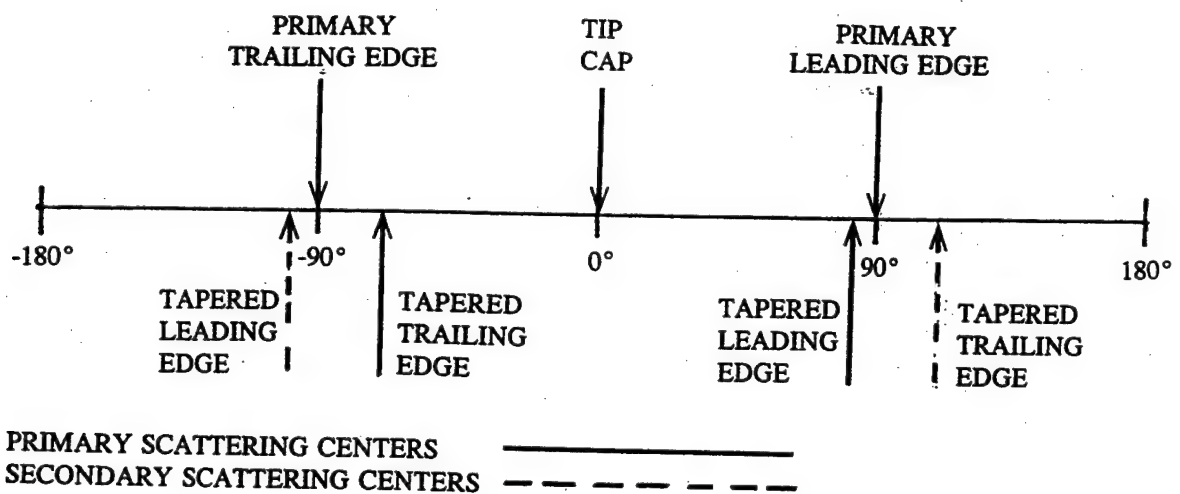
Figure B-2. Location of Primary and Secondary Scattering Centers.

blade spar nose block made of S-glass/epoxy with higher permittivity, the overall radar backscatter results from the combined effect of both the nose block and the EPS. The thicker nose block of higher permittivity S-glass dominates the overall effect of the combination and hence the radar reflection from the primary leading edge. As the thickness of the new EPS is expected to be the same as the current erosion boot and is significantly thinner than the nose block, the slight change due to a small dielectric constant variation in the EPS should be imperceptible to a threat radar.

For a two bladed rotor system, the scattering from the primary trailing edge of the retreating blade will line up with the scattering from the primary leading edge of the advancing blade, partially obscuring any possible change in the RCS due to changing the EPS of the primary leading edge.

Replacing the erosion protection system (EPS) with the new EPS from Station 75 to Station 261 on the primary leading edge could only change the K747 blade radar reflectivity pattern for only one of the potential scattering angles and that change would be partially obscured as mentioned above. No significant RCS variation is anticipated and the radar detectability of the helicopter with modified K747 blades will remain unchanged.

Sheet 1 (Parts List / Application)

KAMAN AEROSPACE CORPORATION, BLOOMFIELD, CONNECTICUT
CAGE CODE B4955
GUARD-L.E. EROSION MATERIALS TEST
PL XK747-216 **REV** A **SH** 1 **OF** 1

CONTRACT NO. DAAJ02-91-C-0045

APPLICATION						
P/N	NEXT ASSY	USED ON	P/N	NEXT ASSY	USED ON	EFFECTIVITY
-011	XK747-215	AH-1				
-013	XK747-215	AH-1				

NOTES: UNLESS OTHERWISE SPECIFIED

1. ⚠ REQUIRED MARKING TO BE IN THIS AREA PER KPS 215, CLASS D (BAG & TAG).

2. THE PURPOSE OF THIS DRAWING IS TO DEFINE A LEADING EDGE EROSION GUARD FABRICATED FROM TWO DIFFERENT MATERIALS FOR TEST AND EVALUATION. THE -011 GUARD WILL BE FABRICATED FROM A LIQUID AND THE -013 FROM SHEET MATERIAL.

3. -011 MATERIALS AND PROCESS INFORMATION. THE GUARD IS FABRICATED FROM A PREPOLYMER, N8#535330-A, A CURATIVE W, BAYTEC CURATIVE W, AND A BLACK COLOR CONCENTRATE DESCRIBED BELOW.

USING SUITABLE METERING, MIXING AND DEGASSING EQUIPMENT, PROCESS THE EPOSION GUARD MATERIAL AS FOLLOWS: MIX THE PREPOLYMER AT 85°C (185°F), AND THE CURATIVE AND COLOR CONCENTRATE AT ROOM TEMPERATURE. MIX 100 PARTS BY WEIGHT (pbw) OF THE PREPOLYMER TO THE APPROPRIATE AMOUNTS OF CURATIVE AND COLOR CONCENTRATE TO ACHIEVE AN EQUIVALENT MOLE RATIO OF CURATIVE TO PREPOLYMER. HORIZONTAL LOADING OF 0.98 pbw. MOLD TEMPERATURE SHOULD BE 110°C (230°F). THE MATERIAL CAN BE DEMOLDED AFTER 45 MINUTES. POST CURE FOR 8 HOURS AT 110°C (230°F).

THE BLACK COLOR CONCENTRATE IS PRODUCED FROM BAYTEC CURATIVE W, BLACK 2980 PIGMENT AND ANTI-TERRA-U100 DISPERSANT BY GRINDING THE PIGMENT INTO THE CURATIVE USING 3% SOLIDS DISPERSANT BASED ON PIGMENT SOLIDS ON TOTAL PIGMENT SOLIDS DEPEND ON MANUFACTURING PROCESS REQUIREMENTS. GRIND TO A HEGMAN 7 OR FINER USING A SAND MILL, BALL MILL, OR EQUIVALENT.

REV STATUS OF SHEETS	REV	A	A																											
	SHT	PL	1	2	3	4	5	6	7	8	9	10	11	12	13	14	15	16	17	18	19	20	21	22	23	24	25	26		

	APPROVAL	DATE			APPROVAL	DATE
DRAWN	G.W.HAIRE			PROJECT	W.D.WEIGEL	
CHECKED	B.HOCK					
DESIGN				MATERIAL	W.D.WEIGEL	
ENGR	C.P.HARDERSEN			SAFETY	A.BURNHAM	

Sheet 2 (Notes continued)

KAMAN AEROSPACE CORPORATION, BLOOMFIELD, CONNECTICUT
CAGE CODE B4955
GUARD-L.E. EROSION MATERIALS TEST
PL XK747-216 **REV** A **SH** 2 **OF** 1

CONTRACT NO. DAAJ02-91-C-0045

NOTES: CONTINUED FROM SHEET 1

-013 MATERIALS AND PROCESS INFORMATION. THE GUARD IS FABRICATED FROM NPE 2918 BLACK URETHANE SHEET MATERIAL PURCHASED FROM THE 3M COMPANY, St. PAUL, MN.

FOR ADDITIONAL MATERIALS AND PROCESS INFORMATION, CONTACT KAMAN AEROSPACE CORP. MATERIALS AND PROCESS DEPT, BLOOMFIELD CT.

4. ⚠ STEPS ARE PERMITTED ON THIS SURFACE.

5. INSPECTION CRITERIA INBOARD OF STA. 213.50: ALL REGIONS: THE PART SHALL BE FREE FROM THRU CUTS, TEARS AND CRACKS. THE PART MAY HAVE LOCAL REGION A1 CRACKS FROM PITS, SUCH AS VARIATIONS OR INDENTATIONS THAT ARE NOT CAUSED BY DISCREPANCY IN THICKNESS. SUCH DEFECTS MUST NOT CONTAIN STEPS ON THE OUTER SURFACE AND MUST NOT EXCEED 1.50 IN. IN LENGTH OR A DEPTH OF .012 IN.

6. INSPECTION CRITERIA OUTBOARD OF STA. 213.50: REGION A1, THE EXTERNAL SURFACE OF THE PART SHALL BE FREE FROM CUTS, TEARS, PITS, HOLES, BLISTERS, CRACKS AND STEPS. THESE DEFECTS ARE ACCEPTABLE EXCEPT FOR STEPS. IF LESS THAN 1.50 IN. THE INTERNAL SURFACE OF STEPS MUST NOT BE RESULTANT NPE INTERNAL SURFACE DEVIATION OR ANY KIND OF LOCAL DEFECT SHALL NOT BE LESS THAN .045 IN. AND GREATER THAN .50 SQ. IN. IN SURFACE AREA.

REGION B: THE EXTERNAL SURFACE OF THE PART SHALL BE FREE FROM THRU CUTS, TEARS, CRACKS AND STEPS. FOR BOTH EXTERNAL AND INTERNAL SURFACES, BETWEEN STA 219.50 AND STA 242.00 PIN HOLES TO .040 IN. MAX. ACCEPTABLE. NO MORE THAN NINE PER SURFACE. IN THE THICKNESS EXCEPT FOR STEPS ON THE UPPER SURFACE WITH DEPTH OF .025 IN. OR LESS ARE ACCEPTABLE IF BLENDED OUT. THE INTERNAL SURFACE MAY HAVE RAISED SCRIBE LINES.

REGION C: THE EXTERNAL SURFACE SHALL BE FREE OF STEPS, FOR BOTH THE EXTERNAL AND INTERNAL SURFACES, THE PART SHALL BE FREE FROM THRU CUTS, TEARS, AND CRACKS. ALL OTHER DEFECTS ARE ACCEPTABLE.

7. THE PART SHALL BE WRAPPED INTERNALLY AND EXTERNALLY WITH .002 IN. THICK POLYETHYLENE FILM OR EQUIV. RELEASE MATERIAL, TO PREVENT STICKING AFTER CURING.

8. USE FRECOTE 44NC MOLD RELEASE OR KAC ENGINEERING APPROVED EQUIVALENT.

Parts List (upper right)

KAMAN AEROSPACE CORPORATION, BLOOMFIELD, CONNECTICUT
CAGE CODE B4955
GUARD-L.E. EROSION MATERIALS TEST
PL XK747-216 **REV** A **SH** 1 **OF** 1

CONTRACT NO. DAAJ02-91-C-0045

QTY REQD	DIT	CODE	ZONE	PART OR IDENTIFYING NO.	NOMENCLATURE OR DESCRIPTION	STOCK SIZE	MATERIAL	MATERIAL SPEC	NOTE CODE
-013				-011	GUARD			535330-A	2,3
			1A3	-013	GUARD	NPE 2918 BLACK URETHANE SHEET	3M CO. St; PAUL, MN.		2,3
	AR			N8# 535330-A	PREPOLYMER		MILES INC., PITTSBURGH, PA.		
	AR			BAYTEC CURATIVE W			MILES INC., PITTSBURGH PA.		
	AR			2980 BLACK	PIGMENT		CEROEC CORP., WASHINGTON, PA.		
	AR			ANTI-TERRA-U100	DISPERSANT		BYK-CHEMIE USA, WALLINGFORD, CT.		
	AR			NPE 2918	BLACK URETHANE SHEET		3M CO. St. PAUL, MN.		

Revision Notice (RN)

KAMAN AEROSPACE CORPORATION, BLOOMFIELD, CONNECTICUT
CAGE CODE B4955
GUARD-L.E. EROSION MATERIALS TEST
RN XK747-216 **REV** A **SH** 1 **OF**

CONTRACT NO.

REV NOTE	DISPOSITION OF PARTS UNDER: [1] MAY BE REWORKED [2] CANNOT BE REWORKED [3] RECORD [4] USE AS IS					DISP
	EFFECTIVITY	E.O. NO.	ZONE	DESCRIPTION OF REVISION		
ENG. REL. NO.						
			O/N B/M	① IN O/N AND NOTE 3, (WAS)NO. 154-9-A BLACK PIGMENT, (NOW) BLACK 2980 PIGMENT....		3
			O/N	② IN NOTE 3 (WAS) GRIND TO A HEGMAN 8 OR FINER.... (NOW) GRIND TO A HEGMAN 7 OR FINER...		3
			1A1	① IN F/O ADDED NOTE "FOR -011 OXLY"		3

	APPROVAL	DATE		APPROVAL	DATE
DRAWN	RICH LAY		PROJECT		
CHECKED			MFG		
DESIGN			MATERIAL		
ENGR			SAFETY		

Sheet 1 of 2

KAMAN AEROSPACE CORPORATION
BLOOMFIELD, CONNECTICUT
CASE CODE 84955
CONTRACT NO. DAAJ02-91-C-0045

BLADE ASSY MATERIALS TEST

PL XK747-215 REV -

CAD/CAM DWG SH 1 OF 2

APPLICATION

P/N	NEXT ASSY	USED ON	EFFECTIVITY	QTY REQD NEXT ASSY	QTY REQD AIRCRAFT
-001	NONE	AH-1	NONE	AS REQ	AS REQ
-003	NONE	AH-1	NONE	AS REQ	AS REQ

NOTES: UNLESS OTHERWISE SPECIFIED

1. △1 STENCIL WITH ONE INCH WHITE CHARACTERS USING MIL-C-83286 POLYURETHANE PER FED. STD-595 COLOR NO. 17925.

    EXPERIMENTAL
    PART NO. XK747-215-00X
    SERIAL NO.

2. INSTALL EROSION GUARD IN ACCORDANCE WITH KPS.146. USE 120 GLASS FABRIC IN BOND JOINT. A 180° PEEL TEST SAMPLE REPRESENTATIVE OF THE PROCESS AND MATERIALS USED SHALL BE BONDED TO THE SPAR AND WHEN TESTED SHALL MEET OR EXCEED THE PEEL STRENGTH REQUIREMENT OF 10 POUNDS PER INCH WIDTH MINIMUM. VOIDS NOT TO AN EDGE, NOT LARGER THAN ONE INCH MAX. DIMENSION, AND ADJACENT VOIDS NOT CLOSER THAN FOUR INCHES ARE ACCEPTABLE EXCEPT THAT IF THE VOID EXHIBITS A BUBBLE, IT SHALL BE FILLED WITH REPAIR ADHESIVE AND ROLLED FLAT. EDGE VOIDS NOT DEEPER THAN .50 AND NOT LONGER THAN 4.0 SHALL BE REBONDED WITH REPAIR ADHESIVE. REPAIR ADHESIVE SHALL BE IN ACCORDANCE WITH KPS 146.

3. FOR THE -001 & -003 ASSY'S, (WITH THE K747-210-011 CRES GUARD REMOVED AND THE K747-209-011 SHIELDS INSTALLED).
    TOTAL WEIGHT----- 246.28 +4.00/-2.00 LBS.
    CHORDWISE C.G.--- 7.716/7.806 IN. FROM L.E.
    SPAN MOMENT----- 34,117 +0.0/-10.0 IN. LBS. AT CENTER OF ROTATION

REV STATUS OF DRAWING SHEETS & PL

APPROVAL	DATE	APPROVAL	DATE	APPROVAL	DATE	APPROVAL	DATE
DRAWN G.W.HAIRE	93-09-03	DESIGN G.W.HAIRE	93-09-03	LOGISTICS		PROJECT	
CHECKED		WEIGHT		STANDARDS		MFG	
GR ENGR		MATERIAL		SAFETY		ENG.REL.NO.	
STRESS		REL & MAINT		MANF FAB		ENG.RELEASE	

Sheet 2 of 2

KAMAN AEROSPACE CORPORATION
BLOOMFIELD, CONNECTICUT
CASE CODE 84955
CONTRACT NO. DAAJ02-91-C-0045

BLADE ASSY MATERIALS TEST

PL XK747-215 REV -

CAD/CAM DWG SH 2 OF 2

QTY REQD -001	QTY REQD -003	CASE CODE	ZONE	PART OR IDENTIFYING NO.	NOMENCLATURE OR DESCRIPTION	STOCK SIZE	MATERIAL	MATERIAL SPEC
				-001	BLADE ASSY	MAKE FROM	K747-003-403	
				-003	BLADE ASSY	MAKE FROM	K747-003-403	
			1	XK747-216-011	EROSION GUARD			
	1			XK747-216-013	EROSION GUARD			
	8	8		K747-209-011	SHIELD			
	2	2		NAS1189E4P8B	SCREW			
	8	8		NAS1189E5P8B	SCREW			
	AR	AR			ADHESIVE	PER KPS 146		
					REMOVAL LIST			
	1	1		K747-116-15	EROSION GUARD			
	1	1		K747-210-011	EROSION GUARD			

APPENDIX E

Analysis of Polyurethane Advanced Rotor Blade Erosion Protection System

W. F. Adler
D. J. Mihora

March 28, 1993

TABLE OF CONTENTS

i

LIST OF ILLUSTRATIONS

iv

LIST OF TABLES

APPENDIX A LIST OF ILLUSTRATIONS

APPENDIX B LIST OF ILLUSTRATIONS

1.0   INTRODUCTION

The nucleation and subsequent growth of rain erosion damage in polymeric coatings on helicopter rotor blades is not fully understood in terms of the material properties of the polymeric coatings. The majority of the rain erosion tests of the candidate coating systems have evaluated the endurance of these systems for long duration run times usually until significant degradation of the coating takes place. The analysis completed in this program provides a physically realistic model for the waterdrop impact event so that meaningful correlations can be developed between the waterdrop impact damage modes and the material and geometrical parameters of the coatings.

The analyses of coatings on materials when exposed to waterdrop impacts are quite limited. The previous analyses are either one-dimensional stress wave calculations (Engle, 1974; Rieger and Boche, 1974; Haynie, 1989; Kalumuck, Chahine, and Haynie, 1987) or are quasistatic models of a solid body pushing on the coating (Matthewson, 1979, 1982). The computational model developed at General Research Corporation (GRC) is a three-dimensional finite element analysis of a waterdrop impacting a structured target material. The three-dimensional model is applicable to non-normal impact conditions. By using a finite-element approach, which is only feasible for the waterdrop impact problem due to the computer developments which have become available over the last few years, structural features of the target can be accurately modeled. In the present case the target can be a multiple layered construction.

Previous computational analyses of a waterdrop collision have been based on finite difference approaches (summarized by Adler, 1979). The complexity of these analyses at the time they were done limited them to waterdrop impacts normal to the surface of the target. The target was either rigid or a homogeneous elastic material. It is difficult to consider a structurally or materially complex target in the context of a finite difference approach.

A waterdrop collision on a leading edge rotor blade material is a highly transient event. The duration of this impact event is on the order of a few millionths of a second. In this time period the impacting waterdrop is compressed and distorted to extreme levels. The impact process generates stress waves in both the water and the polymeric layer. The compressional

1

wave in the waterdrop travels through the water and the waterdrop distorts more rapidly than the compliant polymer. The momentum transfer from the waterdrop causes large pressures to develop at the distorting interface between these two compliant materials. Both the waterdrop and the polyurethane simultaneously undergo large strains.

The impacted polyurethane layer can develop a deep crater and substantially alter the evolving waterdrop shape. By contrast, waterdrop impacts on the surfaces of metals and ceramics do not undergo the extreme interactions with the targets as in the case of polymeric layers. These large distortions influence the mechanics of loading the polyurethane layer and the temporal and spatial development of the stress waves and pressure distribution over the contact area. This situation represents a very complex impact mechanics problem that is solvable only using large deflection finite element codes such as DYNA3D. DYNA3D was originally developed by Lawrence Livermore National Laboratory for weapons development more than a decade ago. Over the last several years this code has been adapted by GRC to hydrometeor impact problems by including an increased number of elements and incorporating an equation of state for water and realistic properties for the target materials.

Different polymeric materials when used as leading edge rotor blade protection guards have different useful lives when exposed to rain and sand environments. There are few insights into the cause of leading edge rain erosion of polymers in the literature. There is also a lack of any guidance as to the preferred material properties that may enhance the wear protection of these materials. It is difficult to postulate properties improvements because the mechanics occurring during the repeated waterdrop impacts has not been adequately described or understood. As a very important first step in understanding this process the analysis of the behavior of a single waterdrop collision is a meaningful starting point for investigating the multiple impact sequences that produce leading edge erosion.

The finite element modeling of the impact between a waterdrop and polyurethane layers was successful after adjusting for numerical computational problems which arose in conjunction with the extreme distortions of the finite element grid. The predicted elongations (strains) are considered to be very significant in the damage assessment. Although radial stresses under the

2

impacting waterdrop are primarily compressive in nature, large tensile strains develop in the circumferential direction under the waterdrop and around the edge of the crater. These tensile strains reached 80 percent in some cases. However tensile failures are not predicted by the computational simulations since even the weakest polyurethane material candidate exhibited 210 percent strain to failure under dynamic loading conditions.

The finite element modeling indicated the time to reach the maximum tensile strains was 4 to 8 μs which is long compared to waterdrop impacts on more rigid materials where times on the order of a fraction of a microsecond are typical. Even with the long time durations strain rates exceeding 2.5×10^5 s^{-1} are predicted. These high strain rates were also accompanied by large strain levels. Slightly oblique impacts appear to be more damaging than normal impacts with larger regions of high tensile strains developing.

The requirement for mechanical properties at large strains and high strain rates for a viscoelastic material placed a constraint on accurately describing the response of the polymeric layer to the waterdrop impact. Since the typical viscoelastic material property measurements are for frequency-dependent, small strain loading conditions, sources for the more relevant property measurements at large strains were sought.

A literature survey was carried out. The literature survey confirmed that a negligible amount of work had been done on attaining high frequency, large strain property measurements. Several suppliers for viscoelastic property measurement equipment were contacted. Only a few of the available test techniques were able to approach strain levels of 10 percent when more than 50 percent is required.

General Research developed the experimental capability to obtain large strain, high strain rate material properties to failure for flexible polymeric materials. This facility provides the relevant material property data which is required in the computational modeling. This unique capability has significantly expanded our knowledge of the performance of the candidate polyurethanes. The polyurethanes tested under large strain conditions do not exhibit the anticipated tendency toward more brittle behavior at the 10^4 to 10^5 s^{-1} strain rates associated with

3

the waterdrop impact. These materials display surprisingly low hyperelastic modulii during large strain extensions.

The dynamic mechanical response of five different polyurethane-based materials selected by Kaman Aerospace Corporation is described for realistic waterdrop impact conditions. The finite element modeling is made material specific with the proper constitutive equations as implemented with the experimentally determined material properties. The final calculations indicate a single waterdrop impact can not initiate failure of the polyurethane coating. The failure process is more complex, however the work completed provides an initial quantitative approach for a physically-realistic failure model. It is hypothesized that repeated large strain extensions may lead to fatigue as the nucleating mechanism for erosion damage.

4

2.0 FINITE ELEMENT MODELING OF A WATERDROP COLLISION ON A POLYMERIC LAYER

Numerical modeling tools used at GRC to assess hydrometeor and particulate impact behavior include TURBAN, DYNA3D and AUTODYNE. TURBAN is a two-dimensional, high-fidelity finite difference solution of the early time wave propagation in an elastic substrate. DYNA3D is a discretized, three-dimensional Lagrangian finite element code that explicitly steps forward in time to solve transient response problems. AUTODYNE is a two-dimensional Eulerian finite element code with rezoning capability when large element distortions occur. DYNA3D is the most versatile but also the most difficult of these codes to implement for the waterdrop impact conditions.

2.1 Description of the DYNA3D Finite Element Model

DYNA3D and the associated pre-and post-processing codes were developed by Lawrence Livermore National Laboratory (LLNL) for very short-time events. These codes have been used extensively by government and industry over the last decade. The codes require large RAM and disk space and a fast CPU processor to provide efficient problem solving. General Research has modified versions of these mainframe codes running on the Stellar computer, and i860 and i486 workstations.

The simulation of a waterdrop impact onto a polyurethane layer is an extreme case of large deflections of two very flexible media. Numerical instabilities for this problem category were overcome and stable solutions were generated. As the impact process proceeds the waterdrop distortions becomes quite severe, but methods were developed to accommodate the extreme elemental distortions in the finite element formulation of the problem. When the waterdrop deforms into a pancake shape, the cratering in the polyurethane is significant. DYNA3D can accommodate these large distortions which occur in the elements first making contact between the two media.

The DYNA3D code is an explicit solver and inexpensively solves each incremental time step. However, the number of time steps can be large when long time periods are needed to

5

describe the event and rapid changes are taking place. There are no large matrix inversions required as used in alternate implicit large deflection codes like ABAQUS and MARC. The code is fast because nearly all the code is vectorized. The explicit central difference method is used to integrate the equations of motion in time. The code is conditionally stable provided the computational time increment is governed by the Courant limit. For waterdrop impacts this limit is essentially the time required for an elastic wave to propagate across the shortest dimension of the smallest element in the waterdrop. The code automatically calculates the time step size at each step of the solution and adjusts the time step size accordingly to minimize the number of time steps in the solution.

DYNA3D solves a vectorized equation. No matrices are generated and only internal force vectors are determined for all elements with no decompositions required. An explicit scheme calculates the acceleration based upon the current loads. Force values are available because of the lumped mass formulation. The diagonal mass matrix, M, produces an uncoupled set of equations of the form:

$$M \ a_{n+1} = p^{ext} - f^{int}$$

In the above equation, p^{ext} are the applied external forces and f^{int} are the internal forces on an element. The energy equation is used to evaluate the waterdrop compression using

$$E = V \ s_{ij} \ \xi_{ij} - (p + q) \ V$$

where s_{ij} is the deviatoric stress

ξ_{ij} is the strain tensor

p is the pressure

q is the bulk viscosity

V is the relative volume

A versatile linear polynomial equation-of-state of the form

$$p = C_1 \ \mu + C_2 \ \mu^2 + C_3 \mu^3$$

6

represents the waterdrop for moderate levels of compression (<25 kbar) where:

$C_1 = 3.1907 \times 10^5$ psi

$C_2 = 1.3836 \times 10^6$ psi

$C_3 = 2.1130 \times 10^6$ psi

The element compression, μ, is given by

$\mu = \rho/\rho_o - 1$.

where ρ is the current density and ρ_o is the initial density.

A critical attribute of the code is the contact - impact algorithm. The finite element nodes in the waterdrop and the polyurethane are prevented from crossing two defined slide surfaces. There is a master slide surface attached to the underside of the waterdrop. There is a separate slave slide surface attached to the impacted surface of the polyurethane. Each surface goes through an algorithm to check if a node penetrates the other surface. When penetration is detected, a normal force is applied to the element with a magnitude which relocates the node on the penetrated slide surface. A looping process occurs first for each node in the master slide surface to detect penetration into the slave surface. The process is repeated with each node of the slave surface to detect penetration into the master surface. The combined check of the nodes for both surfaces provides the robustness of the algorithm. The contact algorithm can include a shear force. In the present model, only normal forces are transmitted between the waterdrop and polyurethane.

The accuracy of the finite element predictions is controlled by how well the constitutive equations for the waterdrop and the substrate represent the physical aspects of the waterdrop collision. The equation-of-state modeling for water provides a much higher accuracy than the substrate. The substrate modeling is governed by the capability to obtain finite strain, high frequency material property measurements. A failure criterion is also required to complete this modeling of the response of the polyurethane layer to the waterdrop impact. There are a variety of constitutive representations to fit the experimental data. For the present computations constitutive equations were introduced representing hyperelastic, viscoelastic, and elastic-plastic

response. An attribute of DYNA3D is the abundance of constitutive representations available to model large strains.

The viscoelastic constitutive equations use the same relationship for the bulk and shear relaxation.

$$G(t) = G_i + (G_o - G_i) \, e^{-Bt}$$

where $G_o = E_o/2(1+v)$ early time shear constant, at $t = 10^{-7}$ s

$G_i = E_i/2(1+v)$ long time shear constant, at $t = 10^{-5}$ s

$v = 0.45$ (representative value of Poisson's ratio)

B = decay constant between G_o and G_i, e.g. 4×10^6 s^{-1}.

The deviatoric and principal stresses use the same decay constant for shear and bulk relaxation. They are calculated from the expressions

$$\sigma_{ij} = 2 \int G(t-\tau) \dot{\xi}_{ij} d\tau \qquad\qquad \sigma_{kk} = 3 \int G(t-\tau) \dot{\xi}_{kk} d\tau$$

The volumetric strain is assumed to be elastic, and the pressure is computed from the volumetric strain using

$$p = - K \xi_v$$

where the elastic bulk modulus is

$$K = 3 \, E_i$$

and the volumetric strain is

$$\xi_v = (\xi_x + \xi_y + \xi_z)$$

The three-dimensional finite element model can describe both normal and oblique waterdrop impacts on soft polymeric layers. Examples of the finite element analysis at a

8

particular instant during the impact event are shown in Figure 2.1. These examples show the large distortions of the elements which are accommodated in the approach developed by GRC.

2.2   Initial Waterdrop Impact Calculations

The typical grid layout is shown in Figure 2.2 for the waterdrop and the polymeric layer. The waterdrop diameter is 2 mm and the coating is 0.1 in thick. The elements making up the waterdrop have approximately the same volumes. The coating has high zoning under the region where the waterdrop will deform. The far-field region of the coating does not require the same fidelity. The far-field region does allow large distortions and wave propagation. The near- and far-field regions are connected by a tied slide line. The lower part of the substrate also can be represented by a coarser finite element grid since the gradients in the stress components are not as large as at the impact face. The only boundary condition applied to the model is at the base of the substrate. The base is constrained not to displace or rotate.

An impact velocity of 1000 fps was selected as being the upper limit on the waterdrop impact range for the main motor. The impact conditions evaluated represent upper bounds on the strains the polyurethane layer must resist.

An oblique view of a crater formed in the polyurethane layer for a 2 mm waterdrop impact at 1000 fps at 2 μs after contact is shown in Figure 2.3 with the waterdrop removed. The largest element distortions in the polyurethane are at the centerline and at the edge of the crater. The polyurethane distortions are regular as expected. The initial simulations were not as good as this example because of element collapse and hourglassing of surface elements which limited the temporal length of the run. Figure 2.4 shows an example of the hourglassing instability.

Hourglassing is a element shape instability that does not alter the element's internal energy. The hourglass modes tend to form over a very short time as compared to the time to form the crater. If the hourglass instability occurs, it propagates very rapidly and is very evident. LLNL recommends the introduction of viscous damping as the approach for inhibiting unde-

9
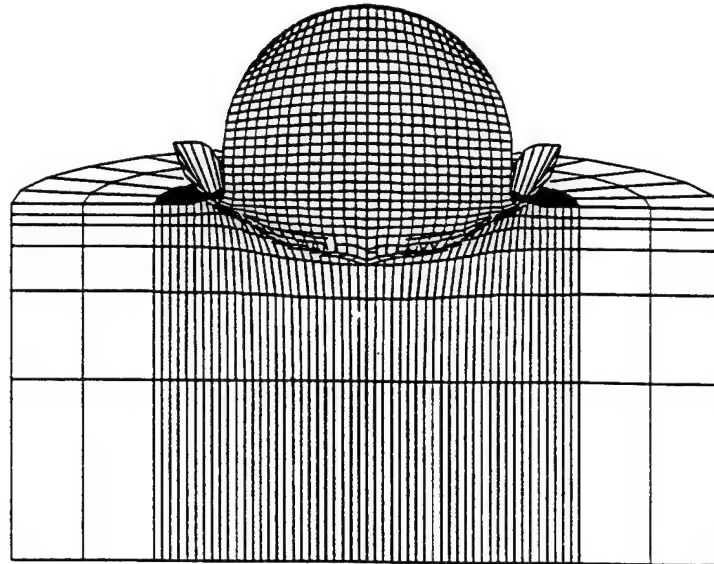
a. Normal impact condition at 2 μs.
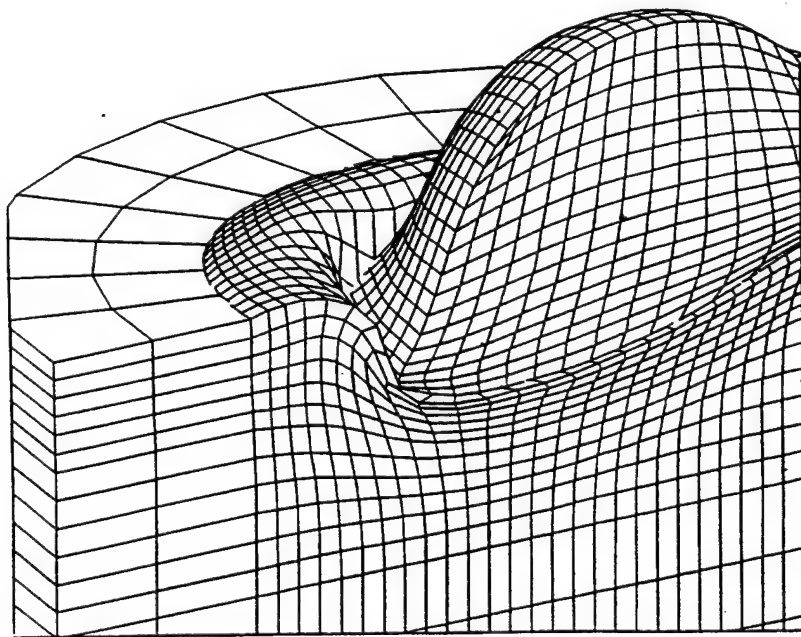
b. A 45° oblique impact condition at 5 μs. The waterdrop impact is from left to right.

Figure 2.1. Finite element representations for a 2 mm waterdrop impacting at 1000 fps on a polymeric layer.

10
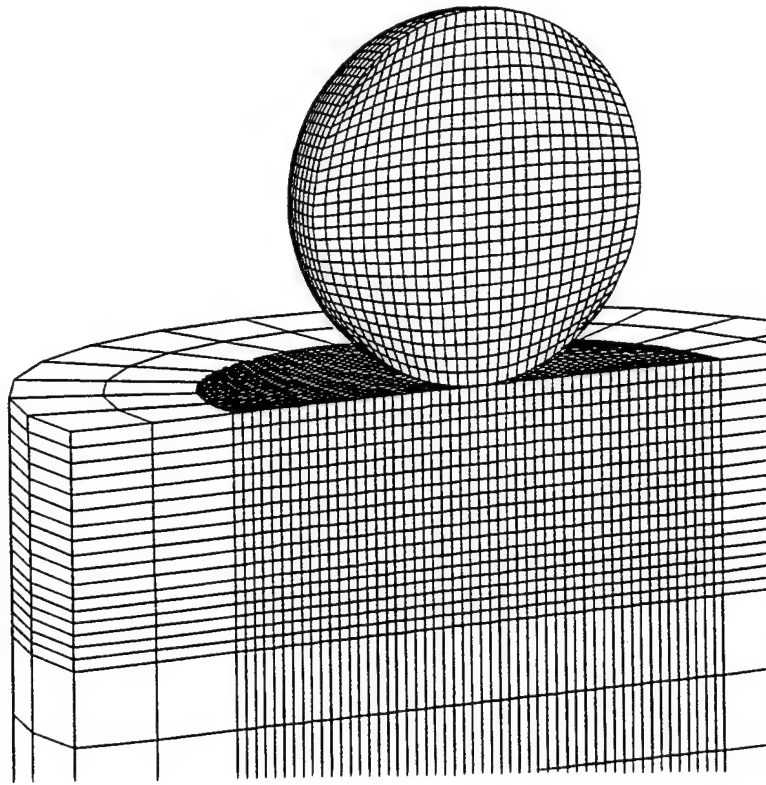
Figure 2.2 Finite element grid configuration for the waterdrop impact simulation.
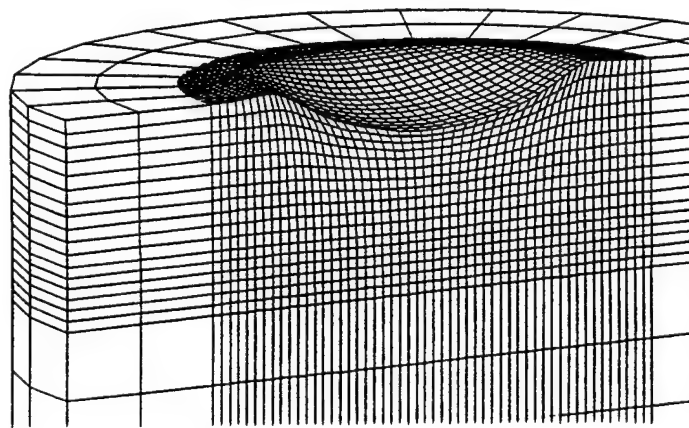
Figure 2.3   Crater formation using the high fidelity gridding for a 2 mm waterdrop impact
               at 1000 fps after 2 μs.

11

sirable hourglassing which has negligible effect on the stable global distortion under the waterdrop. An alternate hourglass control uses a form of structural damping.
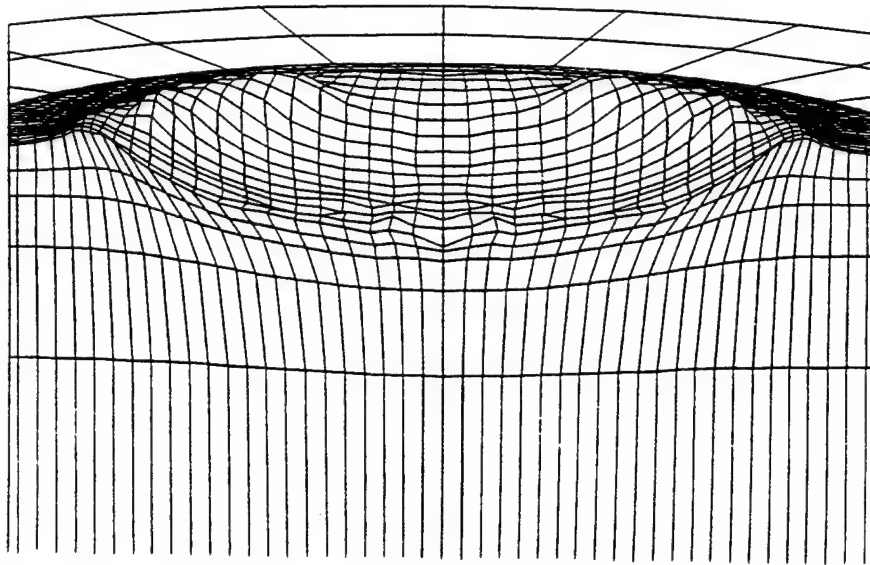
Figure 2.4   Crater formation using course finite element gridding for a 2 mm waterdrop impact at 1000 fps after 2 μs illustrating the hourglass effect in the interfacial elements.

The calculated strains listed in Table 2.1 obtained from the preliminary modeling effort are the largest tensile values predicted during the waterdrop interaction/distortion with a polyurethane coating for a waterdrop diameter of 2 mm impacting normal to the surface at 1000 fps. The viscoelastic parameters in Table 2.1 are selected to provide insights into the response of a hypothetical polymeric layer; the appropriate material properties for the five polyurethane candidate materials are determined experimentally in Section 5.

The prediction of strains from 3 to 18.8 percent illustrate that there can be large localized deformations. The larger strains are associated with the lower stiffness materials. One might expect lower stiffness polyurethanes generally have a larger ultimate strain capability. The lower stiffness polyurethanes experience larger distortions and appear to be better able to survive, but this conclusion is conjecture. For each material a comparison of the predicted strains and measured ultimate strains can lead to an understanding of the erosion resistance of these materials.

12

Table 2.1   Summary of the Strains for a 2 mm Waterdrop Impact at 1000 fps on a Polymeric Coating Using Parametric Values for the Viscoelastic Properties.

t (μs)	B (s^{-1})	K (ksi)	G_o (ksi)	G_i (ksi)	$(\sigma_{rr})_{max}$ (ksi)	$(\xi_{rr})_{max}$ Strain
1.0	1.e7	4.44e5	4.e5	4.e3	14.8	0.0308
1.0	1.e5	4.44e5	4.e5	4.e3	30.8	.0334
0.6	1.e6	4.44e5	4.e5	4.e3	30.0	.035
21.0	1.e7	4.44e4	4.e5	4.e3	15.5	.062
0.9	1.e5	4.44e4	4.e5	4.e3	33.6	.065
1.0	1.e6	4.44e4	4.e4	4.e3	7.0	.117
1.2	1.e7	4.44e4	4.e4	4.e3	0.13	.188

A waterdrop impact simulation run to useful completion requires an intimate working knowledge of element sizing. The sizing and resizing of the elements must be performed at the beginning of the simulation. In the future, there is a possibility that active rezoning can be realized. With the current inability to rezone late in the run time, the initial element sizing is crucial. The main detractor of fixed zoning is the sequential decrease in the computation time increment as the contact elements are squashed.

Only simple eight node elements are used to represent the waterdrop and the polymeric layer. The number of elements is large to achieve high fidelity. Nominally 24,800 elements are used in the normal impact simulation, while about 32,000 elements are used in the oblique impact simulations. The large number of elements add to the long CPU requirements. Reduction in the number of elements could be implemented in some cases by forcing cyclic symmetry or axisymmetric modeling. There is no mechanism to degenerate DYNA3D into cyclic symmetric or axisymmetric. There is a separate code, DYNA2D, for axisymemetric problems, but unfortunately the input requirements are different. The axisymmetric model is essentially a completely different formulation.

Two symmetry models were implemented in the current simulations as a procedure to reduce the element numbers and CPU time. A quarter model was employed for normal

13

waterdrop collisions with reflections about the xz and yz planes. For oblique waterdrop impacts a half model is employed with symmetry about the xz plane.

3.0   MATERIAL PROPERTY EVALUATIONS (BACKGROUND)

As indicated in Section 2.2 a number of waterdrop impact conditions were evaluated initially using estimates for the viscoelastic parameters obtained from the data collected from several sources. These preliminary computations provided an indication of the strain levels and strain rates the polyurethane coating experiences during the waterdrop impact event. The strain rates were found to fall within a range where the stiffness modulus is quite variable below its nearly constant high-frequency value. The tensile strains in the vicinity of the boundary of the contact zone between the drop and the coating were also found to be quite high (on the order of 20 percent from Table 2.1). These preliminary computations helped to define the type of viscoelastic property data that is required to provide accurate estimates of the coating performance. The additional material response parameter that is required in the computational model is a failure criterion. An experimental capability for obtaining these material property measurements was developed at GRC. The required material property measurements were found to be essentially unavailable.

While small strain, high frequency viscoelastic property measurements are readily obtained, there are only a few sources for large strain, high frequency viscoelastic property evaluations. There is a negligible amount of work on the failure of viscoelastic materials at high rates of loading. After reviewing all of the options that are available for obtaining this data, it was concluded that GRC has specialized capabilities which made it possible to carry out an innovative approach to provide the material property data required to implement the computational model. The test procedure formulated for this purpose is described.

3.1   Thermomechanical Behavior of Polyurethane

Polyurethanes have the attributes of exceptional toughness and abrasion resistance among polymeric materials. As a protective coating or paint they are well known for their high elongation to break during quasistatic tension tests. The foundation of the polyurethanes is the isocyanates. This organic functional group is capable of an enormously diverse range of chemical reactions and mechanical properties. Plasticizer additives, fillers and impact modifiers

15

are also used to change the dynamic mechanical properties. The flexural modulus at 20°C ranges from below 4000 psi to well over 400,000 psi. Ultimate strain values at 20°C range from a few percent to greater than 1500 percent.

Polyurethane properties vary significantly with temperature. At reduced temperatures, the material becomes very stiff. The glass transition temperatures generally range from -90 to 20°C. The material stiffening caused by a 10°C temperature drop can be equal to the stiffening caused by a 100 Hz frequency increase. Thus, the higher frequency response is similar to the low frequency response at reduced temperatures where the material is also very stiff. The change in the viscoelastic parameters for a 3M unfilled polyurethane referenced to a temperature of 25°C is shown in Figure 3.1. The frequency range which has been found to be most relevant to waterdrop collisions described by the GRC computational model is denoted in Figure 3.1.
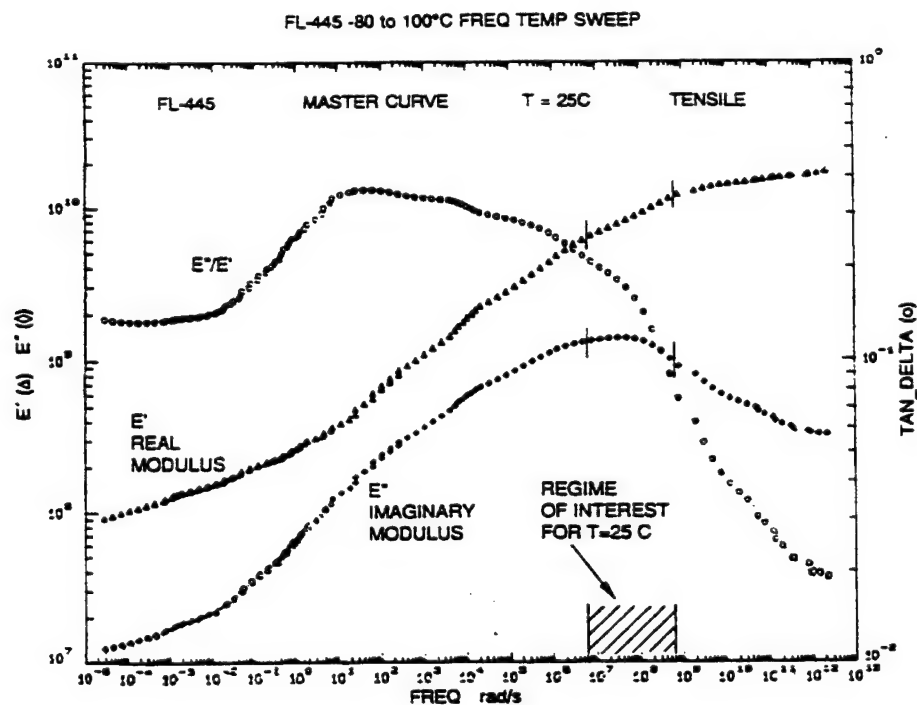
Figure 3.1   Linear viscoelastic properties over an extended frequency range for a polyurethane material (FL-445). These results are for very small strains.

16

The linear viscoelastic behavior of materials illustrated by Figure 3.1 for small cyclic oscillations is most useful for assessing very small deflection response such as material damping trends. The theory of acoustic response utilizes this form of data -- particularly the ratio of real modules, E′, to the imaginary modulus E″, which is denoted as "tan_delta" in Figure 3.1. However, waterdrop impacts do not involve damping or small strains but are a large deflection, large strain response phenomenon.

Impact tests utilize material property representations in the time domain and not in terms of the frequency as in Figure 3.1. The waterdrop impacts on rotor blades are highly transient events. The waterdrop impact introduces a very high-rate transient pressure buildup. The viscoelastic material experiences a very rapidly increasing stress field that leads to a distortion that is not equal to the applied force. In a perfectly elastic material, the stress gives rise to strains which are related by Young's modulus. In a viscoelastic material, the instantaneous response will be followed by an additional strain which increases with time.

For the waterdrop impact it is assumed that a localized impulse is applied to the material and the subsequent strain relaxation must be determined. This transient material behavior can be obtained from the frequency response data shown in Figure 3.1 by transforming the data from the frequency to the time domain. This is achieved by performing an inverse Fourier transform on the E′ and E″ data set. Figure 3.2 shows the transform which produces either the relaxation function or conversely the creep function. The creep function is determined when an instantaneous stress is applied at t=0; the relaxation function is evaluated when an instantaneous strain is applied at t = 0. The data at 25 °C that is important for the waterdrop impact analysis is associated with a time less than 10^{-6}s or synonymously a frequency greater than 10^6 Hz.

A review of the literature indicates that most polyurethanes at ambient conditions are in a transition regime at 10^6 to 10^7 Hz which is the critical range for the waterdrop collisions. It is known that plasticizers, fillers and impact modifiers substantially alter the stiffness values at these frequencies. Table 3.1 summarizes stiffness data from small strain periodic forced oscillations where the data was temperature to frequency converted to approximately 10^6 Hz.

17
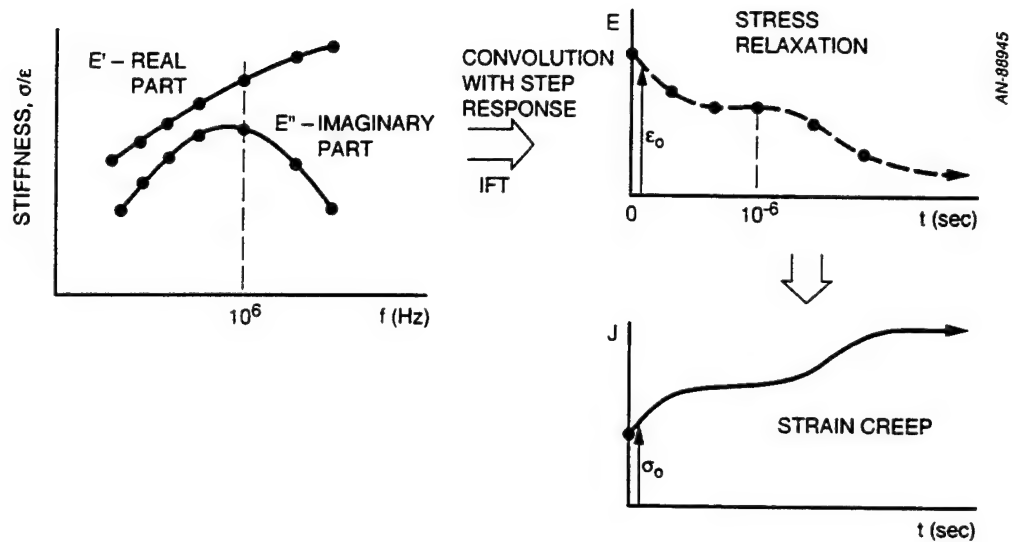
Figure 3.2   Construction of impulse material response for the computational modeling utilizing linear cyclic stiffness data.

Table 3.1. Polyurethane Stiffness Measurements at Approximately 10^6 Hz Frequency.

Reference	Temperature (°C)	Frequency (MHz)	Linear Modulus E′ (ksi)
Madigosky (1984)	10	1	580
Lewis (1991)			
Material No. 476	24	0.2	250
Material No. 478	25	4	425
Christensen and Wu (1988)	0	1	63
3M - FL-445	25	1	87
Dlubac, et al., (1990)	10	1	95

The accurate description of the rain erosion resistance of polymeric coatings resides in both the computational dynamic response modeling and the high strain rate testing to failure.

18

The use of low frequency data for the waterdrop impacts is very risky because the trends as a function of frequency are not known. A polyurethane that exhibits low ultimate strain at low temperature may be acceptable at high frequencies (high strain rates). The extremely compliant polyurethanes introduce much larger strains (because of the lower modulus) than the stiffer polyurethanes. The more compliant polyurethanes probably realize higher ultimate strains but it is unclear if the increases in ultimate strain adequately compensate for the higher tensile strains which are present.

3.2   Viscoelastic Property Measurements

It is well known that viscoelastic material properties vary greatly with the rate of deformation. Approximately 25 years ago Dupont introduced the Dynamic Mechanical Analyzer (DMA) to characterize the sinusoidal behavior of polymers. Since that time many additional test devices have become available. Most of the available test instrumentation is associated with linear, periodic deformations. Although this form of testing is useful, it does not satisfy the requirements for describing material damage caused by large amplitude, transient loadings. Test methods for assessing viscoelastic response due to impact loadings have never been adequately developed. Several transient measurement techniques will be discussed which could provide material property data for the loading conditions representative of waterdrop impacts.

The high strain rates associated with impact loads usually result in stiff, brittle material response when compared to the more common linear static and creep properties of polymers. Little data is available on viscoelastic failure characteristics for strain rates above 1000 s^{-1} which is still a low frequency for the waterdrop impacts. The true strains in the surface layer at these high strain rates can be in the range of 1 to 20 percent as indicated in the example in Table 2.1 It is reasonable to suppose that erosion resistance is correlated with the large strain capability of the polymeric materials at these very high strain rates. Figure 3.3 illustrates the substantial reduction in ultimate strain for a viscoelastic material as a function of strain rate (and a_T, the temperature-frequency shift factor). There is no comparable polyurethane data base of ultimate tensile strain at high strain rates to guide the selection of the preferred polyurethane compositions.

19
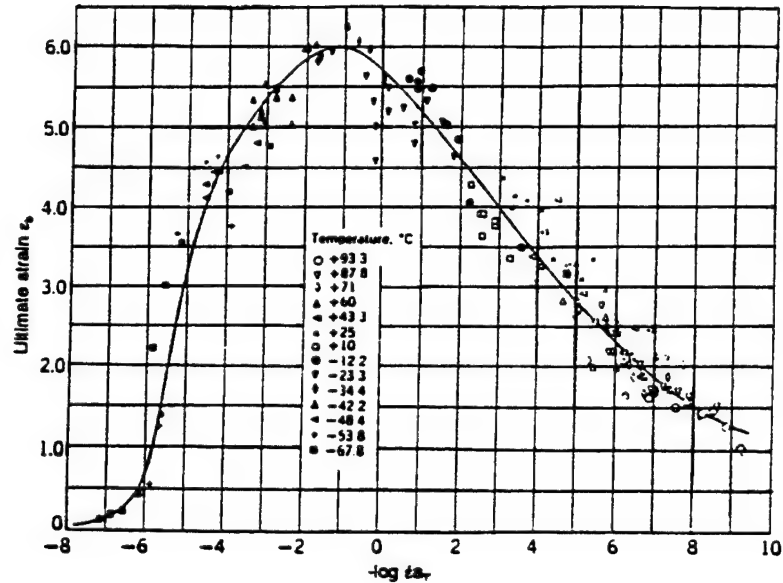
Figure 3.3   Tensile Strain at break plotted against the logarithm of strain rate reduced to -10°C for a cross-linked styrene-butadiene rubber at 14 temperatures.

The types of viscoelastic test methods that are available can be categorized as follows:

- Periodic forced oscillations are used to evaluate linear stiffness properties for small deformations.
- Impact tests are used to identify the onset of rupture and ultimate failure.
- Impact fatigue tests are used to record the rapid growth of microscopic ruptures into major tears.

3.2.1   Periodic Forced Oscillations

Mechanical or acoustic tests are not able to excite the polyurethane materials at the high frequencies required in the waterdrop impact event. Stiffness data at 10^6 to 10^8 Hz is needed to characterize the response when the waterdrop distorts the surface during the few microseconds subsequent to initial contact.   At such frequencies and for ambient temperatures most

20

polyurethane materials start approaching their glassy region and the specimen stiffness becomes too high to be excited by the standard measurement equipment. Equivalent behavior corresponding to the high frequency response is produced at low temperatures using lower frequency excitations. This temperature-frequency shift factor generally follows the Arhenius model for viscoelastic materials. Data is available to support this model for small strains but negligible data is available for large strain behavior.

3.2.2 Single Impacts

The development of microscopic flaws is primarily associated with the tension field that exists outside of the waterdrop contact region. The tensile strain magnitude to failure at high rates of loading is a significant factor for erosion resistance. Although there are numerous compression impact test procedures, the data base for tension testing is essentially non-existent.

3.2.3 Impact Fatigue

Local tensile rupture in a viscoelastic material is not well understood. Tensile rupture is the primary material property that relates to particulate erosion. There are a scattered number of documents concerning impact fatigue but the test data base is less than the analytical papers on the subject. The phenomenology is associated with the following:

- Repeated application of large strains (>10 percent).
- Initiation of small tension cracks.
- Rapid growth of the microcracks into large tears leading to macroscopic material removal.

The experimentation and theory in crack growth in viscoelastic materials have been carried out primarily for stiff polymeric materials such as polymethylmethacrylate. Mueller and Knauss (1971) have measured the crack speed in a low modulus polyurethane at strain levels of 10 to 30 percent. Crack nucleation (initiation) and growth are definitely present when the rate of load application is high as in the case of sand and waterdrop impacts.

21

Linear elastic data is the starting point for acquiring stiffness data. However, it must be recognized for the waterdrop impacts the materials experience large strains (exceeding 20 percent). The reduction in stiffness with large strain can be measured by both cyclic and transient test equipment. However many more concerns exist with the cyclic testing than the transient testing because of the internal heating and possible cumulative damage as the test proceeds and the added difficulty of holding the samples during repeated tension/compression cycles. Cyclic test equipment (Dynamic Mechanical Analyzers) are readily available from many sources. None of the DMA's have the ability to induce large strains in polyurethanes at high frequencies.

3.3   Viscoelastic Material Test Procedures

Both extension or torsional tests can provide useful data when performed at the effective high strain rates. In addition to commercial equipment, a significant number of investigators have developed unique instruments, often for special purposes. Some of the better known instruments are summarized in Table 3.2. In general, the cyclic test instrumentation provides only linear response. Knowledge of the shift factor between temperature and frequency allows measurements to be taken at low frequencies and various temperatures which will be equivalent to those at high frequencies and various temperatures. This is necessary because most excitation systems and sample geometries are likely to limit the upper frequency range to around 1000 Hz. The widely used DMA instruments only provide cyclic loadings to 10 Hz.

The only testing laboratory identified by GRC with experience in forced oscillation measurements at large strain levels is Anatrol Corporation. They have proposed to use a one-degree-of-freedom impedance oscillator for shear stiffness measurements at levels up to ten percent strain. A thermocouple would be used to determine the sample's temperature during the oscillations.

22

Table 3.2   Cyclic Forced Oscillation Instrumentation for Viscoelastic Property Measurements.

Instrumentation	Organization
Dynamic Mechanical Analyzer (DMA)	Dupont, TA Instruments
Vibrating Beam	ASTM E756-80
Autovibron DDVIII (Rheovibron)	Toyo Instruments
Torsional Braid Analyzer	PAC
Viscoanalyzer	Metravib
RSA III	Rheometrics
Impedance Oscillator	NSWC, Anatrol

Table 3.3 summarizes the transient response instrumentation which provides both linear and non-linear mechanical properties. Impact testing can provide both linear and large strain data to failure. Data from the impact loadings is preferred since it actually represents the waterdrop impact time domain event. Alternatively, the transient behavior of a material has to be inferred from the cyclically excited samples. The data in the frequency domain must then be converted to a time domain representation with the use of the inverse Fourier transform. It is desirable to obtain data directly in the time domain and avoid the frequency to time domain transforms, although these relationships have been developed by GRC.

Table 3.3. Transient Response Instrumentation

Instrumentation	Organization
• Universal Testing Machines (Fixed Rate)	• Plastechon (offers the highest loading rate machine)
• Spherical Indenter	• Dynalizer/Lemmons
• Instrumented Drop Weight Systems	• DYNATUP®/GRC
• Impedance Technique	• Many
• Flyer Plates	• Gas guns, powder guns, electrical discharge procedures at GRC

The universal testing machines can only realize the desired high strain rates by using the temperature-frequency shift factors.

23

A very attractive alternative test procedure for acquiring the basic viscoelastic properties is with a dynamic impact test apparatus manufactured by J.W. Lemmons (Belgium) called the Dynalizer. This instrument determines the short time relaxation constant directly without the added effort of requiring numerous data points at many frequencies and then the subsequent frequency to time conversions. The dynamic impact spherical indenter shown in Figure 3.4 can measure compression relaxation to 10^3 s^{-1}. Discussions with the commercial developer of this test procedure indicate that a substantial increase in strain rate is likely with minor modifications.

$\varepsilon = $ VARIABLE

$\dot{\varepsilon} \leq 10^3$ s^{-1}

OUTPUT: $E(t) = A + Bt^{-\alpha} = \dfrac{0.48}{R^{0.59} D^{1.33}} F(t)$

$E'(f) E''(f)$
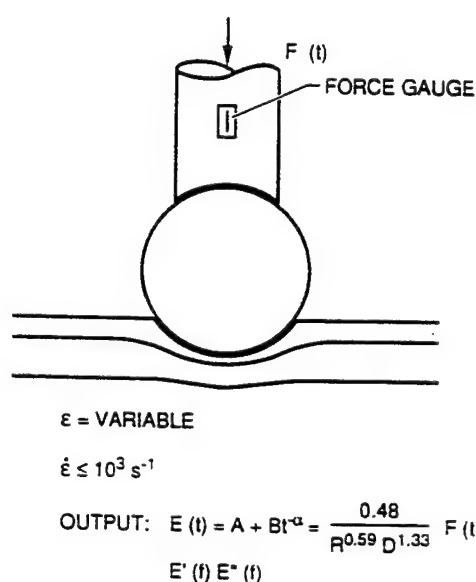
Figure 3.4 Dynalizer-spherical dynamic indenter with strain control.

Within GRC's DYNATUP® Products Group are impact testing experts for plastics and composites using a family of instrumented drop weight systems (an example of this equipment is shown in Figure 3.5. A modified drop tower arrangement can use a cantilever beam actuator shown schematically in Figure 3.6 to measure the tensile strength in the test specimen. The maximum realizable strain rate is about 7×10^3 s^{-1} for the current fixture.

24

CONTROL HOUSING

HOIST CHAIN

GUIDE POST (2)

SUPPORT POST (2)

HEIGHT INDICATOR SCALE

RELEASE LATCH HOUSING

HAMMER

BRAKE SWITCH

INSTRUMENTED TUP

STOP BLOCK (2)

BASE
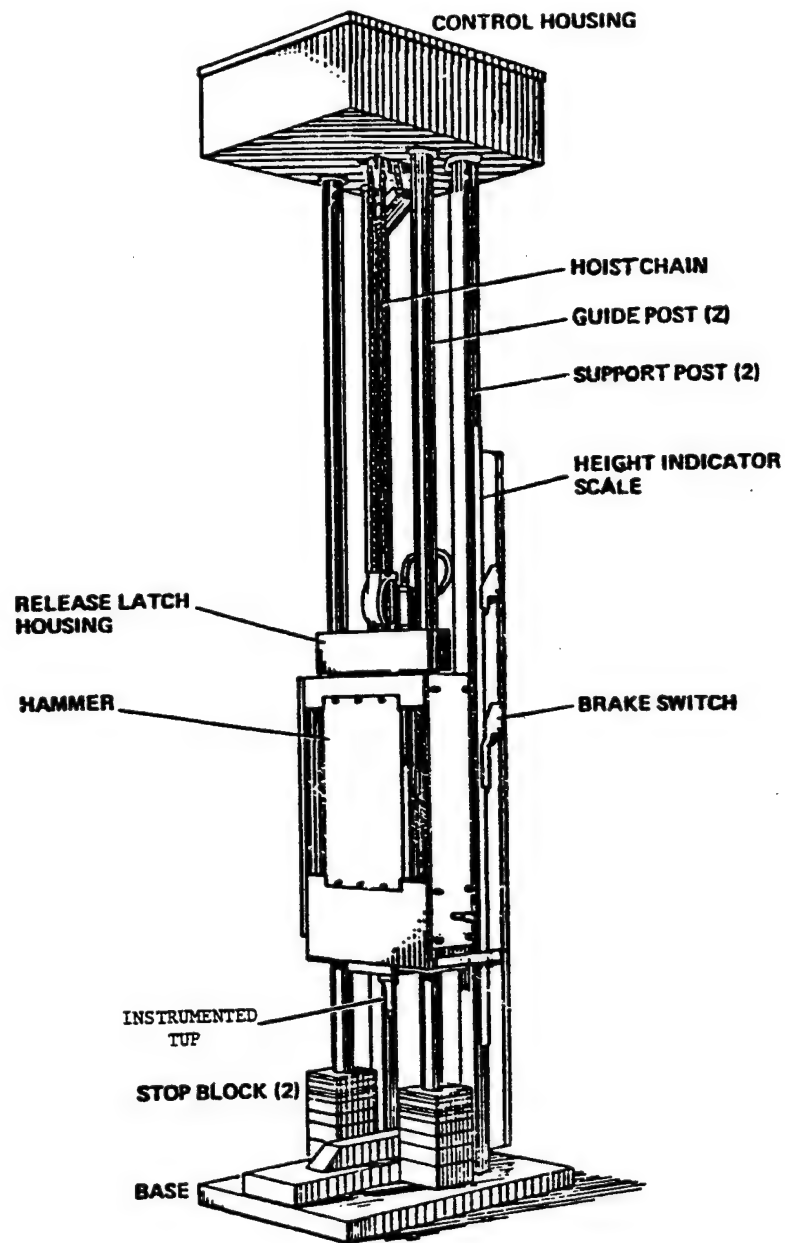
Figure 3.5   Schematic of drop weight system.

25

131

Anatrol proposed to use their proven shock impedance technique to acquire viscoelastic data at high strain rates. Figure 3.7 shows the one-degree-of-freedom model they proposed to use in their approach. A mass is mounted at four corners of a frame. A miniature accelerometer is attached to the mass which records the one-degree-of-freedom response. The mass is excited by an instrumented impact hammer. Increasing the impact force of the hammer results in larger strains. The temporal data is recorded and subsequently converted to the frequency domain. The highest frequency expected by this technique is probably 1000 Hz. The impact excitation could be applied to generate either extensional or shear deformations. The temperature-frequency shift factor is required for each material to predict the properties up to strain rates of 2×10^5 s^{-1}.
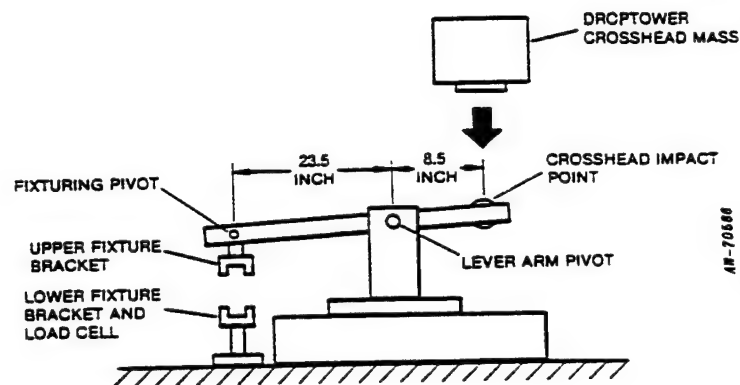
Figure 3.6 Drop tower with mechanical advantage in tension impact tests.
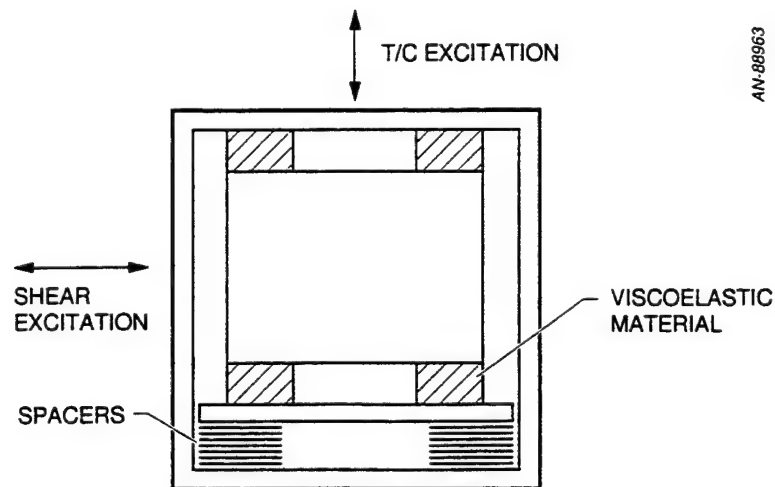
Figure 3.7. Schematic drawing of the test specimen used for impedance technique.

26

4.0 HIGH-FREQUENCY, LARGE STRAIN MATERIAL PROPERTY MEASUREMENTS

High-frequency viscoelastic properties data is not readily available for the polyurethane coating candidates selected for rotor erosion protection. As described in Section 3 the preferred measurement technique to obtain the viscoelastic response data is a transient force measurement rather than periodic force measurements. The transient force data can be taken at the operational temperatures and the stress-strain data used directly without a temperature-frequency conversion factor (shift factor). The principal attribute of the transient data acquisition procedure is that the representative test conditions are achieved directly: namely, large strain and high strain rates up to material failure. Data obtained from the GRC high-velocity impact test procedure to be described can readily provide the needed large strain, high strain rate data including tensile failure of the material.

General Research performs many routine measurements on materials at strain rates exceeding 10^5 s^{-1} using its gas gun and powder gun facilities. A gas or explosively driven projectile is suddenly accelerated or decelerated to apply high loading rates. The response of materials due to these shock wave loadings is recorded by high speed event recorders. Hugoniot and transient stress data can be acquired in many forms with the existing experimental capabilities at GRC.

For the proposed test configuration a 50 mm diameter powder gun was used to provide the impulsive loading on the polyurethane sample. An overview of the GRC ballistic range is shown in Figure 4.1. The GRC 50 mm ballistic range facility is designed to launch 200 g payloads at velocities from 650 to 8500 fps. The range is used for various impact experiments and with a minimum of modification was adapted to the acquisition of polyurethane material property measurements. The test section for the 50 mm powder gun is in the foreground of the photograph in Figure 4.2.

The final arrangement for the test configuration is shown schematically in Figure 4.3. An aluminum projectile is launched with the gun on the left side of Figure 4.3a. The projectile

27

133
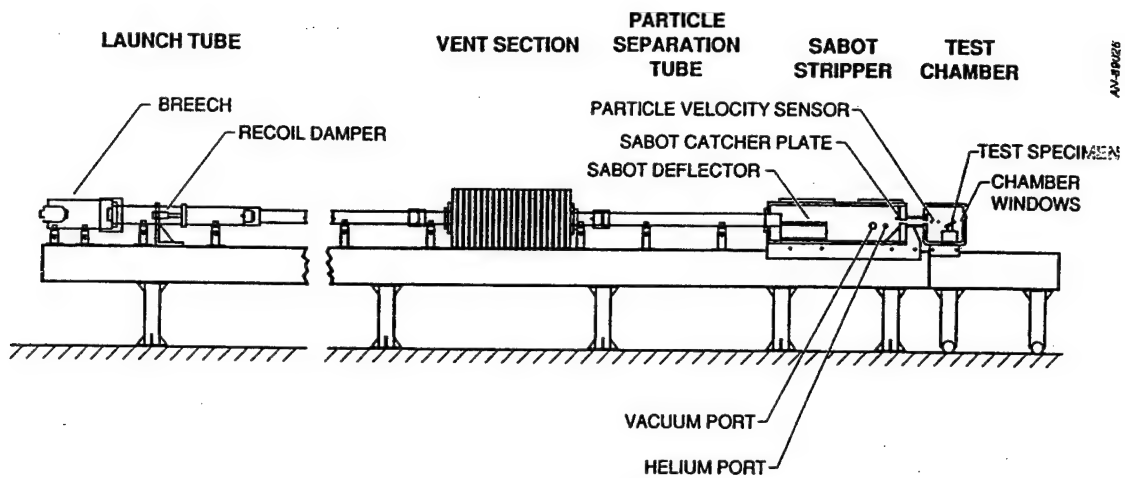
Figure 4.1   Overview of the ballistic range.
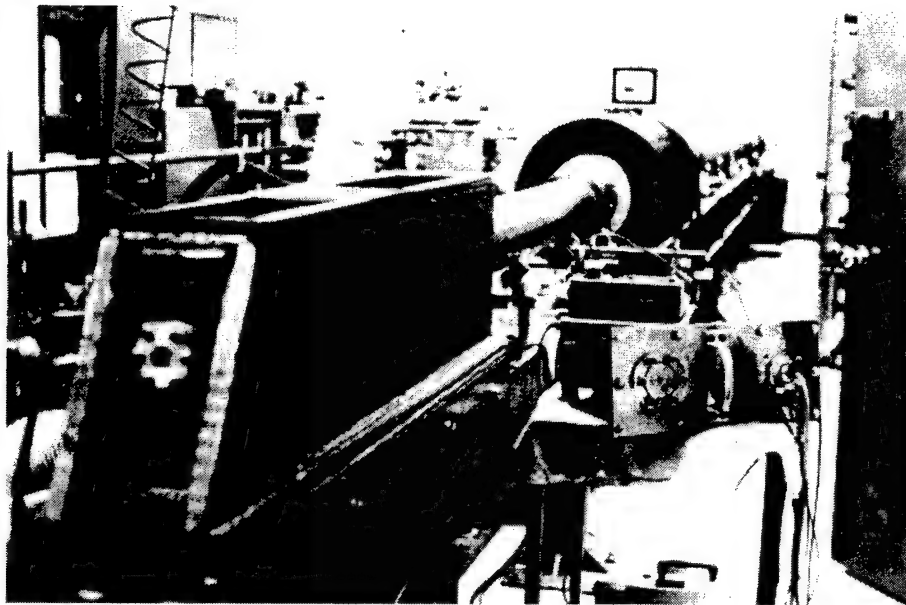
Figure 4.2   GRC 50 mm power gun facility configured for high strain rate tension testing of polymeric materials.   Impact chamber is in foreground and gun barrel is in background.

28
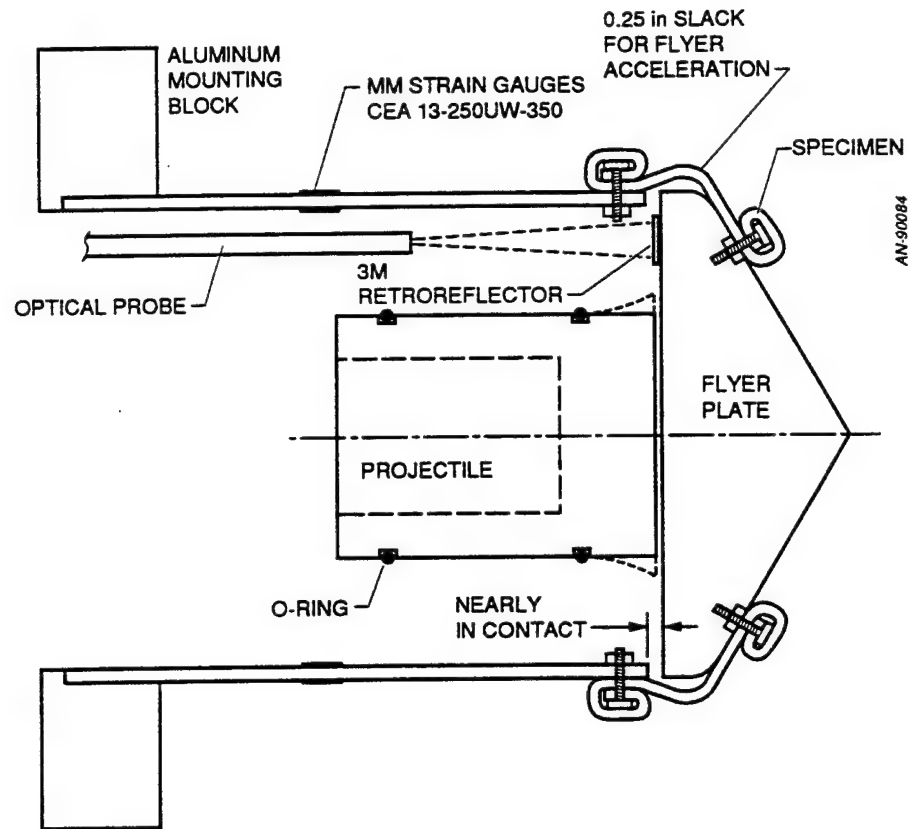
a. Overview of specimen loading configuration.
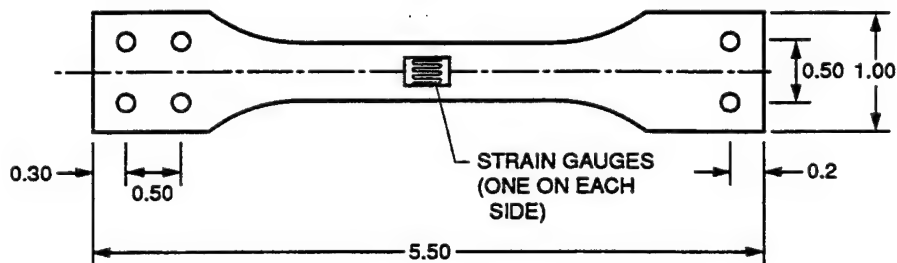
b. Detail of load cell Plate.

Figure 4.3. General test configuration for high strain rate tests for polymeric materials.

29

impacts the flyer plate which is held in place by plastic adjustment screws. The momentum from the projectile is transferred to the flyer plate which is accelerated to moderately high velocities (currently up to 1800 fps). The specimen is mounted to the flyer plate and an aluminum strip with strain gages (shown in Figure 4.3b) to measure the force applied to the polymeric sample. The mass and acceleration of the flyer plate are large compared to mass of the material sample, so the sample is stretched under fairly controlled conditions. The actual test setup can be seen in Figure 4.4. The projectile just making contact with the flyer plate is shown in Figure 4.5.

The complete tensile stress as a function of strain curve at designated strain rates can be obtained for each polymeric specimen. The force measurements are obtained from calibrated strain gages mounted on a 0.5 in. wide by 0.067 in. thick aluminum plate (Figure 4.3b). The strain gage signal is amplified by a LeCroy Model 8100 amplifier which has a frequency linearity to 1 MHz.

The facility can use two aluminum plates to acquire simultaneous stress data on two samples. The flyer plate velocity is recorded by a custom modified MTI-2000 photonic range sensor with a bandwidth of 800 MHz. Data is acquired and stored on a two-channel LeCroy 9410 digital storage scope and a two-channel Nicolet 204A oscilloscope. The scopes have a time resolution to 10 ns. These oscilloscopes are triggered using the signal from the MTI probe. Figure 4.3a shows the baseline shapes of the projectile, flyer plate, and the relative locations of the sensor instrumentation.

The MTI-2000 fiber optic probe performs better than the usual specifications because of circuitry modifications requested from the manufacturer that increase the bandwidth and gain. The optical circuitry has no attenuation to 600 MHz. The signal drift is insignificant after a half-hour warm-up. The probe is capable of accurately measuring the separation distance from the target over several inches using micro-miniature corner cube reflectors bonded to the flyer plates. The preferred reflective tape is Type 3970 G manufactured by 3M. The tape applied to the flyer

30
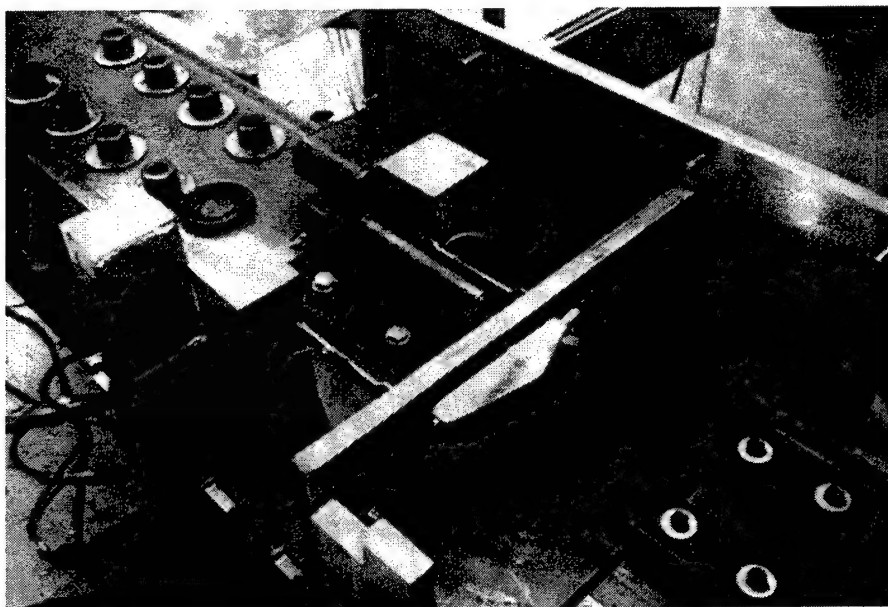
Figure 4.4   View of the test section showing the flyer plate in place, the optical probe, and aluminum load cell attached to the polymeric strip.
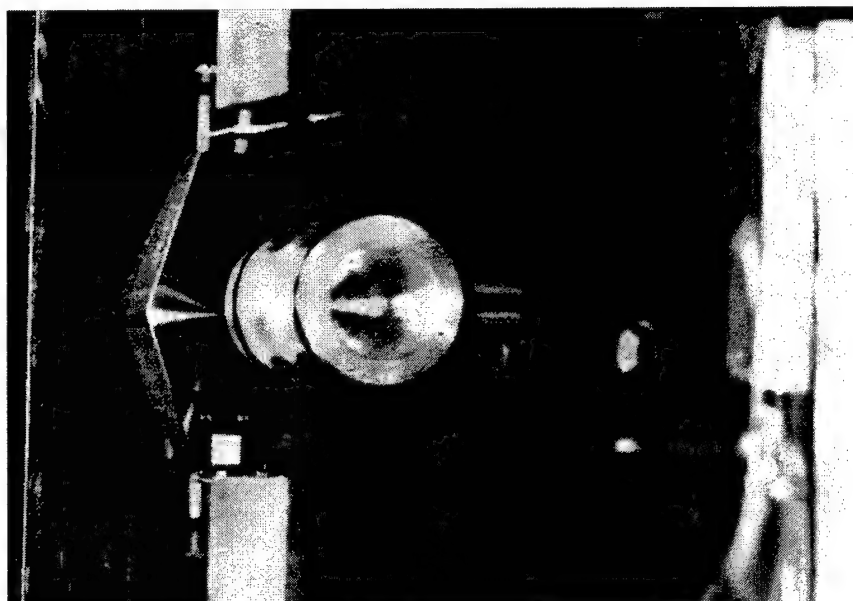
Figure 4.5.   View of 50 mm aluminum projectile prior to impacting the flyer plate.

31

plate measures only 0.375 in by 0.375 in by 0.005 in thick. The probe is spaced initially 2.0 in from the corner cube. The corner cube provides an excellent return signal that is relatively insensitive to tilt. This arrangement produces 0.526 in/V signal at the 2.0 in. spacing.

The optical probe measures the time history of the test specimen as the impact event takes place. The velocity measurements are important in order to evaluate how much of the velocity of the projectile is transferred to the flyer plate during the time the specimen is elongated to failure.

Figures 4.6 and 4.7 are examples of the data output from a test using material 17. The oscilloscope trace in Figure 4.6 is the displacement of the flyer plate. This trace is the output of the MTI fiber optic probe which is calibrated to read displacements from 1.5 to 4.0 in. The specimen extension as a function of voltage is a nonlinear relationship. The ordinate is the voltage and the abscissa is time. The oscillations are attributed to the modal vibrations of the flyer plate from the impact with the projectile. In this example, the flyer plate reaches a steady speed of 786 fps. The velocity is determined from a linear fit to the slope of the displacement/time plot. The plate is subjected to 300,000 g's average acceleration during the ramp-up.

The displacement of the flyer plate is measured using the MTI probe which relies on reflected light. The light intensity is converted to an analog voltage in the range of 0 to 5.0 volts which corresponds to a displacement of 1.5 to 4.0 in. The voltage/displacement relationship is nonlinear. Strongly influencing the relationship is the type and size of the retroreflector bonded to the flyer plate. The signal is weak at a displacement of 4 inches which constitutes the maximum usable range. For a 0.375 by 0.375 inch reflector tape, the displacement/voltage relationship is

$$d = 5.634 - 1.552 \, V + 0.165 \, V^2$$

where V is volts and d is the displacement in inches. Most impact events were aligned with an initial deflection of 1.8 to 2.2 inches or a nominal voltage of 3.5 volts. When the center of
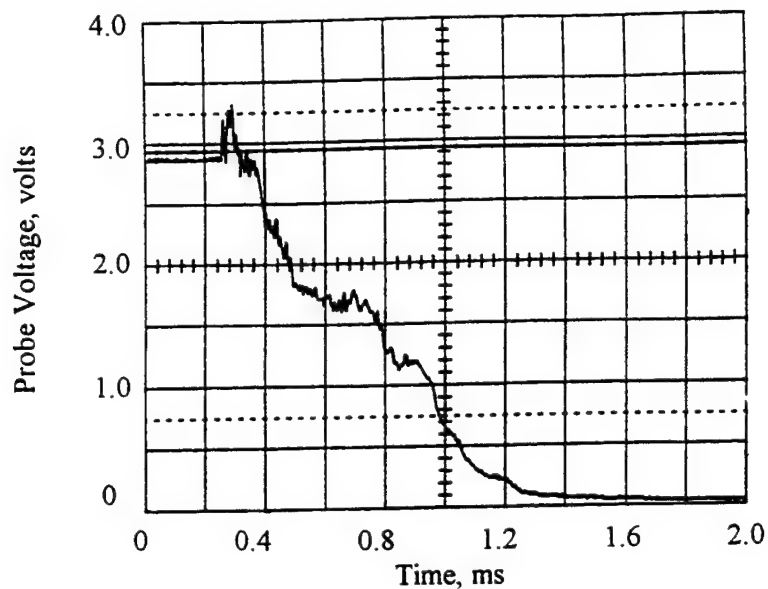
Figure 4.6   Flyer plate displacement recorded with MTI-2000 photonic range sensor for Material 17, Run 12-1 (Refer to Appendix A).
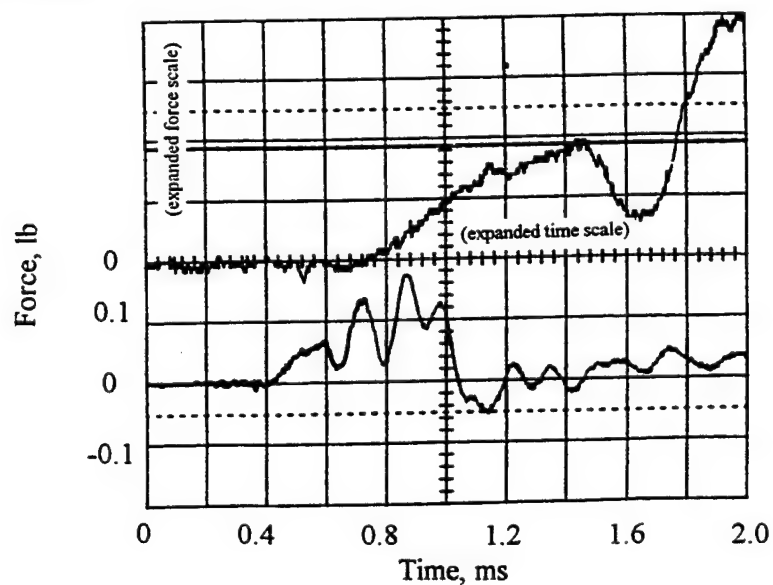
Figure 4.7   Load/time trace for evaluation of the stresses in polyurethane Material 17, Run 12-1. (Refer to Appendix A). The upper trace provides an expanded scale of the forces during the loading phase.

33

the flyer plate is impacted, the two ends of the flyer plate deflect opposite to the direction of the central impact zone. This lowest mode bending deflection causes the voltage to increase slightly and subsequently to asymptotically decrease to zero as the plate moves down the tube. A best fit line through the oscillations is used to calculate the average velocity of the accelerated flyer plate.

Perturbations and changes to the shape and size of the retroreflector yielded slightly different relationships for most firings. However, the average speeds were close to one another in the four regimes of interest, namely, 310, 510, 875 and 1100 fps. At the present time only the average velocities are calculated from the MTI readouts.

The lower trace in Figure 4.7 is the strain gage reading which is calibrated to provide the force in the polyurethane strip. This trace is linear with the scaling relationship of 266.7 lb/V. It is seen that the strain readings have harmonic content. This is attributed to the mass of the aluminum strain plate that has cross sectional dimensions of 0.5 in. wide by 0.067 in. thick. A guideplate was installed with the aluminum strain plate in order to reduce the bending strains. The relevant portion of the strain gage reading is shown on an expanded scale as the upper trace in Figure 4.7.

The shape and mass of the aluminum sabot and aluminum flyer plate for the high strain tests have been standardized for production mode testing. With the current configuration the sabot impact velocity was in the range from 300 to 1800 fps. The reliability of this facility continues to improved as experience is gained with the electronic and mechanical components.

The projectile and flyer plate designs followed an evolutionary process. Initially polymeric projectiles were considered. Several candidate materials for the projectile were evaluated. A candidate material which did not break-up or distort excessively prior to completion of the test was desirable. These experiments were guided by modeling the impact mechanics occurring between the polymeric plug and the impacted plate. This process was accurately simulated using the DYNA3D finite element code. A parametric model was developed and eleven cases were considered. The principal observations from these runs are as follows:

34

- Large plastic distortions of the projectile occur at impact velocities exceeding 2500 fps. These distortions do not affect the momentum transfer to the flyer plate. However, to prevent the distorted projectile material from impacting the test specimen, the specimen must be several inches away from the projectile impact site.

- Aluminum flyer plates greater than 0.5 in. thick at the impact location are required to survive projectile punch through or fracturing. A thickness of 1.5 in. is desirable to minimize edge deformations. However, the higher mass reduces the velocity transferred from the projectile. The impacted flyer plate should therefore not be a circular plate in order to reduce the mass but something closer to a rectangular plate with dimensions of 2.5 by 4.0 in. across and 0.75 to 1.5 in. thick.

- The thickness of the impacted flyer plate is dictated in part by the MTI fiber optic sensor used for the displacement measurements. This sensor can not read plate motion if at the same time large rotations are occurring.

The computational models provided valuable insights into the interactions that occur when the flyer plate is struck by the projectile at high velocity. The initial impact tests without specimens or instrumentation in place successfully demonstrated that the calculated projectile and flyer plate designs survived without breaking apart. The extent of the deformations agreed with the results from the computer model.

Nominally the projectile is 2.0 in. in diameter by 2.75 in. long. In-house experience favored using polymeric materials for the projectile which is fired down the 50 mm diameter range. Currently polystyrene is used but better overall performance was expected from the alternative polymers listed in Table 4.1. This information was obtained from several sources which included manufacturers and those involved in ballistic impact experimentation. The claims of the suppliers for some of these materials regarding the ballistic behavior of their materials were verified in the GRC facility and did not provide the anticipated performance. Fragmentation and large deformation of the impacting projectile have to be avoided in order to eliminate damage to the instrumentation that is used in the high strain rate tests.

Table 4.1 Impact Behavior of Polymeric Projectile Materials.

Polymer	Impact Characteristics	GRC Results
Propolux 944	Easy to machine. Polypropylene copolymer used by ballistic ranges for non-fragmenting impacts to 9000 fps.	Effective up to 3200 fps but severe front face melting and mushrooming to two times it initial diameter made it undesirable for this application.
Zelux M	Machinable polycarbonate. Sabots can be launched to 600 fps and impact surfaces without fragmenting.	Fractures into several pieces at 2200 fps. Fragments are not acceptable due to interference with instrumentation.
Hi-Impact Polystyrene	Far better than the standard polystyrene	Exhibits large plastic flow and extreme deformations at 2200 fps.
Nylotron GS	High shear strength nylon with polydisulfide	Fragmented into almost a dust at 3200 fps.
Polyproplyene	Not a good ballistic material since it is brittle at high strain rates.	Excessive deformations which can interfere with instrumentation.

None of the polymeric projectile materials was acceptable within the constraints imposed in the GRC high strain impact facility. This led to the use of an aluminum projectile which would not fragment or distort excessively for the range of impact velocities required to achieve the high strain rates. the extent of the posttest deformations of the aluminum projectiles is shown in Figure 4.8. The aluminum projectiles experience an 11 percent permanent compression shortening and an 11 percent radial expansion at the impact face. This level of distortion is quite acceptable and does not interfere with the optical displacement signal. The characteristic difference between the polymeric and the aluminum projectiles is the mushrooming or cracking of the polymers. Results using aluminum projectiles are sensitive to the shape of the projectile face impacting the planar flyer plate. The preferred shape is a concave front which shifts the early loading to the outer annulus of the projectile.

A flyer plate also had to be designed which would not fracture during the loading cycle. The impact event at projectile velocities in the vicinity of 2000 fps is fairly violent. The major limitation on the maximum velocity that can be used reliability in the polymeric impact tests is the onset of fracture in the flyer plate. This was a critical limitation until the flyer plate shape

36
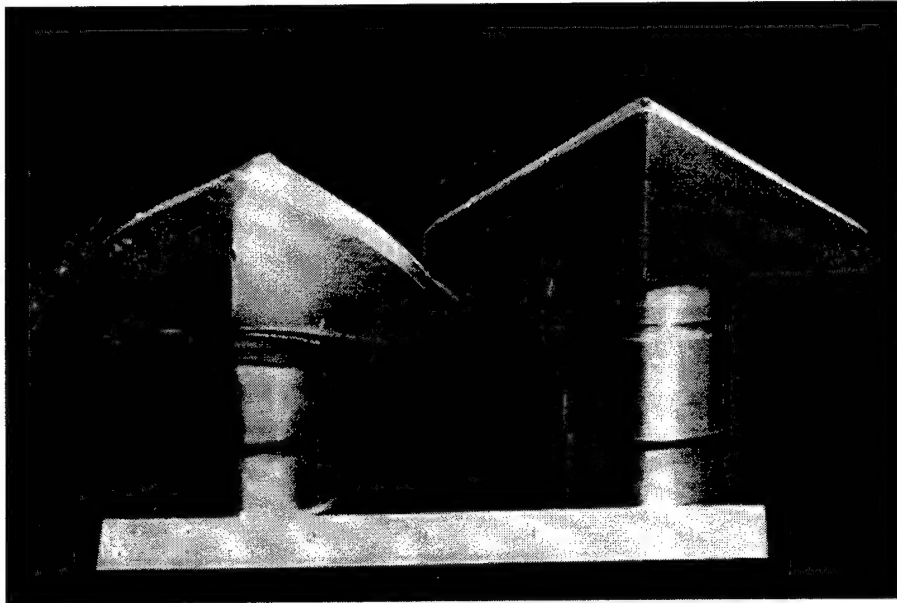
a. Pre-and posttest flyer plates and sabots used in 16000 in/in/s strain rate tests.

b. Deformation of 220 g aluminum projectile after 1800 fps impact.

Figure 4.8. Initial and posttest condition of the aluminum projectile.

37

shown in Figure 4.8 was developed. This geometry strengthens the flyer plate at locations which are highly stressed while minimizing the overall mass of the plate. A maximum projectile velocity of 2000 fps can currently be achieved. No significant effort has been devoted to optimizing the flyer plate's geometry so that it can effectively survive higher impact velocities: which translates into higher strain rates.

Three alternative techniques for gripping the flexible polyurethane specimens during the test have been designed. The primary problem in gripping the specimen is slippage at the supports which will reduce the rate of strain that can be achieved.

- Long strips of the flexible test materials are rolled onto a shaft. The applied tension during the loading phase produces lateral contractions which lock the material on the shaft. The thinned gage section is between two shafts which are being separated at a rapid rate during the loading cycle.

- The specimen can also be held by a wedge-type gripping arrangement such that as the tension increases the jaws of the wedge apply compressive loadings to the specimen to hold it in place.

- Finally, the simplest arrangement is to adhesively bond the specimen to the flyer plate and a fixed support. The bonded area can be made much larger than the gage cross section of the specimen so the shear strength of the adhesive may be sufficient to resist the impulsive loadings that will be generated during the test.

A combination of the first gripping method with adhesive bonding was finally found to provide satisfactory results. This arrangement was developed after several test firings in the facility. This gripping system is shown in Figure 4.9 with a failed specimen showing the failure occurring in the reduced section. The specimen mounted on the flyer plate and the aluminum load cell is shown in Figure 4.10 prior to testing.

Static tests using a Tinius Olsen Universal Test Machine were used to determine strain to failure at low strain rates and to experiment with various gripping techniques. The very simple, inexpensive mounting technique which was devised for attaching the polyurethane specimen to the flyer plate was used in these tests which were a further check on whether any specimen pull out was taking place. Quasistatic tension tests have produced true strains to failure of 500 to 800 percent in the candidate materials.

38
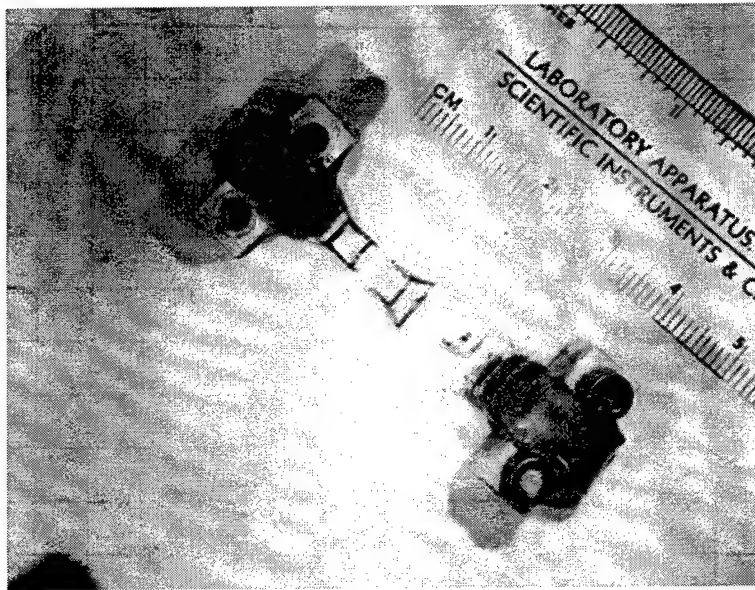
Figure 4.9. Failed polyurethane specimen with successful mounting arrangement.

Figure 4.10. View of the flyer plate and mounted polyurethane specimen prior to testing.

5.0   MATERIAL PROPERTY TEST RESULTS

The GRC transient high strain to failure test capability described in Section 4 was used to obtain the relevant material property measurements for five polyurethane materials. The five candidate materials are identified by the KAC assigned sample number. The materials evaluated were the following: Material No. 4, Material No. 11, Material No. 17, Material No. 44, and Material No. 45. The specimen requirements for these materials are strips nominally 5.3 in. long by 0.3 in. wide and approximately 0.060 in. thick.

As outlined in Section 4 the tension testing was accomplished by attaching one end of the specimen to a rigid base and the other end to a freely-supported flyer plate. The flyer plate was rapidly displaced by the impact and efficient momentum transfer from an aluminum projectile that was fired into the aluminum flyer plate.

It was not possible to attach stress/strain monitoring equipment directly onto the polyurethane strips. Instead, the strain was recorded by monitoring flyer plate motion and stress was obtained by recording strain in a lightweight aluminum plate that was attached to one end of the polyurethane strips as described in detail in Section 4. The interpretation of the acquired test data requires an understanding of the wave propagation path through the material specimen and into the sensors and data acquisition instrumentation. The determination of constitutive properties from the test data was obtained from these measurements. Time limitations precluded digital data conversion of the raw data to a functional set of relations. Instead, the analog data was manually converted to several simple parameters such as ultimate stress and ultimate strain.

The stress measurements provide an envelope of peak stresses in the polyurethane specimen when undergoing elongation. An example of these measurements is shown in Figure 4.7. The high-frequency stresses at the beginning of the linear loading cycle are not available. However, a history of stress to failure is measured by an envelope which typically has 4 to 6 peaks within the defined stress-strain envelope. This portion of the force time record is reproduced in Figures 5.1 to 5.5 for one test of each material candidate. The curves in Figures 5.1 to 5.5 are the first part of the representative curve show for Material 17 in Figure 4.7. The

41
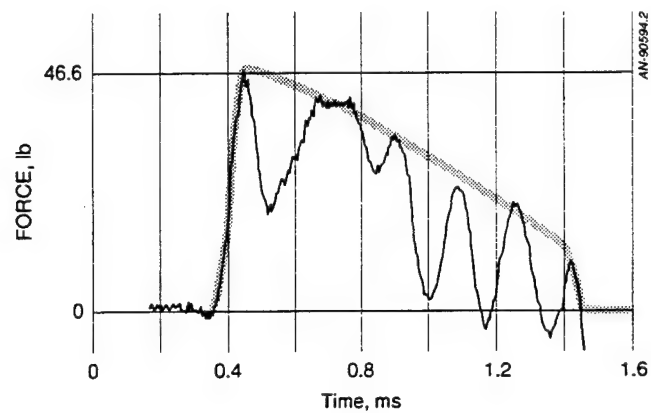
Figure 5.1 Force/Time History for Material 4 (Run 1-17).
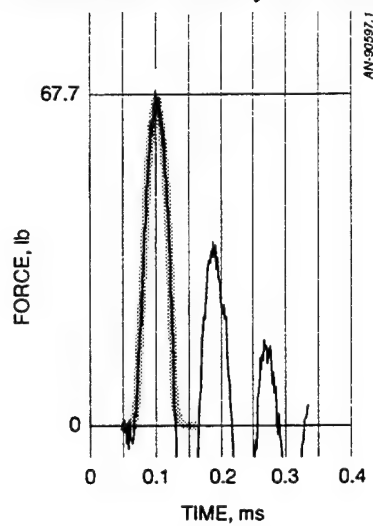
Figure 5.2. Force/Time History for Material 11 (Run 1-6).
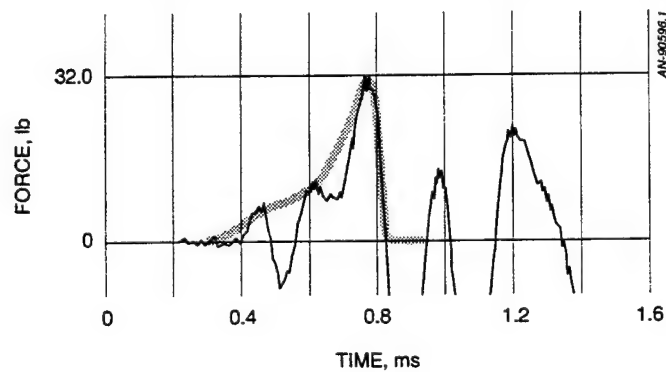
Figure 5.3. Force/Time History for Material 17 (Run 1-15).

42
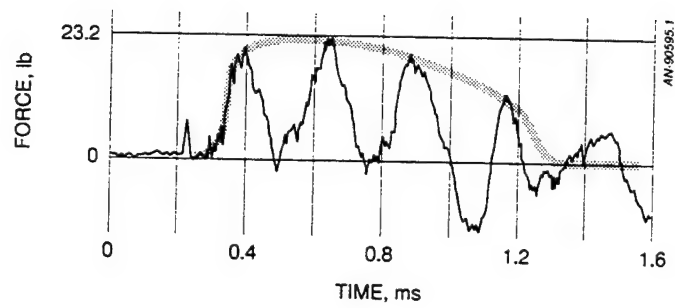
Figure 5.4. Force/Time History for Material 44 (Run 12-22).
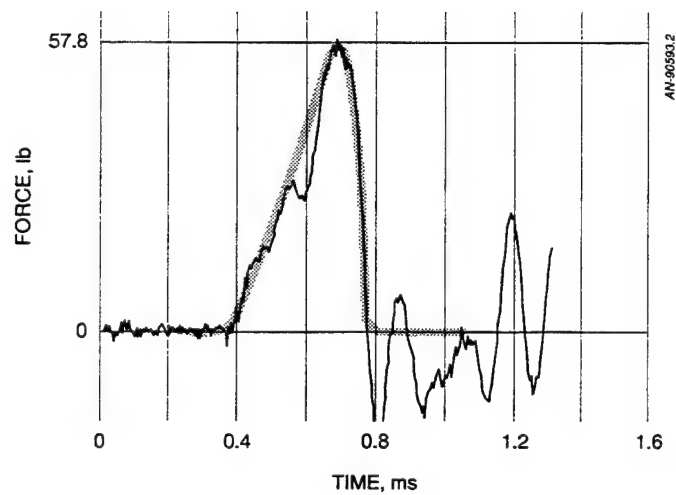
Figure 5.5. Force/Time History for Material 45 (Run 1-12a).

43

period of the oscillations observed in these figures is attributed to the in-plane wave propagation of the polyurethane specimen and the aluminum test plate. All the data collected on the five polyurethane materials at different loading rates is compiled in Appendix A.

Figures 5.1 to 5.5 show the raw data output from the aluminum load cell which monitored the force in the polyurethane test specimens. The five data sets were replotted to the same x/y scales to better illustrate the trends. The shaded envelope drawn around the cyclically varying force data is the approximate force-time history. The data in these figures is for an average flyer plate speed of about 1100 fps achieved after impact with the projectile traveling at 1530 fps (for a momentum conversion efficiency of 87 per cent). The stress wave progression leaving the polyurethane and traveling into the aluminum load cell provides only a few data points at the sinusoid peaks.

The force/time histories shown in Figures 5.1 through 5.5 are the direct strain gage readouts multiplied by a gain factor. The strain gages are recording an in-plane wave propagating through the aluminum strip. Special design of this fixture and the aluminum strip inhibits lateral bending vibrations. Therefore the strains are only due to in-plane wave propagation. Once the tension wave passes over the strain gage, the wave continues to the end of the strip where it is reflected as a compression wave. The compression wave traverses the strain gage which produces a reduced signal. Thus, there are periods of in-plane wave oscillations similar to an acoustic pipe frequency. With the wave speed in aluminum at 0.25 in/μs and an aluminum test plate length of 8 inches, a period of at least 32 μs is expected in the data. Hammer impacts to the aluminum test plate with the specimen in place produces a period of in-plane oscillation from 100 to 160 μs. Part of this longer period is attributed to the reduced wave speed traveling through the polyurethane specimen which is attached to the end of the aluminum test plate. The wave speed through polyurethane is very low as compared with aluminum.

Interpreting the force/time history traces is difficult because of the in-plane wave oscillations. In numerous tests using a hammer impact for calibration and very low velocity impacts, it became evident that the envelope around the cyclic oscillations characterizes

44

the average force/time history. The oscillations reduce the actual strains present. In Figures 5.1 to 5.5, the shaded envelope provides a filtered form of the force/time response which minimizes the effect of the higher-frequency oscillations. The response is seen to be quite different for the five materials.

The response of the five polyurethanes shows surprisingly large ultimate strains to failure with the exception of material 11. The test data does not support an earlier conjecture that these polyurethanes exhibit a tendency toward a more brittle behavior (stiffen) as the strain rates approach 10^5 s^{-1}. The polyurethane elongations were found to be very large. The ultimate strains with increasing strain rate from 10^4 s^{-1} do not change significantly from their lower-frequency values. These materials also exhibit a very large reduction in cross sectional area commensurate with the large recorded elongations.

The measured stiffness values for the polyurethanes are quite low. The maximum secant stiffness recorded during the large distortion stage varies from 0.5 to 13.3 ksi. Large strain data is not available for these or other polymers from alternate sources to compare these material responses. Data from dynamic mechanical analyzers for alternate polymers acquired at infinitesimal strains can not be related to the measurements made in the current program for large strain. It is found that the stiffness decreases as the measured strain magnitude increases in contrast to the small strain relations.

The constitutive properties of the polyurethanes can only be approximated with the high strain data shown in Figures 5.1 to 5.5. Although the data is measured to failure, as explained previously the data is effectively filtered as it passes through the specimen and into the aluminum bar where the strain gages are located. As a result the data is lacking high frequency detail including the early time deformations. Attempts to better understand the material's constitutive nature are limited by this low-pass filtering of the stress/strain data. Interpolation is required between the 4 to 16 accurate data points (peaks of the sinusoids) that currently define the response envelope. The force-time history is combined with the strain data to determine stress. True stress is calculated by including the correction for the change in the cross-sectional area of

45

the specimen, i.e. $A_o/A = 1 + \varepsilon$, where A_o is the initial area, A is the current area, and ε is the tensile strain component.

Large strain values were measured for all materials except for material 11 which is quite stiff even at low strain rates. The uncertainties in the data and variability in the samples favors taking averages of multiple runs. Multiple tests for material 17 were used to obtain an average stiffness for the five samples tested.

Failure data was acquired over a range of strain rates. Table 5.1 summarizes the properties data for the five polyurethanes tested to failure. The ultimate strength, ultimate strain and secant modulus are listed in order from the most compliant to the stiffest: material 4,44,17, 45, and 11. Data is provided for several strain rates, categorized as fast, medium, slow and very slow. These designation corresponds to a nominal strain rate of 10200, 8120, 4730, and 2875 s^{-1}. The values listed in Table 5.1 in parentheses define the number of averaged test specimens. The largest number of specimens tested was for material 11 and the least number tested was for material 4 (which represents the current polyurethane coating for the K747 main rotor).

The determination of the parameters in Table 5.1 is illustrated using the data in Figure 5.5 for material 45. From Figure 5.5 the peak force in the polyurethane strip as measured by the strain gages on the aluminum test strip is 57.8 lb. This force occurred 300 μs after impact. The true strain in the narrow cross-section of the dog-bone specimen is given by

$$\varepsilon = \left(\frac{\delta_2}{\Delta}\right)\left(\frac{\Delta}{\ell_2}\right)$$

where

$$\frac{\delta_2}{\Delta} = \left[1 + \left(\frac{\ell_1}{\ell_2}\right)\left(\frac{w_2}{w_1}\right)\right]^{-1}$$

The sum $\ell_1 + \ell_2$ is the length of the specimen between the clamped ends; ℓ_2 is the length of the thin section of the dog bone and w_1 and w_2 are the corresponding widths. The dimensions for

46

Table 5.1
Summary of High Strain Rate Properties of Five Polyurethanes
in Tension Tests to Failure.

No. Rank	1	2	3	4	5
Material No.	4	44	17	45	11
Color	Black	Dk. Yellow	Amber	Clear	Black
Ultimate Strength, σ (ksi)					
Fast	3.9	11.9 (4)	47.8 (6)	36.1	21.5 (2)
Medium	—	10.1	27.2 (4)	—	24.9
Slow	—	—	—	28.9	—
Very Slow	1.51	1.69	8.67	30.1	8.9
Ultimate Strain, ε					
Fast	6.87	4.66	6.60 (6)	4.10	1.64 (2)
Medium	—	4.13	5.12 (4)	—	1.90
Slow	3.6	—	—	5.8	—
Very Slow	5.72	1.47	3.18	4.56	2.98
Ultimate Strength / Ultimate Strain = E (ksi)					
Fast	0.58	4.49 (4)	6.47 (6)	8.78	13.1 (2)
Medium	—	2.44	5.31 (4)	—	12.74
Slow		—	—	6.45	—
Very Slow	0.26	1.20	2.73	6.63	2.99

AN-90629

( ) Indicates the number of tests included in the average
value in the table.

47

the dog bone are $\ell_1 = 1.33$ in, $\ell_2 = 0.3$ in, $w_1 = 0.3$ in, and $w_2 = 0.15$ in. The total elongation of the specimen

$$\Delta = \delta_1 + \delta_2 = vt$$

where δ_2 is the elongation of the thin section of the dog bone and v is the average velocity of the flyer plate over the time t. So

$$\varepsilon = 0.311\frac{vt}{\ell_2}$$

In the example in Figure 5.5 the specimen length increases by $\Delta = (1.32 \times 10^4$ in/s) $(300 \times 10^{-6}$s) = 3.96 in. The true strain is $\varepsilon = 1.036(3.96) = 4.1$ (410 per cent axial elongation).

The true stress,

$$\sigma = \frac{F}{A_o}\left(\frac{A_o}{A}\right)$$

requires a prediction of the reduced cross-section, A, in the narrow dog-bone region. It can be shown for elastic materials with a Poisson's ratio $v>0.4$ that the area ratio is simply $A_o/A = 1 + \varepsilon$ or $A_o/A = 6.3$. The cross-sectional area A_o is 0.00816 in^2 so the stress is

$$\sigma = \frac{57.8\,(5.1)}{0.00816} = 36,125 \text{ psi}$$

The hyperelastic modulus for this condition is E = 35,125/4.1 = 8811 psi

In the cases where the data comprises multiple sinusoids (e.g., Figure 5.1 to 5.4) the stress and strain values must be computed at each sinusoidal peak to determine the hyperelastic modulus. In many cases (e.g., Figure 5.1), the true stress remains nearly constant to failure. The stress in Figure 5.4 is increasing with each sinusoid and reaches its peak value at the fourth sinusoid when the specimen fails.

48

Program constraints prevented the acquisition of more test data. The data presented is representative of large strain response but lacks an adequate statistical base to provide high confidence in the absolute values.

There is little difference in the GRC high strain rate data between the fast and medium strain rates: especially with respect to viscoelastic behavior. However, viscoelastic behavior is very evident for the small-deflection, linear response shown in Figure 3.1.

There is a strong variation in stiffness as a function of frequency.

For the waterdrop impact conditions the times of interest (0.1 to 10 μs) convert to 6.3×10^5 to 6.3×10^7 rad/s. From Figure 3.1 the small-strain linear modulus E' is 58 to 123 ksi. This larger stiffness is expected. The DMA data is not very useful in the finite element simulations because the strains are small. The large strain hyperelastic modulus is about 8.8 ksi. Limited DMA testing at 10 percent strain has shown a significant lowering of stiffness. The DMA data can be used in the first 0.1 μs of the impact event when the strains are still small. However, the material behavior in the 4 to 8 μs time duration where the strains are large is minimally influenced by the stiffer properties in the first 0.1 μs. Using a viscoelastic constitutive model, the small strain results from the DMA data were combined with the large strain data from the GRC powder gun tests to run several finite element viscoelastic impact simulations.

An enhancement in the data interpretation is achieved in some instances by using single data traces rather than averaging the data traces as was done previously. Table 5.2 summarizes five specific test cases: one for each of the polyurethanes. Constitutive data is summarized using hyperelastic, elastic-plastic and average secant modulii. The large strain transient data is plotted in terms of a stress/strain curve for a given strain rate. The various forms of material response are indicated in Figure 5.6. The elastic-plastic response uses a two slope representation based on $\tan \alpha_1$ and $\tan \alpha_2$. The two cases for materials 11 and 45 display linear hyperelastic behavior to failure. For materials 4, 17 and 44 the plasticity values are measured starting from the linear hyperelastic stress.

49

Table 5.2
Representative Material Properties at the Highest
Measured Strain Rate (10,200s^{-1})

Material	4	44	17	45	11
Test ID	1 – 7a	12 – 22	1 – 15	1 – 12a	1 – 6
Hyperelastic Values					
E$_1$ (ksi)	2.3	2.5	3.4	8.8	12.9
σ$_1$ (ksi)	2.90	1.31	2.62	36.1	21.2
ε$_1$	1.28	0.52	0.78	4.10	1.64
Plastic Values					
E$_2$ (ksi)	0.57	0.94	4.12	—	—
σ$_2$ (ksi)	3.89	4.23	16.93	—	—
ε$_2$	6.8	4.46	4.09	—	—
Average Secant Modulus for All Specimens at this Strain Rate					
E$_s$ at Failure (ksi)	2.3	4.5	6.5	8.8	13.3
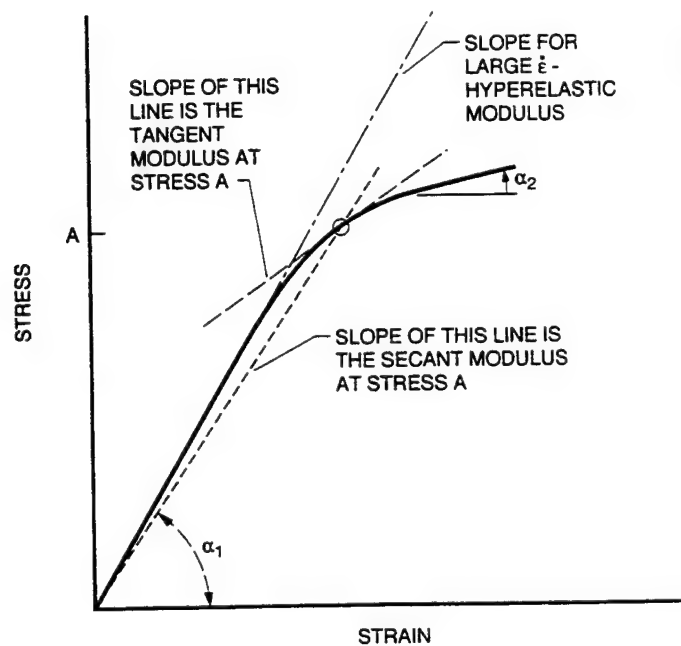
Figure 5.6.   Definition of various modulii for high strain, transient impact stress/strain curve.

The experimental measurements of the behavior of the candidate polyurethane materials show that visoelastic modeling is more important in the early extensional stage of the impact cycle, while plastic flow modeling may be more important when the strains are extremely large.

The plastic flow modeling is likely to be more important than the viscoelastic modeling in terms of the damage phenomenology. The tests indicate that the behavior of materials 1, 17 and 44 is complicated by the introduction of plastic flow when the strains are large (e.g. $\varepsilon > 100$ per cent). Surprisingly, the plastic flow may not be important in the present modeling because the tensile strains do not reach the high strain threshold where plastic flow dominates. Materials 11 and 45 behave as hyperelastic materials over the tested ranges and do not exhibit an elastic-plastic response. Materials 4, 17 and 44 are represented with hyperelastic properties for strain values $\varepsilon < 100$ per cent. It appears reasonable within the current program constraints that the waterdrop response can be studied for all five materials using hyperelastic constitutive properties -- provided the ranges of applicability are noted.

51

6.0   FINITE ELEMENT EVALUATION

The initial finite element calculations were carried out with assumed values for the viscoelastic properties for the polyurethane layer. (Initial calculations referred to in Section 2.2.) Three values of the high-frequency, linear viscoelastic moduli were selected in order to compare the differences in the response. The high-frequency moduli were arbitrarily assumed to be 4000, 40,000 and 400,000 psi. A 2 mm waterdrop impacted these materials at 1000 fps. The calculated results appear well-behaved for substrates with higher stiffnesses (E' = 40,000 to 400,000 psi). At the lower stiffness of 4000 psi the finite element mesh had to be modified to account for the large distortion of the surface layer. The magnitude of the maximum strain experienced in the polyurethane layer with the lowest modulus is 30 percent. The higher stiffness materials experienced maximum strains of 5 percent (E' = 40,000 psi) and 0.15 percent (E' = 400,000 psi). The significance of the selections of the most representative constitutive relations for the polyurethane coatings is clearly evident from these examples.

Based on the available small strain evaluations the magnitude of the material coefficients seemed to be reasonable, however the subsequent test results obtained at GRC for finite strains show that the measured magnitudes of the material coefficients were considerably less than the assumed values used in the finite element calculations. This means that the response of the polyurethane layers is much softer than anticipated even at the very high strain rates. Accordingly the duration of the interaction of the waterdrop with the polymeric layer was at least an order of magnitude larger than assumed initially. This condition required that the total time for the computer runs describing the waterdrop impact event had to be extended which produced extreme distortions in the elements comprising the waterdrop. Special care had to be used to track the highly-distorted elements so adjustments could be made for the long run times required to describe the waterdrop impact. Instead of the initial computer runs covering real times of 2μs, real times in excess of 8μs were required to follow the waterdrop loading process. Table 6.1 summarizes the finite element simulations that were obtained subsequent to the high strain rate tests to obtain relevant material properties for the five candidate polyurethane materials listed in Table 5.1. A nominal 0.1 in. coating thickness was used in all of the DYNA3D calculations except for Run Number 10 which was for a 0.25 inch thick coating. A 2 mm spherical

53

157

Table 6.1
Summary of the Finite Element Waterdrop Impacts
onto 0.1 in. Thick Polyurethanes at 1000 fps

Run Number	D mm	θ deg	E psi	T μs	σ_{x+} ksi	σ_{x-} ksi	σ_{y+} ksi	σ_{y-} ksi	σ_{z+} ksi	σ_{z-} ksi	ε_{y+}	ε_{y-}	ε_{z+}	ε_{z-}	Comment
1	2	90	25,000	1.4	2.78	−10.0	2.78	−10.0	1.23	−12.1	0.171	−0.232	0.200	−0.312	Shows early stiff response like viscoelastic materials
2	2	90	12,000	2.0	1.1	−6.6	1.1	−6.6	0.47	−6.9	0.29	−0.244	0.211	−0.425	Material 11 hyperelastic
3	2	90	6.000	2.0	0.15	−4.1	0.15	−4.1	0.24	−5.9	0.3	−0.28	0.23	−0.51	Material 17 hyperelastic
4	2	90	2,000	2.0	0.1	−2.22	0.1	−2.22	0.1	−3.9	0.34	−0.29	0.244	−0.624	Material 4 hyperelastic
5	2	45	12,000	4.0	2.36	−10.1	1.72	−10.1	2.03	−10.1	0.125	−0.178	0.161		Material 11 hyperelastic
6	2	45	6,000	4.0	1.28	−12.3	1.09	−12.3	1.68	−12.3	0.24	−0.904	0.314	−0.598	Material 17 hyperelastic
7	2	45	2,000 / 2,000	8.0 / 4.0	1.51 / 1.9	−3.31 / −4.22	1.23 / 1.08	−2.88 / −4.51	1.84 / 1.89	−3.42 / −4.76	0.845 / 0.464	−0.848 / −0.516	0.744 / 0.765	−1.1 / −1.04	Material 4 hyperelastic Material 4 hyperelastic
8	6	90	6,000	8.0	1.19	−8.8	1.19	−8.8	1.92	−12.2	0.435	−0.383	0.581	−0.644	Material 17: 6 mm waterdrop
9	2	90	visco	2.0 / 4.0	2.01 / 2.12	−1.99 / −1.25	2.01 / 2.12	−1.99 / −1.25	1.11 / 0.6	−19.9 / −5.9	0.384 / 0.221	−0.101 / −0.155	0.284 / 0.04	−0.701 / −0.562	Material 17 viscoelastic
10	2	90	visco	4.0	1.48	−1.29	1.49	−1.29	0.53	−4,97	0.216	−0.149	0.0446	−0.554	Material 17: 0.25 inch thick viscoelastic

54

158

waterdrop traveling at 1000 fps was allowed to impact the polyurethane layer. No surface friction was prescribed between the contacting surfaces. The simulations included both normal and oblique impacts. A normal impact simulation was also carried out for a large 6 mm waterdrop in order to determine the effect of more severe impact conditions (Run No. 8).

The first four simulations shown in Table 6.1 are for 2 mm waterdrops impacting at normal incidence into hyperelastic materials. The modulii for the polyurethane was varied from 2 to 25 ksi which bounded the experimental data in Table 5.2. The modulii used in these calculations are substantially lower than those considered in the first phase of this program. The present finite element simulations produce large craters which provide numerical challenges because of the large strains at the interface between the waterdrop and polyurethane layer. These issues were discussed in Section 2. The numerical difficulties were overcome and the results provide insights into the waterdrop impact process not previously available. The computations are now straightforward but they are CPU intensive. All of the numerical problems associated with the finite element model have been resolved. The series of parametric computer runs completed are assembled in Appendix B.

The principal numerical problems were manifest in the "hourglassing" of the surface elements and the excessive distortions of elements near the rim of the developing crater. Variable size elements using rezoning corrected the element distortion anomalies. A number of simulation runs were made with varying types and levels of artificial viscosity to limit the hourglassing. The selected viscosity values that eliminate hourglassing do not have an effect on the tensile or compressive strains. There are two forms of hourglass control: viscous and stiffness. It was found that the viscous form is preferred.

Compared to metals and ceramics the stress waves in polyurethanes travel at very low speeds. The largest stresses in the polyurethane layer develop when a substantial momentum in the waterdrop is lost to the substrate. It became apparent as more simulations were completed that the very late time dynamic response was more important than the early time impact response. For very hard materials the peak transient stresses occur early in the waterdrop deformation cycle before there is significant lateral outflow as the drop is collapsing onto the surface. By contrast,

the maximum stresses in the polyurethane layers develop late in the waterdrop distortion cycle when severe distortions of the drop are present. Accordingly, the run times were advanced from 2 to 4 to 8 μs as the final simulation cases were carried out.

Computational run times to simulate the 8 μs history of the waterdrop collision are extremely long because of the number of elements and the nature of this explicit finite element code. The increment in computational time is controlled by the period in which the compressional wave in the water traverses the smallest element dimension in the waterdrop model. This time increment has been as short as $6x10^{-10}$ s during the large deformation stage. The code performs calculations at each time increment for all of the 25,000 elements in the model. For a simulation time of 8 μs all 25,000 elements are being updated $8x10^{-6}/10^{-10} = 80,000$ times. The CPU times to perform these computations are from 3000 to 8000 minutes on the Stellar and i860 platforms. These computational times probably can be reduced by a factor of 4 to 10 by decreasing the fidelity of the waterdrop. When a waterdrop impacts a ceramic material, the 25,000 element model is necessary to capture the transient event and the waterdrop outflow mechanism. However, these calculations have shown that overall momentum transfer determines the peak tensile strain. The momentum transfer probably can be modeled with significantly fewer elements. It was decided to be conservative in these initial evaluations and maintain the high fidelity of the impact process. Future simulations can contain fewer elements for both the waterdrop and polyurethane coating once the difference in the accuracy which can be tolerated for the lower fidelity model is established.

The 45° waterdrop impact simulations in Table 6.1 used a reduced number of elements for the waterdrop and required a longer simulation time for the peak damage to develop in the polyurethane layer. Although the strains are quite large, they do not approach the measured ultimate strains evaluated at high strain rates as listed in Table 5.1. The calculated strains are large enough possibly to initiate plastic flow for materials 4, 17 and 44. Materials 11 and 45 display hyperelastic modulii of 13.1 and 8.8 ksi to failure.

For a normal waterdrop impact at 2.0 μs the five types of polyurethanes experience larger regions for and higher magnitude of compressive stresses than the tensile stresses. The

compressive and tensile strain magnitudes are comparable. Unfortunately, these simulations ended prematurely because of numerical problems associated with the "hourglassing" effect described previously and extreme compression of the elements at the centerline. The stresses and strains have not yet reached peak values as was achieved in the later DYNA3D simulations.

The damage in materials is generally increased as the waterdrop diameter increases. The effect of a reasonably sized larger equivalent drop diameter on the polyurethane protective layers is evaluated in Run Number 8. The strains which are generated in the polyurethane layer for a 6 mm waterdrop diameter impact at normal incidence listed in Table 6.1 do not display a significant increase over those generated by the 2 mm waterdrop impacts. Failure is not predicted.

Table 6.2 provides comparisons of the large margin between the predicted maximum tensile strains and the measured ultimate strains in Table 5.1. These predictions although preliminary do provide a quantitative evaluation of the effects of a single impacting waterdrop on flexible polyurethane layers. The finite element model offers the most physically-based representation of the transient interactions of the waterdrop and the polyurethane layers. This is a first step in constructing a meaningful perspective on what coating properties are required for improved rain erosion protection.

Table 6.2
Strain Relationships for 1000 fps Waterdrop Impacts into the
Polyurethane Layers.

Material	4	44	17	45	11
E_s (ksi) Secant Modulus at Failure	2.3	4.5	6.5	8.8	13.3
$+\varepsilon_{max}$ (in/in) Experimental	6.87	4.66	6.60	4.10	1.64
@ 2µs $\theta = 90°$ ε_+ $\varepsilon_+ / \varepsilon_{max}$	0.34 0.049	0.32 0.069	0.30 0.045	0.295 0.072	0.29 0.177
@ 4 µs $\theta = 45°$ ε_+ $\varepsilon_+ / \varepsilon_{max}$	0.464 0.068	0.35 0.075	0.24 0.036	0.18 0.044	0.125 0.076
@ 8 µs $\theta = 45°$ ε_+ $\varepsilon_+ / \varepsilon_{max}$	0.845 0.123				
@ 4 µs viscoelastic $\varepsilon_+ / \varepsilon_{max}$			0.221 0.034		
@ 4 µs visco (thick) $\varepsilon_+ / \varepsilon_{max}$			0.216 0.033		

58

162

7.0 CONCLUSIONS

The dynamic finite element modeling for waterdrop impacts on polymeric layers is a significant advance over the previously available analyses. The computational model provides an accurate description of the waterdrop interacting with the highly deformable, polymeric layer. The duration and general features of the waterdrop process can now be quantified with respect to the material properties of the polymeric layer.

Another significant advance was achieved in obtaining strain to failure measurements for the polymeric candidates for the erosion protection system at high strain rates. No source for this data could be identified so a novel test method was developed to determine the constitutive behavior of the coatings.

The invention and implementation of the Mihora/Adler Flyer Plate (MAFP) can become of similar importance as the split Hopkinson bar. The split Hopkinson bar is used routinely in shock physics for small strain measurements. The MAFP has the distinct advantage of large strain testing at strain rates that are much higher than the split Hopkinson bar tests.

The measured material properties are inserted in the finite element analysis to obtain the transient stress and strain component distributions for the various polymeric materials. The strain to failure measurements for the five candidate polymers did not display a large variation from material to material. The large strain/high strain rate measurements also did not exhibit the significantly reduced strains to failure typically associated with high loading rates. All of the polymeric materials remained rubbery with minimal strains to failure around 300 percent. The maximum calculated strains for the waterdrop impacts were around 80 percent. On the basis of these results, the first time a realistic simulation of the waterdrop impact has been achieved, a single waterdrop impact would not be capable of initiating the coating failure for the materials evaluated.

59

These calculations and the associated material property measurements can now be used to explore other forms of coating degradation. Alternative to scenarios for the onset of damage can be envisioned.

The statistical nature of the waterdrop impacts should be considered in order to establish if any critical conditions can occur due to the synergistic effect of two or more waterdrops impacting in close proximity to each other at nearly the same time. While in service the polymeric coatings will experience solid particle impacts which may tend to lower their resistance to tearing. This is analogous to a notch sensitivity for the material in more conventional mechanical property evaluations. The role of material fatigue processes can also be investigated in a context which is physically representative of the multiple raindrop/sand impact environments. Apparently the acceptable rain erosion response of four of the five candidate materials (i.e. materials 4, 17, 44, 45) is due to the desirable attributes they possess: the ability to maintain high elongation at high loading rates, high dynamic tear strength, and good low-cycle fatigue resistance.

The large strain, high strain rate tests indicate that single waterdrop impacts are not the direct cause of erosion damage. It is concluded that ultimate strain and modulus are significant, however additional factors need to be considered to develop a figure of merit for ranking erosion damage. From the quantitative analyses of the single waterdrop impacts it is hypothesized that the repeated high strain fatigue life is a potential contributor to promoting erosion damage. The DYNA3D simulations provide guidance for specifying fatigue test parameters. It is accordingly proposed to develop a cyclic test apparatus that can produce high strain repetitive loadings that can be used to rank the erosion resistance of candidate coatings. The DYNA3D simulations point toward an instrument that cyclically applies a nearly hemispherical indentation at high rates. Issues which will have to be resolved include the unnatural heating of the specimen if the indentations are too closely spaced in time and the form of the deflection verses time relation. These design parameters can be evaluated using the DYNA3D code and the understanding of the measured high strain rate properties acquired from this effort.

60

The outcome of the computational and experimental effort is that the tools are now in place to evaluate the physically-realistic properties of protective coatings for helicopter rotor blades that are needed to optimize the coating systems. Further work is required however to develop a series of innovative mechanical tests that will effectively screen the candidate materials in terms of the environmental conditions to which they will be exposed. The suggested approach yields meaningful quantitative results for relating coating performance to the appropriate material property measurements. This relationship can now be established and used to improve in-service coating lifetimes.

APPENDIX A
HIGH STRAIN RATE TEST DATA FOR THE CANDIDATE
POLYURETHANE MATERIALS

The recorded oscilloscope data for force and deflection for the five different polyurethane materials listed in Table 5.1 are included in this Appendix. Two polyurethane specimen configurations were used in the tensile tests. Most of the tests employed a 1.6 in. long by 0.3 in. wide active test section. When the material is spiral looped and bonded to the two slitted attachment posts the sample length required is 5.2 in. Near the middle of the active region a "dogbone" cutout is made so that the test section is 0.3 in. long by 0.15 in. wide. These specimens always failed in this dogbone cutout region. A small number of specimens had a straight test section without the dogbone cutout.

The records displayed in this Appendix are from a digital recorder. The digital data is obtained from a LeCroy 9410 digital scope with a storage rate of 4 Gs/s. The strain gages on the aluminum load cell are amplified using an LeCroy 8100 amplifier that has frequency linearity to 1 MHz. The amplifier is powered using a LeCroy 8013A crate. The force/time output data is linear. The displacement/time data is acquired from the MTI Instruments 2000 photonic sensor with a frequency response to 800 KHz. The displacement signal relies on a corner cube retroreflector tape Type 3970G manufactured by 3M. The deflection determine from the output voltage is a nonlinear function.

All of the recorded data in this Appendix is for the aluminum projectile and flyer plate. The early tests using polymeric projectiles are not included.

Two signal data traces are presented on each plot. The first data trace for each material shows a long time window of 2.0 ms (0.2 ms/div). The long time traces are to assure that the impact event and complete polyurethane extension to failure are captured. A second plot shown for each test with expanded x/y scale is included to highlight the part of the record that contains the polyurethane response. The time scale for each expanded plot is marked on the grid lines, however the general interpretation of the test results is complicated by the various gain factors that were used and the nonlinearity of the voltage output for the deflection measurements. The reduction of this data is described in conjunction with Figures 4.6 and 4.7.

A-1

Table 1 summarizes the tests completed for each material type. The run designation is the date that the test was carried out. The data records are organized according to the material in descending order of the flyer plate velocity. The entries marked with a (W) in Table A1 denote the wide specimens which were not cut into a dogbone configuration for the test section. The specified speeds for the flyer plates of 1100, 875, 510, and 310 fps are the mean values after the flyer plates have reached a steady speed. Time is the abscissa of each plot and the ordinate is either the MTI voltage signal or the strain gage signal. At the earliest times (initial x-value) the MTI voltage output (related to the displacement of the specimen) is displayed as the upper ordinate curve and the lower ordinate curve is the strain gage reading (related to the load on the specimen).

Table A1. Run Number for Tests of the Candidate Polyurethane Materials
Using the GRC Large Strain, High Strain Rate Facility.

Average Flyer Plate Speed (fps)	Material				
	4	11	17	44	45
1100	1-7a(W)	12-9 1-6	12-2 12-31 1-14a 1-14b 1-15	12-22(W) 1-18(W)	1-12a
875		12-8b	11-11 11-17 11-18 11-19 11-25 12-1 12-8a	12-15	
510	1-7b(W)				1-12b
310	1-19a(W)	2-16	2-11 2-15	1-19b(W)	2-12

A-2

0 0.2ms

a. Displacement and Load Time Records

0 50μs
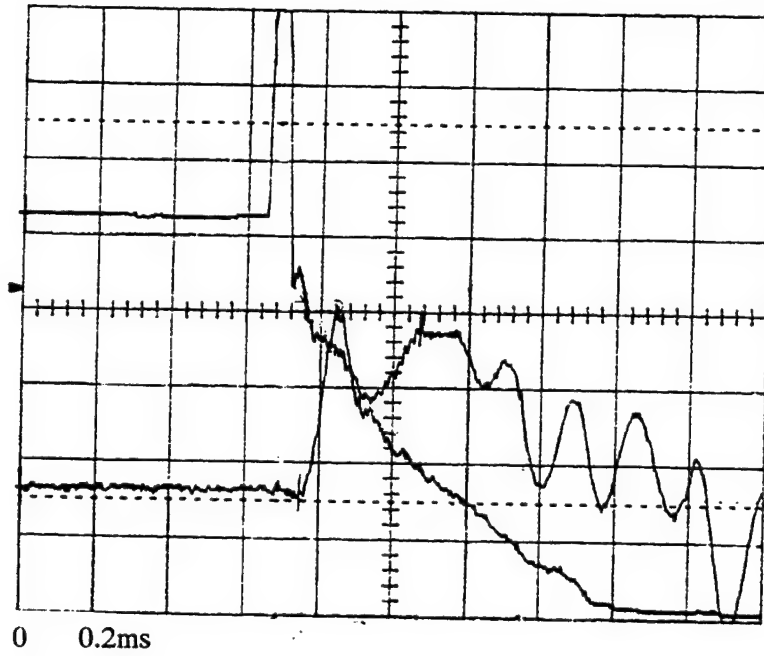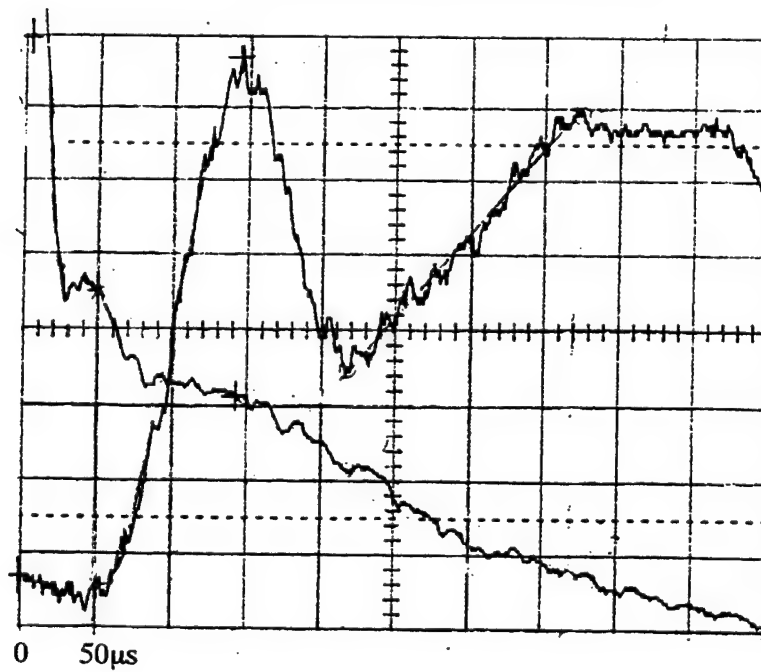
b. Expanded Load Trace

Figure A1. Run No. 1-7a for Material 4 Impacted at 1100 fps.

A-3

170

0   0.5ms

a. Displacement and Load Time Records

0   208μs
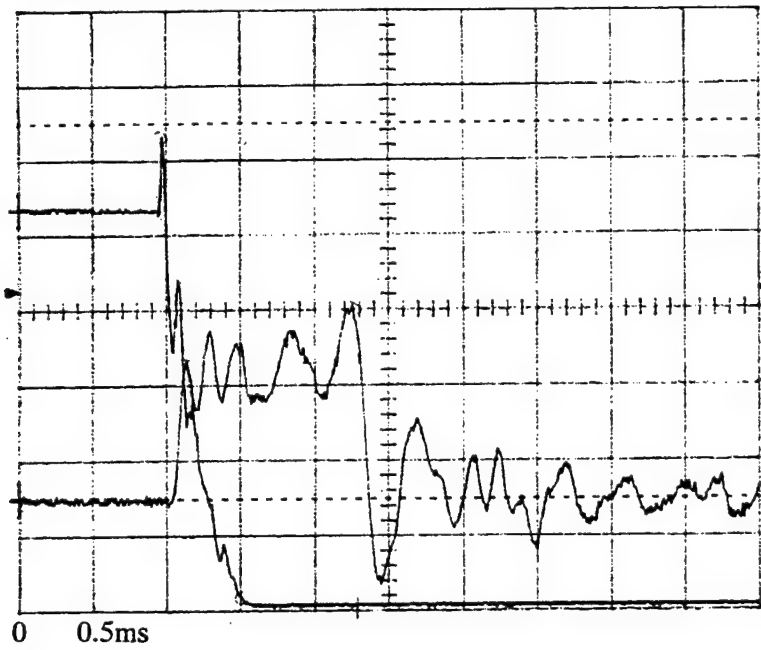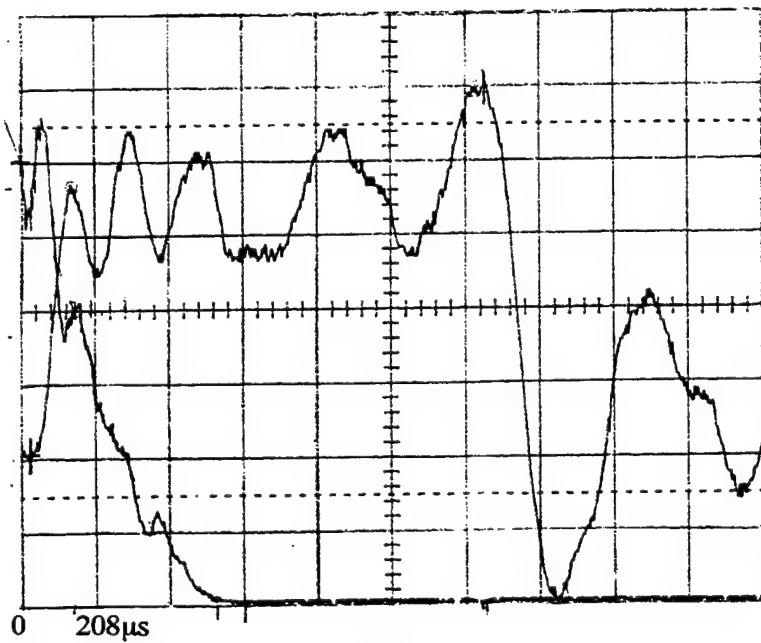
b. Expanded Load Trace

Figure A2. Run No. 1-7b for Material 4 Impacted at 510 fps.

A-4

171

0   0.5ms
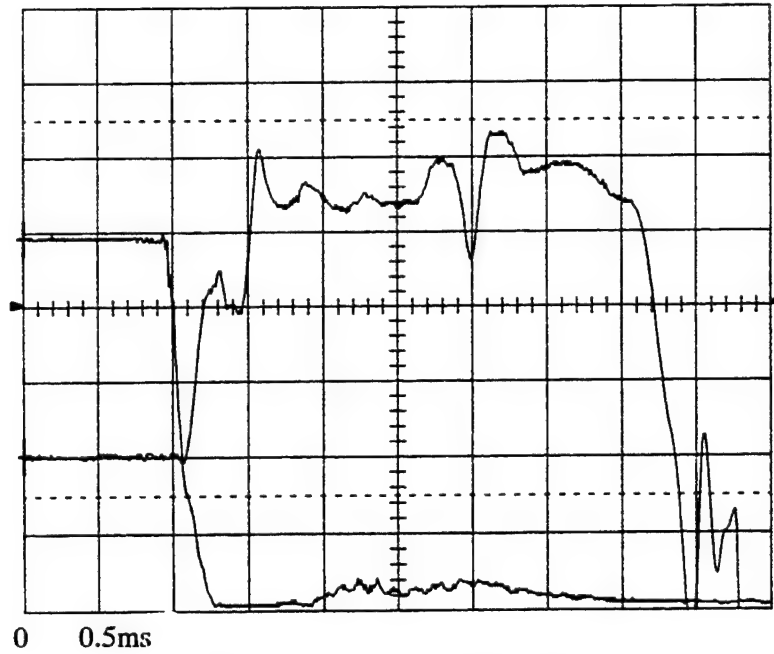
a. Displacement and Load Time Records

NOT AVAILABLE

b. Expanded Load Trace

Figure A3. Run No. 1-19a for Material 4 Impacted at 310 fps.

A-5

172

0   0.1ms

a. Displacement and Load Time Records

0   20µs
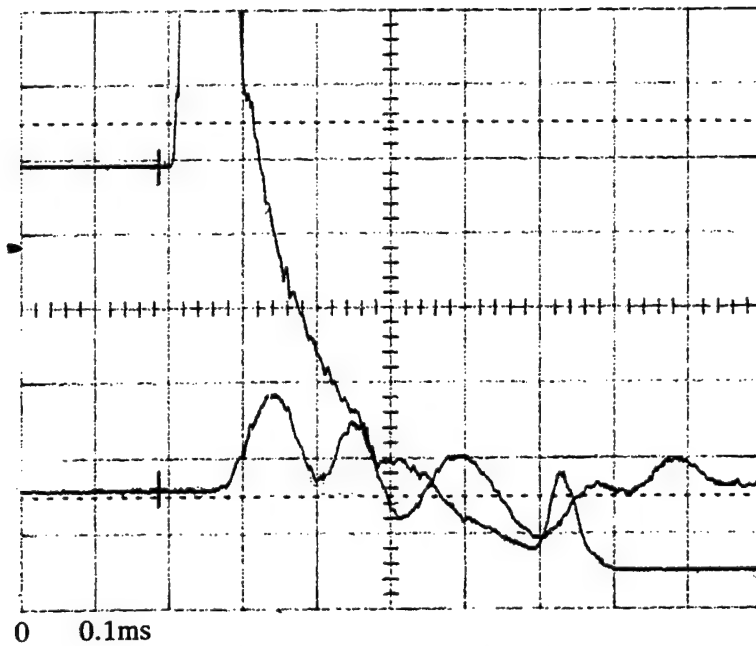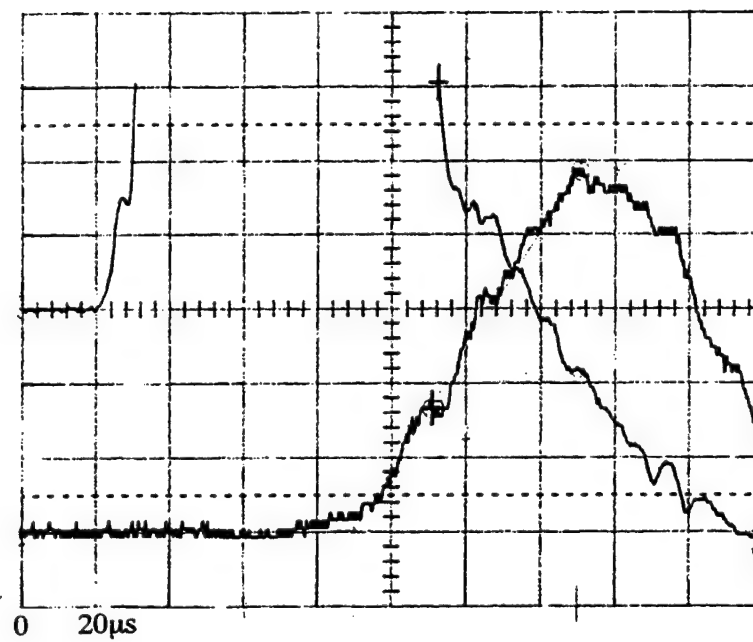
b. Expanded Load Trace

Figure A4. Run No. 12-9 for Material No. 11 Impacted at 1100 fps.

A-6

0   0.1ms

a. Displacement and Load Time Records

0   20µs
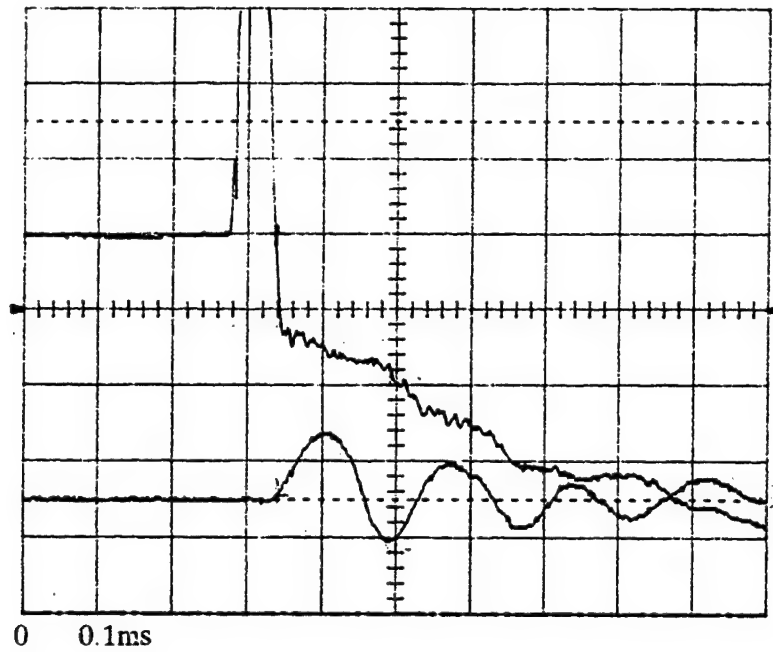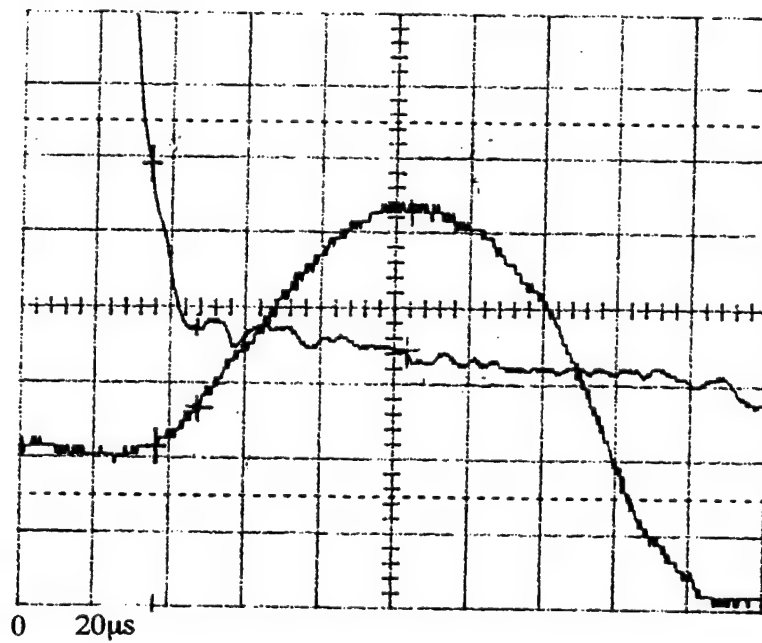
b. Expanded Load Trace

Figure A5. Run No. 1-6 for Material 11 Impacted at 1100 fps.

A-7

174
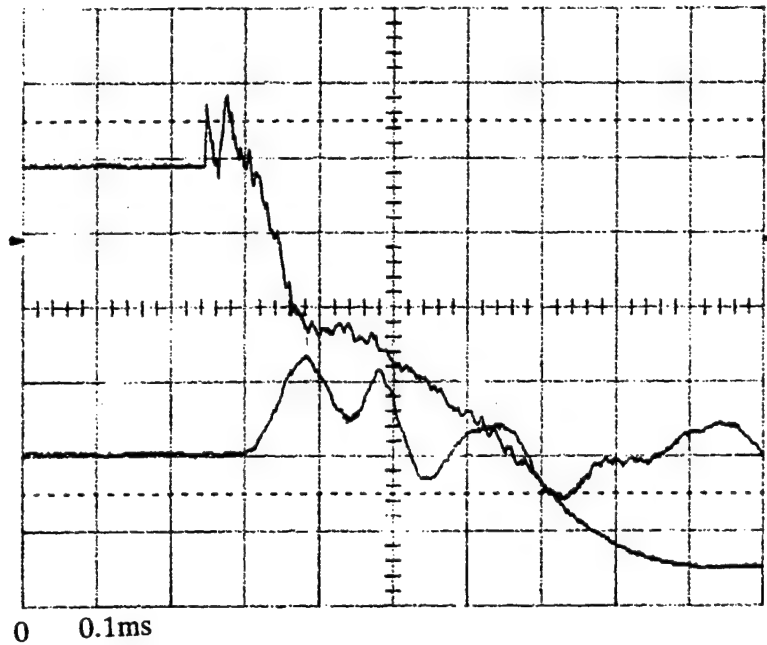
a. Displacement and Load Time Records
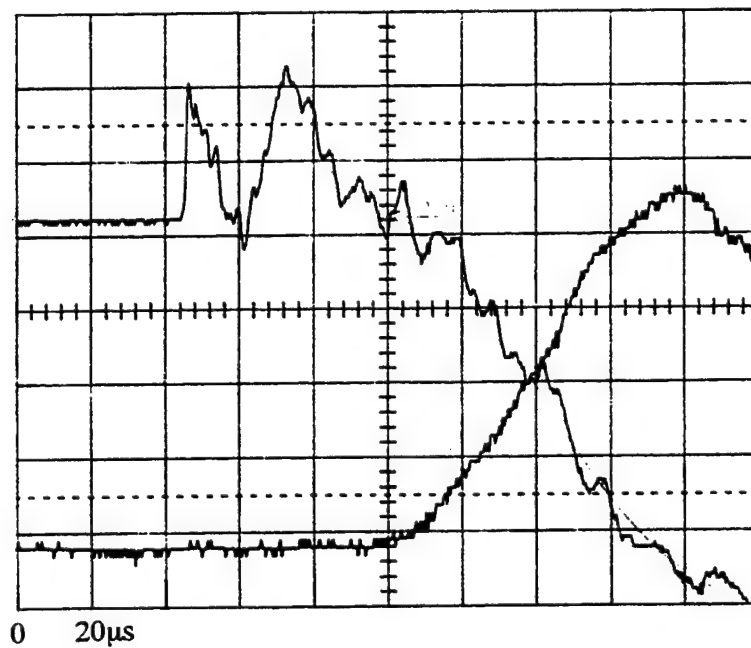
b. Expanded Load Trace

Figure A6. Run No. 12-8b for Material No 11 Impacted at 875 fps.

A-8

175

a. Displacement and Load Time Records

0   0.5ms

0   102μs
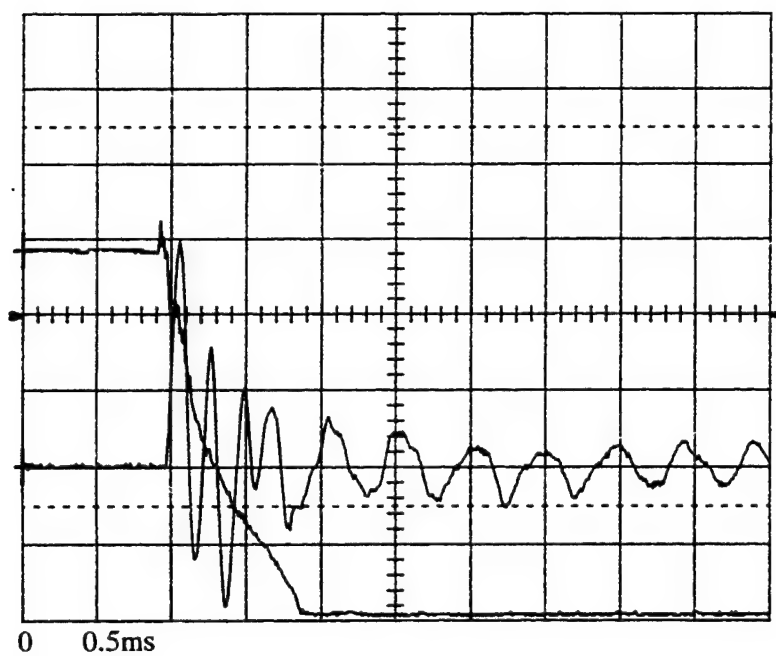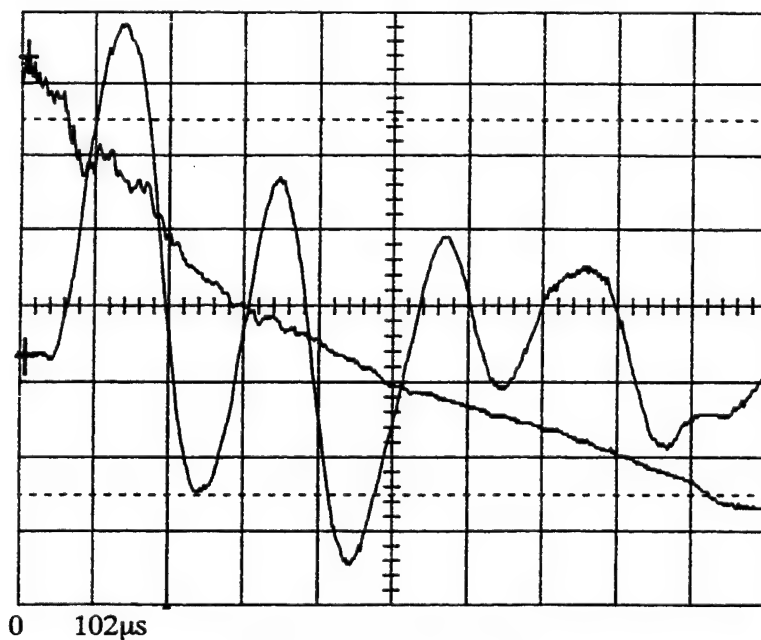
b. Expanded Load Trace

Figure A7. Run No. 2-16 for Material 11 Impacted at 310 fps.

A-9

176
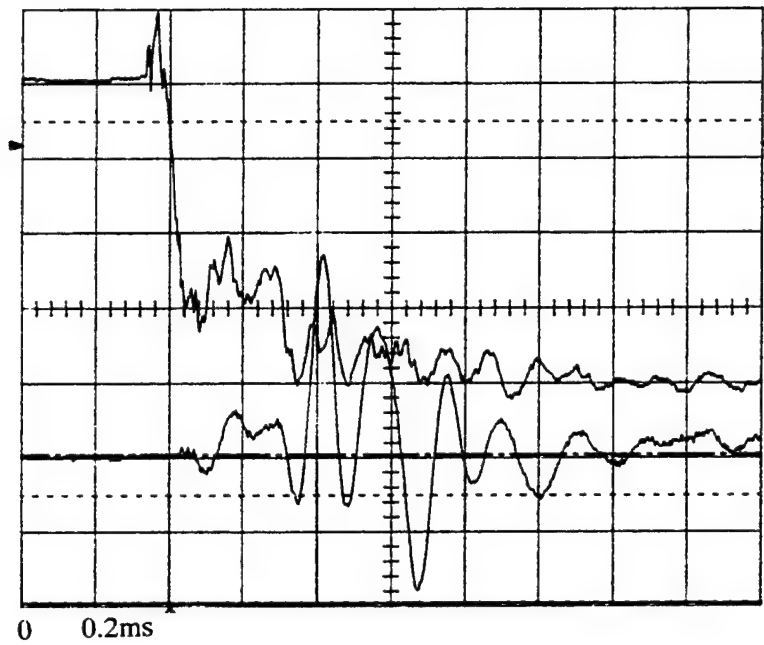
a. Displacement and Load Time Records
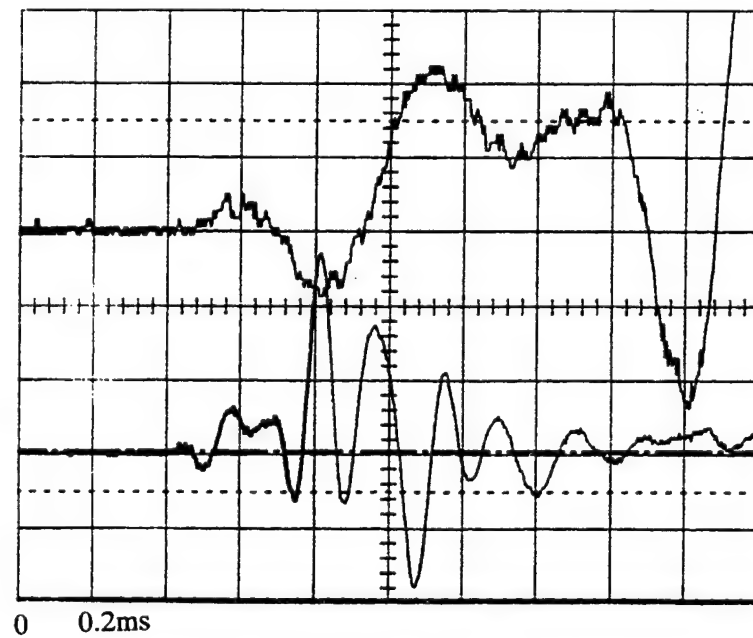
b. Expanded Load Trace

Figure A8. Run No. 12-2 for Material 17 Impacted at 1100 fps.

A-10

0   0.2ms

a. Displacement and Load Time Records

0   50μs
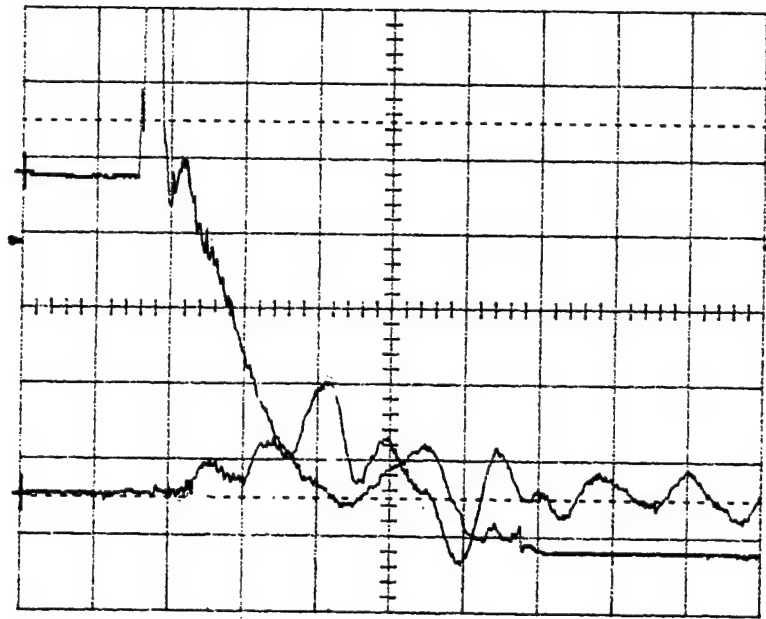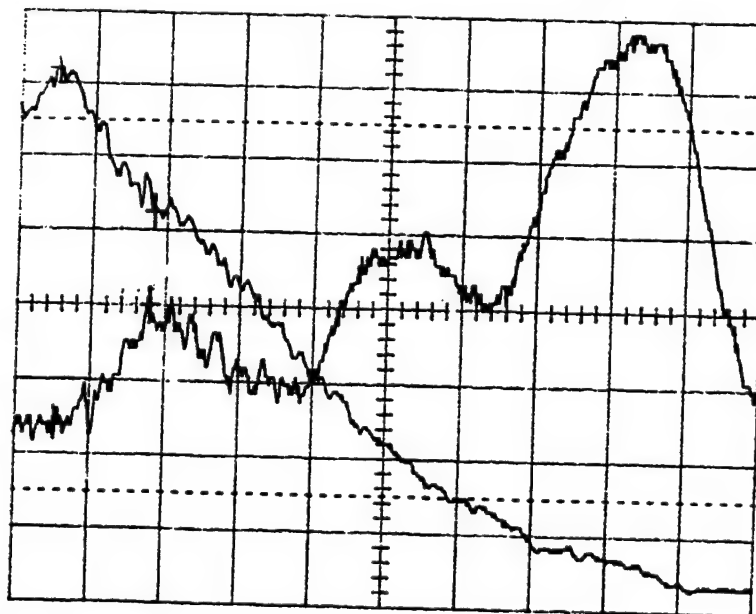
b. Expanded Load Trace

Figure A9. Run No. 12-31 for Material 17 Impacted at 1100 fps.

A-11
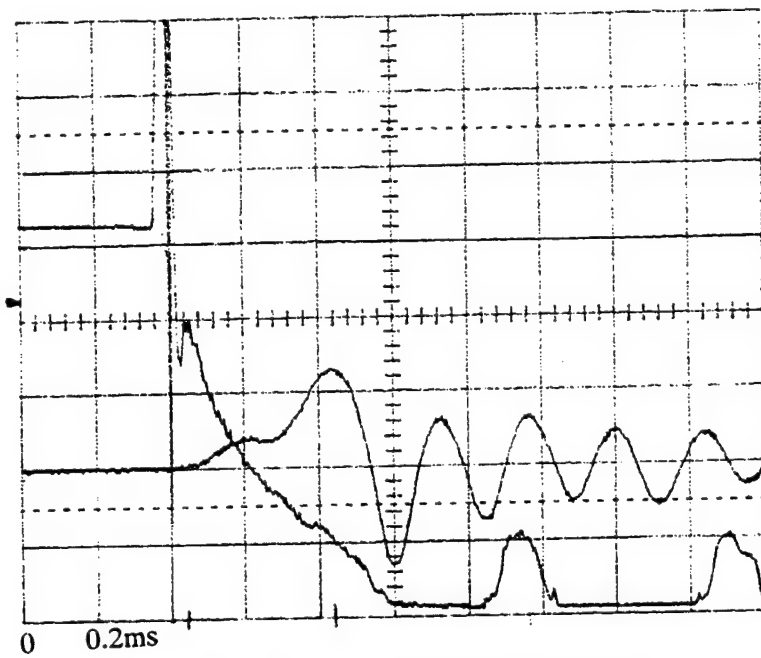
a. Displacement and Load Time Records
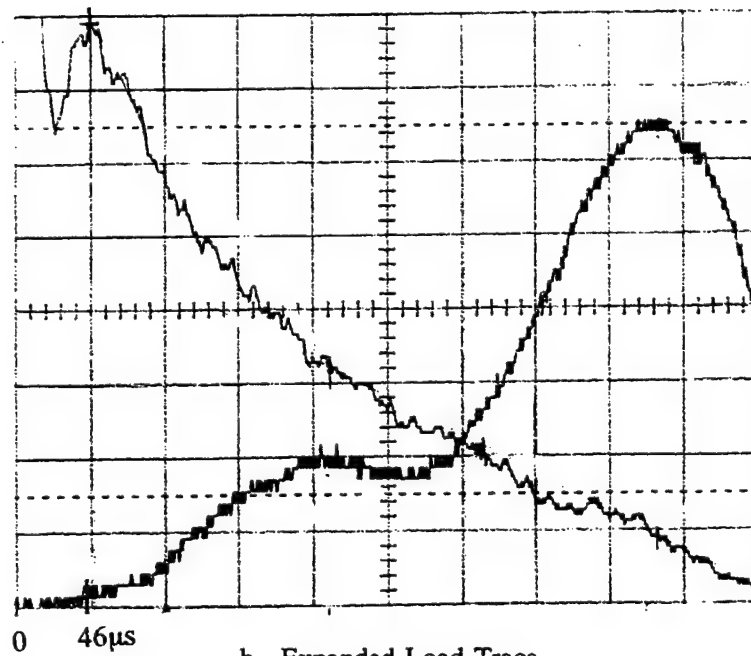
b. Expanded Load Trace

Figure A10. Run No. 1-14a for Material 17 Impacted at 1100 fps.

A-12

179

0   0.2ms

a. Displacement and Load Time Records

0   50µs
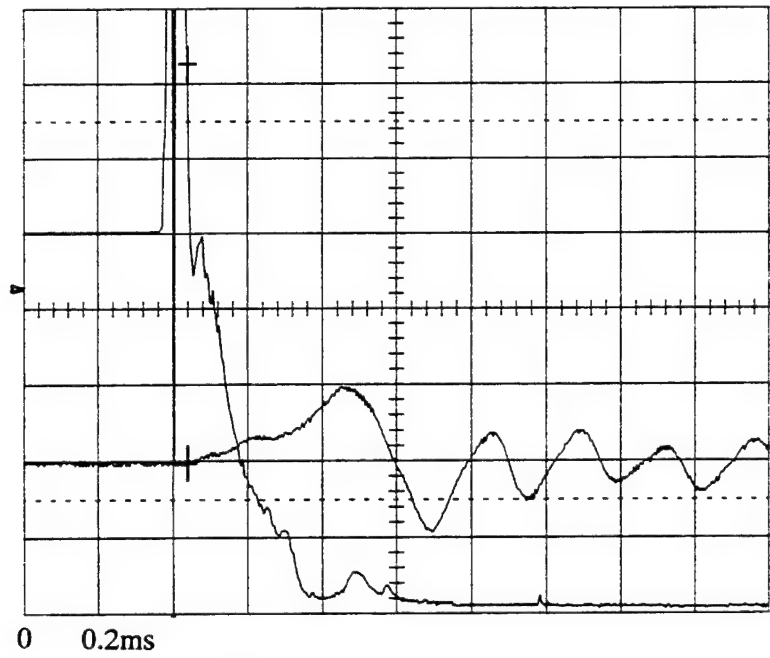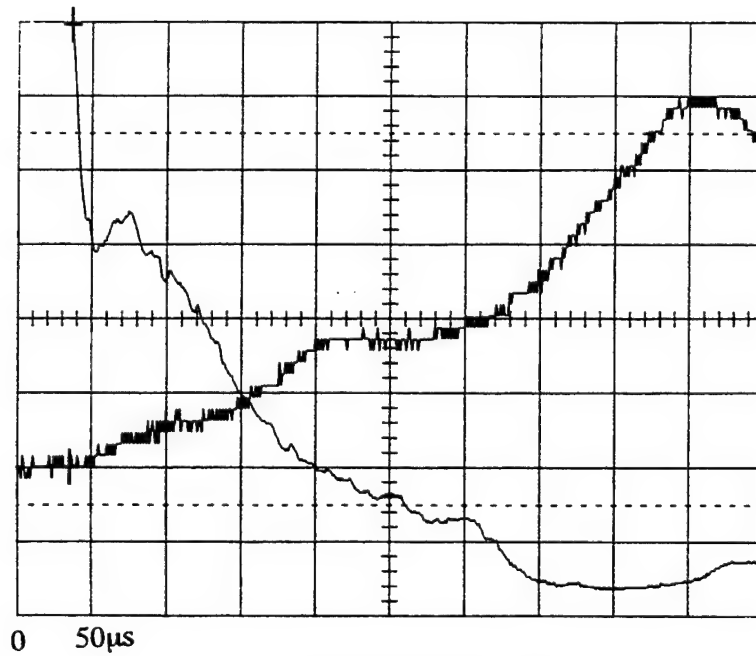
b. Expanded Load Trace

Figure A11. Run No. 1-14b for Material 17 Impacted at 1100 fps.

A-13

180
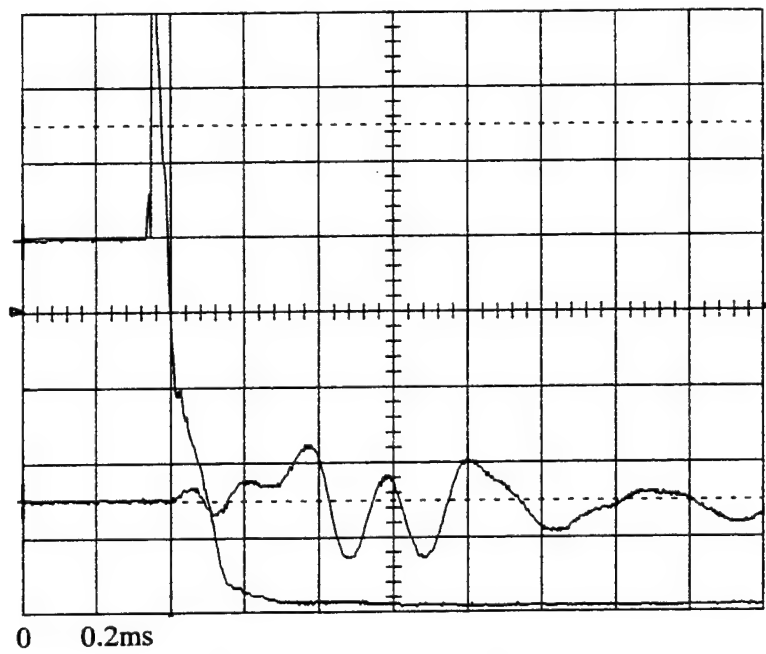
a. Displacement and Load Time Records
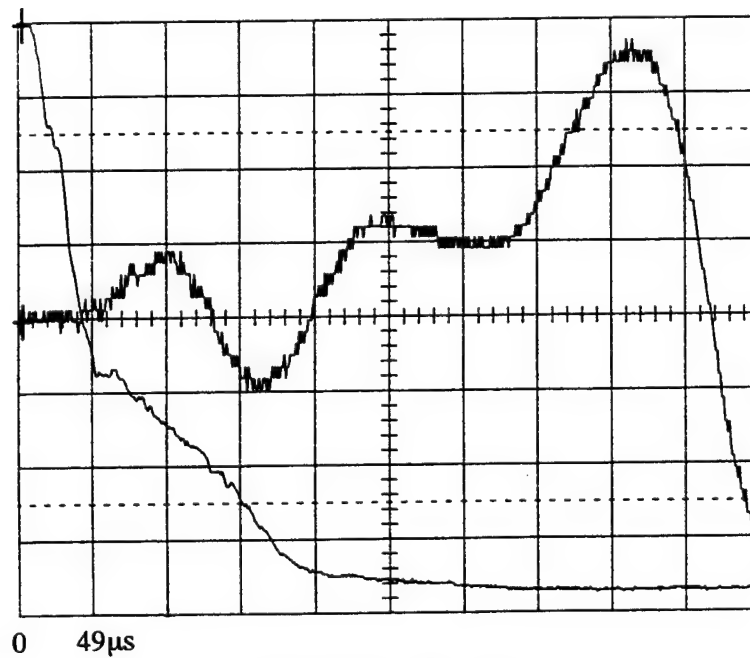
b. Expanded Load Trace

Figure A12. Run No. 1-15 for Material 17 Impacted at 1100 fps.

A-14

181

0   50µs
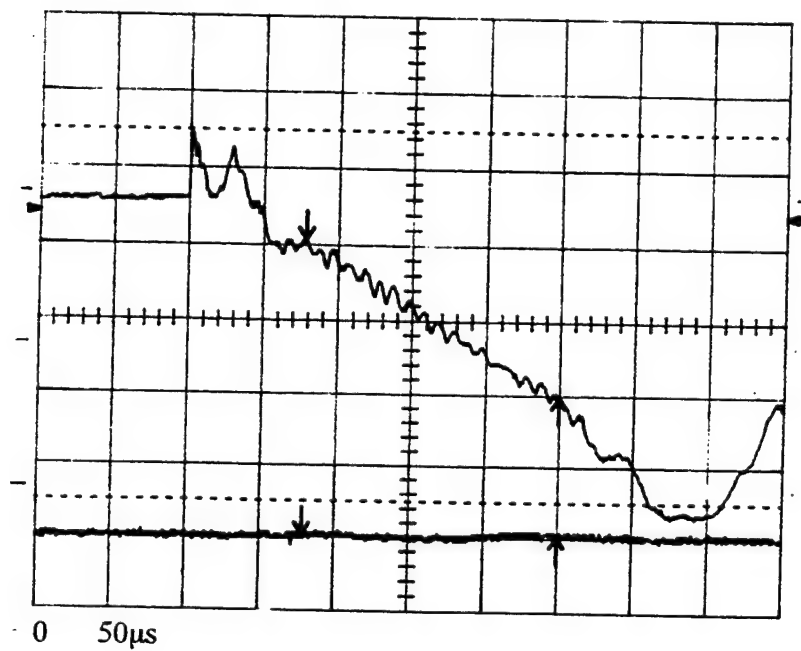
Figure A13.   Run No. 11-11 for Material 17 Impacted at 875 fps.

A-15

0   20μs
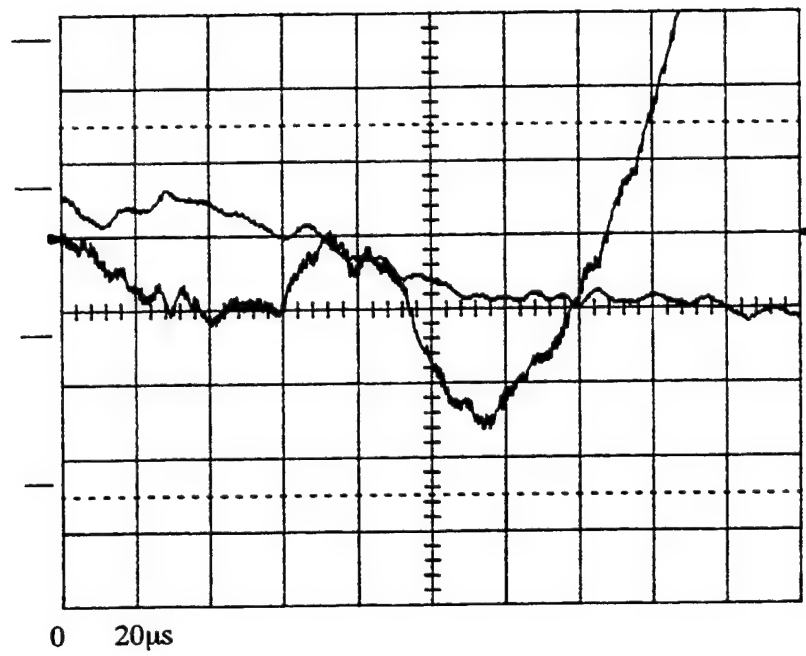
Figure A14. Run No. 11-18 for Material 17 Impacted at 875 fps.

A-16

0   50μs
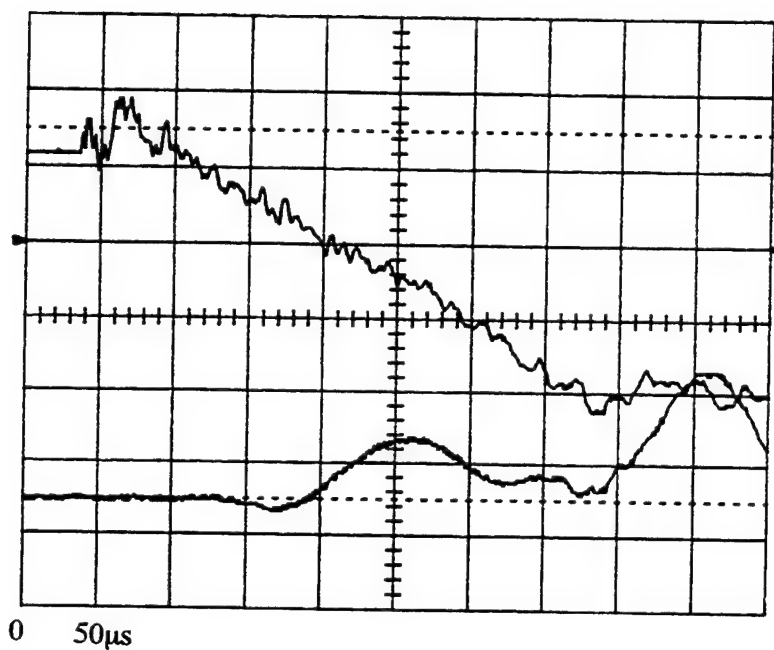
Figure A15. Run No. 11-19 for Material 17 Impacted at 875 fps.

A-17

184

0   0.1ms
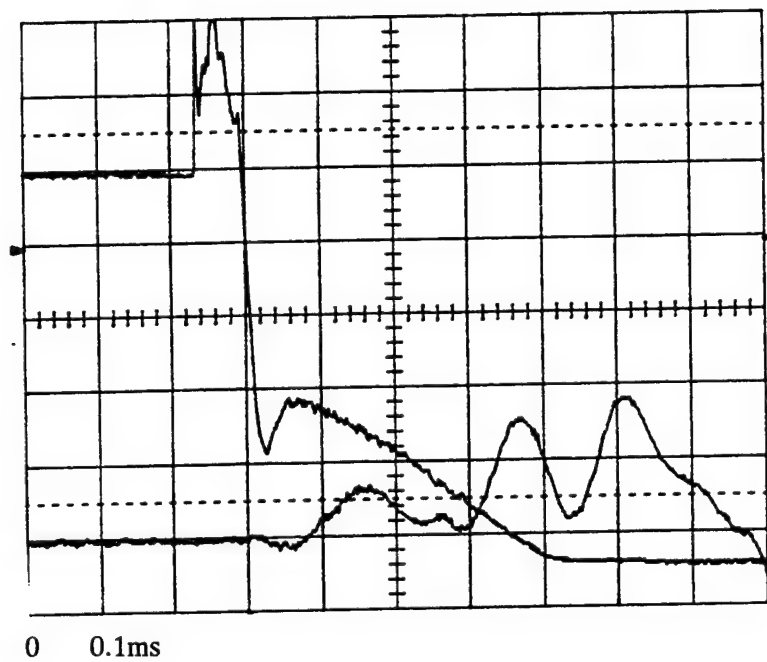
Figure A16. Run No. 11-25 for Material 17 Impacted at 875 fps.

A-18

185

0   0.2ms

a. Displacement and Load Time Records

0   0.2ms
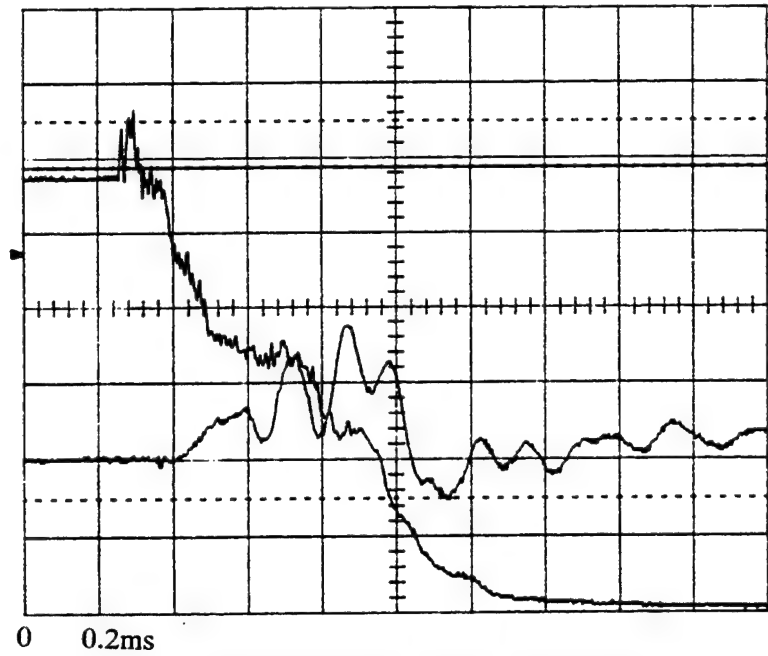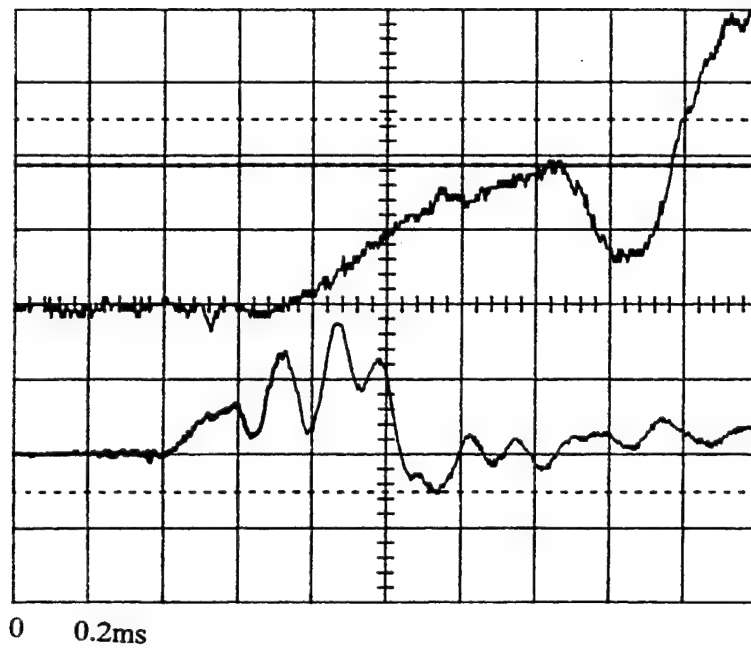
b. Expanded Load Trace

Figure A17. Run No. 12-1 for Material 17 Impacted at 875 fps.

A-19

0   0.2ms

a. Displacement and Load Time Records

0   0.2ms
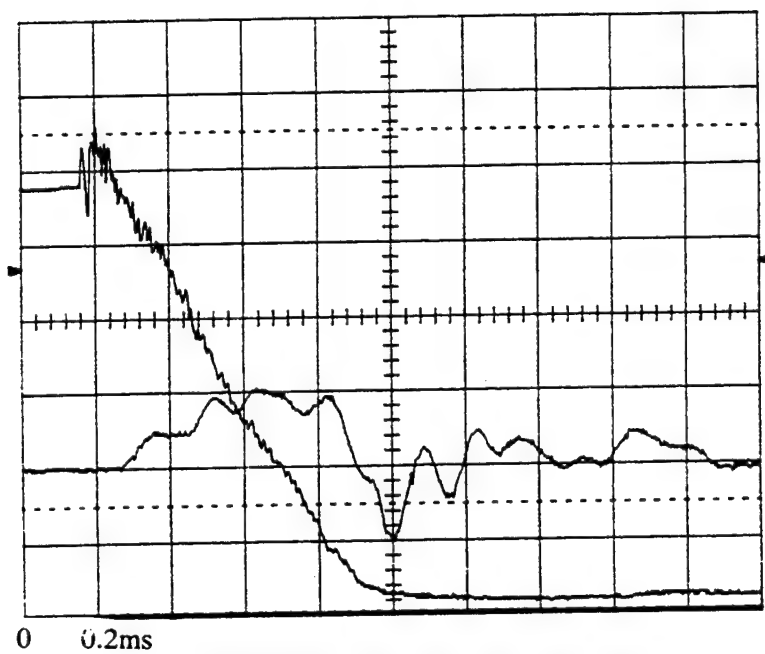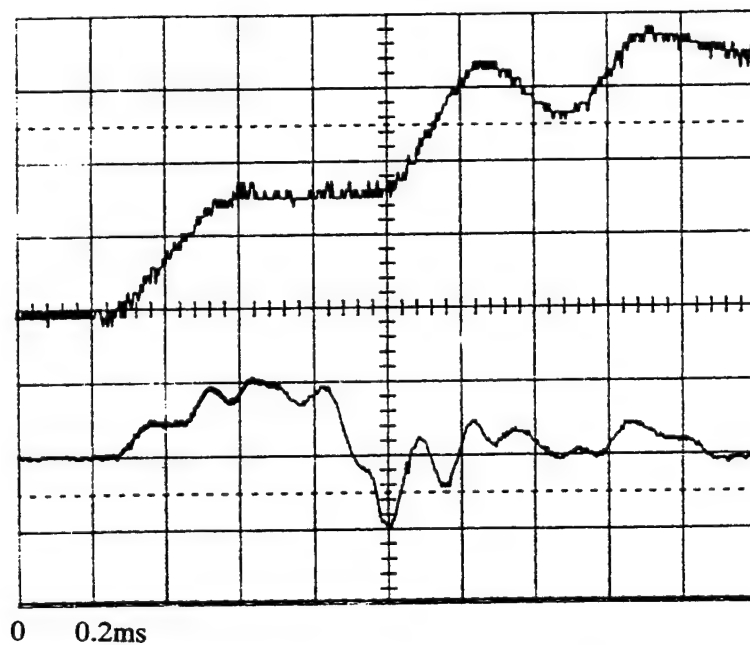
b. Expanded Load Trace

Figure A18. Run No. 12-8a for Material 17 Impacted at 875 fps.

A-20

187
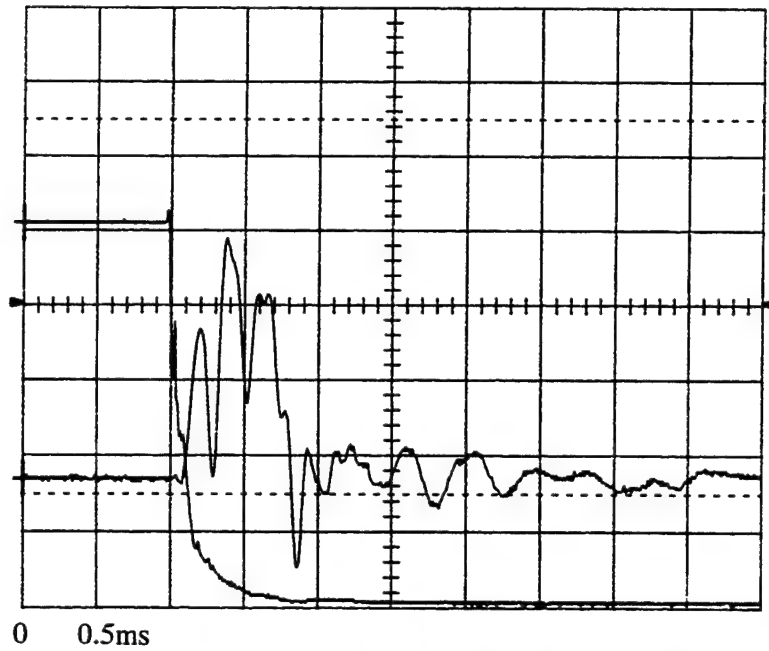
a. Displacement and Load Time Records
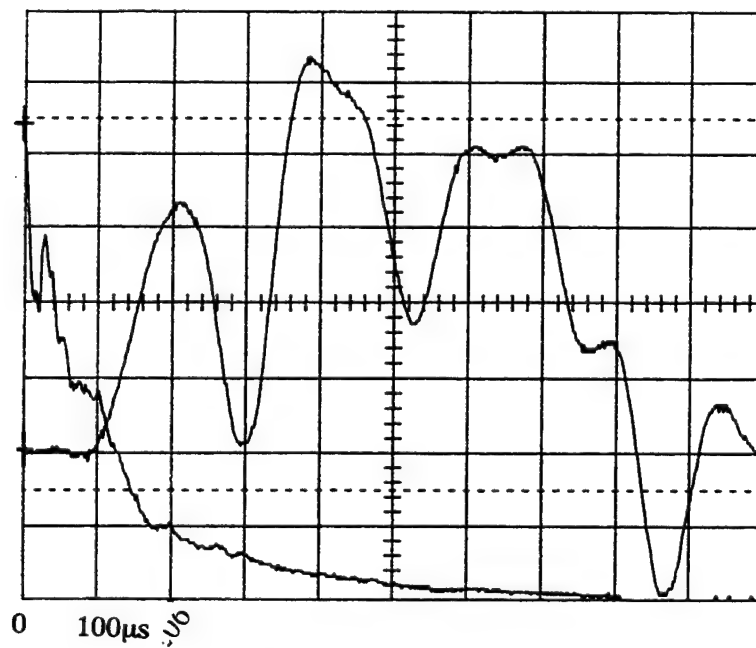
b. Expanded Load Trace

Figure A19. Run No. 2-11 for Material 17 Impacted at 310 fps.

A-21

188

0   0.5ms

a. Displacement and Load Time Records

0   100μs
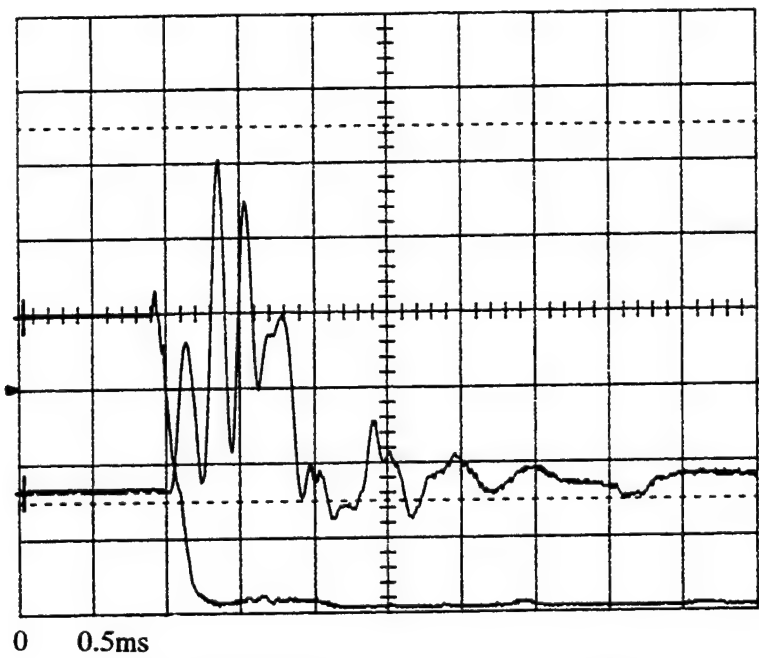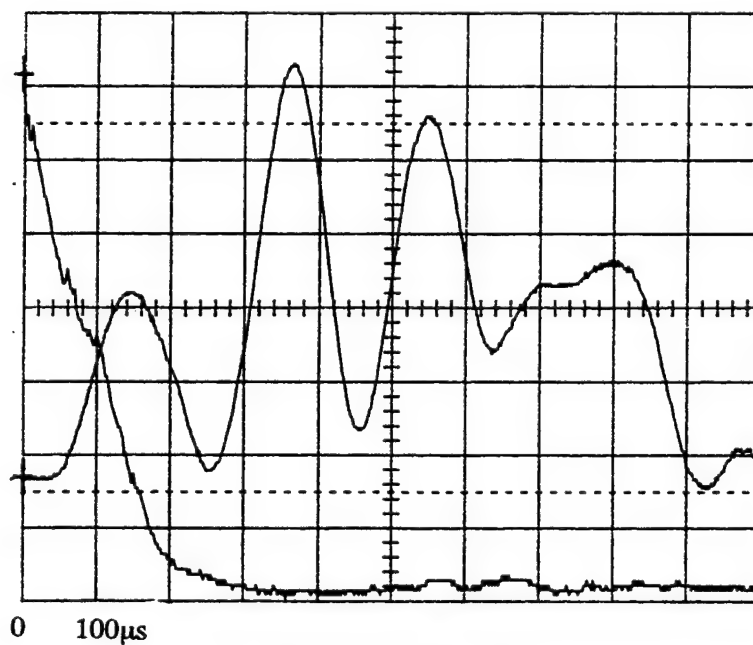
b. Expanded Load Trace

Figure A20. Run No. 2-15 for Material 17 Impacted at 310 fps.

A-22

0   0.2ms

a. Displacement and Load Time Records

0   48μs
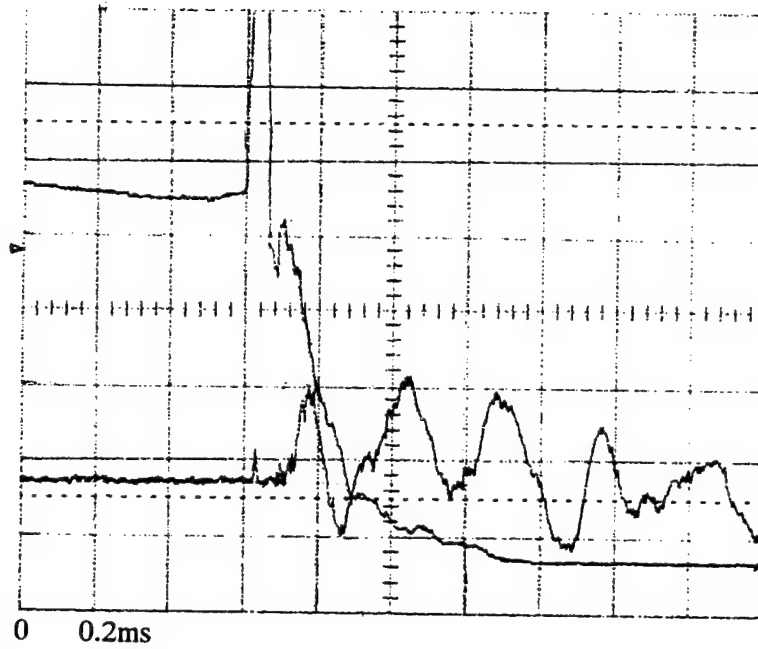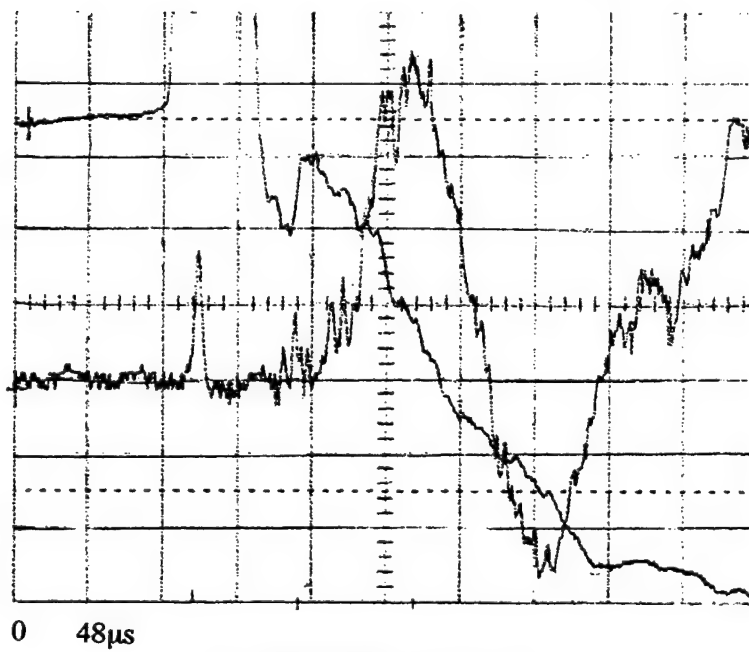
b. Expanded Load Trace

Figure A21. Run No. 12-22 for Material 44 Impacted at 1100 fps.

A-23

190
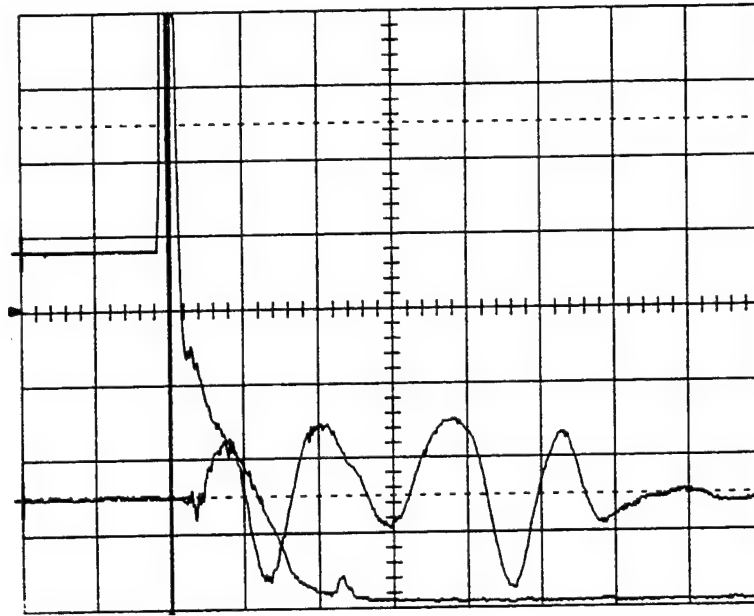
0   0.2ms a. Displacement and Load Time Records
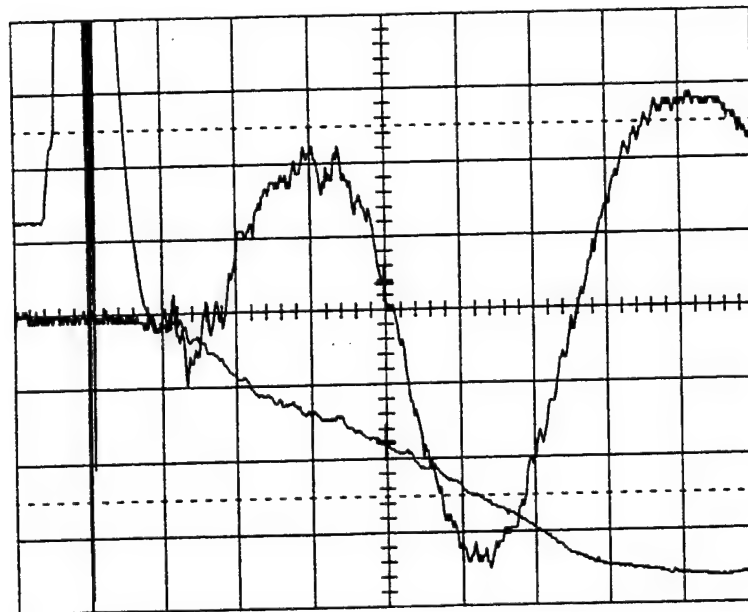
0   50μs

b. Expanded Load Trace

Figure A22. Run No. 1-18 for Material 44 Impacted at 1100 fps.

A-24
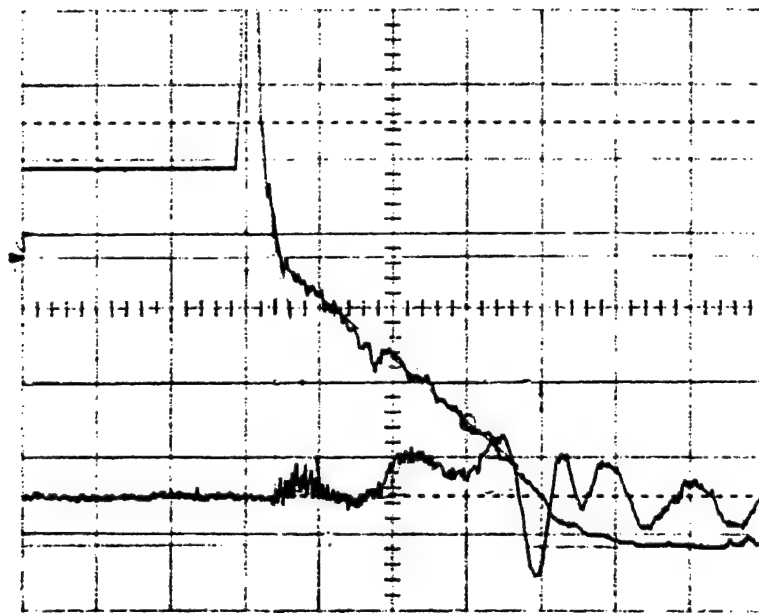
0   0.2ms

a. Displacement and Load Time Records
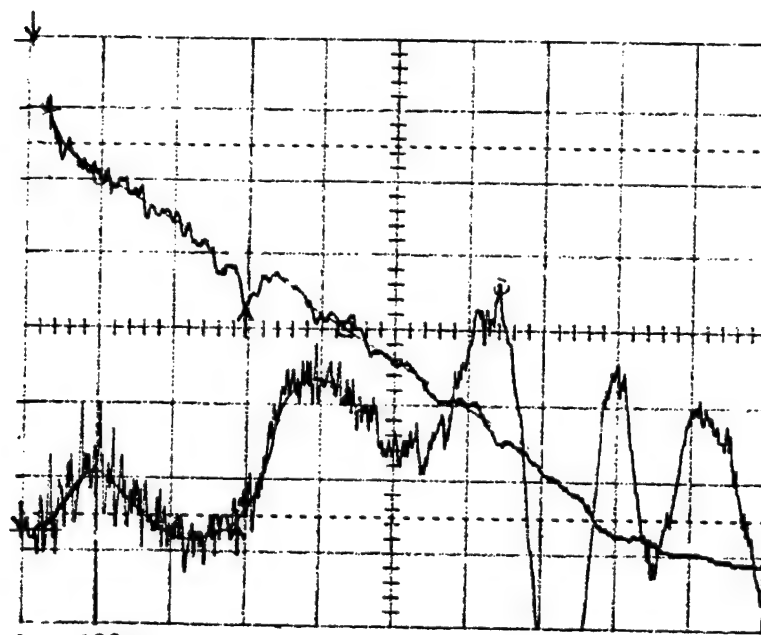
0   100µs

b. Expanded Load Trace

Figure A23. Run No. 12-15 for Material 44 Impacted at 875 fps.

A-25
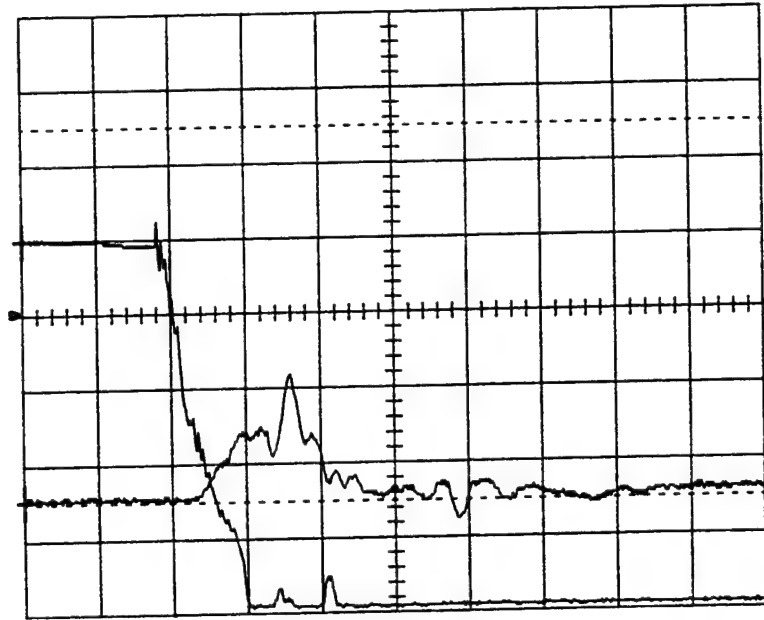
a. Displacement and Load Time Records
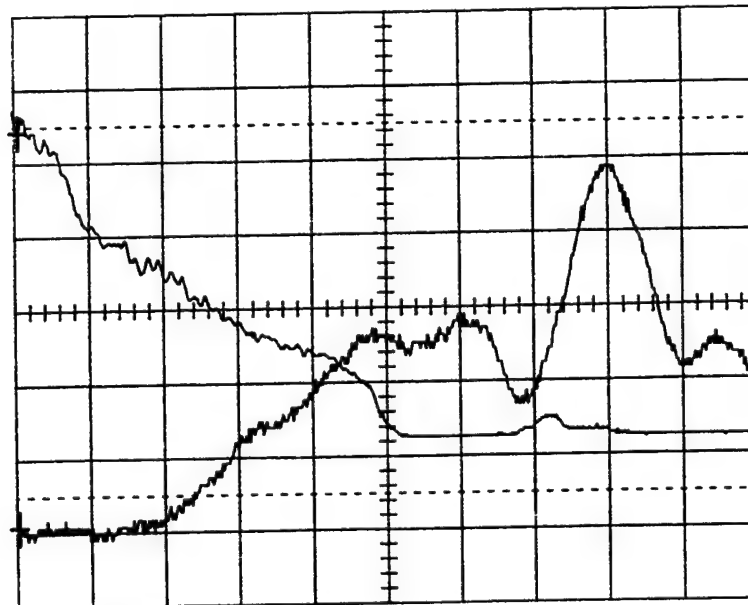
b. Expanded Load Trace

Figure A24. Run No. 1-19b for Material 44 Impacted at 310 fps.

A-26

193

0   0.2ms

a. Displacement and Load Time Records

0   50μs
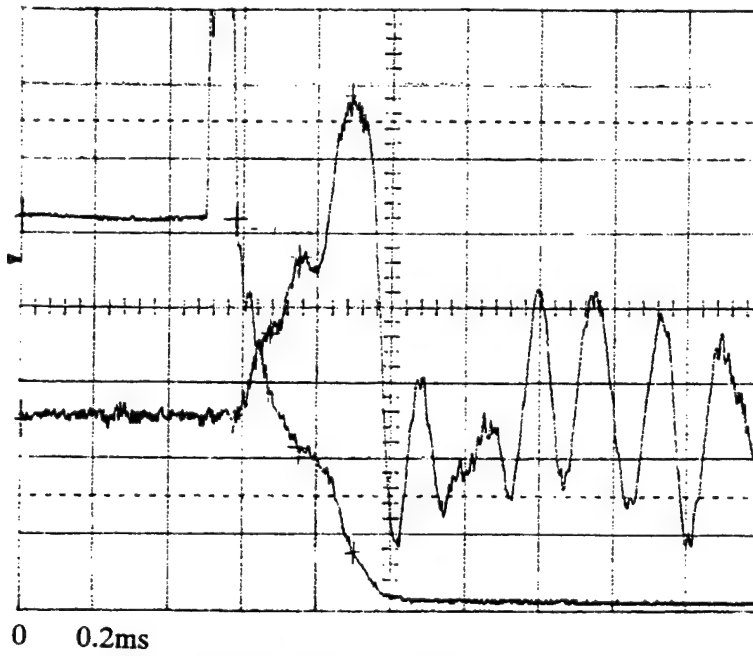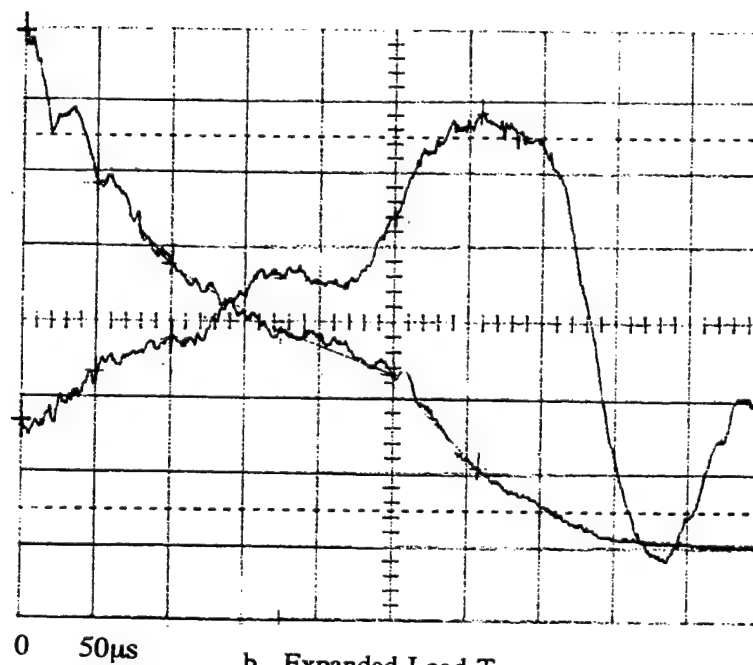
b. Expanded Load Trace

Figure A25. Run No. 1-12a for Material 45 Impacted at 1100 fps.

A-27

194

a. Displacement and Load Time Records

0   0.5ms

b. Expanded Load Trace

0   100μs
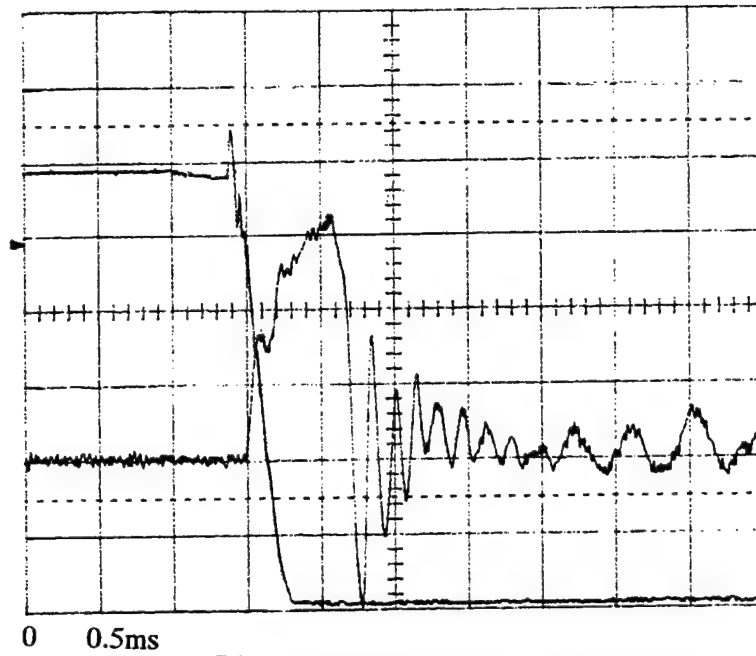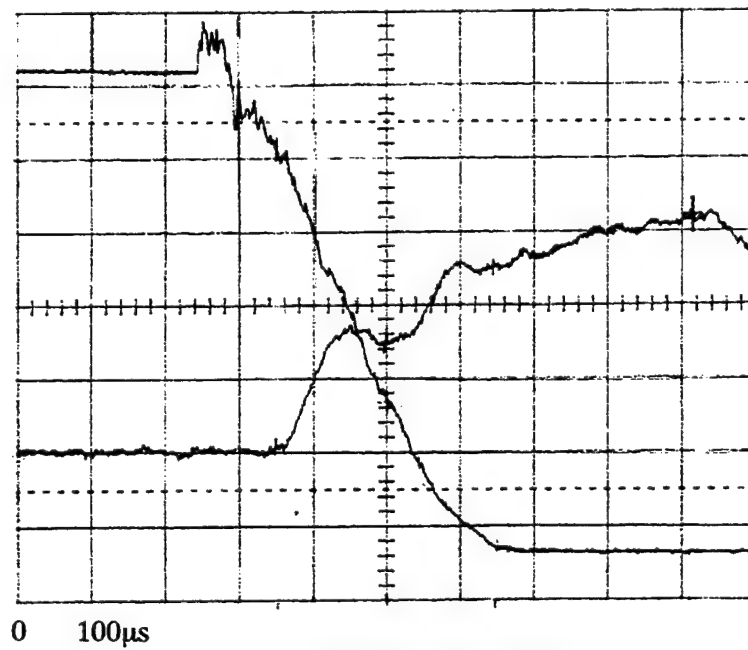
Figure A26. Run No. 1-12b for Material 45 Impacted at 570 fps.

A-28

195

0   0.5ms

a. Displacement and Load Time Records

0   195μs
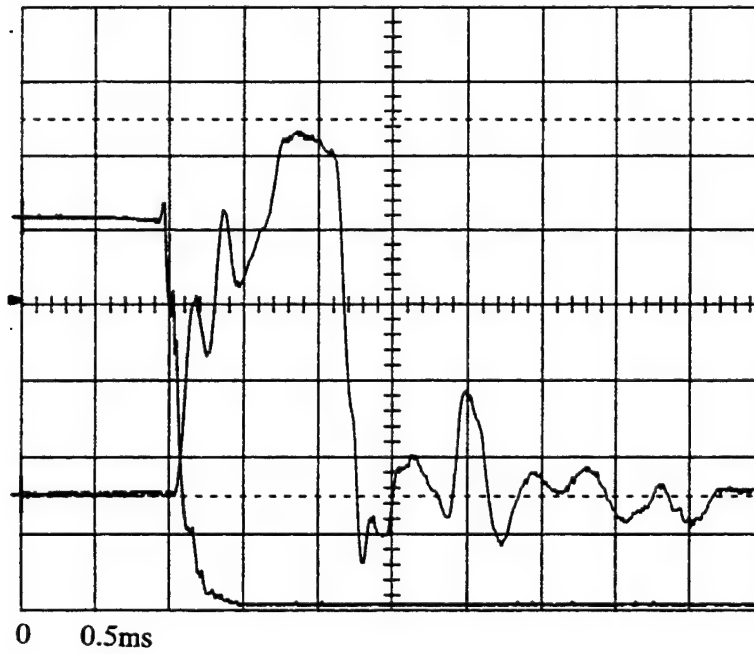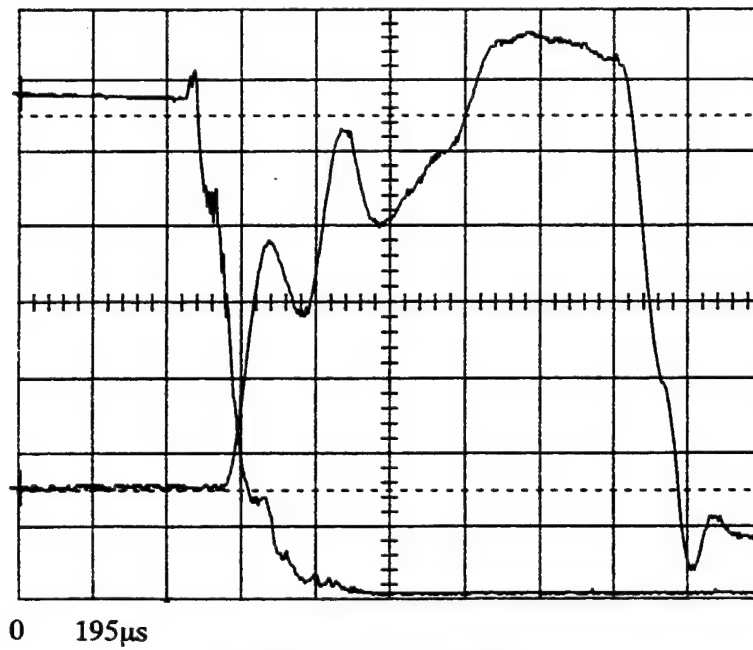
b. Expanded Load Trace

Figure A27. Run No. 2-12 for Material 45 Impacted at 310 fps.

A-29

196

APPENDIX B

**Finite Element Simulations of Waterdrop Impacts on
Polyurethane Layers at 1000 fps**

The initial finite element calculations were used to construct and refine the basic model. Material properties for the polyurethane layers were assumed to show the effect of the stiffness modulii when they were varied over two orders of magnitude. Fairly extensive modeling was completed to examine the influence of a range of grid geometries on the calculated stress and strain components. The final waterdrop impact calculations summarized here used the optimized grid arrays.

Once the actual material properties for the five polyurethane candidates were evaluated as documented in Section 5 the waterdrop impact simulations could be carried out. The measured stiffness values turned out to be quite low (in the lower range of the modulii selected for the initial finite element calculations) and they were within a narrow range for the five polyurethane materials. This result required longer computational run times than used initially in order to reach the maximum stress and strain states. The simulations completed are summarized in Table B1.

Representative results for the ten finite element simulations are contained in this Appendix. The primary results from these simulations are listed in Table 6.1. The totality of the finite element calculations is much more extensive than the cases collected in this Appendix, however there was no effective means for conveniently summarizing these results due to both the spatial and temporal variations in the quantities being evaluated. Contour plots were used extensively as shown in Figures B1 to B6. The range of values for the contours can include the minimum to maximum values or the range could be confined to specific limits to determine a particular detail in the response of the polyurethane layer. The convention used in these plots is that positive values are tensile while negative values are compressive.

The alternative mode for plotting the data is shown in Figures B41 to B46 where the variation of the mechanical parameter with time is provided at a specific location (designated by a given finite element grid). The grid points in Figures B41 to B46 are at the surface of the polyurethane layer beginning at the initial contact point and then moving radially outward. The increasing alphabetical designation corresponds to increasing radial distance.

The results from the finite element computations can be presented in several ways, but further work is required to develop plot routines for this purpose. The results from the computations to date were manually reviewed and the critical features of the computations documented.

Table B1. Finite Element Calculations for 2 mm Waterdrop
Impacts on a Polyurethane Layer at 1000 fps.

Simulation	Impact Angle (degrees)	Material	Material Representation	Modulus (psi)	Total Run Time (μs)	Remarks
1	90	-	Hyperelastic	25,000	1.5	
2	90	11	Hyperelastic	12,000	2.0	
3	90	17	Hyperelastic	6,000	2.0	
4	90	4	Hyperelastic	2,000	2.4	
5	45	11	Hyperelastic	12,000	4.0	
6	45	17	Hyperelastic	6,000	4.0	
7	45	4	Hyperelastic	2,000	8.0	
8	90	17	Hyperelastic	6,000	8.0	6mm drop diameter
9	90	17	Viscoelastic	Variable	4.0	
10	90	17	Viscoelastic	Variable	4.0	0.25 in. thick polyure-thane layer

Simulation 1

Hyperelastic Modulus is 25 ksi

2 mm Waterdrop Impact at Normal Incidence

```
1/4 drop 2 mm 1 Kfps Polyureth
  time =  0.13999E-05
contours of x-stress
min=-0.100E+05 in element   5390
max= 0.278E+04 in element   4961
```

```
contour values
  A=-8.94E+03
  B=-7.61E+03
  C=-6.28E+03
  D=-4.94E+03
  E=-3.61E+03
  F=-2.28E+03
  G=-9.52E+02
  H= 3.78E+02
  I= 1.71E+03
```
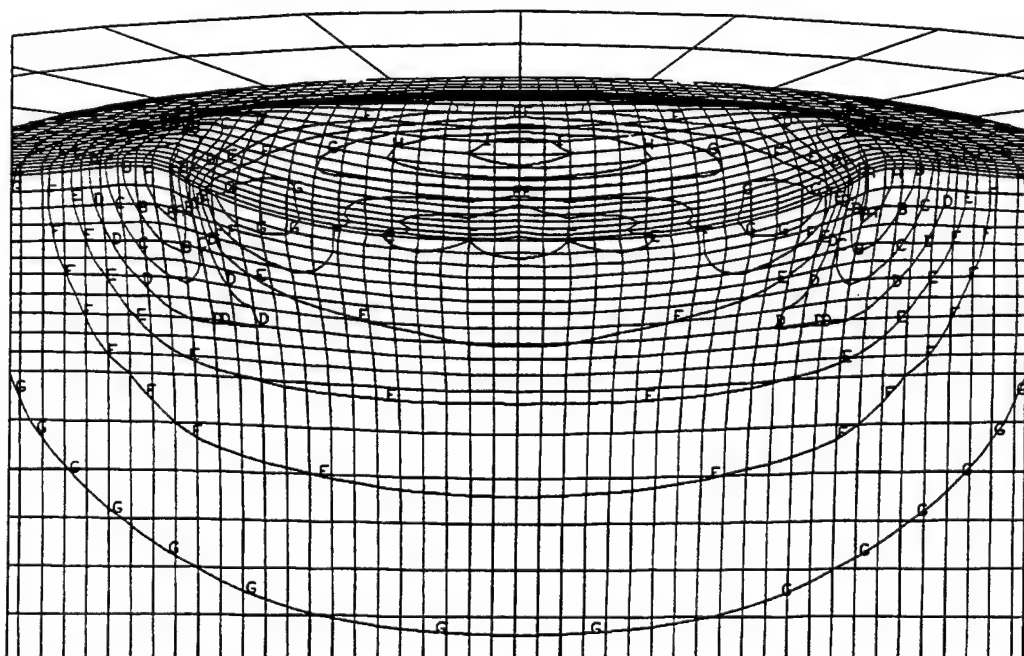
Figure B1. Radial stress distribution for Simulation 1 at 1.4 μs.

B-3

```
1/4 drop 2 mm 1 Kfps Polyureth
 time =  0.13999E-05
contours of y-stress
min=-0.100E+05 in element  5690
max= 0.278E+04 in element  4686
```

```
contour values
 A=-8.94E+03
 B=-7.61E+03
 C=-6.28E+03
 D=-4.94E+03
 E=-3.61E+03
 F=-2.28E+03
 G=-9.53E+02
 H= 3.78E+02
 I= 1.71E+03
```
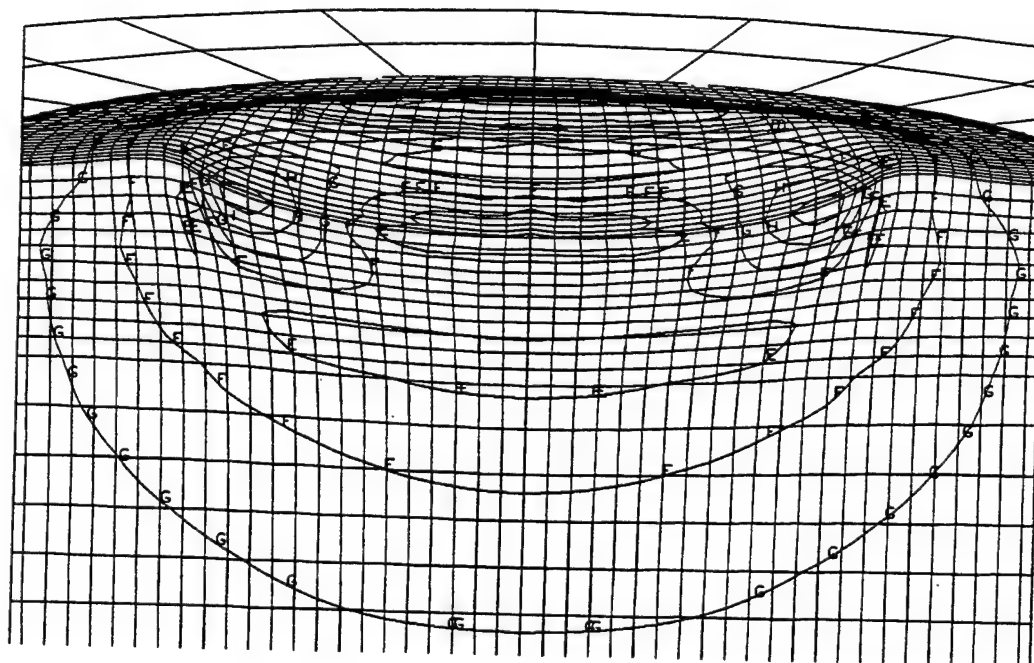
Figure B2.   Circumferential stress distribution for Simulation 1 at 1.4 μs.

```
1/4 drop 2 mm 1 Kfps Polyureth
  time =   0.13999E-05
contours of z-stress
min=-0.121E+05 in element   4729
max= 0.123E+04 in element   5053
```

```
contour values
  A=-1.10E+04
  B=-9.62E+03
  C=-8.23E+03
  D=-6.84E+03
  E=-5.45E+03
  F=-4.06E+03
  G=-2.67E+03
  H=-1.28E+03
  I= 1.06E+02
```
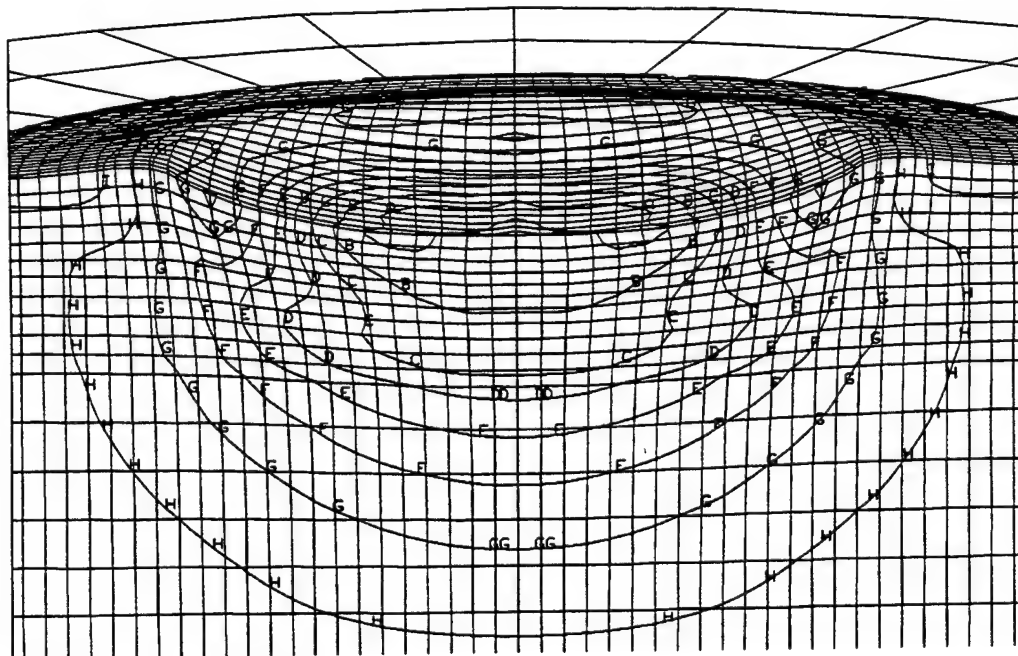
Figure B3. Axial stress distribution for Simulation 1 at 1.4 μs.

B-5

203

1/4 drop 2 mm 1 Kfps Polyureth
 time = 0.13999E-05
contours of x-strain
 (infinitesimal)
min=-0.232E+00 in element   4690
max= 0.171E+00 in element   4682

contour values
 A=-1.98E-01
 B=-1.56E-01
 C=-1.15E-01
 D=-7.26E-02
 E=-3.07E-02
 F= 1.12E-02
 G= 5.31E-02
 H= 9.50E-02
 I= 1.37E-01
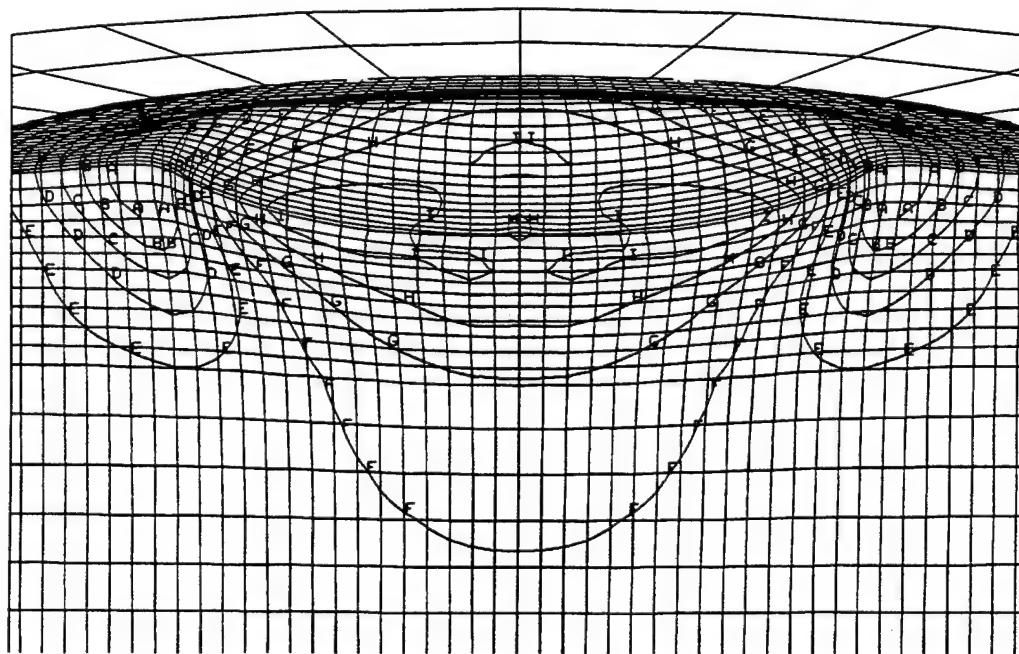
Figure B4. Radial strain distribution for Simulation 1 at 1.4 μs.

B-6

204

```
1/4 drop 2 mm 1 Kfps Polyureth
 time =  0.13999E-05

contours of y-strain
  (infinitesimal)

min=-0.232E+00 in element  5065
max= 0.171E+00 in element  4857
```

```
contour values
 A=-1.98E-01
 B=-1.56E-01
 C=-1.15E-01
 D=-7.26E-02
 E=-3.07E-02
 F= 1.12E-02
 G= 5.31E-02
 H= 9.50E-02
 I= 1.37E-01
```
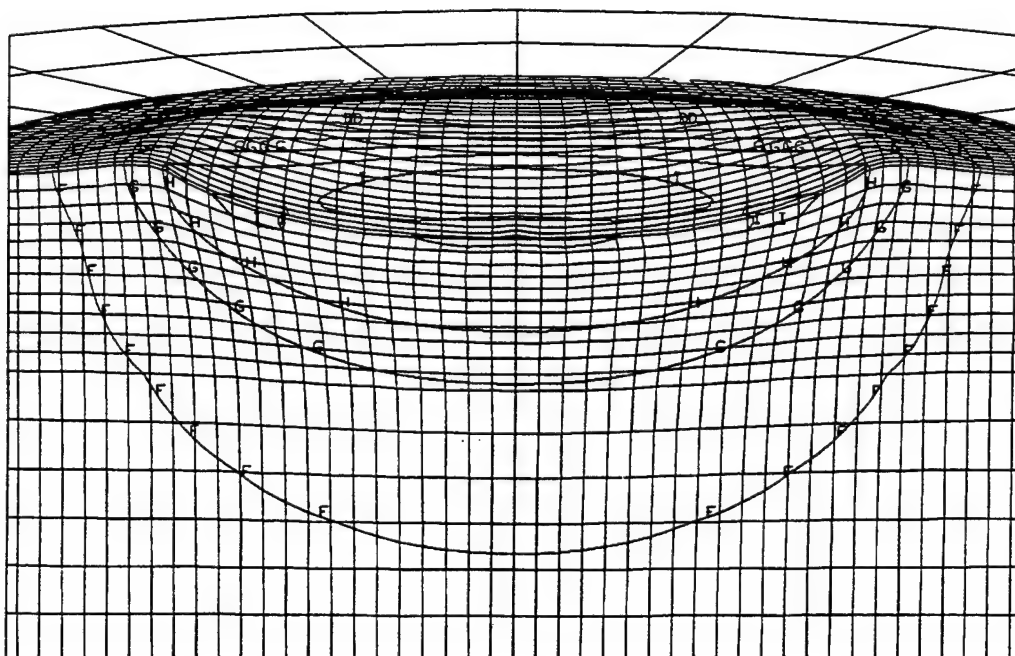
Figure B5. Circumferential strain distribution for Simulation 1 at 1.4 μs.

B-7

205

```
1/4 drop 2 mm 1 Kfps Polyureth
 time =  0.13999E-05
contours of z-strain
  (infinitesimal)
min=-0.312E+00 in element  4784
max= 0.200E+00 in element  5675
```

```
contour values
 A=-2.69E-01
 B=-2.16E-01
 C=-1.63E-01
 D=-1.09E-01
 E=-5.60E-02
 F=-2.62E-03
 G= 5.07E-02
 H= 1.04E-01
 I= 1.57E-01
```
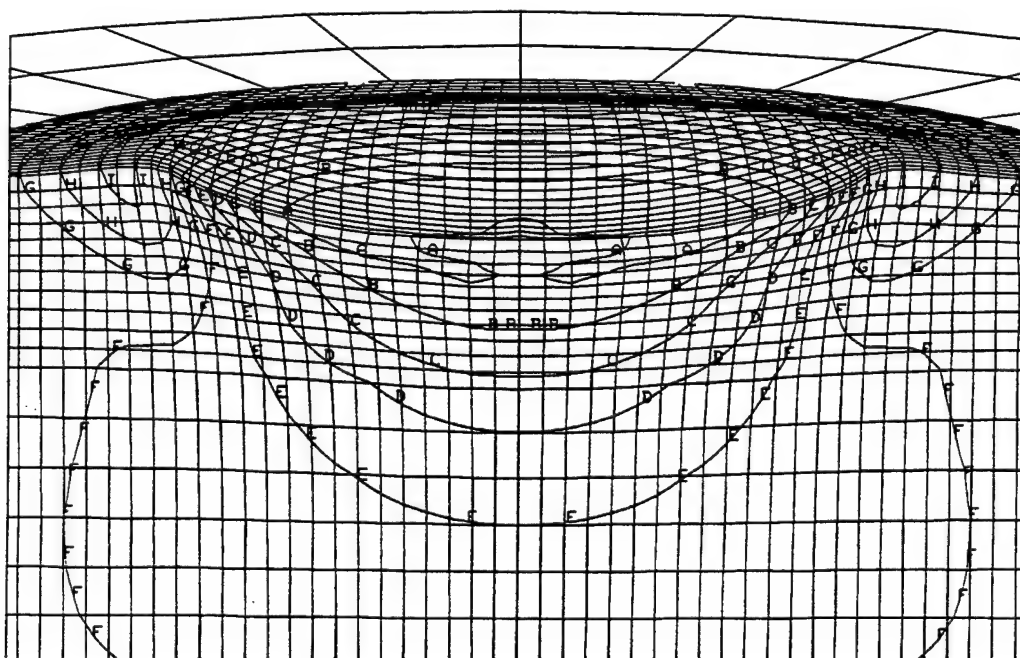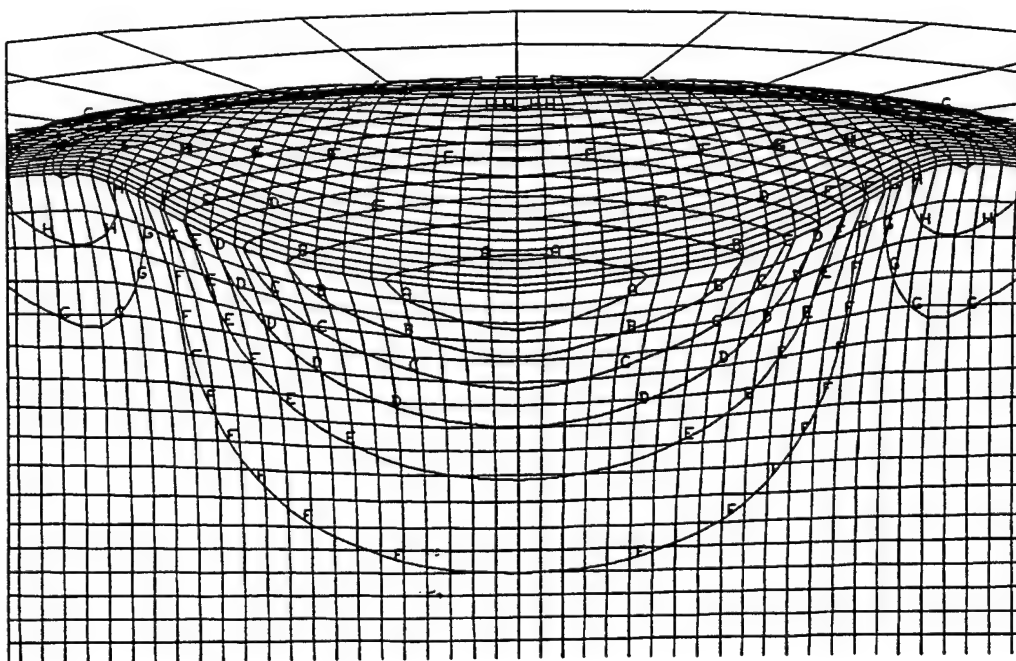
Figure B6. Axial strain distribution for Simulation 1 at 1.4 μs.

B-8

Simulation 2

Hyperelastic Modulus is 12 ksi (Material 11)

2 mm Waterdrop Impact at Normal Incidence

PolyUrethane e 12000 H2O 2mm 1000fps
 time = 0.20000E-05
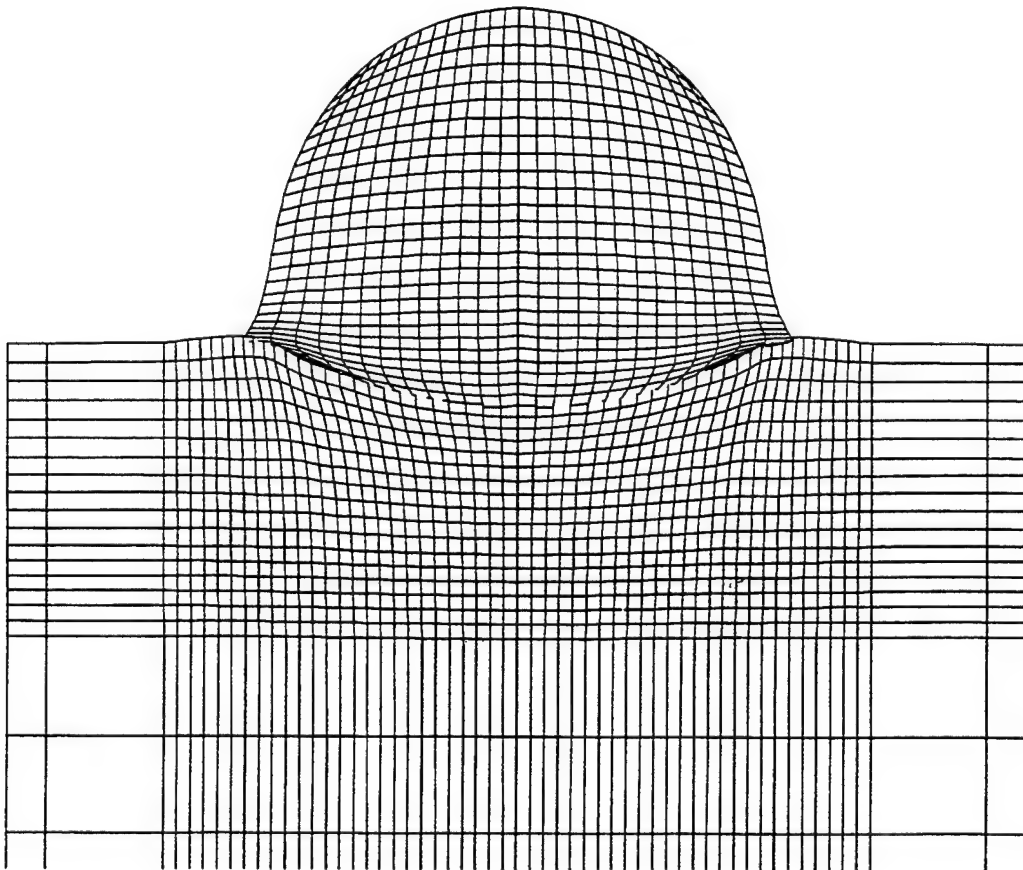
Figure B7. Waterdrop and polyurethane layer grid configuration for Simulation 2 at 2.0 μs.

B-9

PolyUrethane e 12000 H20 2mm 1000fps
time = 0.20000E-05
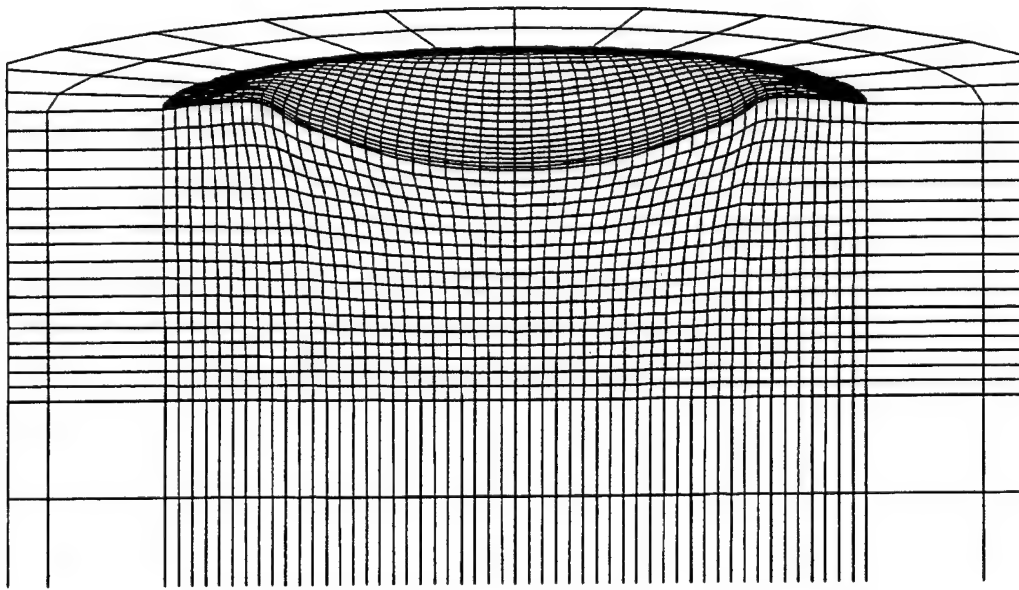
Figure B8. Distortion of polyurethane layer (Material 11) for Simulation 2 at 2.0 μs.

B-10

209

Figure B9. Radial stress distribution for Simulation 2 at 2.0 μs.

B-11

H2O 2 mm 90 deg Polyurethane e 12000 hyperelastic
time = 0.20000E-05
contours of y-stress
min=-0.655E+04 in element 5741
max= 0.110E+04 in element 4688

contour values
A=-6.33E+03
B=-5.95E+03
C=-5.57E+03
D=-5.19E+03
E=-4.81E+03
F=-4.43E+03
G=-4.05E+03
H=-3.67E+03
I=-3.29E+03
J=-2.91E+03
K=-2.53E+03
L=-2.16E+03
M=-1.78E+03
N=-1.40E+03
O=-1.02E+03
P=-6.39E+02
Q=-2.60E+02
R= 1.19E+02
S= 4.99E+02
T= 8.78E+02

Figure B10. Circumferential stress distribution for Simulation 2 at 2.0 μs.

B-12

211

Figure B11. Axial stress distribution for Simulation 2 at 2.0 μs.

H2O 2 mm 90 deg Polyurethane e 12000 hyperelastic
time = 0.20000E-05
contours of x-strain
 (infinitesimal)
min=-0.244E+00 in element   4693
max= 0.299E+00 in element   4702

contour values
A=-2.28E-01
B=-2.01E-01
C=-1.74E-01
D=-1.47E-01
E=-1.20E-01
F=-9.33E-02
G=-6.65E-02
H=-3.96E-02
I=-1.28E-02
J= 1.41E-02
K= 4.09E-02
L= 6.78E-02
M= 9.46E-02
N= 1.22E-01
O= 1.48E-01
P= 1.75E-01
Q= 2.02E-01
R= 2.29E-01
S= 2.56E-01
T= 2.83E-01
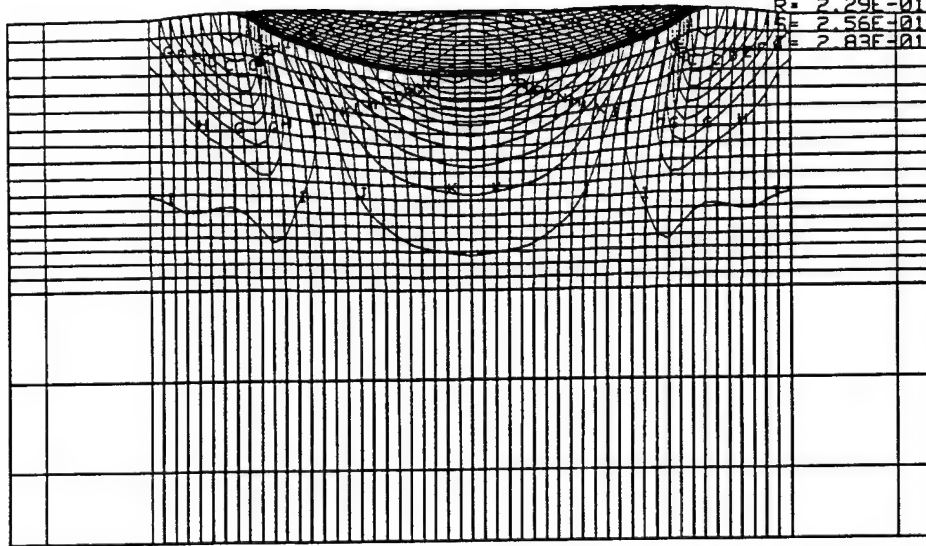
Figure B12. Radial strain distribution for Simulation 2 at 2.0 µs.

B-14

213

H2O 2 mm 90 deg Polyurethane e 12000 hyperelastic
time = 0.20000E-05

contours of y-strain
 (infinitesimal)
min=-0.244E+00 in element 5143
max= 0.299E+00 in element 4702

contour values
A=-2.28E-01
B=-2.01E-01
C=-1.74E-01
D=-1.47E-01
E=-1.20E-01
F=-9.33E-02
G=-6.65E-02
H=-3.96E-02
I=-1.28E-02
J= 1.41E-02
K= 4.09E-02
L= 6.78E-02
M= 9.46E-02
N= 1.22E-01
O= 1.48E-01
P= 1.75E-01
Q= 2.02E-01
R= 2.29E-01
S= 2.56E-01
T= 2.83E-01

Figure B13. Circumferential strain distribution for Simulation 2 at 2.0 μs.

Figure B14. Axial strain distribution for Simulation 2 at 2.0 µs.

2 mm v 1000 H2O Polyurethane e 6e3
 time = 0.19999E-05
contours of z-displacement
min=-0.111E-02 in element 5052
max= 0.108E-01 in element 4675

contour values
 A=-1.11E-04
 B= 1.12E-03
 C= 2.36E-03
 D= 3.59E-03
 E= 4.83E-03
 F= 6.07E-03
 G= 7.30E-03
 H= 8.54E-03
 I = 9.77E-03
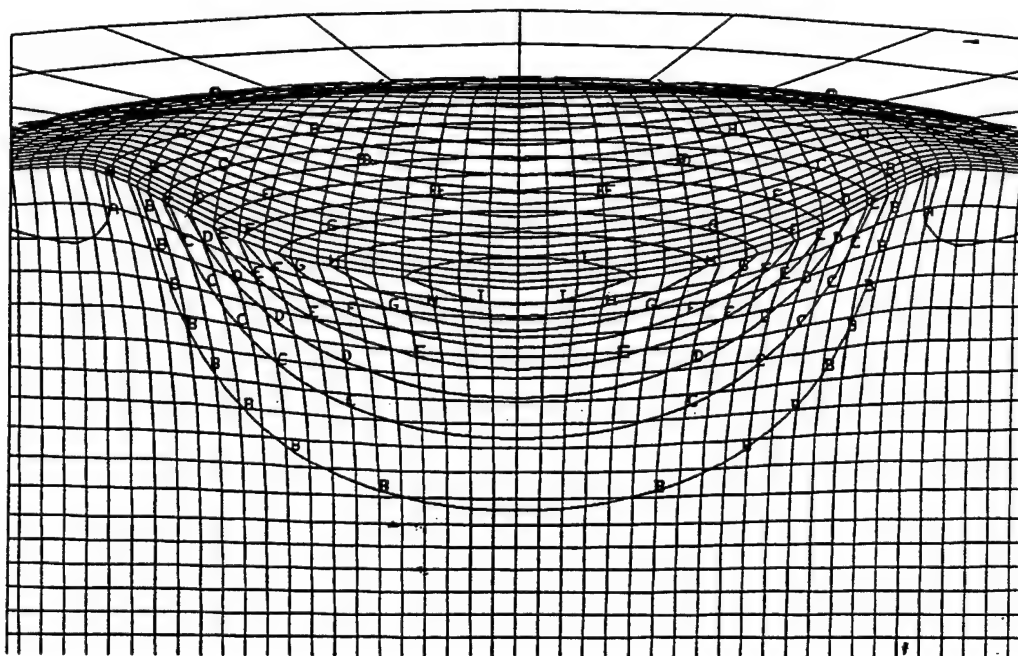
Figure B15. Contours of axial displacement for Simulation 2 at 2.0 μs.

E-17

216

Simulation 3

Hyperelastic Modulus is 6 ksi (Material 17)

2 mm Waterdrop Impact at Normal Incidence

```
2 mm v 1000   H2O Polyurethane e 6e3
 time =  0.19999E-05                          contour values
                                                A=-3.77E+03
contours of x-stress                            B=-3.33E+03
                                                C=-2.88E+03
min=-0.413E+04 in element   4689                D=-2.43E+03
max= 0.155E+03 in element   4401                E=-1.99E+03
                                                F=-1.54E+03
                                                G=-1.10E+03
                                                H=-6.51E+02
                                                I=-2.05E+02
```
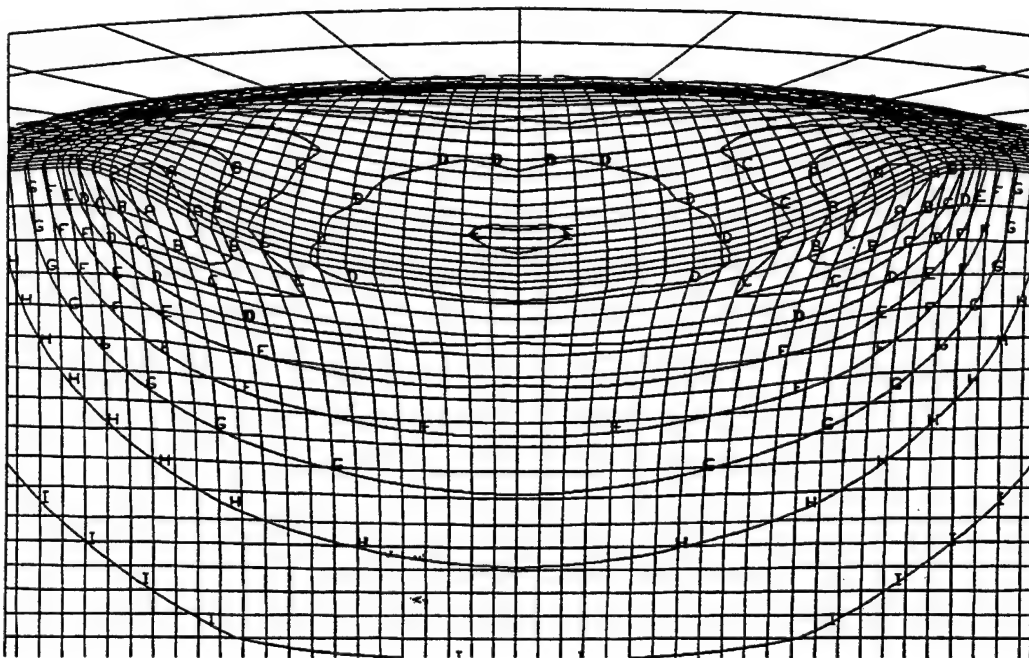
Figure B16. Radial stress distribution for Simulation 3 at 2.0 µs.

```
2 mm v 1000  H2O Polyurethane e 6e3
  time =   0.19999E-05
contours of y-stress
min=-0.413E+04 in element  5039
max= 0.155E+03 in element  4395
```

```
contour values
 A=-3.77E+03
 B=-3.32E+03
 C=-2.88E+03
 D=-2.43E+03
 E=-1.99E+03
 F=-1.54E+03
 G=-1.10E+03
 H=-6.50E+02
 I=-2.05E+02
```
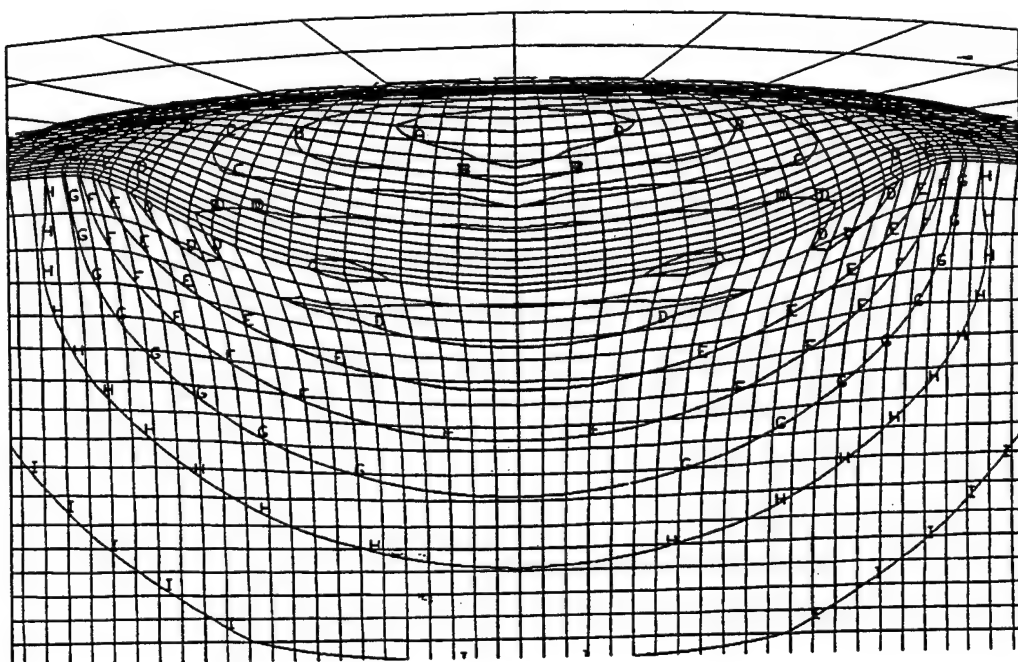
Figure B17. Circumferential stress distribution for Simulation 3 at 2.0 μs.

B-19

```
2 mm v 1000   H2O Polyurethane e 6e3
  time =   0.19999E-05                          contour values
                                                  A=-5.40E+03
contours of z-stress                              B=-4.76E+03
                                                  C=-4.12E+03
min=-0.591E+04 in element   5351                  D=-3.48E+03
max= 0.224E+03 in element   4931                  E=-2.84E+03
                                                  F=-2.21E+03
                                                  G=-1.57E+03
                                                  H=-9.29E+02
                                                  I=-2.91E+02
```
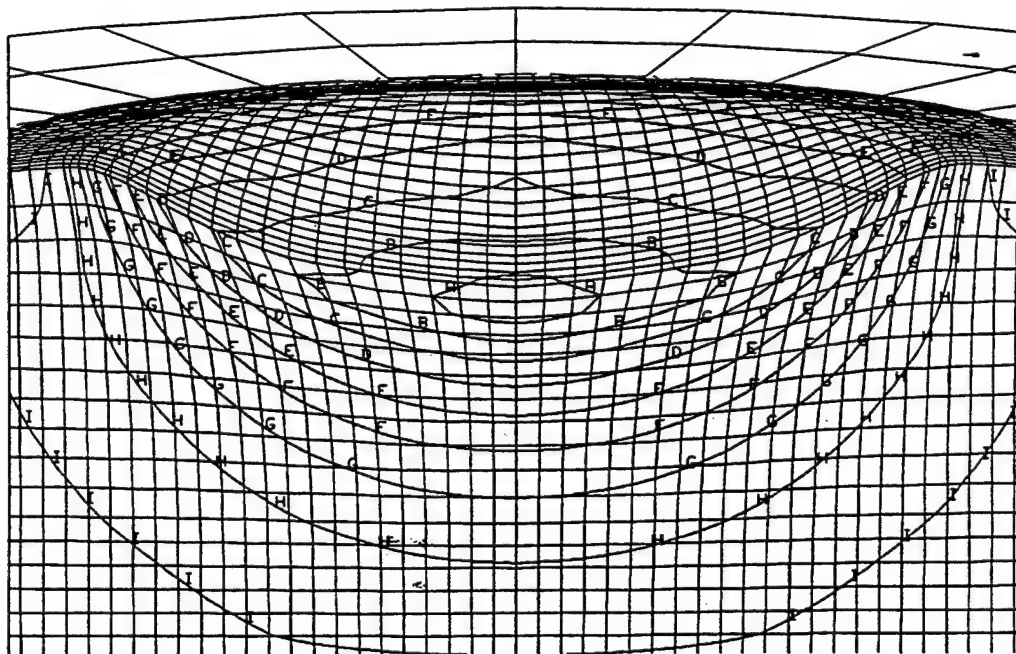
Figure B18. Axial stress distribution for Simulation 3 at 2.0 μs.

B-20

220

2 mm v 1000 H2O Polyurethane e 6e3
  time = 0.19999E-05

contours of x-strain
  (infinitesimal)

min=-0.280E+00 in element   4692
max= 0.299E+00 in element   4675

contour values
  A=-2.32E-01
  B=-1.71E-01
  C=-1.11E-01
  D=-5.09E-02
  E= 9.41E-03
  F= 6.97E-02
  G= 1.30E-01
  H= 1.90E-01
  I= 2.51E-01
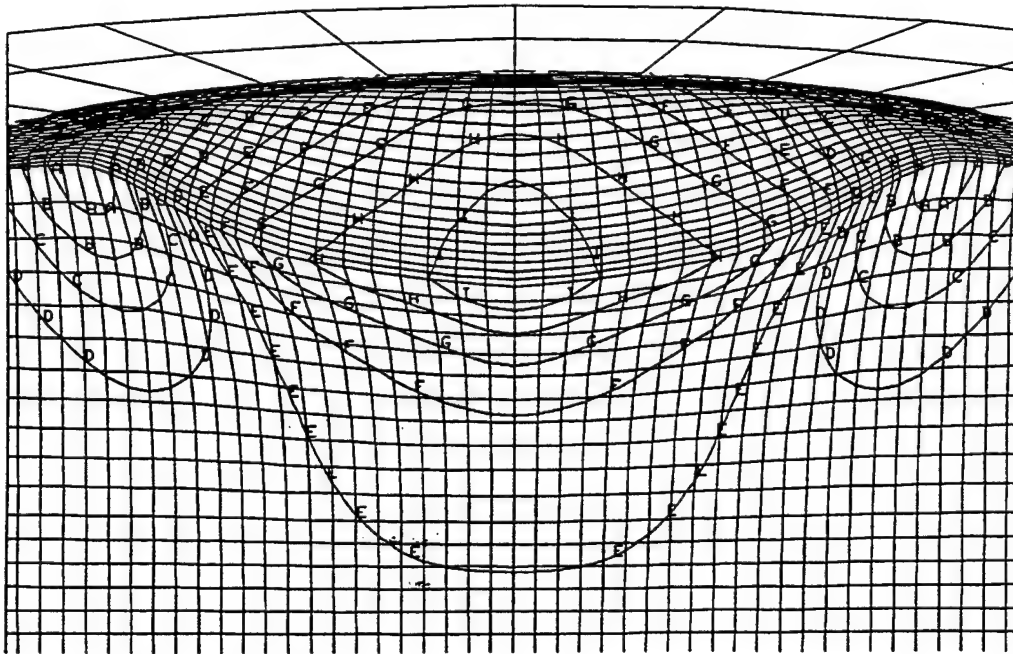
Figure B19. Radial strain distribution for Simulation 3 at 2.0 μs.

B-21

221

```
2 mm v 1000   H2O Polyurethane e 6e3
 time =  0.19999E-05
contours of y-strain
  (infinitesimal)
min=-0.280E+00 in element  5117
max= 0.300E+00 in element  4675
```

```
contour values
 A=-2.32E-01
 B=-1.71E-01
 C=-1.11E-01
 D=-5.07E-02
 E= 9.65E-03
 F= 7.00E-02
 G= 1.30E-01
 H= 1.91E-01
 I= 2.51E-01
```
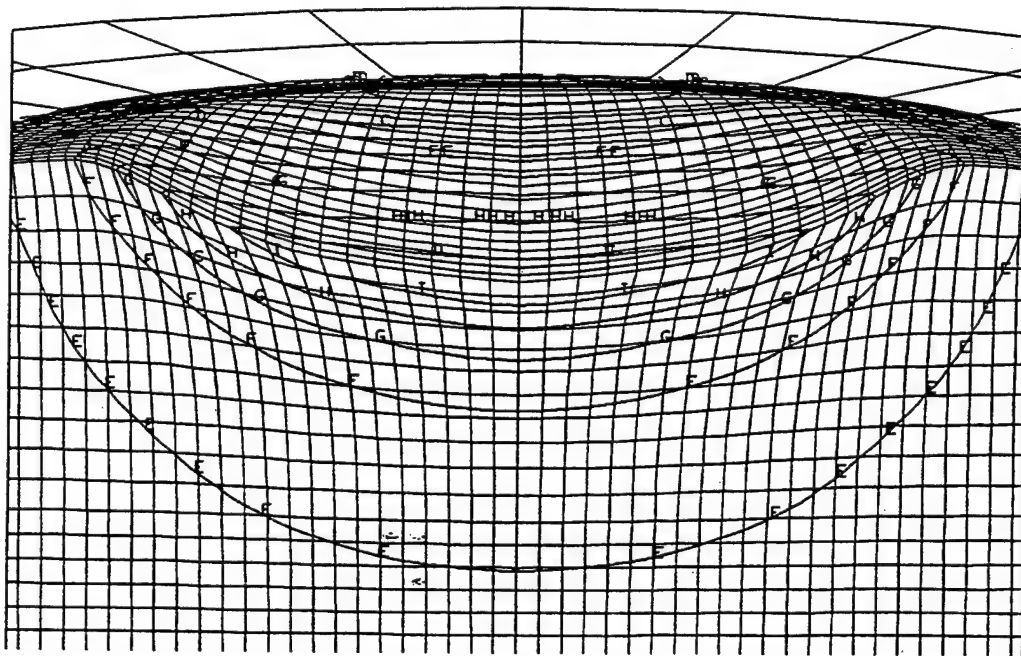
Figure B20. Circumferential strain distribution for Simulation 3 at 2.0 µs.

B-22

```
2 mm v 1000   H2O Polyurethane e 5e3
 time =   0.19999E-05                              contour values
contours of z-strain                                A=-4.50E-01
  (infinitesimal)                                   B=-3.72E-01
                                                    C=-2.94E-01
min=-0.513E+00 in element   4675                    D=-2.17E-01
max= 0.235E+00 in element   5026                    E=-1.39E-01
                                                    F=-6.10E-02
                                                    G= 1.68E-02
                                                    H= 9.46E-02
                                                    I= 1.72E-01
```
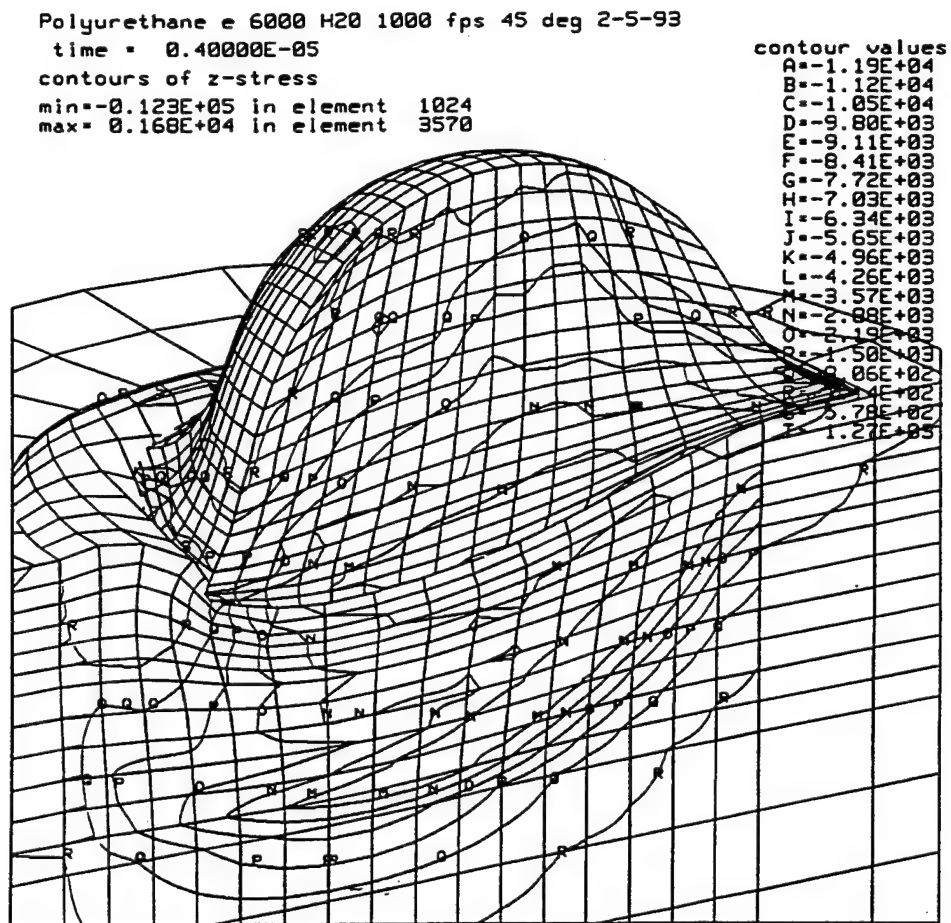

Figure B21. Axial strain distribution for Simulation 3 at 2.0 µs.

B-23

223

Simulation 4

Hyperelastic Modulus is 2 ksi (Material 4)

2 mm Waterdrop Impact at Normal Incidence

PolyUrethane e 2000 H2O 2mm 1000fps
 time = 0.24000E-05
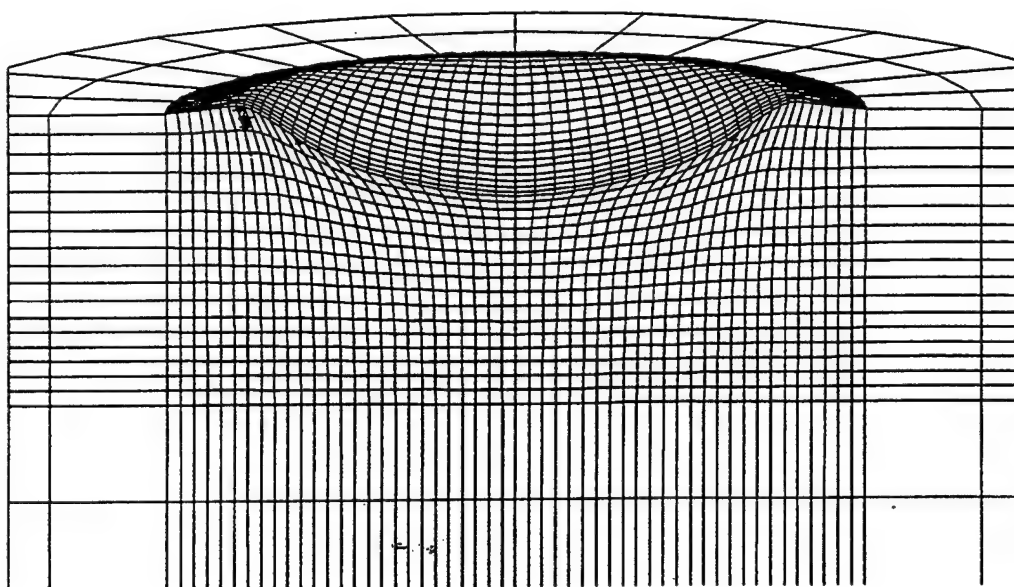
Figure B22. Deformed finite element grid for Simulation 4 at 2.4 μs.

```
Hyperelastic e 2e3 H20 2 mm 1000 fps
 time =  0.19999E-05
contours of x-stress
min=-0.655E+04 in element   5366
max= 0.110E+04 in element   5013
```

contour values
```
A=-5.91E+03
B=-5.11E+03
C=-4.32E+03
D=-3.52E+03
E=-2.73E+03
F=-1.93E+03
G=-1.13E+03
H=-3.36E+02
I= 4.60E+02
```
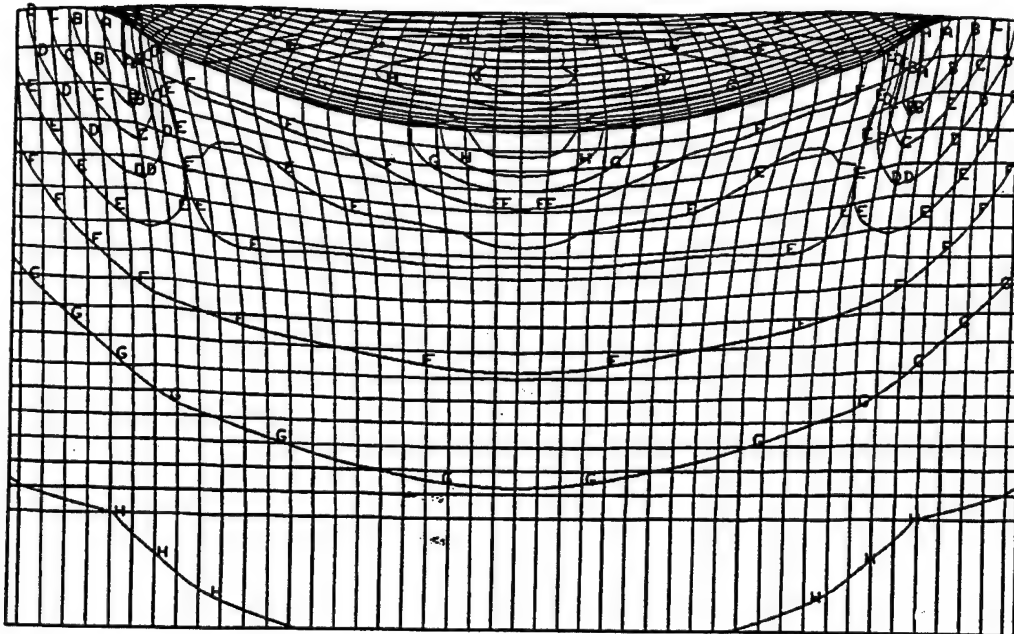

Figure B23. Radial stress distribution for Simulation 4 at 2.0 μs.

B-25

226

Hyperelastic e 2e3 H20 2 mm 1000 fps
 time = 0.19999E-05
contours of y-stress
min=-0.655E+04 in element 5741
max= 0.110E+04 in element 4688

contour values
 A=-5.91E+03
 B=-5.11E+03
 C=-4.32E+03
 D=-3.52E+03
 E=-2.73E+03
 F=-1.93E+03
 G=-1.13E+03
 H=-3.36E+02
 I= 4.60E+02
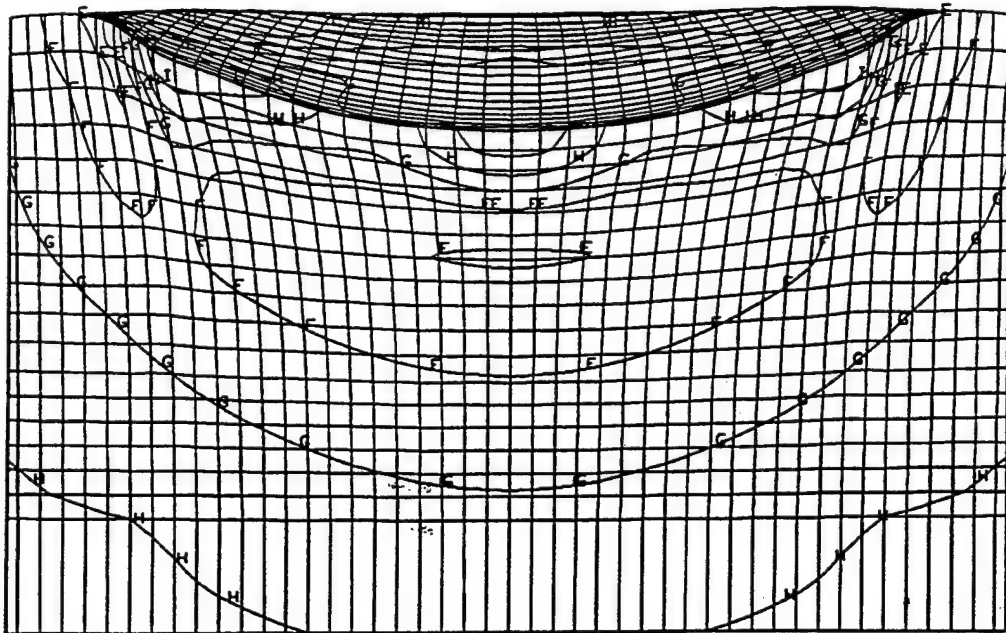
Figure B24. Circumferential stress distribution for Simulation 4 at 2.0 μs.

B-26

227

Hyperelastic e 2e3 H20 2 mm 1000 fps
time = 0.19999E-05
contours of z-stress
min=-0.693E+04 in element   4755
max= 0.471E+03 in element   4401

contour values
A=-6.31E+03
B=-5.54E+03
C=-4.77E+03
D=-4.00E+03
E=-3.23E+03
F=-2.46E+03
G=-1.69E+03
H=-9.21E+02
I=-1.51E+02
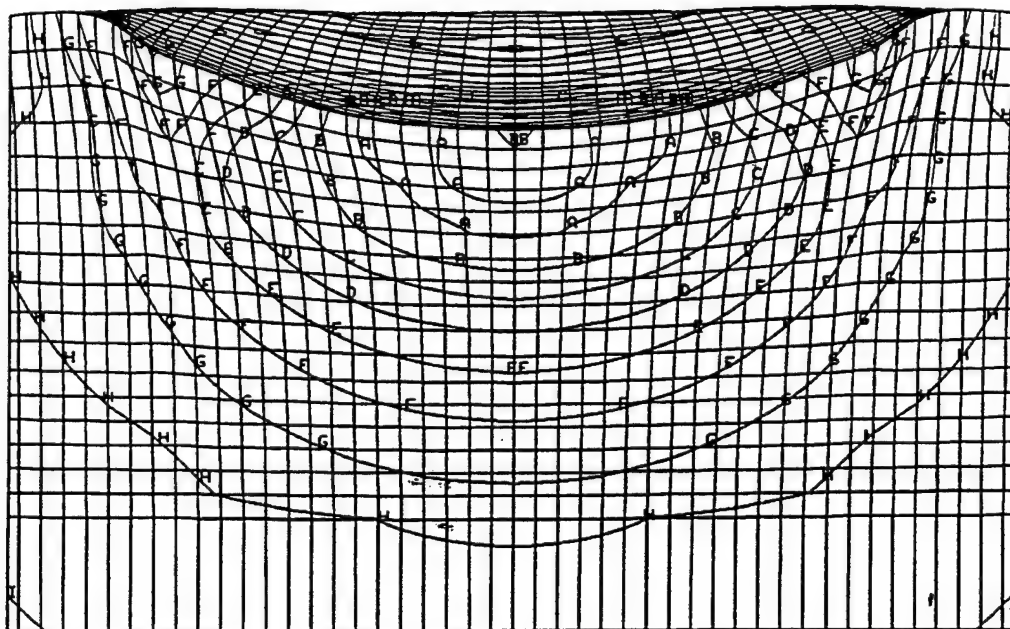
Figure B25. Axial stress distribution for Simulation 4 at 2.0 μs.

B-27

228

Hyperelastic e 2e3 H20 2 mm 1000 fps
 time = 0.19999E-05
contours of x-strain
 (infinitesimal)
min=-0.244E+00 in element 4693
max= 0.299E+00 in element 4702

contour values
 A=-1.98E-01
 B=-1.42E-01
 C=-8.53E-02
 D=-2.89E-02
 E= 2.75E-02
 F= 8.39E-02
 G= 1.40E-01
 H= 1.97E-01
 I= 2.53E-01
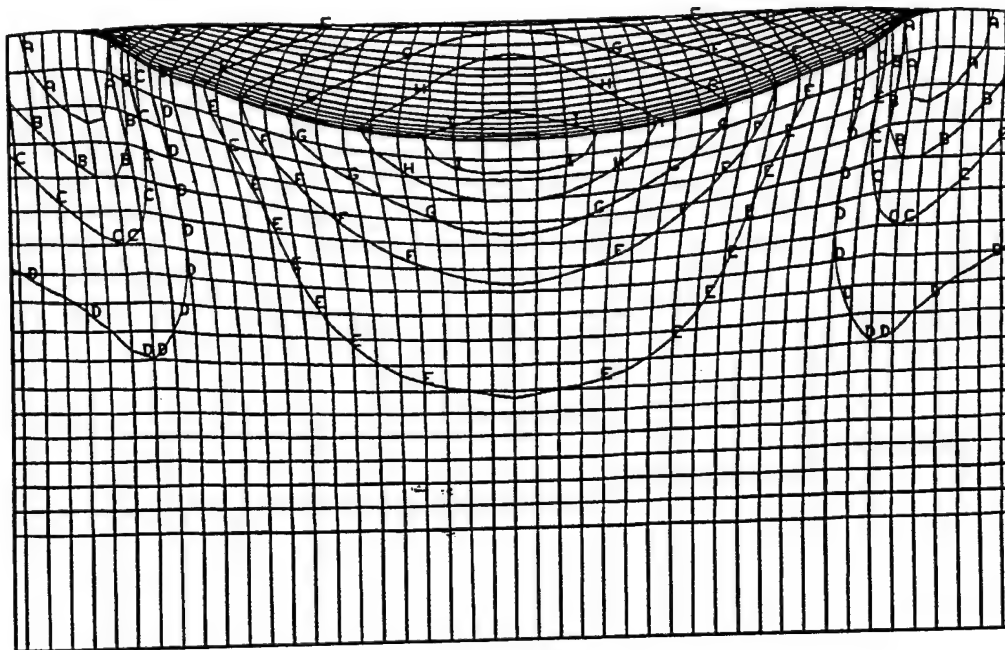
Figure B26. Radial strain distribution for Simulation 4 at 2.0 μs.

B-28

229
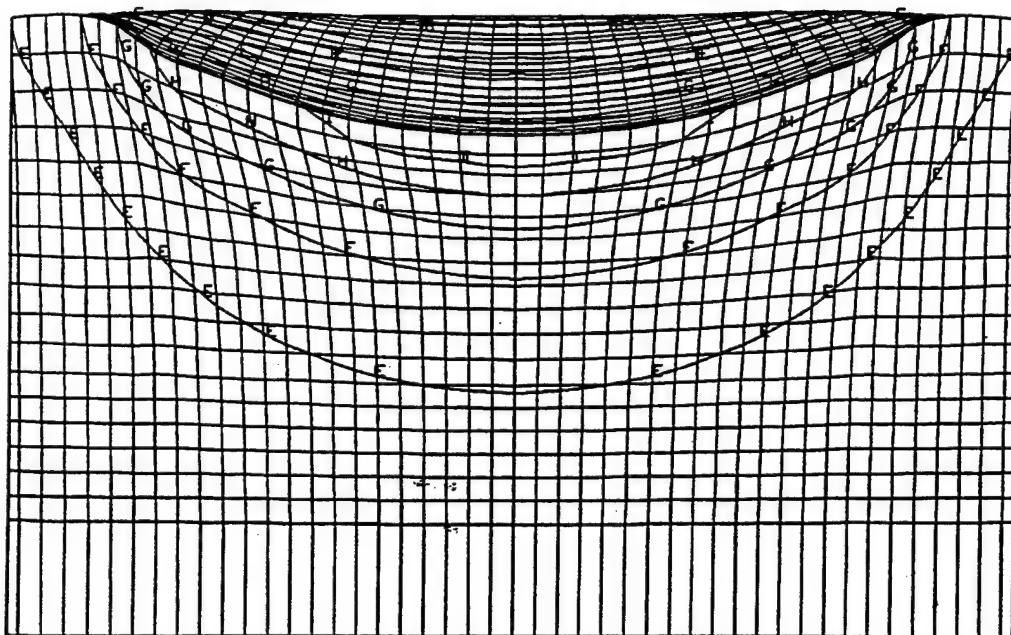
Figure B27. Circumferential strain distribution for Simulation 4 at 2.0 μs.

Hyperelastic e 2e3 H20 2 mm 1000 fps
 time = 0.19999E-05
contours of z-strain
  (infinitesimal)
min=-0.425E+00 in element 4702
max= 0.211E+00 in element 5079

contour values
 A=-3.72E-01
 B=-3.06E-01
 C=-2.40E-01
 D=-1.74E-01
 E=-1.07E-01
 F=-4.13E-02
 G= 2.48E-02
 H= 9.10E-02
 I= 1.57E-01
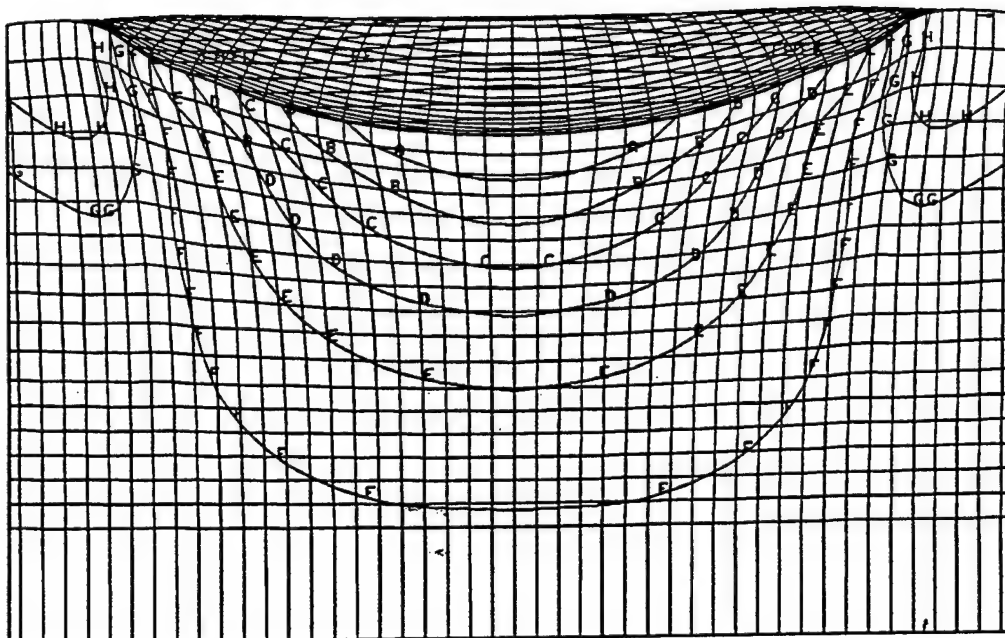
Figure B28. Axial strain distribution for Simulation 4 at 2.0 μs.

B-30

231

Simulation 5

Hyperelastic Modulus is 12 ksi (Material 11)

2 mm Oblique Waterdrop Impact at 45°
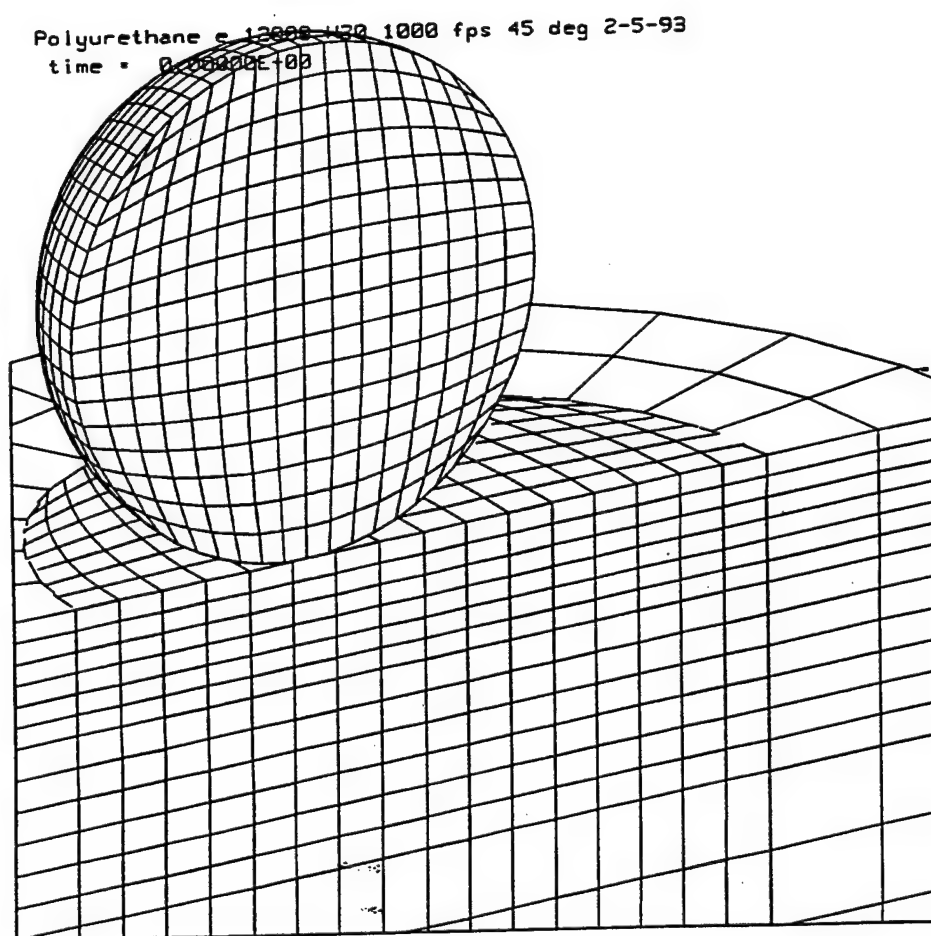
Figure B29. Initial finite element grid for Simulation 5.

B-31

233

Polyurethane e 12000 H20 1000 fps 45 deg 2-5-93
  time = 0.40000E-05
contours of x-stress
min=-0.101E+05 in element 1015
max= 0.236E+04 in element 3527

contour values
A=-9.72E+03
B=-9.10E+03
C=-8.48E+03
D=-7.87E+03
E=-7.25E+03
F=-6.63E+03
G=-6.02E+03
H=-5.40E+03
I=-4.79E+03
J=-4.17E+03
K=-3.55E+03
L=-2.94E+03
M=-2.32E+03
N=-1.70E+03
O=-1.09E+03
P=-4.71E+02
Q=1.45E+02
R=7.62E+02
S=1.38E+03
T=1.99E+03
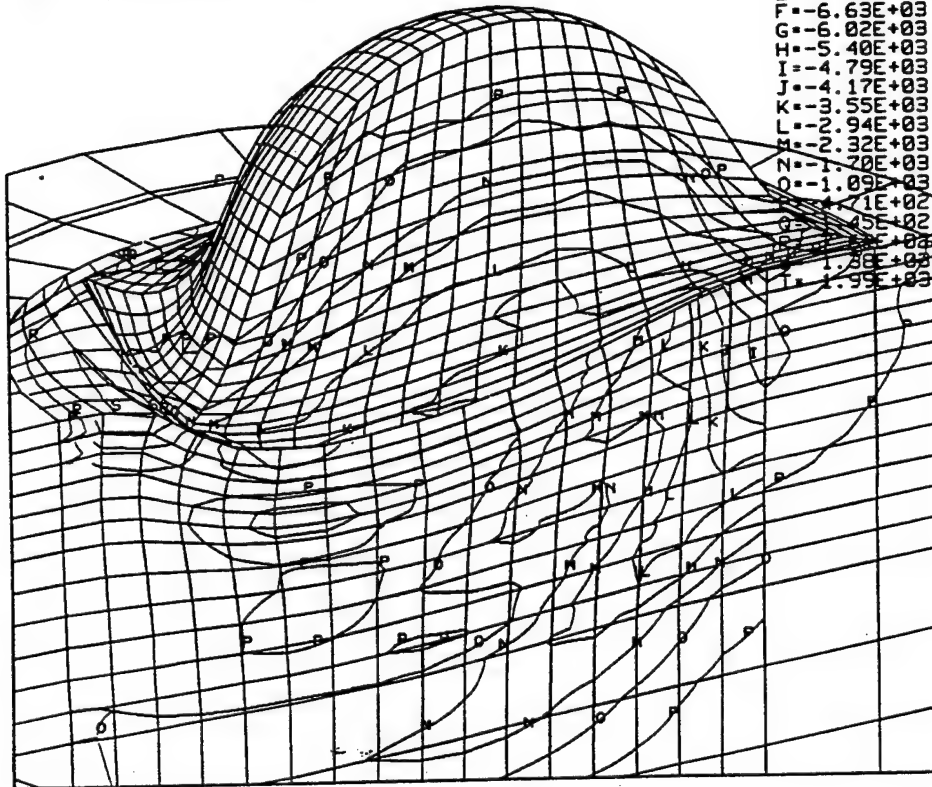
Figure B30. Radial stress distribution for Simulation 5 at 4.0 μs.

B-32

234

Polyurethane e 12000 H20 1000 fps 45 deg 2-5-93
 time = 0.40000E-05
contours of y-stress
min=-0.101E+05 in element 1015
max= 0.172E+04 in element 3565

contour values
A=-9.73E+03
B=-9.15E+03
C=-8.57E+03
D=-7.98E+03
E=-7.40E+03
F=-6.81E+03
G=-6.23E+03
H=-5.64E+03
I=-5.06E+03
J=-4.47E+03
K=-3.89E+03
L=-3.31E+03
M=-2.72E+03
N=-2.14E+03
O=-1.55E+03
P=-9.67E+02
Q=-3.83E+02
R=1.86E+02
T=1.30E+03
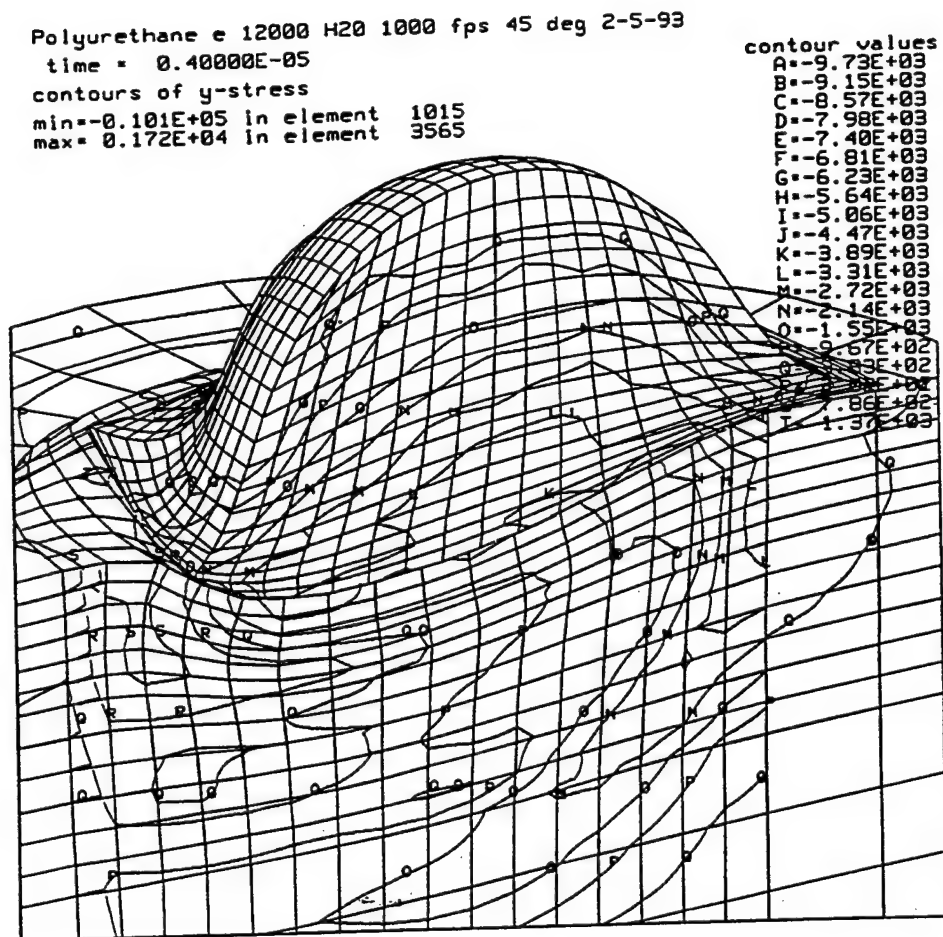
Figure B31. Circumferential stress distribution for Simulation 5 at 4.0 μs.

B-33

```
Polyurethane e 12000 H20 1000 fps 45 deg 2-5-93
  time =  0.40000E-05                              contour values
contours of z-stress                                A=-9.73E+03
                                                    B=-9.13E+03
min=-0.101E+05 in element   1015                    C=-8.53E+03
max= 0.203E+04 in element   3578                    D=-7.93E+03
                                                    E=-7.33E+03
                                                    F=-6.73E+03
                                                    G=-6.13E+03
                                                    H=-5.53E+03
                                                    I=-4.93E+03
                                                    J=-4.33E+03
                                                    K=-3.73E+03
                                                    L=-3.13E+03
                                                    M=-2.53E+03
                                                    N=-1.93E+03
                                                    O=-1.33E+03
                                                    P=-7.26E+02
                                                    Q=-1.28E+02
                                                    R= 4.74E+02
                                                    S= 1.07E+03
                                                    T= 1.67E+03
```
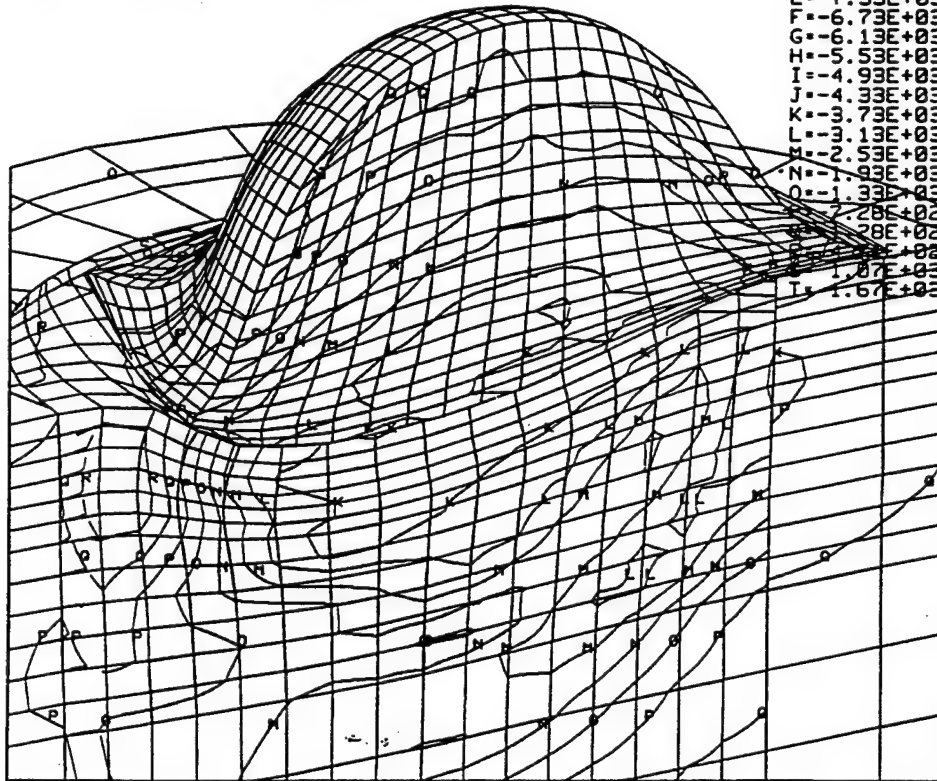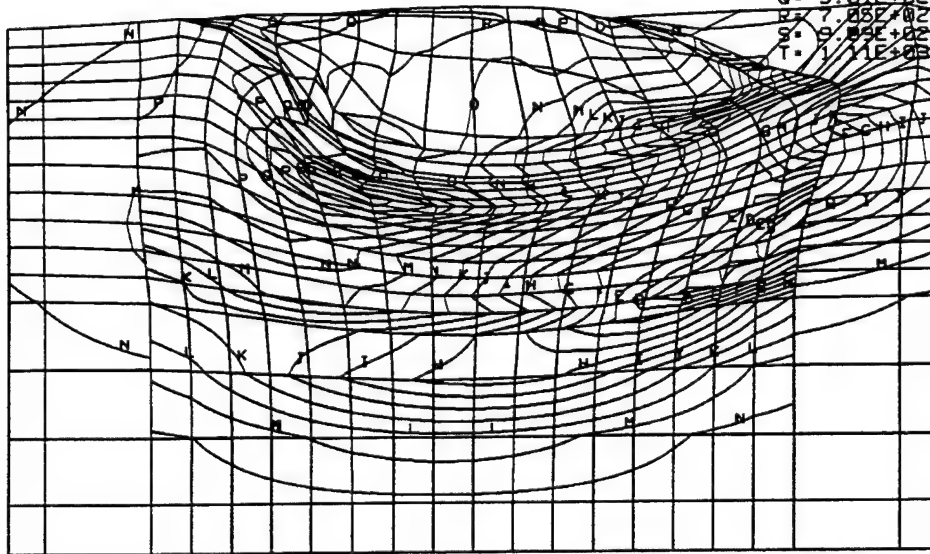
Figure B32. Axial stress distribution for Simulation 5 at 4.0 μs.

B-34

236

Simulation 6

Hyperelastic Modulus is 6 ksi (Material 17)

2 mm Oblique Waterdrop Impact at 45°

Polyurethane e 6000 H20 1000 fps 45 deg 2-5-93
   time = 0.40000E-05
contours of x-stress

min=-0.123E+05 in element 1024
max= 0.128E+04 in element 3526

contour values
A=-1.19E+04
B=-1.12E+04
C=-1.05E+04
D=-9.87E+03
E=-9.20E+03
F=-8.53E+03
G=-7.85E+03
H=-7.18E+03
I=-6.51E+03
J=-5.84E+03
K=-5.17E+03
L=-4.49E+03
M=-3.82E+03
N=-3.15E+03
O=-2.48E+03
P=-1.81E+03
Q=-1.13E+03
R=-4.58E+02
S= 2.10E+02
T= 8.81E+02
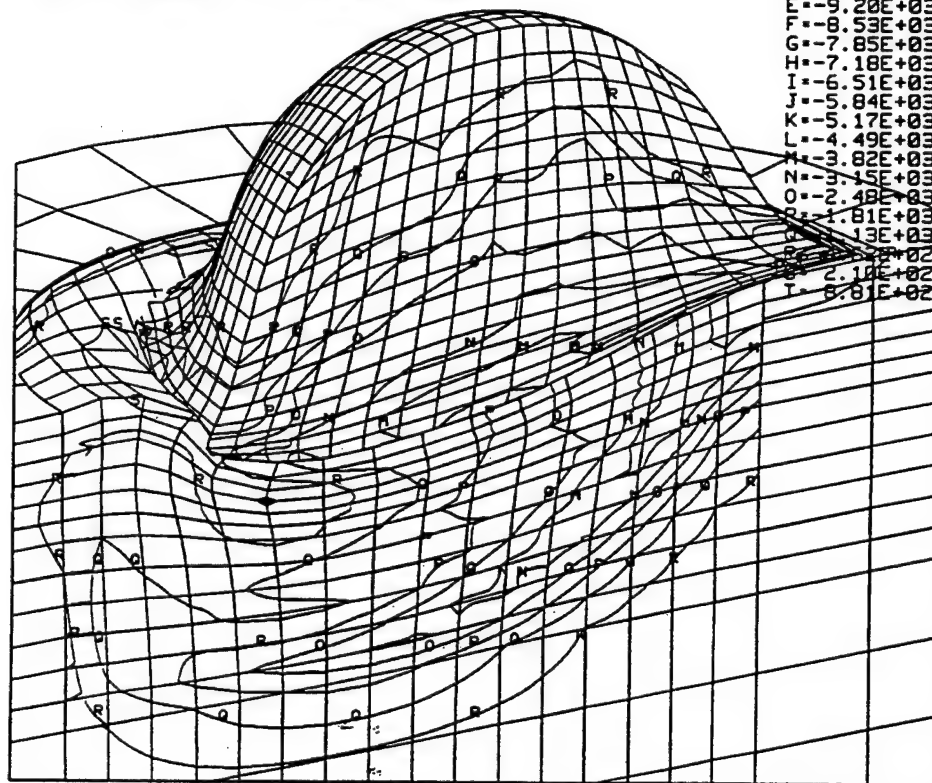
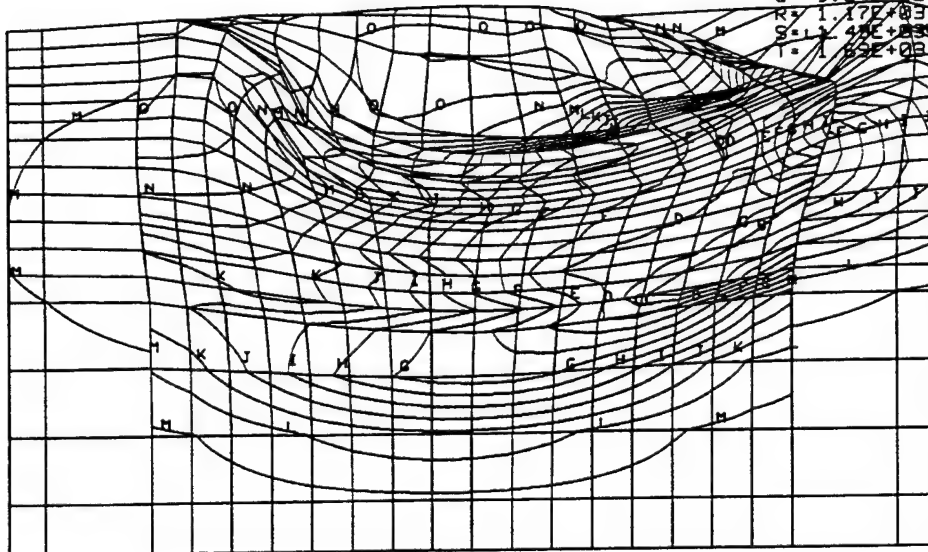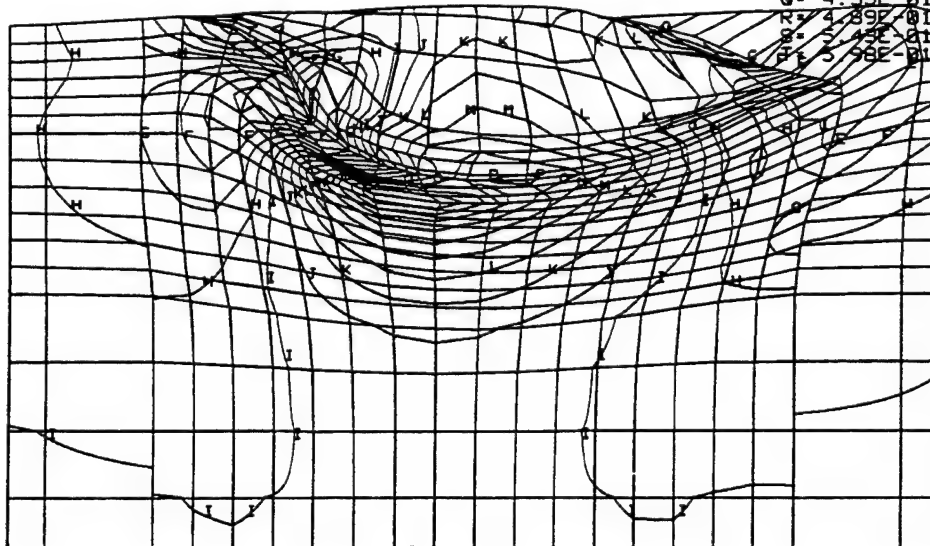Figure B33. Radial stress distribution for Simulation 6 at 4.0 μs.

B-35
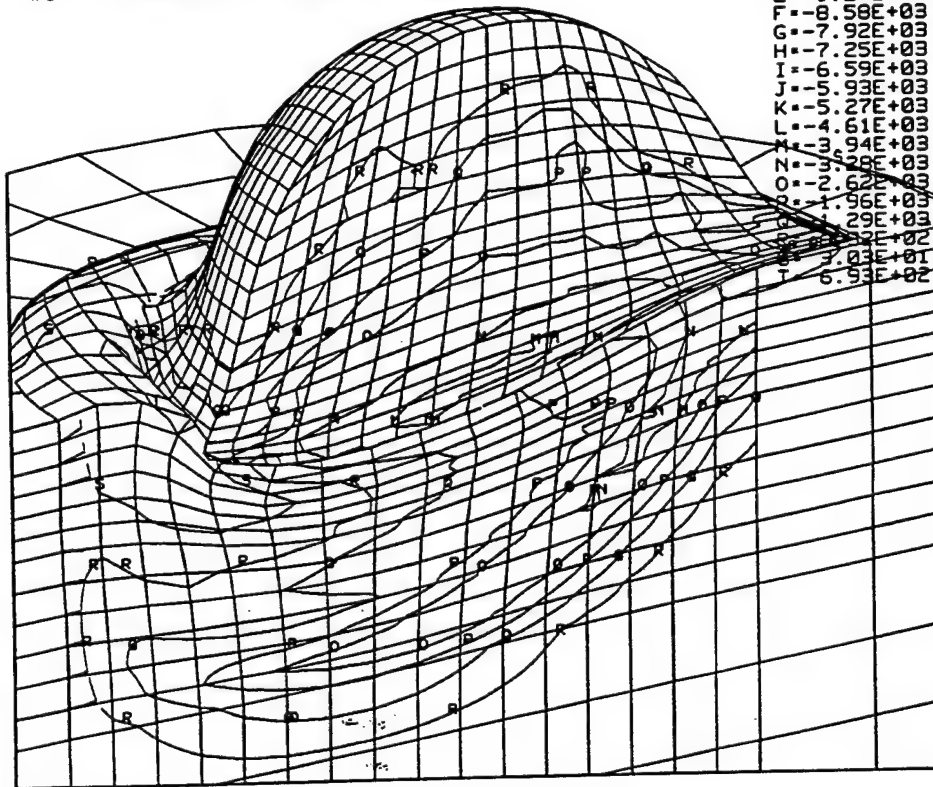
Figure B34. Circumferential stress distribution for Simulation 6 at 4.0 μs.

Polyurethane e 6000 H20 1000 fps 45 deg 2-5-93
 time = 0.40000E-05
contours of z-stress
min=-0.123E+05 in element 1024
max= 0.168E+04 in element 3570

contour values
A=-1.19E+04
B=-1.12E+04
C=-1.05E+04
D=-9.80E+03
E=-9.11E+03
F=-8.41E+03
G=-7.72E+03
H=-7.03E+03
I=-6.34E+03
J=-5.65E+03
K=-4.96E+03
L=-4.26E+03
M=-3.57E+03
N=-2.88E+03
O=-2.19E+03
P=-1.50E+03
Q=-8.06E+02
R=-1.14E+02
S=5.78E+02
T=1.27E+03

Figure B35. Axial stress distribution for Simulation 6 at 4.0 μs.

B-37

240

Simulation 7

Hyperelastic Modulus is 2 ksi (Material 4)

2 mm Oblique Waterdrop Impact at 45°

Polyurethane e 2000 H20 1000 fps 45 deg 2-5-93
time = 0.10000E-05
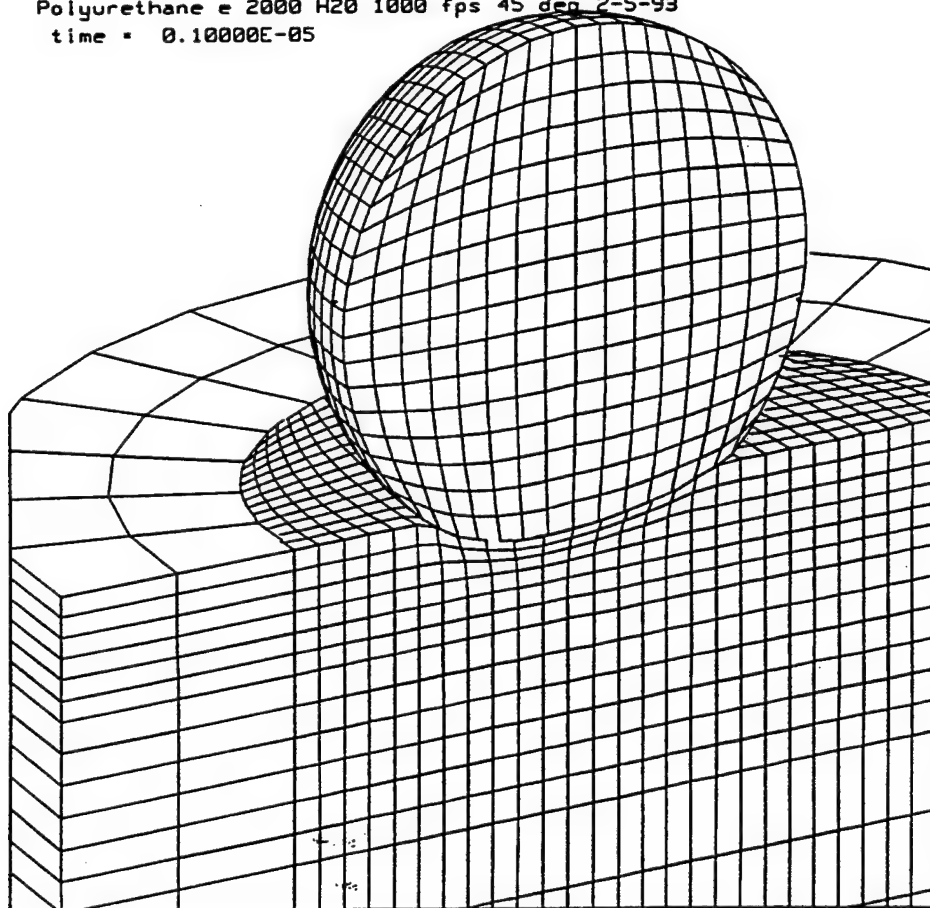
Figure B36. Finite element grid distortion for Simulation 7 at 1.0 μs.

Polyurethane e 2000 H20 1000 fps 45 deg 2-5-93
  time = 0.20000E-05
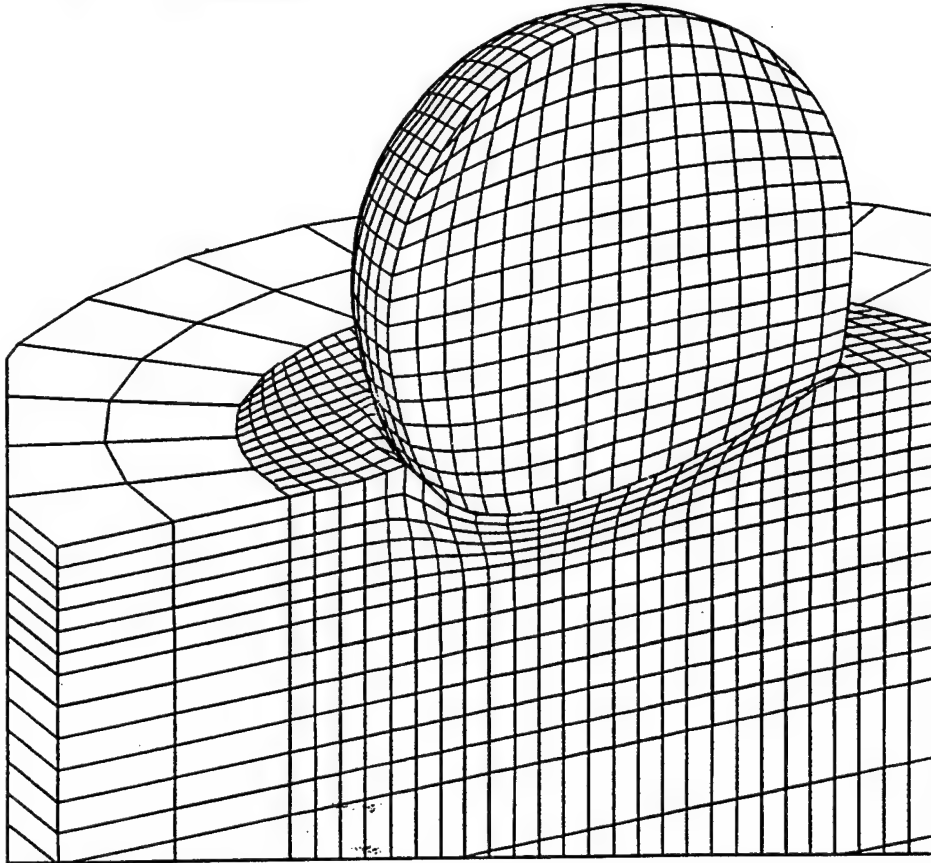
Figure B37. Finite element grid distortion for Simulation 7 at 2.0 μs.

Polyurethane e 2000 H20 1000 fps 45 deg 2-5-93
 time = 0.30000E-05
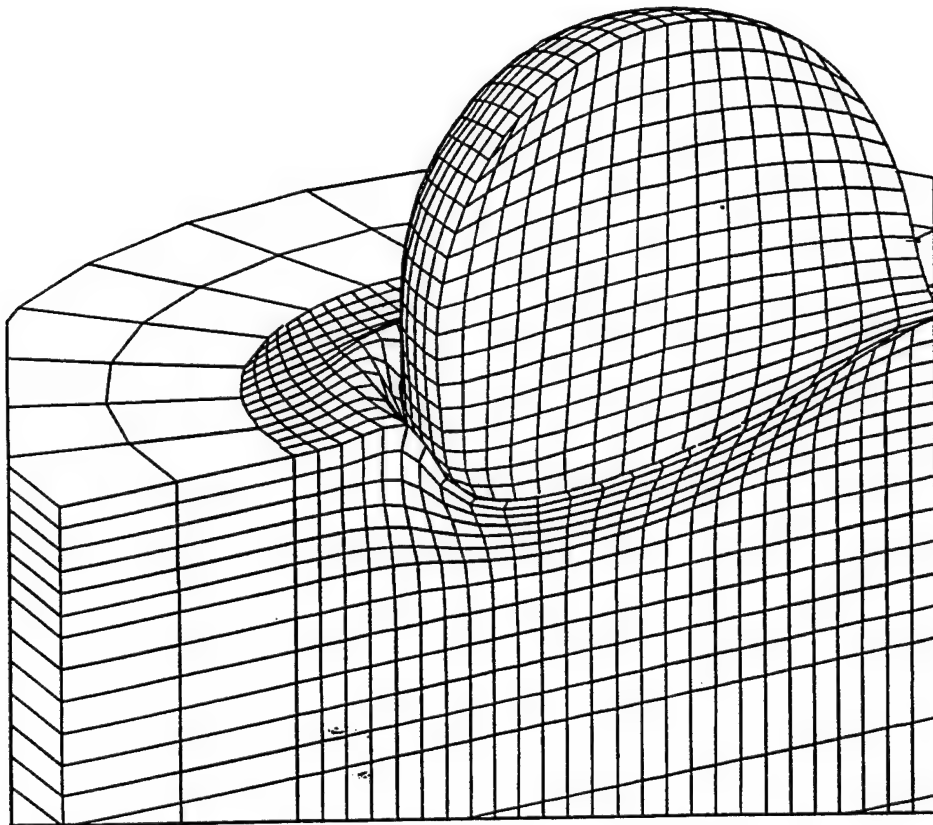
Figure B38. Finite element grid distortion for Simulation 7 at 3.0 μs.

B-40

Polyurethane e 2000 H20 1000 fps 45 deg 2-5-93
  time = 0.40000E-05
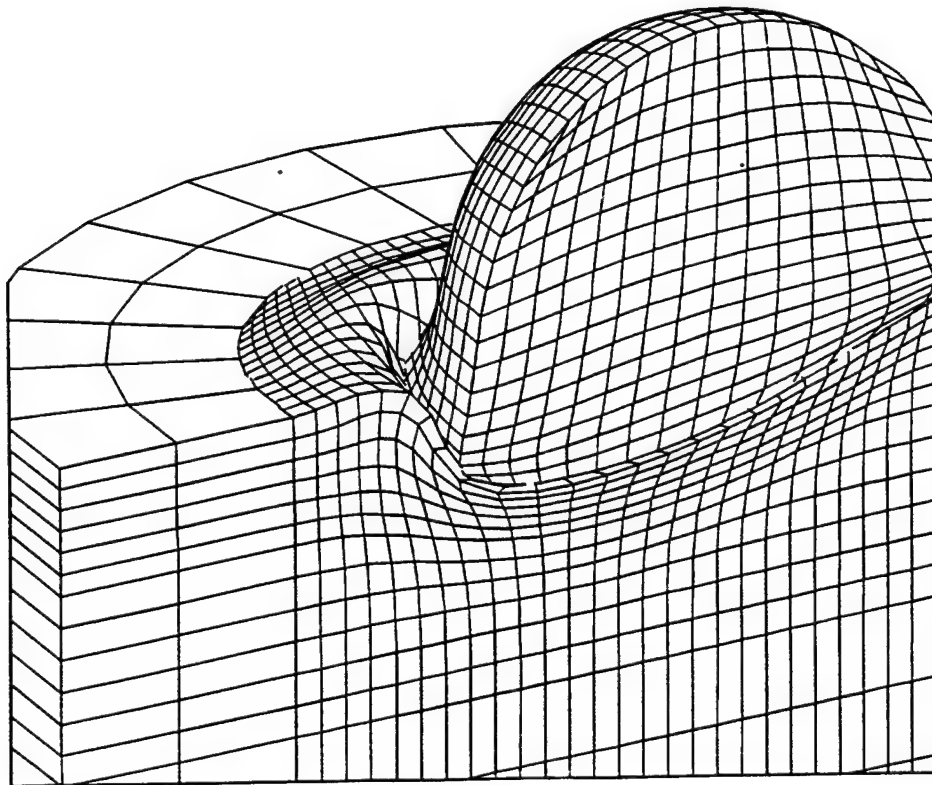
Figure B39. Finite element grid distortion for Simulation 7 at 4.0 μs.

Polyurethane e 2000 H20 1000 fps 45 deg 2-8-92
    time = 0.80000E-05
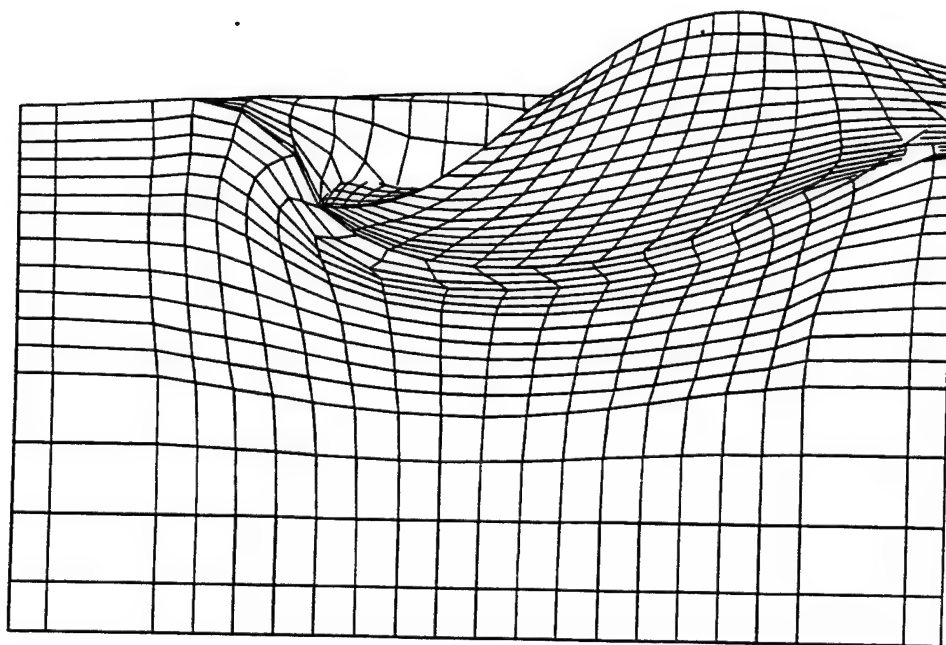
Figure B40. Finite element grid distortion for Simulation 7 at 8.0 µs.

B-42
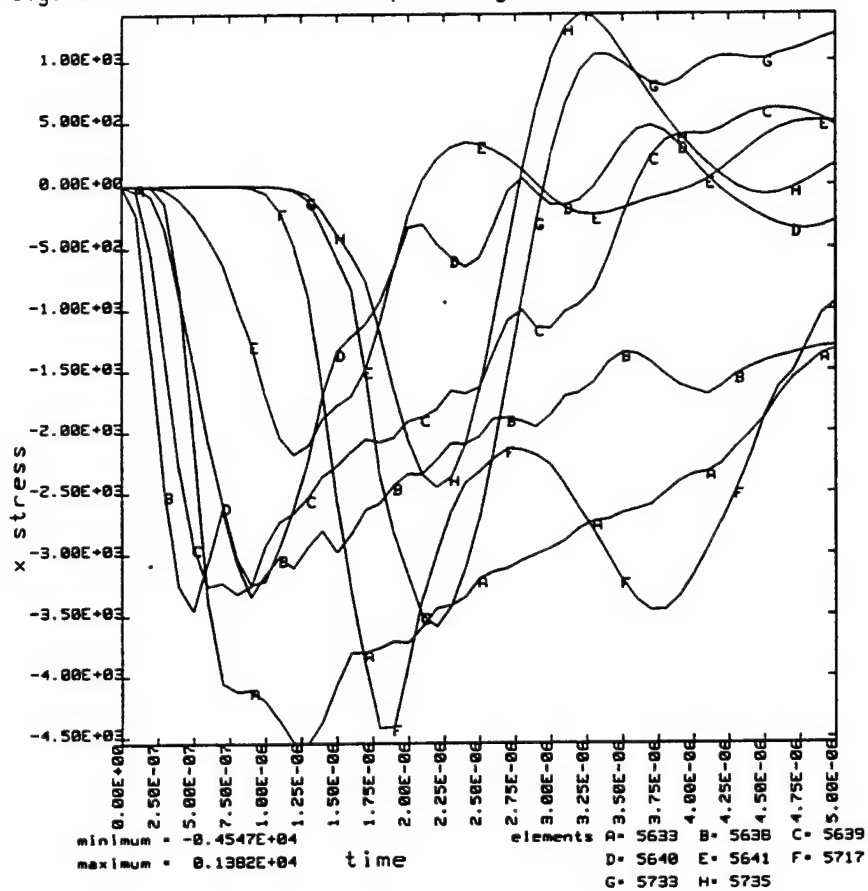
Figure B41.　　Radial stress components as a function of time at selected radial locations for Simulation 7.

Figure B42.   Circumferential stress components as a function of time at selected radial locations for Simulation 7.

Figure B43.   Axial stress components as a function of time at selected radial locations for Simulation 7.

B-45

249
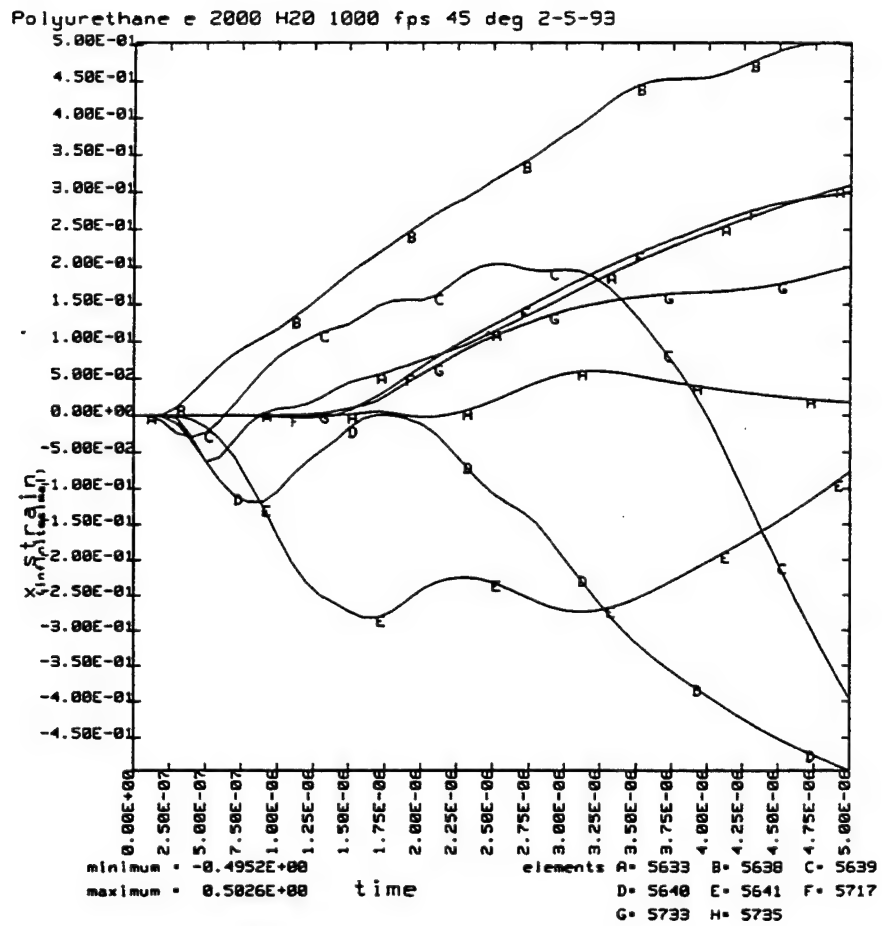
Figure B44.   Radial strain components as a function of time at selected
radial locations for Simulation 7.

Figure B45.   Circumferential strain components as a function of time at
selected radial locations for Simulation 7.

3-47

251
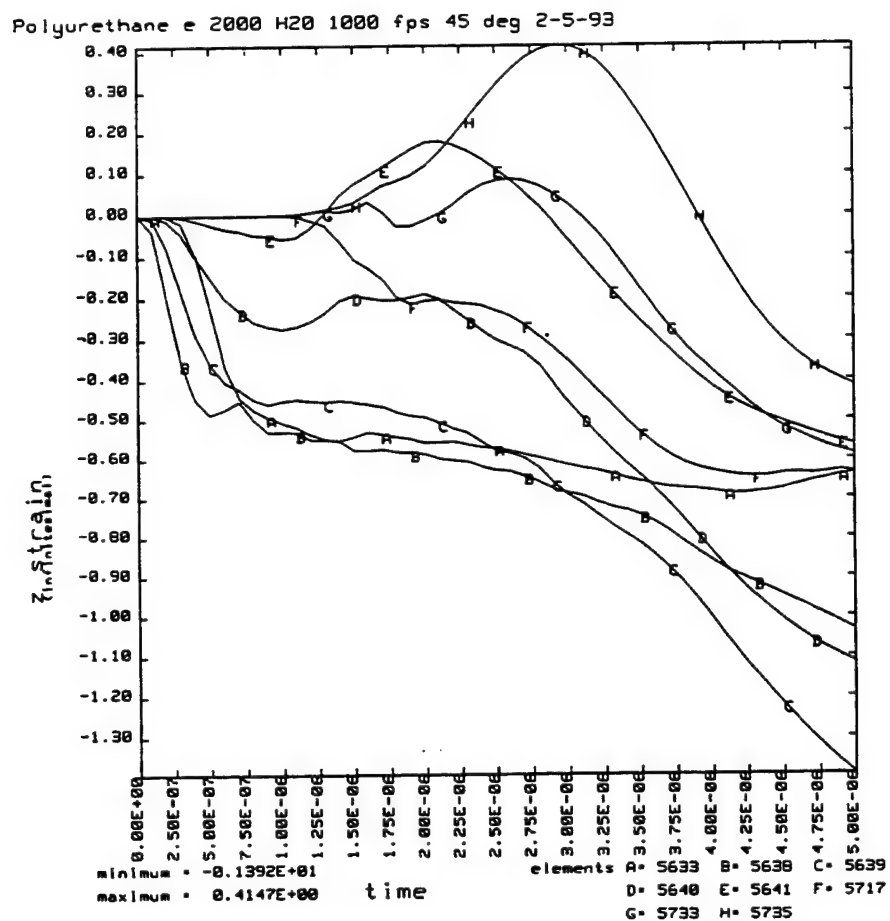
Figure B46.   Axial strain components as a function of time at selected
radial locations for Simulation 7.

Polyurethane e 2000 H20 1000 fps 45 deg 2-8-92
 time = 0.80000E-05
contours of x-stress
min=-0.331E+04 in element 3009
max= 0.151E+04 in element 2540

contour values
A=-3.17E+03
B=-2.93E+03
C=-2.69E+03
D=-2.45E+03
E=-2.21E+03
F=-1.98E+03
G=-1.74E+03
H=-1.50E+03
I=-1.26E+03
J=-1.02E+03
K=-7.82E+02
L=-5.43E+02
M=-3.04E+02
N=-6.57E+01
O= 1.73E+02
P= 4.12E+02
Q= 6.51E+02
R= 8.90E+02
S= 1.13E+03
T= 1.37E+03
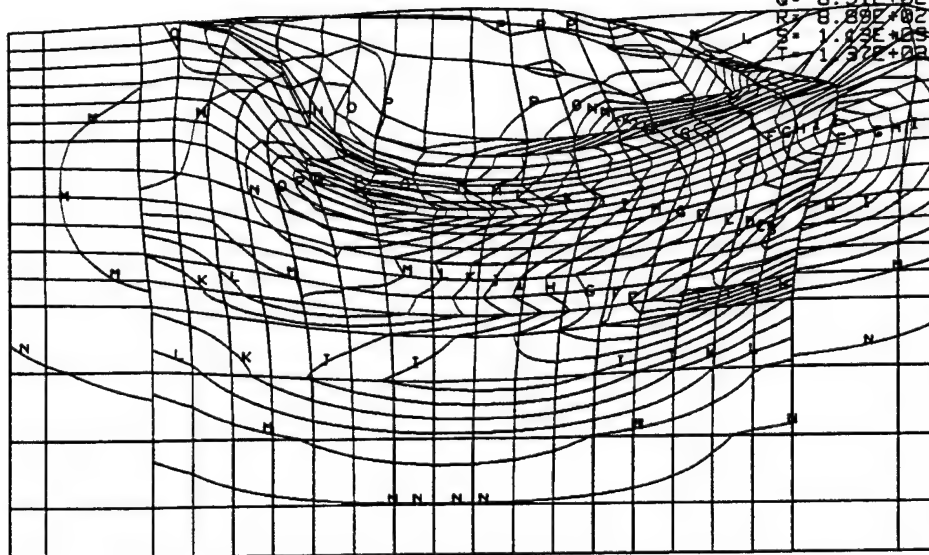
Figure B47. Radial stress distribution for Simulation 7 at 8.0 μs.

Figure B48. Circumferential stress distribution for Simulation 7 at 8.0 μs.

B-50

254

Figure B49. Axial stress distribution for Simulation 7 at 8.0 μs.

Figure B50. Radial strain distribution for Simulation 7 at 8.0 μs.
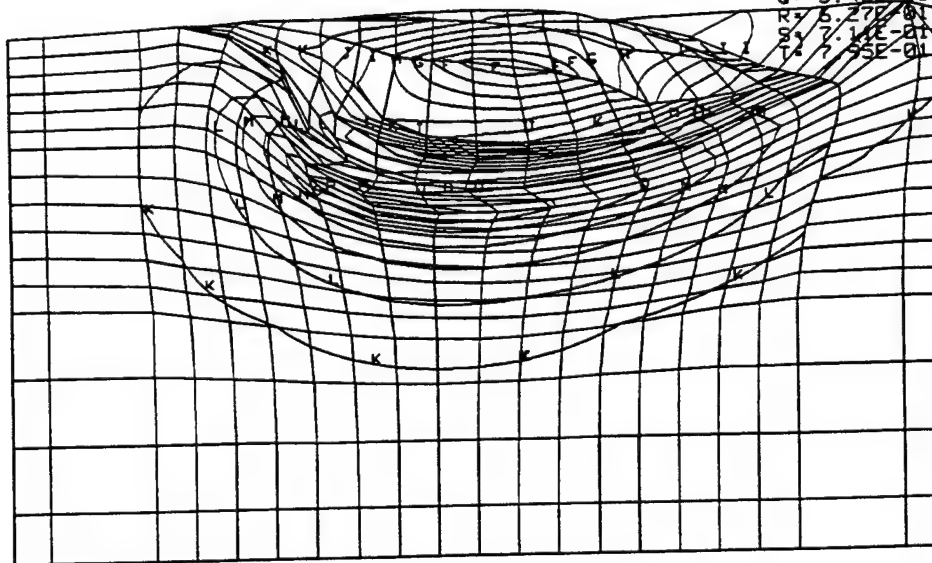
Figure B51. Circumferential strain distribution for Simulation 7 at 8.0 μs.
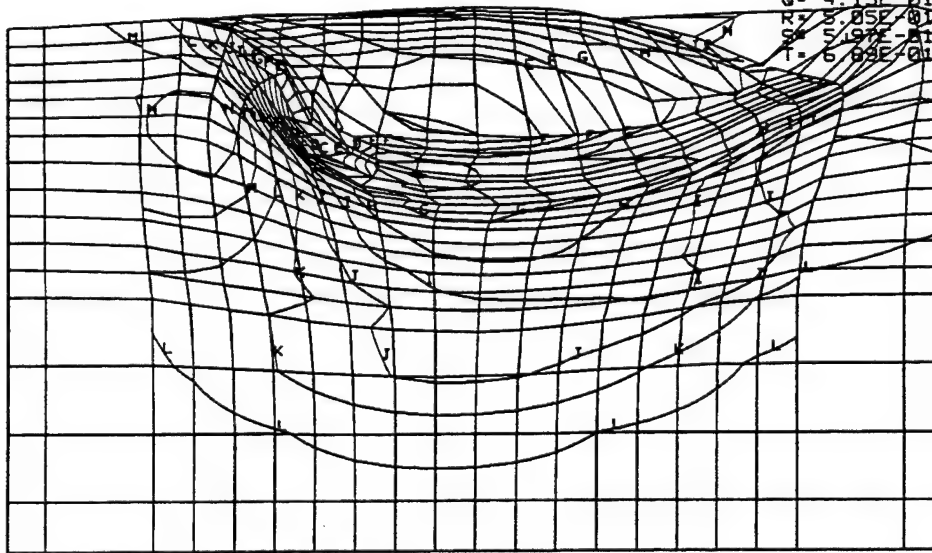
Figure B52. Axial strain distribution for Simulation 7 at 8.0 µs.

Simulation 8

Hyperelastic Modulus is 6 ksi (Material 17)

6 mm Waterdrop Impact at Normal Incidence

```
1/4 drop 6 mm 1 Kfps Polyureth
 time =  0.80000E-05
contours of y-strain
  (infinitesimal)
min=-0.383E+00 in element  2177
max= 0.435E+00 in element  1778
```

```
contour values
A=-3.58E-01
B=-3.18E-01
C=-2.77E-01
D=-2.37E-01
E=-1.96E-01
F=-1.56E-01
G=-1.15E-01
H=-7.49E-02
I=-3.44E-02
J= 6.11E-03
K= 4.66E-02
L= 8.71E-02
M= 1.28E-01
N= 1.68E-01
O= 2.09E-01
P= 2.49E-01
Q= 2.90E-01
R= 3.30E-01
S= 3.71E-01
T= 4.11E-01
```
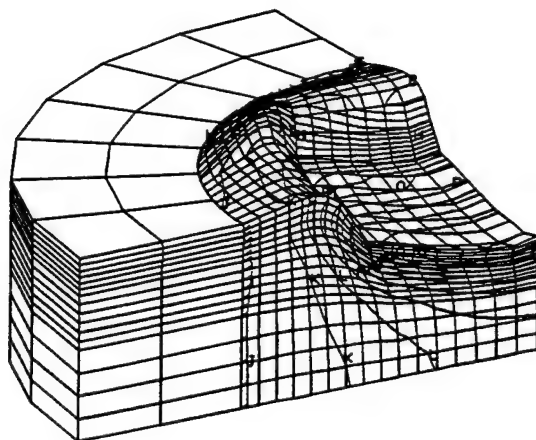
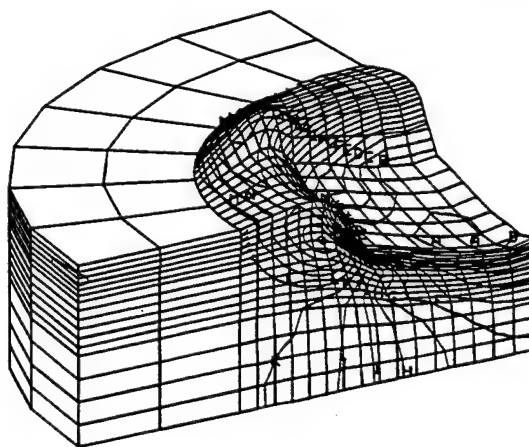Figure B53. Circumferential strain distribution for Simulation 8 at 8.0 μs (limited).

Figure B54. Axial stress distribution for Simulation 8 at 8.0 µs (limited).

B-56

Simulation 9

Viscoeleastic Material Representation of Material 17

2 mm Waterdrop Impact at Normal Incidence

H2O 2 mm 90 1000 fps deg Polyurethane # 17 Viscoelastic
time = 0.40000E-05
contours of x-stress
min=-0.125E+04 in element 6051
max= 0.212E+04 in element 4675

contour values
A=-1.15E+03
B=-9.82E+02
C=-8.15E+02
D=-6.48E+02
E=-4.81E+02
F=-3.14E+02
G=-1.48E+02
H= 1.93E+01
I= 1.86E+02
J= 3.53E+02
K= 5.20E+02
L= 6.86E+02
M= 8.53E+02
N= 1.02E+03
O= 1.19E+03
P= 1.35E+03
Q= 1.52E+03
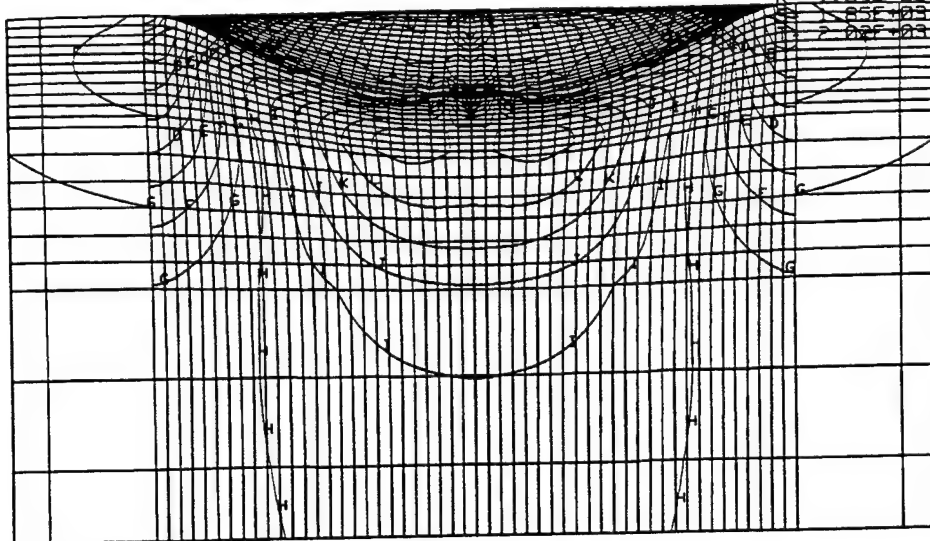R= 1.69E+03
S= 1.85E+03
T= 2.02E+03

Figure B55. Radial stress distribution for Simulation 9 at 4.0 μs.

H2O 2 mm 90 1000 fps deg Polyurethane # 17 Viscoelastic
time = 0.40000E-05
contours of y-stress
min=-0.125E+04 in element 6651
max= 0.212E+04 in element 4675

contour values
A=-1.15E+03
B=-9.82E+02
C=-8.16E+02
D=-6.49E+02
E=-4.82E+02
F=-3.15E+02
G=-1.49E+02
H= 1.81E+01
I= 1.85E+02
J= 3.52E+02
K= 5.18E+02
L= 6.85E+02
M= 8.52E+02
N= 1.02E+03
O= 1.19E+03
P= 1.35E+03
Q= 1.52E+03
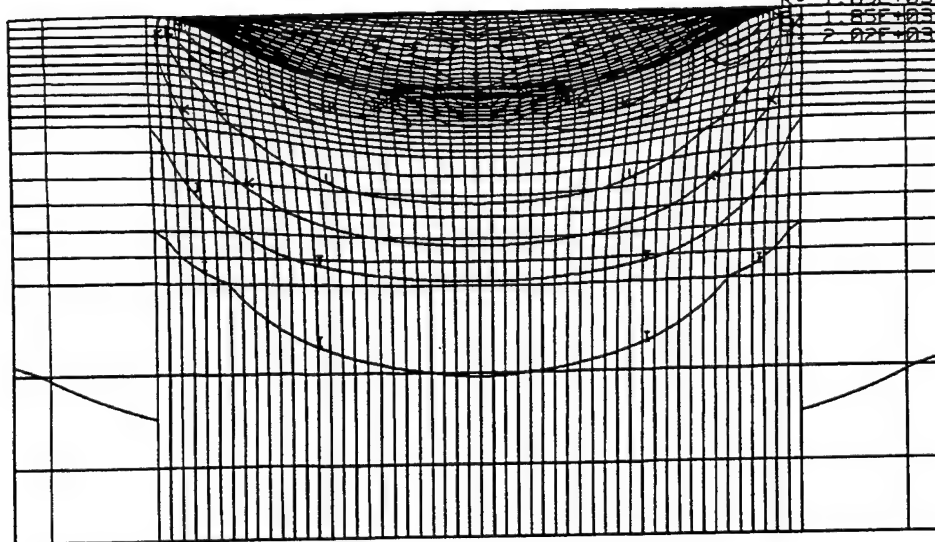R= 1.69E+03
S= 1.85E+03
T= 2.02E+03

Figure B56. Circumferential stress distribution for Simulation 9 at 4.0 μs.

B-58

H2O 2 mm 90 1000 fps deg Polyurethane # 17 Viscoelastic
time = 0.40000E-05

contours of z-stress

min=-0.595E+04 in element   4675
max= 0.608E+03 in element   8054

contour values
A=-5.76E+03
B=-5.43E+03
C=-5.11E+03
D=-4.78E+03
E=-4.46E+03
F=-4.13E+03
G=-3.81E+03
H=-3.48E+03
I=-3.16E+03
J=-2.83E+03
K=-2.51E+03
L=-2.18E+03
M=-1.86E+03
N=-1.53E+03
O=-1.21E+03
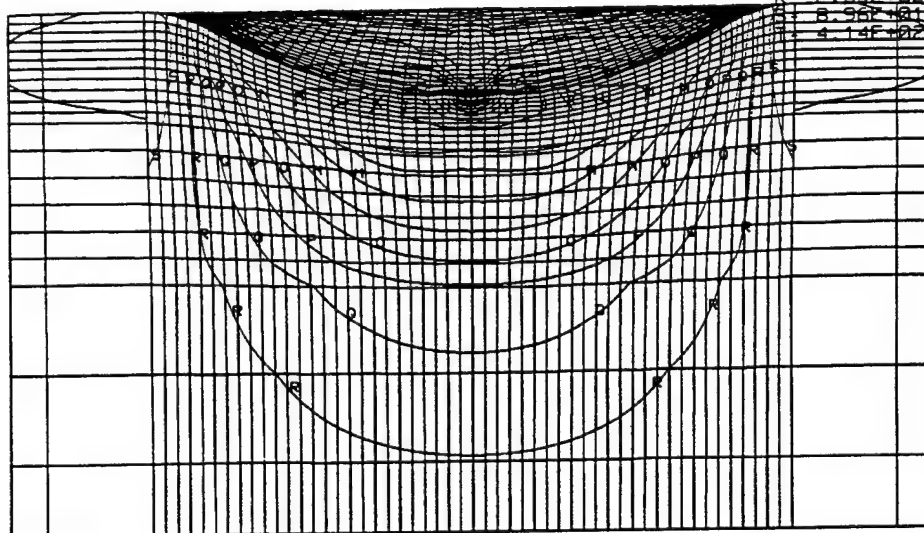P=-8.84E+02
Q=-5.60E+02
R=-2.35E+02
S=8.96E+01
4.14E+02

Figure B57. Axial stress distribution for Simulation 9 at 4.0 μs.

B-59

265

H2O 2 mm 90 1000 fps deg Polyurethane # 17 Viscoelastic
time = 0.40000E-05
contours of x-strain
 (infinitesimal)
min=-0.155E+00 in element 4696
max= 0.221E+00 in element 4675

contour values
A=-1.44E-01
B=-1.25E-01
C=-1.07E-01
D=-8.80E-02
E=-6.94E-02
F=-5.07E-02
G=-3.21E-02
H=-1.35E-02
I= 5.18E-03
J= 2.38E-02
K= 4.24E-02
L= 6.11E-02
M= 7.97E-02
N= 9.84E-02
O= 1.17E-01
P= 1.36E-01
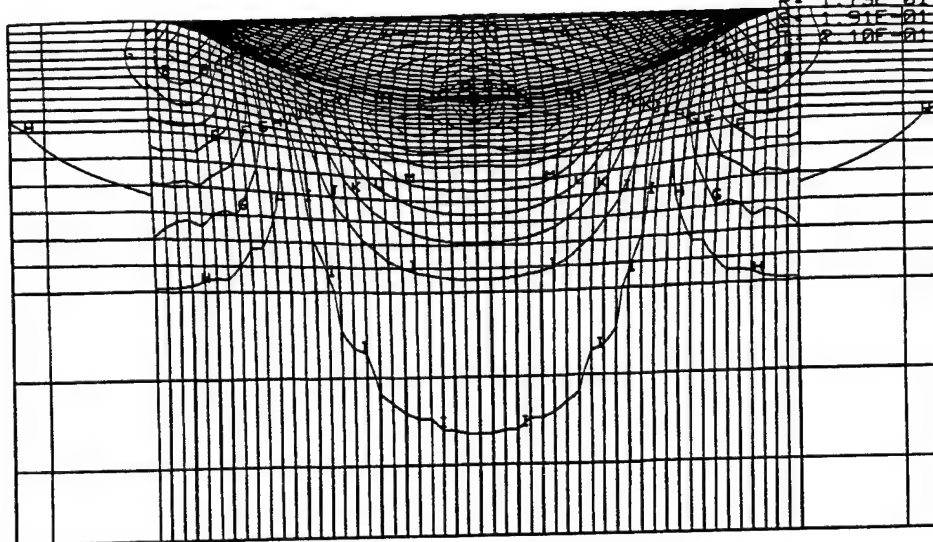Q= 1.54E-01
R= 1.73E-01
S= 1.91E-01
T= 2.10E-01

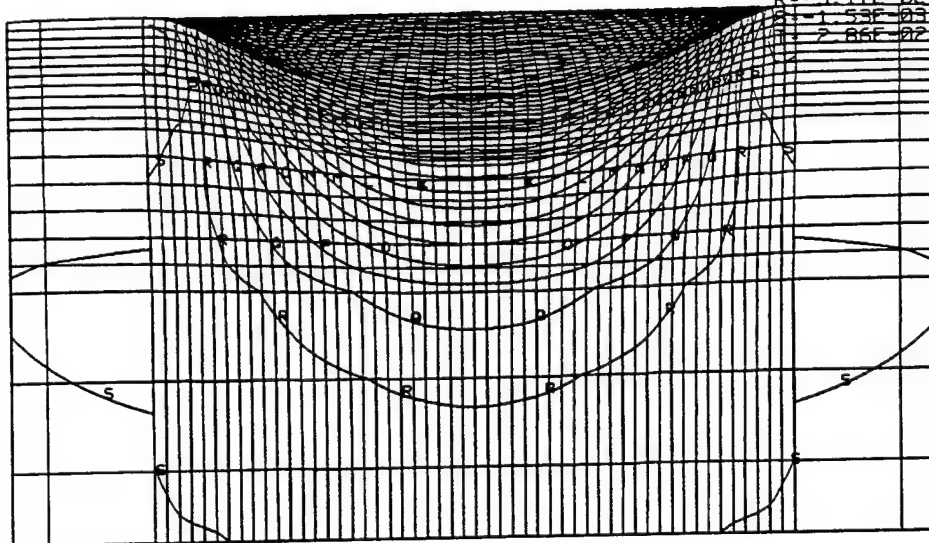Figure B58. Radial strain distribution for Simulation 9 at 4.0 μs.

Figure B59. Axial strain distribution for Simulation 9 at 4.0 μs.

Simulation 10

Viscoelastic Material Representative of Material 17

2 mm Waterdrop Impact at Normal Incidence

0.25 in. Thick Polyurethane Layer

Figure B60. Radial stress distribution for Simulation 10 at 4.0 µs.

H2O 2 mm 90 deg 1000 fps Polyurethane #17 0.25 in VISCO

time = 0.40000E-05

contours of y-stress

min=-0.129E+04 in element 4861
max= 0.149E+04 in element 4731

contour values
A=-1.21E+03
B=-1.07E+03
C=-9.34E+02
D=-7.96E+02
E=-6.58E+02
F=-5.20E+02
G=-3.82E+02
H=-2.44E+02
I=-1.06E+02
J= 3.19E+01
K= 1.70E+02
L= 3.08E+02
M= 4.46E+02
N= 5.84E+02
O= 7.22E+02
P= 8.60E+02
Q= 9.98E+02
R= 1.14E+03
S= 1.27E+03
T= 1.41E+03

Figure B61. Circumferential stress distribution for Simulation 10 at 4.0 μs.

Figure B62. Axial stress distribution for Simulation 10 at 4.0 µs.

H2O 2 mm 90 deg 1000 fps Polyurethane #17 0.25 in VISCO
time = 0.40000E-05
contours of x-strain
  (infinitesimal)
min=-0.149E+00 in element   6105
max= 0.216E+00 in element   4731

contour values
A=-1.39E-01
B=-1.20E-01
C=-1.02E-01
D=-8.43E-02
E=-6.62E-02
F=-4.81E-02
G=-3.00E-02
H=-1.19E-02
I= 6.21E-03
J= 2.43E-02
K= 4.24E-02
L= 6.05E-02
M= 7.86E-02
N= 9.67E-02
O= 1.15E-01
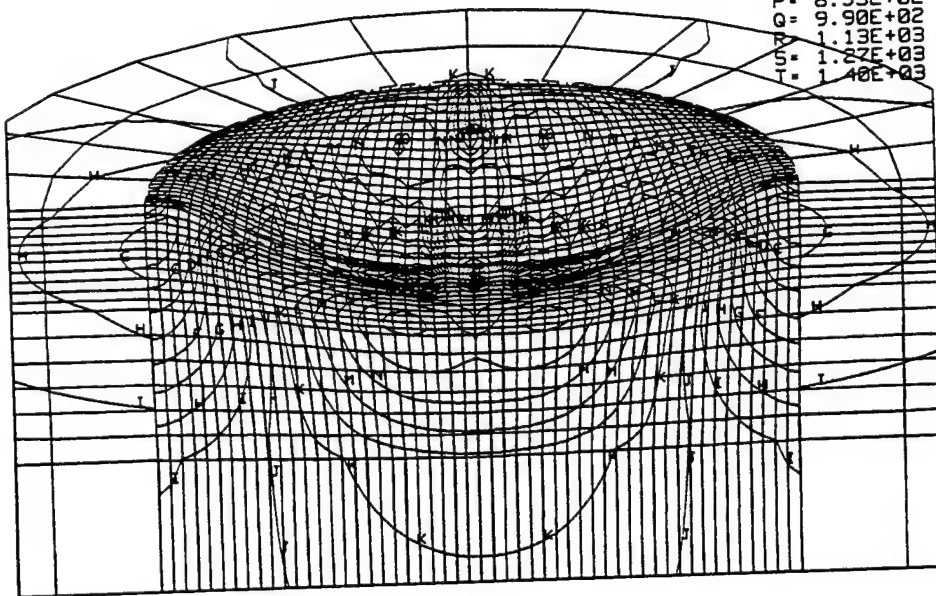P= 1.33E-01
Q= 1.51E-01
R= 1.69E-01
S= 1.87E-01
T= 2.05E-01

Figure B63. Radial strain distribution for Simulation 10 at 4.0 µs.

H2O 2 mm 90 deg 1000 fps Polyurethane #17 0.25 in VISCO

time = 0.40000E-05

contours of y-strain
  (infinitesimal)

min=-0.149E+00 in element 6655
max= 0.216E+00 in element 4731

contour values
A=-1.39E-01
B=-1.20E-01
C=-1.02E-01
D=-8.42E-02
E=-6.61E-02
F=-4.80E-02
G=-2.99E-02
H=-1.18E-02
I= 6.29E-03
J= 2.44E-02
K= 4.25E-02
L= 6.06E-02
M= 7.87E-02
N= 9.68E-02
O= 1.15E-01
P= 1.33E-01
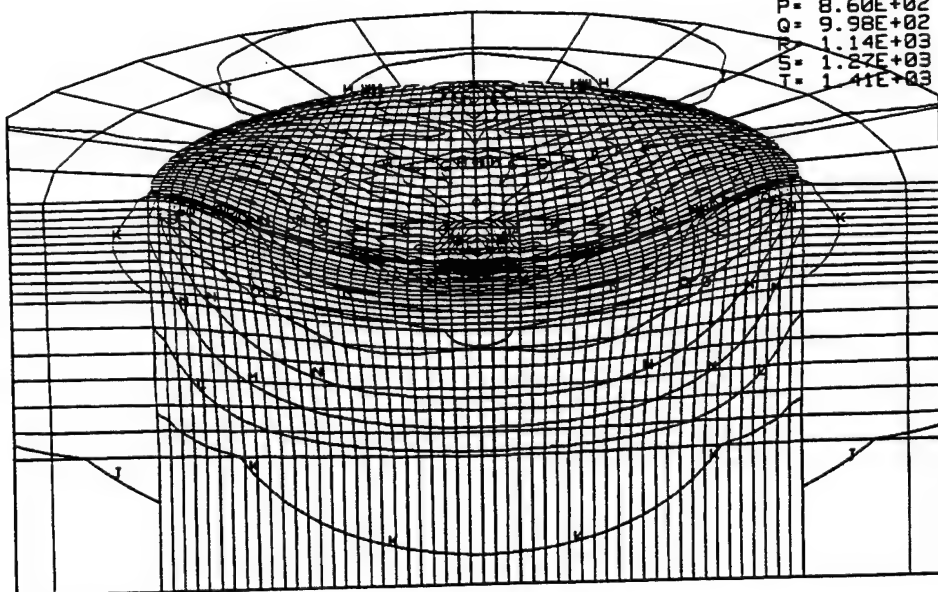Q= 1.51E-01
R= 1.69E-01
S= 1.87E-01
T= 2.06E-01

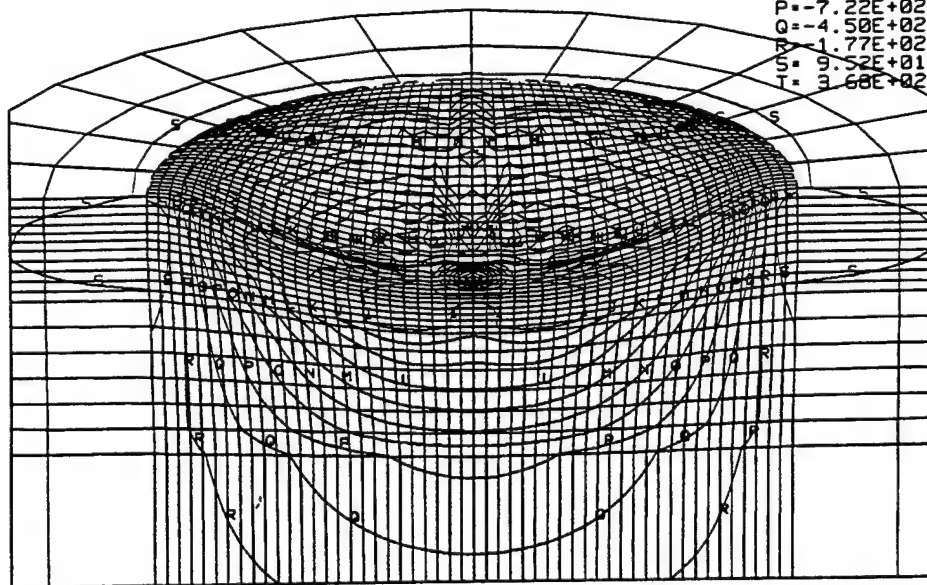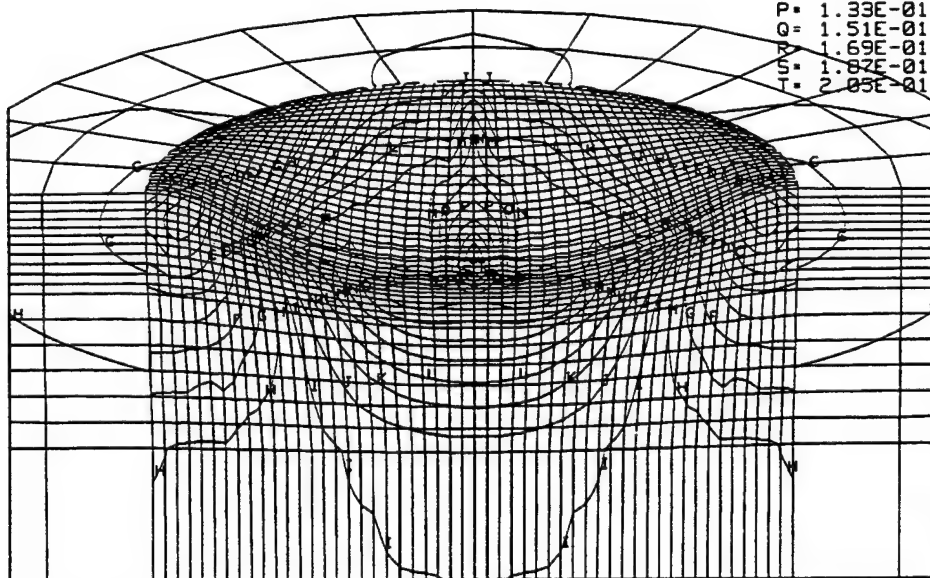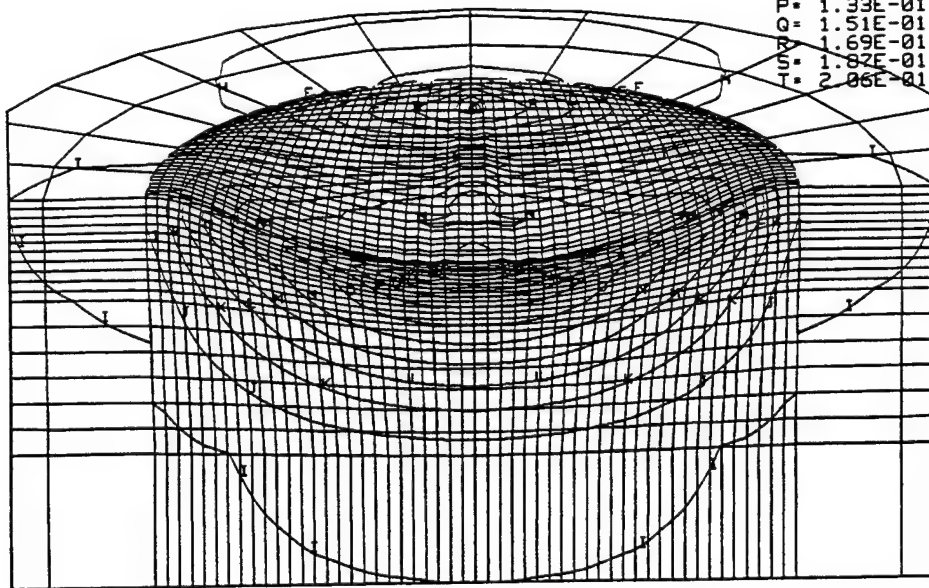Figure B64. Circumferential strain distribution for Simulation 10 at 4.0 µs.

H2O 2 mm 90 deg 1000 fps Polyurethane #17 0.25 in VISCO

```
 time =  0.40000E-05                              contour values
                                                   A=-5.36E-01
contours of z-strain                               B=-5.07E-01
  (infinitesimal)                                  C=-4.77E-01
                                                   D=-4.47E-01
min=-0.554E+00 in element   4967                   E=-4.18E-01
max= 0.446E-01 in element   6710                   F=-3.88E-01
                                                   G=-3.59E-01
                                                   H=-3.29E-01
                                                   I=-2.99E-01
                                                   J=-2.70E-01
                                                   K=-2.40E-01
                                                   L=-2.10E-01
                                                   M=-1.81E-01
                                                   N=-1.51E-01
                                                   O=-1.21E-01
                                                   P=-9.17E-02
                                                   Q=-6.20E-02
                                                   R=-3.24E-02
                                                   S=-2.72E-03
                                                   T= 2.69E-02
```
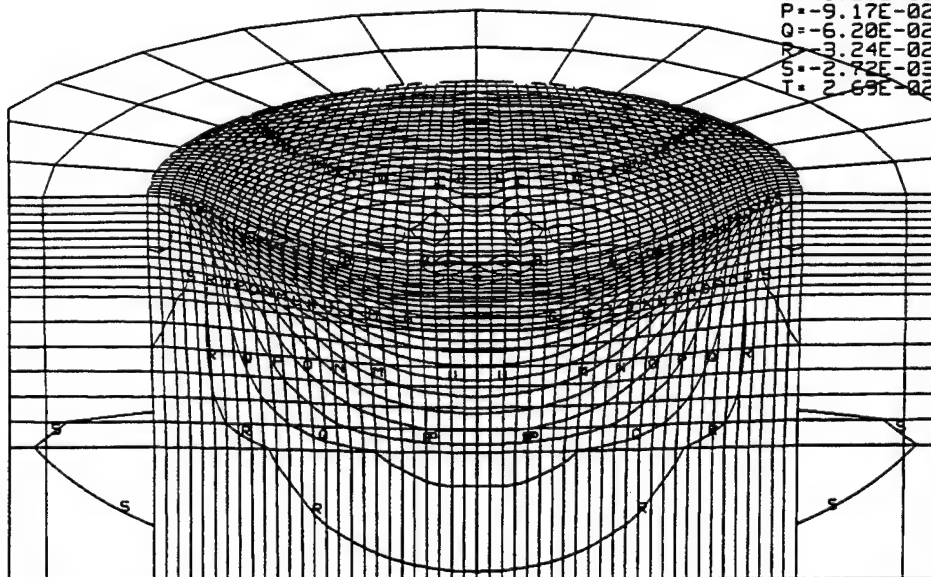

Figure B65. Axial strain distribution for Simulation 10 at 4.0 μs.

REFERENCES

W.F. Adler (1979). "The Mechanics of Liquid Impact," <u>Treatise on Materials Science and Technology</u>, <u>16</u> (C.M. Preece, ed), New York: Academic Press, 127-183.

R.M. Christensen and E.M. Wu (1988). "A Theory of Crack Growth in Viscoelastic Materials," <u>Engineering Fracture Mechanics</u>, <u>14</u>, 215-225.

J.J. Dlubac, G.F. Lee, J.V. Duffey, R.J. Deigan, and J.D. Lee (1990). "Comparison of the Complex Dynamic Modulus as Measured by Three Apparatus," <u>Sound and Vibration Damping with Polymers</u> (R.D. Corsaro and L.H. Sperling, editors), Washington D.C: American Chemical Society, 49-62.

O.G. Engle (1974). "A Study of Composite Coatings for Rain-Erosion Protection of Radomes," <u>Proceedings of the Fourth International Conference on Rain Erosion and Associated Phenomena</u>, Meersburg, Germany, 8 to 10 May 1974.

D.A. Haynie (1989). Rotor Blade Erosion Protection Systems, Final Report for Contract DAAK51-84-C-0033, USAAVSCOM TR-88-D-24.

K.M. Kalumuck, G.L. Chahine, and D.A. Haynie (1987). "Helicopter Blade Leading Edge Erosion Protection Study," <u>Proc. 7th International Conference on Erosion by Liquid and Solid Impact</u>, Cambridge, England, 7 to 10 September 1987.

T. Lewis (1991). "Effects of Dynamic Strain Amplitude and Static Prestrain on the Properties of Viscoelastic Materials," SAE Noise and Vibration Conference, Traverse City, MI.

W. Madigosky (1984). "Improved Extensional Modulus Measurements for Polymers and Metal Matrix Composites," <u>Proceedings Vibration Damping Workshop</u>, (27 February 1984), Long Beach, CA, Q-1 to Q-12.

M.J. Matthewson (1979). "Theoretical Aspects of Thin Protective Coatings," <u>Proceedings of the Fifth International Conference on Erosion by Liquid and Solid Impact</u>, Cambridge, England, 3 to 7 September 1979.

M.J. Matthewson (1987). "The Effect of a Thin Compliant Protective Coating on Hertzian Contact Stresses," <u>J. Phys. D: Appl. Phys.</u>, <u>15</u>, 237-249.

H.K. Muller and W.G. Knauss (1971). "Crack Propagation in a Linearly Viscoelastic Strip," <u>J. Appl. Mech.</u>, <u>38</u>, 483.

H. Rieger and H. Boche (1974). "Erosion Behaviour of Surface Coatings," <u>Proceedings of the Fourth International Conference on Rain Erosion and Associated Phenomena</u>, Meersburg, Germany, 8 to 10 May 1974.

R-1

APPENDIX F
DESIGN CRITERIA FOR ADVANCED ROTOR BLADE EROSION PROTECTION SYSTEMS

1   SCOPE

This design criteria document has been developed for all main and tail rotor blade erosion protection systems used on Army helicopters.

2   PURPOSE

The intent of this document is to define the environmental conditions for a typical Army rotor blade and establish minimum requirements for the design and wear life of erosion protection systems. Conflicting requirements of referencing documents shall take precedence over this document.

3   DEFINITIONS

3.1 Blade design life. The blade design life is defined as the retirement life of the blade.

3.2 Design wear life. Design wear life is a specified amount of exposure to both sand clouds and rainfall without erosion failure.

3.3 Erosion. Erosion is defined as the gradual wearing away or pitting of the material surface as a result of direct or grazing particle impingement. The erosion damage is typically caused by solid particles up to 1000 microns and liquid particles up to 8000 microns.

3.4 Erosion failure. The blade or erosion protection system is considered failed when the erosion process has progressed sufficiently to cause measurable dynamic or aerodynamic performance loss, exposure of substrate and/or bondline, or gross distortions. There are five basic modes of erosion failure that may be observed during a visual inspection. These are described below.

3.4.1 Cracking. Cracking is generally a result of fatigue. Evidence of cracks exceeding established limits in the erosion protection system or blade requires replacement.

3.4.2 Debonding. Debonding is most prevalent with nonmetallics. Any evidence of debonding that exceeds established limits of the erosion protection system or substrate requires repair or replacement.

3.4.3 Pitting. The same basic criteria that apply to surface wear also apply to pitting. Careful inspection is required to ensure that complete penetration to the substrate has not occurred.

3.4.4 Surface wear. Blade surface is worn. Metals generally wear smooth, whereas nonmetals usually wear rough. The blade contour has been changed and should be checked to determine if it is within the established variation allowances. Even if the blade contour is satisfactory, once the substrate is exposed, the blade shall be repaired or replaced.

3.4.5 Wrinkling. Wrinkling is most prevalent with ductile metals worn to a specific minimum thickness. Once this occurs, repair or replacement is required.

3.5 Foreign object impact. A foreign object impact is defined as an impact with solids larger than those that typically cause erosion. The solids include, but are not limited to, pebbles, rocks, tree branches, and miscellaneous debris.

3.6 Hydrolysis. Hydrolysis is the mechanism by which certain types of nonmetallic materials degrade from exposure to hot, humid environments. This typically occurs in polyester-type polyurethanes.

3.7 Nonrepairable. Any blade or erosion protection systems that cannot have the original contour restored after being worn by sand, rain, or similar environment shall be considered nonrepairable. This includes blades that are permitted to have the leading edges smoothed by sanding but cannot have the original contour restored.

3.8 Repairable/replaceable. Rotor blades and/or erosion protection systems shall be considered repairable if the leading edge surface can be built up to the original contour after being worn by sand, rain, or similar type environment. Likewise, if the system consists of a layer of material for erosion protection that can be removed and replaced, this erosion protection system may be considered replaceable. References to repairable and replaceable may be used interchangeably.

3.9 V_H. The symbol V_H refers to the maximum normal cruise speed in level flight.

4   INTERFACE REQUIREMENTS

4.1 Contour. The aerodynamic contour shall be maintained within the established variation allowances.

4.2 Coverage. The erosion protection system shall cover, as a minimum that portion of the blade that will not provide the specified design wear life with the final paint finish.

4.3 Deicing. The erosion protection system shall not impair the operation of the deicing systems (if applicable).

4.4 Hydrolysis. Nonmetallic erosion protection systems shall survive 1200 hours exposure at 82°C(180°F) and 95-100% relative humidity without significant changes in properties such as hardness, resiliency, strength, and resistance to melting, cracking, swelling, blistering or solvents.

278

4.5 Structural. The erosion protection system shall be structurally compatible with the basic blade. Materials shall also meet any additional requirements for environmental conditions specified for the blade (e.g., ultraviolet, ozone, temperature, humidity, fluid exposure).

4.6 Packaging. Provisions shall be provided for packaging of blades and replacement erosion protection systems to minimize the potential for damage during shipping, handling, or installation.

5   DESIGN WEAR LIFE

5.1 Sand cloud flight spectrum for nonrepairable erosion protection systems

5.1.1 Utility, cargo, and attack aircraft. Utility, cargo, and attack aircraft shall have erosion protection systems designed for operation in sand cloud environments during IGE/NOE maneuvers for a minimum of 10 percent of the blade design life. Blades with unlimited design life shall have repairable erosion protection systems.

5.1.2 Observer aircraft. Observer aircraft shall have erosion protection systems designed for operation in sand cloud environments during IGE/NOE maneuvers for a minimum of 4 percent of the blade design life. Blades with unlimited design life shall have repairable erosion protection systems.

5.2 Sand cloud flight spectrum for repairable erosion protection systems. The erosion protection systems of each repairable rotor blade shall be capable of 12 hours of flight for each equivalent man-hour required for the repair and/or replacement of an erosion protection system for the duration of the blade design life. Equivalent man-hours include an allowance for material cost.

Determination of man-hours for repair/replacement shall include, but not be limited to, the following: blade removal and inspection, preparation for repair/replacement, removal of damaged area of component, attachment of replacement material, painting, final assembly, balancing, and installation of blade onto the aircraft.

To account for material cost, divide the total material cost (i.e., cost to the Army) by the SIC Code 372 labor rate in " Employment and Earnings" published by the U.S. Department of Labor Bureau of Labor Statistics, burdened 50 percent. This will be considered the equivalent man-hours for material costs.

The formula for determining the required Erosion Protection System Designed Life (EPSDL) is as follows:

$$EPSDL = 12 \left[\text{Repair man-hours} + \frac{\text{Material cost}}{(1.5)(\text{SIC labor rate})} \right]$$

To determine the amount of time operating in sand clouds during IGE/NOE maneuvers, use EPSDL in lieu of "blade design life" in paragraphs 5.1.1 and 5.1.2.

5.3 <u>Rainfall flight spectrum for nonrepairable erosion systems</u>. All aircraft shall have erosion protection systems designed for flying in rain with a particle size distribution in accordance with that shown in Figure F-1 and with the following rainfall intensities:

a. One-half inch per hour. For 1.5 percent of the blade design life in 0.5 in/hr rainfall during forward flight at 85 percent of V_H.

b. One inch per hour. For 0.5 percent of the blade design life in 1-in/hr rainfall during forward flight at 85 percent of V_H.

c. Six inches per hour. Retain flight capability for 10 minutes in 6.0-in/hr rainfall after the erosion protection system substrate becomes exposed.

Blades with unlimited design life shall have repairable erosion protection systems.
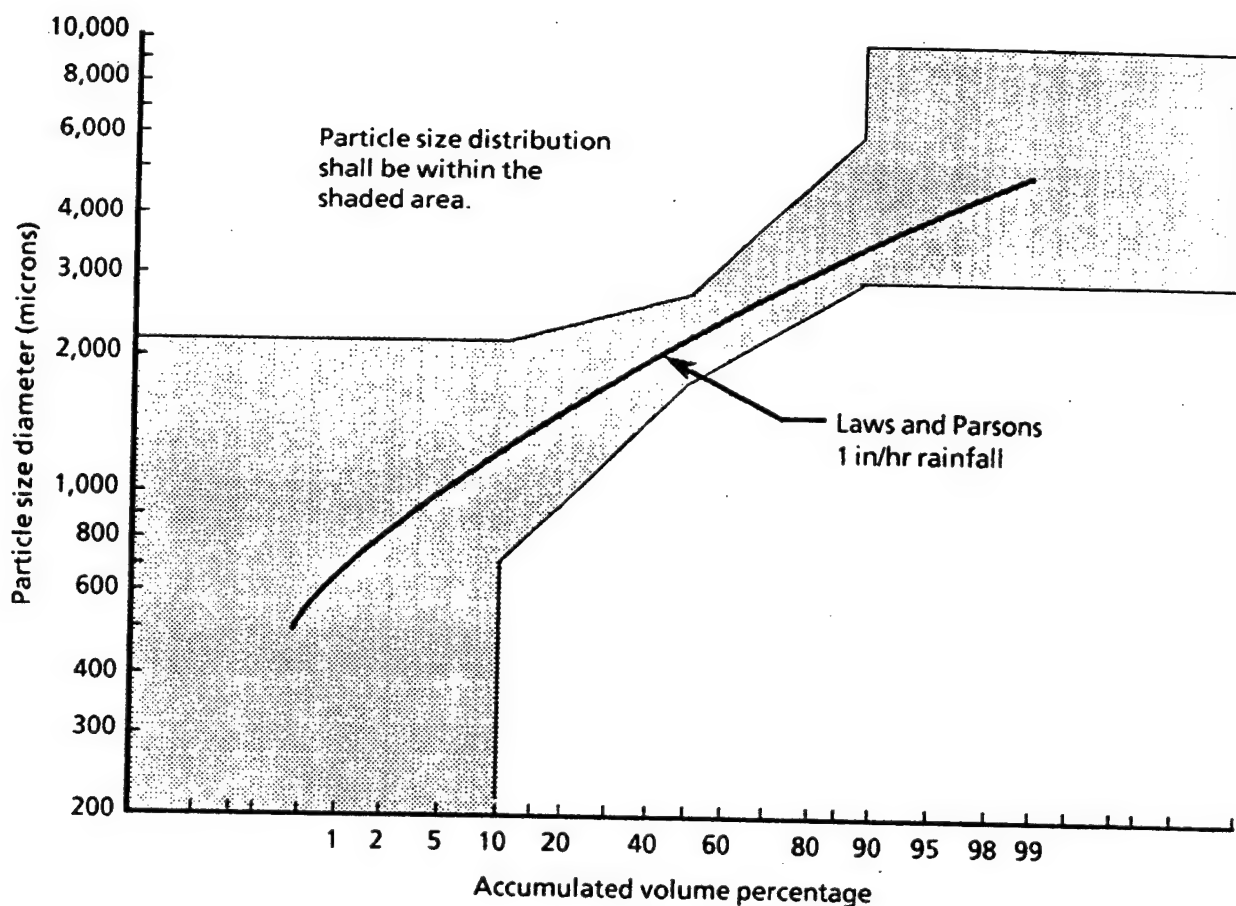

Figure F-1. Particle size distribution for rainfall.

5.4 Rainfall flight spectrum for repairable erosion protection systems. The erosion protection systems of each repairable rotor blade shall be capable of 12 hours of flight for each man-hour required for repair and/or replacement. The EPSDL shall be determined as specified in paragraph 5.2, and the EPSDL shall be used in lieu of "blade design life" in paragraph 5.3.

6 DEFINITION OF SAND CLOUD ENVIRONMENT

6.1 Sand cloud concentration. Sand cloud concentration shall be determined from Figure F-2. Disk loading shall be based on the aircraft's maximum gross weight divided by the main rotor disk area. For tail rotors, use the concentration defined by the main rotor disk loading.
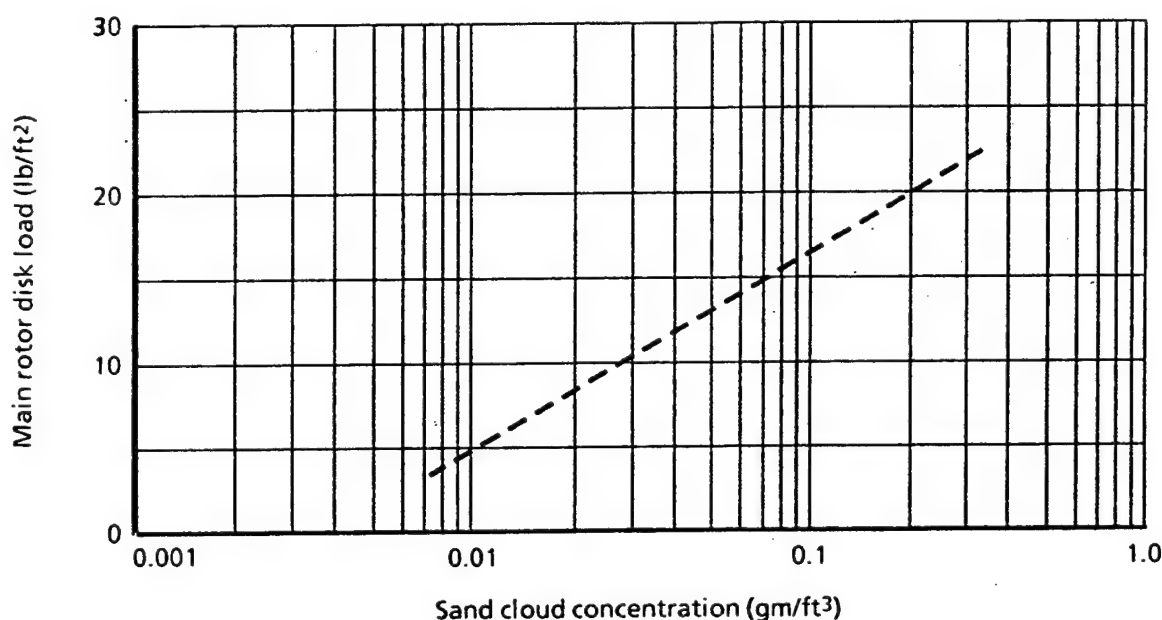

Figure F-2. Dust cloud concentration as a function of main rotor disk load.

6.2 Sand cloud particle description. Any mineral with a sandy texture is suitable, provided the hardness is MOH 7 or greater. Quartz is generally the more common and widely used mineral. The particles shall be approximately spherical in shape and subangular, as defined by Krumbein numbers 0.1 and 0.2 in Figure F-3. Particle size distribution shall be within the limits established by Table F-1.

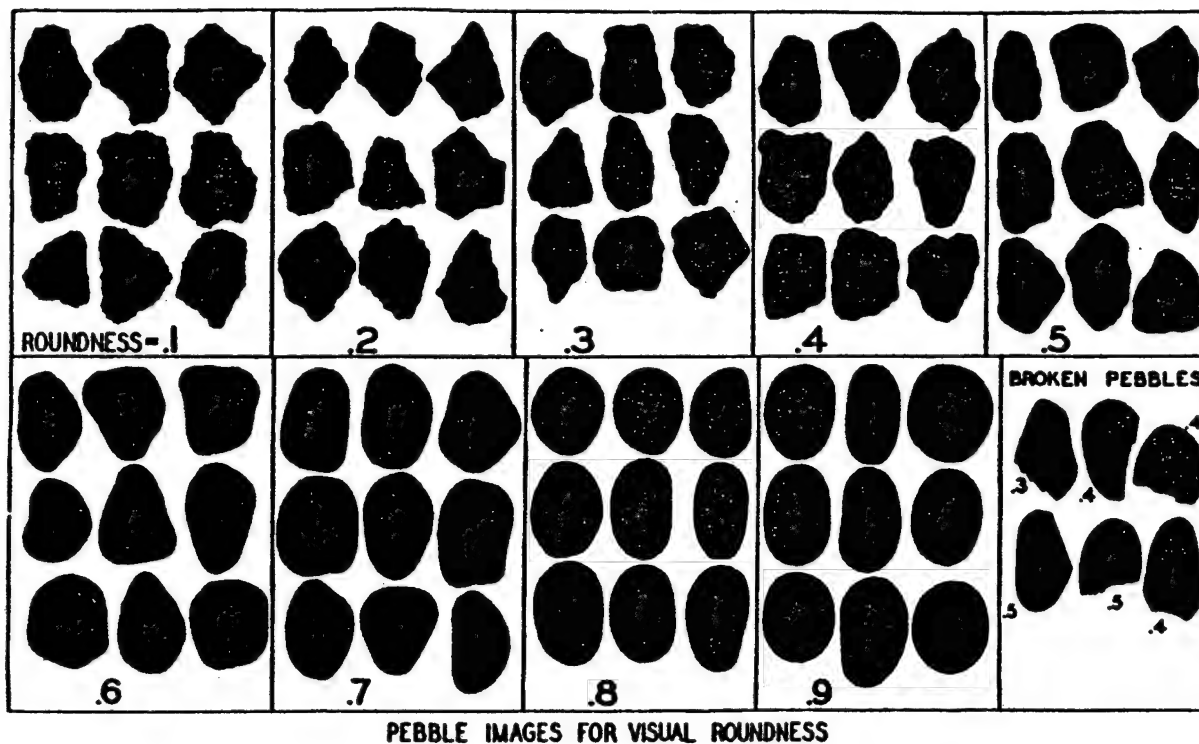PEBBLE IMAGES FOR VISUAL ROUNDNESS

Figure F-3. Krumbein number.

TABLE F-1. SAND PARTICLE SIZE DISTRIBUTION*

Particle Size (microns)	Quantity (percent smaller than particle size, by weight)
1000	100
900	98-99
600	93-97
400	82-86
200	46-50
125	18-22
75	3-7

*Identical to MIL-E-5007D

7   DEFINITION OF RAINFALL ENVIRONMENT

Raindrops shall be considered approximately spherical in shape, and the erosion protection system design shall be based on rainfall intensities of 0.5, 1.0, and 6.0 in/hr. Particle size distribution shall be as plotted in Figure F-1.

8   FOREIGN OBJECT IMPACT

Erosion protection systems shall be capable of enduring strikes of hardwood branches with a diameter equal to 12 percent of the blade's thrust-weighted chord length (but no less than 2 inches in diameter for main rotor blades) without causing an aborted mission. Strikes of hardwood branches with a diameter equal to 6 percent of the blade's thrust-weighted chord length (but no less than 1 inch in diameter for main rotor blades) shall not require unscheduled maintenance other than minor painting.

9   FAILURE CRITERIA

Development of a nonrepairable blade or an erosion protection system shall include an inspection procedure that provides the following.

9.1 Failure modes. The most likely modes of failure for the specific blade or erosion protection system.

9.2 Erosion limits. The allowable limits of wear or failure established for each mode likely to be encountered shall not allow an unacceptable degradation in dynamic or aerodynamic performance or structural integrity.

9.3 Methods of inspection. The methods, equipment, etc., shall be specified to ensure consistency in assessing the extent of erosion damage.

10   QUALIFICATION

Compliance with these design criteria shall be demonstrated by testing in accordance with the Qualification Test Procedure presented in Appendix G.

APPENDIX G
QUALIFICATION TESTING OF
ADVANCED ROTOR BLADE EROSION PROTECTION SYSTEMS

1   SCOPE

The intent of this document is to outline a general test procedure that will point out the parameters of importance in erosion testing. A baseline is set forth from which a detailed test plan can be developed for each erosion protection system being qualified. The specific details of each test plan should be established by mutual agreement between the end user and supplier.

2   DEFINITIONS

2.1 Design wear life. The amount of time the erosion protection system must withstand rain and/or sand without failure as determined by the design criteria document (DCD).

2.2 Erosion. This phenomenon is defined as the gradual wearing away or pitting of the material surface as a result of direct or grazing particle impingement. The erosion damage is typically caused by solid particles up to 1000 microns and liquid particles up to 8000 microns.

2.3 Erosion failure. The blade or erosion protection system is considered failed when the erosion process has progressed sufficiently to cause measurable dynamic or aerodynamic performance loss, exposure of substrate and/or bondline, or gross distortions. There are five basic modes of erosion failure that may be observed during a visual inspection. These are described below.

2.3.1 Cracking. This is generally a result of fatigue. Evidence of cracks exceeding established limits in the erosion protection system or blade requires replacement.

2.3.2 Debonding. This is most prevalent with nonmetallics. Any evidence of debonding that exceeds established limits of the erosion protection system or substrate requires repair or replacement.

2.3.3 Pitting. Same basic criteria as surface wear. Careful inspection is required to ensure that complete penetration to the substrate has not occurred.

2.3.4 Surface wear. Blade surface is worn. Metals generally wear smooth, whereas nonmetals usually wear rough. The blade contour has been changed and should be checked to determine if it is within the established variation allowances. Even if the blade contour is satisfactory, once the substrate is exposed, the blade shall be repaired or replaced.

2.3.5 Wrinkling. This is most prevalent with ductile metals worn to a specific minimum thickness. Once this occurs, repair or replacement is required.

2.4 Hydrolysis. Hydrolysis is the mechanism by which certain types of organic materials degrade from exposure to hot, humid environments. With nonmetallic erosion guard materials, this typically occurs in polyester-type polyurethanes.

3   TEST REQUIREMENTS

3.1 Test setup. Rainfall, sand and impact testing shall be performed with a rotating arm whose radius is not less than 15 percent of the full-scale blade radius being qualified. The minimum cross section of the enclosure shall be a minimum of five times the radius of the rotating arm.

Exceptions to these size restrictions may be granted on the basis of aerodynamic tests that establish the flow around the test coupon to be approximately two-dimensional and/or representative of the intended application. There shall be no enclosure requirement for impact testing.

The rotating arm must be capable of testing the same airfoil geometry as that being qualified. The test airfoil should not be less than 25 percent of the full-scale airfoil.

Either one-or two-bladed arms may be used. However, if sand erosion testing is required, the blade shall be capable of creating a downwash similar to helicopter rotor blades.

3.2 Rainfall test. Rainfall particle size distribution shall be similar to that specified by Laws and Parsons (Ref. 20) for a 1 in/hr rainfall intensity. This is shown plotted in Figure G-1. The simulated rainfall shall be within the shaded area of this figure. The median particle size will be between 1800 and 2500 microns.

Any potable water free of foreign objects may be used. The enclosure shall be free of all loose debris, dirt, and/or sand that may be recirculated during the test. A chemical analysis for record purposes only should be obtained. The analysis should show mineral and chemical content and pH level.

The ideal test intensity is 1 in/hr. However, accelerated testing of up to 4 in/hr is acceptable. Qualification will assume the wear rate is directly proportional to intensity (i.e., 1 hour at 4 in/hr equals 4 hours at 1 in/hr). By using this proportionality relationship, testing at 1 in/hr may be used to qualify for the requirements of ½ in/hr rainfall intensity. Evaluation of test time at different intensities shall be based on the average of all readings taken during the test. However, the maximum intensity shall not exceed 4 in/hr and the minimum shall not be less than ½ in/hr while maintaining the required particle size distribution. Also, the minimum and maximum shall not be more than 1 in/hr from the average (e.g., avg = 1 in/hr, min ≥ ½ in/hr and max ≤ 2 in/hr; or if avg = 3.5, min ≥ 2.5 in/hr and max ≤ 4 in/hr).
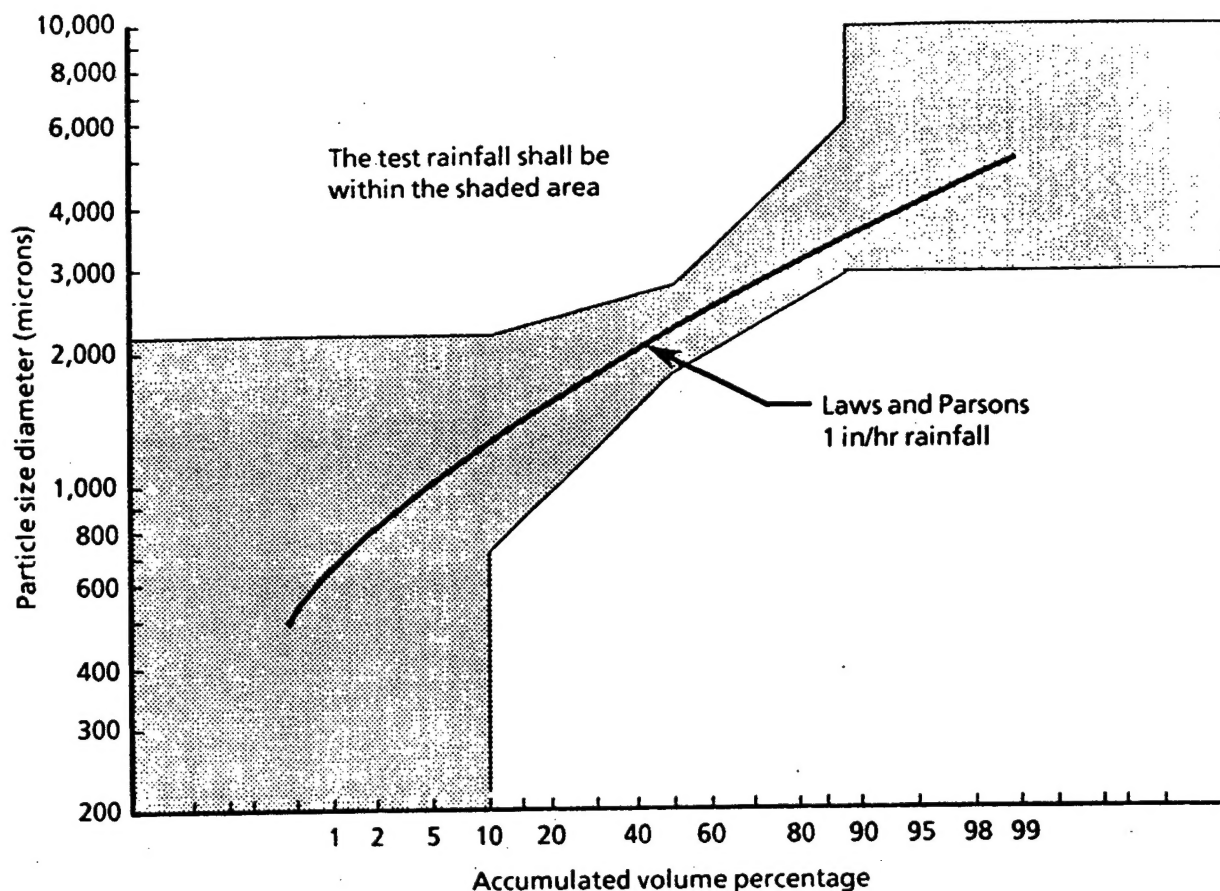
286

Figure G-1. Allowable particle size distribution for test.

3.3 Sand test. Sand shall be made from crushed quartz or any mineral or mixture of minerals with a MOH 7 or greater hardness. ·Particle sizes and shapes shall be within the range of that specified by the Design Criteria Document (DCD). The sand shall be dry to the touch and not be in clumps. The sand shall be replaced when the size and shape of the particles no longer meet the DCD requirements.

The sand cloud is to be maintained by the air recirculation inside the enclosure. Measurements of the cloud concentration shall be made below the rotor disk. The average concentration shall be within 50 percent of that specified by the DCD.

3.4 Test coupons. Test material shall be identical in thickness to that planned for the erosion protection system except for hydrolysis testing. Substrate materials and adhesives shall also be part of the test coupon if they are considered to have an effect on the erosion resistance of the outer layer of material.

3.5 Operation. During the sand tests, tangential velocities at the center of the test coupon shall be equal to the tip velocity of the rotating wing in hover. Higher velocities may be used for rain tests to represent peak velocities encountered during forward flight. For wear rate prediction, flat pitch is acceptable for rain erosion testing. For sand erosion, pitch angles

287

within the normal range of operation shall be used. For wear pattern determination, the pitch angles shall be set so that tests are conducted at both extremes of aerodynamic angle of attack.

3.6 Hydrolysis. Molded and extruded materials shall be sized for durometer hardness testing per ASTM D 2240. Tapes and coatings may be approximately 0.012-0.018 inch thick and shall be applied to appropriate substrate materials. All specimens shall be visually examined prior to exposure. Molded and extruded materials shall be tested for durometer hardness. Tapes and coatings are not usually thick enough for the hardness test. Specimens shall then be exposed to a constant 82°C (180°F) temperature and 95-100% relative humidity until failure or 1200 hours minimum duration. Samples shall be observed for signs of degradation and/or tested for durometer hardness every 72-96 hours for the first 400 hours and less frequently thereafter. Failures occur as a rapid drop in hardness, sometimes followed by melting, within the first several hundred hours of exposure, or by development of brittleness, cracking or irreversible swelling.

3.7 Foreign Object Impact. Impact testing shall be conducted by inserting hardwood dowels of progressively increasing diameters into the path of the test coupons. Specimen centerline tangential velocity shall be 733 ft/sec and coupons shall be in flat pitch. The erosion material shall be assessed for damage after each dowel impact.

4 DOCUMENTATION

4.1 Test plan. A test plan describing the test apparatus, devices used to monitor the environment, and outline of the test conditions shall be submitted for approval by the end user.

4.2 Test report. A final report shall be prepared. This report shall contain sufficient detail to enable a comparison with previous tests and an evaluation of the current test.